

THE UNIVERSITY OF GLASGOW

**NUMERICAL SIMULATION OF NON-EQUILIBRIUM GRADED  
SEDIMENT TRANSPORT**

thesis

submitted to the faculty of engineering  
in candidacy for the degree of doctor of philosophy

DEPARTMENT OF CIVIL ENGINEERING

BY

**QIANG LI**

GLASGOW

THE UNITED KINGDOM

FEBRUARY, 1995

© Qiang Li, 1995

ProQuest Number: 13818451

All rights reserved

INFORMATION TO ALL USERS

The quality of this reproduction is dependent upon the quality of the copy submitted.

In the unlikely event that the author did not send a complete manuscript and there are missing pages, these will be noted. Also, if material had to be removed, a note will indicate the deletion.



ProQuest 13818451

Published by ProQuest LLC (2018). Copyright of the Dissertation is held by the Author.

All rights reserved.

This work is protected against unauthorized copying under Title 17, United States Code  
Microform Edition © ProQuest LLC.

ProQuest LLC.  
789 East Eisenhower Parkway  
P.O. Box 1346  
Ann Arbor, MI 48106 – 1346

Thesis  
10180  
Copy 1

GLASGOW  
UNIVERSITY  
LIBRARY

## Numerical Simulation of Non-equilibrium Graded Sediment Transport

*To my parents, my wife and my son*

## **DECLARATION**

I declare that this thesis is a record of the original work carried out solely by myself in the Department of Civil Engineering at the University of Glasgow in the period of October 1991 to October 1994. The copyright of this thesis therefore belongs to the author under the terms of the United Kingdom Copyright Acts. Due acknowledgement must always be made of the use of any material contained or derived from, this thesis.

Qiang Li, BSc, MSc

February 1995

## **ACKNOWLEDGEMENTS**

I would like to express my sincere thanks to my supervisors Dr G. Pender and Dr D. A. Ervine for their constant inspiration and encouragement during my period of research. Special gratitude is due to Dr Ervine for assisting with my application for a University of Glasgow Postgraduate Scholarship. I am also grateful to Prof. B.B. Willetts (University of Aberdeen) and Drs A. Chan and T. Hoey (University of Glasgow) for their guidance and valuable comments and suggestions. The data made available from the following sources is also acknowledged: Prof. B. B. Willetts and Dr S. Tait (University of Aberdeen), Dr R. Kuhnle (Goodwin Creek Data), Clyde Port Ltd, HR Wallingford, United States Waterway Experimental Station and Gibbs and Neill. I would also like to thank my colleagues Dr P. Addison, Dr R. Manson, Dr B. Zhang, Dr H. Su, Mr B. Mcleod, Mr A. Nisbet, Mr C. Fuller and the late Mr A. Grey for their friendship during my period of study. Finally a special thank is due to my wife Ms Xiaohui Xu for her patience, understanding and encouragement.

This work was funded by a Glasgow University Postgraduate Scholarship and an Overseas Research Scheme award from the Committee of Vice-Chancellors and Principals of the Universities of the United Kingdom. This financial support is gratefully acknowledged.

## ABSTRACT

A comprehensive one-dimensional mathematical model for simulating unsteady non-equilibrium graded sediment transport has been developed and verified with experimental and field data. The model framework is based on non-equilibrium sediment transport, involving the interaction between size fractions, separation simulation of suspended-load and bed load movement, and the exchange of particles between four different model layers.

The implicit finite difference Preissmann scheme is used in the numerical model. This is known to be stable, flexible and robust. The two step operator splitting method, called the two point scheme, is employed to solve the advection-dispersion equation. A Newton-Raphson iteration method is used to linearise the highly non-linear equation system. A fully coupled solution technique, called the double block sweep method, is adopted to reflect the strong physical interrelationship between flow and sediment transport components and to suppress computer errors and divergence of the numerical solution, a problem found in uncoupled or partly coupled methods. The numerical dissipation in the Preissmann scheme can be minimised by selecting the proper space and time weighting factors. In general the space weighting factors for all governing equations are centred. For short term simulation, such as flood events, the time weighting factor is taken as 0.55 to reduce numerical dissipation, for long term simulations a value of 1.0 is used. The model has been tested against standard benchmarks to check the stability, numerical dissipation and performance of the code.

To solve the governing equations empirical sediment relationships must be employed. The main relation is the evaluation of the fractional sediment transport capacity. In this model van Rijn's sediment transport formulae developed for single-sized sediments have been used and modified for graded sediment using the concept of a hiding function. Two hiding functions for use with van Rijn's formulae were developed based on experimental data from HR Wallingford, United States

Waterways Experimental Station and Gibbs & Neill. The first one was developed using Einstein's hiding function definition which adjusts the Shields threshold condition for each size fraction. The second hiding function was developed using Parker's definition of a reduced hiding function which adjusts the threshold condition for each size fraction based on the Shields value for the geometric mean size. In the formulations of the two hiding functions the significance of the Froude number has been assessed and accounted for. Two parameters for grain size distribution, mean size and standard deviation, were used to represent the effect of the bed material composition. The two hiding functions have been verified and compared by simulating the experiments of armour development and formation conducted in Aberdeen University. The results indicated that the reduced hiding function gives a satisfactory agreement between observed and calculated values and the hiding function overestimates the threshold conditions for the finer particles in the mixture. As the base data and optimisation technique are identical for each hiding function it is believed that the reason for the difference is related to the physical nature of graded sediment transport.

The model has been used to simulate field investigations in Goodwin Creek, USA. Four transport events under flood condition were selected based on the availability of information. The model along with the empirical sediment relationships was therefore tested in a very active mobile bed river with graded sediment transport and a bimodal bed material. In order to compare the performance of van Rijn's formulae with a reduced hiding function, Parker's formula with his reduced hiding function was also used to simulate the same events. The effect of sediment inflows and initial bed material composition on the numerical results were also examined during the numerical simulations. The overall results indicated that real life simulation requires extensive data particularly for initial and boundary conditions. Parker's formula is sensitive to the resistance factor therefore the correct estimation of the resistance factor is a necessary condition for using Parker's formula.

The model has been applied in a real medium river system, the River Clyde in Scotland, for long term simulations of the river returning to regime following the cessation of dredging. The numerical results from this model have been compared with ones from a previous study in which the regime method was used. A good comparison of the results between these two studies was obtained. The effect of a new tidal weir, which is planned to be built, on the final regime condition and the river environment was also investigated.

## TABLE OF CONTENTS

	Page
<b>ACKNOWLEDGEMENTS</b>	<b>v</b>
<b>ABSTRACT</b>	<b>vi</b>
<b>TABLE OF CONTENTS</b>	<b>ix</b>
<b>LIST OF ILLUSTRATIONS</b>	<b>xv</b>
<b>LIST OF TABLES</b>	<b>xxiii</b>
<b>NOTATION</b>	<b>xxv</b>
<b>CHAPTER 1 Introduction</b>	<b>1</b>
1.1 Introduction.....	1
1.2 Aims of The Project.....	2
1.3 Main Areas of Research.....	3
1.4 Brief Literature Review .....	3
1.5 State of The Art Survey .....	9
1.6 Layout of The Thesis .....	13
<b>CHAPTER 2 Theory of Non-equilibrium Graded Sediment Transport</b>	<b>16</b>
2.1 Introduction.....	16
2.2 Framework of Sediment Transport of Non-Uniform Material .....	17
2.2.1 Hydrodynamic Equations.....	17
2.2.2 Mechanisms of Sediment Transport.....	19
2.2.2.1 Suspended-load transport .....	20
2.2.2.2 Bedload transport .....	22
2.2.2.3 Bed Material Conservation.....	23
2.2.2.4 Bed Material Sorting .....	23
2.3 Empirical Sediment Relationships.....	24
2.3.1 Hydraulic Resistance.....	24
2.3.2 Fractional Sediment Transport Capacity.....	31

2.3.3 Characteristic Length For Suspended-load .....	33
2.3.4 Travel Length of Bedload .....	36
2.3.5 Fall Velocity.....	38
2.3.6 Mean Velocity of Bedload .....	40
2.3.7 Thickness of Bottom Layer.....	41
2.3.8 Thickness of Active Layer .....	41
2.3.9 Dispersion Coefficient .....	45
<b>CHAPTER 3 Development of Two Hiding Functions For Use With Van Rijn's Sediment Formulae</b>	<b>49</b>
3.1 Introduction.....	49
3.2 Background.....	50
3.3 Effects of Surface Characteristics On Hiding.....	53
3.4 Equal Mobility and Hiding Function.....	54
3.5 Analysis of Hiding Function and Reduced Hiding Function.....	55
3.5.1 Dimension Analysis of Threshold Conditions For Graded Bed Material... 55	
3.5.2 Form of Hiding Function and Reduced Hiding Function .....	58
3.5.2.1 Form of Hiding Function.....	58
3.5.2.2 Form of Reduced Hiding Function.....	59
3.5.3 Relationship Between Hiding Function and Reduced Hiding Function .....	61
3.6 Available Experimental Data.....	61
3.6.1 H.R. Wallingford Data.....	61
3.6.2 USWES Data.....	63
3.6.3 Gibbs & Neill Data .....	65
3.6.4 Grain Size Distributions For All Bed Materials.....	66
3.7 Van Rijn's Sediment Transport Formula .....	67
3.8 Hiding Function Development .....	68
3.8.1 Scaling Size.....	69
3.8.2 Hiding Function .....	69

3.8.3 Verification of The Hiding Function .....	71
3.9 Development of The Reduced Hiding Function .....	71
3.9.1 Reduced Hiding Function .....	71
3.9.2 Reduced Hiding Function Verification .....	73
<b>CHAPTER 4 Numerical Model Development</b>	<b>86</b>
4.1 Equations For Graded Sediment Transport .....	86
4.2 Brief Review of One-Dimensional Mobile Bed Model.....	87
4.3 Numerical Scheme.....	89
4.4 Preissmann Scheme .....	90
4.5 Newton-Raphson Method.....	93
4.5.1 Discretion of Water Continuity Equation .....	95
4.5.2 Discretion of Water Momentum Equation.....	96
4.5.3 Discretion of Suspended-load Transport Equations.....	97
4.5.4 Discretion of Bedload Transport Equation .....	99
4.5.5 Discretion of Bed Material Conservation Equation.....	100
4.5.6 Discretion of Bed Material Sorting Equation .....	101
4.5.7 Final Parameter Matrix .....	103
4.6 Boundary Conditions .....	104
4.7 Need For Fully Coupled Solution.....	105
4.8 Block Double Sweep Method.....	108
4.9 Solution Procedure.....	110
4.10 Stability and Accuracy.....	116
4.10.1 Stability .....	116
4.10.2 Accuracy .....	118
4.11 Lateral Distribution of Deposition or Erosion.....	119
4.12 Effective Depth and Effective Width.....	120
4.13 Multi Functional Model.....	121
<b>CHAPTER 5 Test Applications of The Model</b>	<b>123</b>

5.1 Introduction.....	123
5.2 Performance of The Two Point Scheme.....	123
5.3 Numerical Test For Stability.....	126
5.4 Hydrodynamic Model.....	127
5.5 Trench Infilling Test.....	128
5.6 Test Application of The Armouring.....	130
<b>CHAPTER 6 Application of The Model To Experiments of Static Armour Development</b>	<b>142</b>
6.1 Introduction.....	142
6.2 Experimental Tests In Aberdeen University.....	142
6.2.1 Experimental Apparatus.....	143
6.2.2 Experimental Procedure.....	144
6.2.3 Sampling Techniques.....	145
6.2.4 Initial Experimental Conditions.....	145
6.3 Numerical Model.....	147
6.4 Comparison Between Two Hiding Functions.....	147
6.4.1 Hiding Function.....	147
6.4.2 Reduced Hiding Function.....	148
6.4.3 Difference Between Two Hiding Functions.....	148
6.5 Numerical Simulations.....	148
6.5.1 Experiment 1.....	149
6.5.2 Experiment 2.....	149
6.5.3 Experiment 3.....	150
6.5.4 Experiment 4.....	150
6.6 Analysis and Discussion.....	151
<b>CHAPTER 7 Graded Sediment Transport In Goodwin Creek</b>	<b>168</b>
7.1 Introduction.....	168
7.2 Goodwin Creek.....	169

7.3 Description of Observed Data.....	170
7.4 Empirical Sediment Relationships Used In Goodwin Creek.....	173
7.5 Numerical Model.....	173
7.6 Strategy In Simulations.....	175
7.7 Numerical Results For Model 1.....	175
7.8 Numerical Results From Model 2.....	176
7.9 Numerical Results From Model 3.....	178
7.10 Numerical Results From Model 4.....	178
7.11 Numerical Results From Model 5.....	179
7.12 Numerical Results From Model 6.....	179
7.13 Comparison of $D_{50}$ in Bedload.....	180
7.14 Discussion and Conclusions .....	180
<b>CHAPTER 8 Model Verification Using The River Clyde Data</b>	<b>196</b>
8.1 Introduction.....	196
8.2 Previous Work .....	198
8.3 Descriptions of The River Clyde .....	201
8.3.1 Study Area.....	201
8.3.2 Cross-Section Information .....	202
8.3.3 Properties of Bed Material .....	203
8.4 Boundary Conditions.....	206
8.4.1 Water Inflow .....	206
8.4.2 Sediment Inflow.....	207
8.4.3 Tide Levels.....	208
8.5 Application of Hydrodynamic Model.....	208
8.5.1 Calibration of The River Clyde Model .....	208
8.5.2 Verification of Model.....	210
8.5.3 Water Levels Caused By A 100 Year Tide And A 100 Year Flood .....	211
8.6 Prediction of Final Regime Condition.....	211

8.6.1 Boundary Conditions .....	211
8.6.1.1 Freshwater Inflow.....	212
8.6.1.2 Sediment Inflow .....	212
8.6.1.3 Controlling Water Level At Upstream .....	213
8.6.2 Time To Reach Final Regime Condition .....	214
8.6.3 Cross-Sectional Shape In Final Regime Condition.....	215
8.6.4 Comparison With Previous Regime Calculations.....	217
8.7 Effect of A New Tidal Weir On Final Regime Condition.....	217
8.7.1 Introduction.....	217
8.7.2 Location and Type of The Tidal Weir .....	218
8.7.3 Numerical Treatment of The Tidal Weir .....	218
8.7.4 Effect of A Tidal Weir On Final Bed Profile.....	219
8.8 Conclusion .....	220
<b>CHAPTER 9 Conclusions and Recommendations For Future Work</b>	<b>242</b>
9.1 General.....	242
9.2 Conclusions For Framework of Non-equilibrium Graded Sediment Transport Modelling.....	242
9.3 Conclusions For The Numerical Scheme and Solution Technique .....	244
9.4 Conclusions For The Hiding Functions.....	245
9.5 Conclusions For Applications.....	246
9.5.1 From Applications in Experiments of Armouring Development.....	246
9.5.2 From Application of Goodwin Creek .....	247
9.5.3 From Application of River Clyde .....	247
9.6 Recommendations For Future Work.....	248
<b>REFERENCES</b>	<b>250</b>

## LIST OF ILLUSTRATIONS

Figure	Page
Figure 1.1 Physical Processes of Mobile Bed River System.....	15
Figure 2.1 Water and Sediment Transport In An Mobile Bed River.....	18
Figure 2.2 Conceptualisation of Sediment Transport Layers.....	20
Figure 2.3 Flow Resistance Due To Bedforms.....	27
Figure 2.4 Flow Resistance From Grain Roughness and Bed Form Roughness.....	28
Figure 2.5 Shear Relationship Based On $D_{35}$ of The Parent Material.....	30
Figure 2.6 Measured Variations of Suspended-load with Net Deposition and Net Entrainment .....	34
Figure 2.7 Characteristic Length of Particles Transported in Suspension, Following Different Integration Procedures.....	35
Figure 2.8 Spatial Lag of Bedload in Approaching Equilibrium Condition.....	37
Figure 2.9 Two-Active Layer Depths Below The Bed-Flow Interface.....	43
Figure 2.10 Difference Between Dispersion of Particles and Diffusion of Momentum Exchange .....	47
Figure 2.11 Damping Effect To Dispersion Coefficient.....	49
Figure 3.1 Hiding Functions: (i) Einstein; (ii) Pemberton; (iii) White and Day; (iv) Parker.	78
Figure 3.2 Grain Size Distributions For All Bed Material.....	78
Figure 3.3 Scaling Size $Da$ Verse $\sqrt{D_{84}/D_{16}}$ and $Fr$ .....	79
Figure 3.4 Hiding Function $\epsilon_j$ Against Relative Particle Size $D_j/D_a$ .....	79
Figure 3.5 Comparison of Transport Capacity Between Calculated and Observed Values Without Hiding Function.....	80
Figure 3.6 Comparison of Transport Capacity Between Calculated and Observed Values With Hiding Function.....	80
Figure 3.7 $\Phi$ Value Against $\sigma_g$ and $Fr$ From Data of Day and USWES.....	81
Figure 3.8 $\omega_j$ Value Against Relative Size $D_j/D_g$ .....	81

Figure 3.9 $g_j$ Against $D_j/D_g$ and $\sigma_g$ For $Fr = 0.3$ .....	82
Figure 3.10 $g_j$ Against $D_j/D_g$ and $\sigma_g$ For $Fr = 0.5$ .....	82
Figure 3.11 $g_j$ Against $D_j/D_g$ and $\sigma_g$ For $Fr = 0.7$ .....	83
Figure 3.12 Comparison of Results Between Using Reduced Hiding Function and Single Size Assumption.....	83
Figure 3.13 Comparison Between Observed and Calculated Transport Capacity For HRS and USWES Data Without Hiding Function.....	84
Figure 3.14 Comparison Between Observed and Calculated Transport Capacity For HRS and USWES Data With Reduced Hiding Function.....	84
Figure 3.15 Transport Capacity Results of Using Reduced Hiding Function and $D_{50}$ For HRS and USWES Data .....	85
Figure 3.16 Comparison Between Observed and Calculated Transport Capacity For Gibbs&Neill Data Without Hiding Function.....	85
Figure 3.17 Comparison Between Observed and Calculated Transport Capacity For Gibbs&Neill Data With Reduced Hiding Function.....	86
Figure 4.1 Preissmann Scheme.....	91
Figure 4.2 Lateral Distribution of Deposition or Erosion.....	120
Figure 4.3 Effective Depth and Effective Width At A Cross Section.....	122
Figure 5.1 Numerical Prediction For Plug Source Concentration Distribution From Backward Scheme .....	132
Figure 5.2 Numerical Prediction For Plug Source Concentration Distribution From Central Scheme .....	132
Figure 5.3 Numerical Prediction For Plug Source Concentration Distribution From QUICK Scheme .....	133
Figure 5.4 Numerical Prediction For Plug Source Concentration Distribution From Two Point Scheme .....	133
Figure 5.5 Prediction of Plug Concentration From Two Point Scheme For Different Time Weighting .....	134

Figure 5.6 Prediction of Plug Concentration From Two Point Scheme For Different Courant Number Factor..... 134

Figure 5.7 Numerical Results of Water Level at Upstream and Downstream Boundary..... 135

Figure 5.8 Comparison of Water Level Results Under Different  $\theta$ ..... 135

Figure 5.9 Comparison of Water Level Results Under Different Cr..... 136

Figure 5.10 Infilling Process of Trench For Uniform Material..... 136

Figure 5.11 Infilling Process of Trench For Non-Uniform Material..... 137

Figure 5.12 Distribution of Transport Rate and Capacity of Suspended-load Along Channel After 12 hours..... 137

Figure 5.13 Distribution of Transport Rate and Capacity of Bedload Along Channel After 12 hours ..... 138

Figure 5.14 Distribution of Mean Size In Bed Material Along Channel..... 138

Figure 5.15 Transport Rate Varying With Time During Armouring Development..... 139

Figure 5.16 Suspended-load Transport Rate Distribution Along Channel After 1 day..... 139

Figure 5.17 Bedload Transport Rate Distribution Along Channel After 1 day..... 140

Figure 5.18  $D_{16}$ ,  $D_{50}$  and  $D_{84}$  Varying With Time At 300 m From Inlet..... 140

Figure 5.19 Composition of Bed Material and Transported Material After 50 Days At 300 m From Inlet ..... 141

Figure 6.1 Sketch of Experimental Flume..... 154

Figure 6.2 Cross Section of Bedload Trap..... 154

Figure 6.3 Grain-Size Distributions of Bed Mixtures In Experiments 1, 2, 3 and 4..... 155

Figure 6.4 Simulation of Bedload Rate Experiment No.1 Using The Hiding Function..... 155

Figure 6.5 Comparison of Measured and Computed Size Fraction Transport Rates At Time 361, 614 and 2331 minutes Experiment No.1 Using Hiding Function..... 156

Figure 6.6 Computed Variation of Particle Size Distribution In Active Layer Experiment No.1 Using Hiding Function ..... 157

Figure 6.7 Comparison of Total Bedload Rate Varying With Time From The Reduced Hiding Function..... 157

Figure 6.8 Comparison of Measured and Computed Size Fraction Transport Value For Experiment No.1 At Time 361, 614 and 2331 Minutes.....	158
Figure 6.9 Numerical Results of Bed Material Composition In Active Layer For Experiment No.1 .....	159
Figure 6.10 Comparisons of Composition of Armour layer and Transported Material Between Numerical and Observed Values For Experiment No.1 .....	159
Figure 6.11 Critical Shear Stress For Each Size Fraction For Experimental No.1.....	160
Figure 6.12 Simulation of Bedload Rate For Experiment No.2 Using The Reduced Hiding Function.....	160
Figure 6.13 Numerical Results of Bed Material Composition In Active Layer For Experiment No.2 .....	161
Figure 6.14 Simulation of Bedload Rate For Experiment No.3 Using The Reduced Hiding Function.....	161
Figure 6.15 Comparison of Measured and Computed Size Fraction Transport Value For Experiment No.3 At Time 360, 1256 and 2911 Minutes.....	162
Figure 6.16 Numerical Results of Bed Material Composition In Active Layer For Experiment No.3 .....	163
Figure 6.17 $D_{16}$ , $D_{50}$ and $D_{84}$ Varying With Time For Experiment No.3.....	163
Figure 6.18 Comparisons of Composition of Armour layer and Transported Material Between Computed and Observed Values For Experiment No.3 .....	164
Figure 6.19 Simulation of Bedload Rate For Experiment No.4 Using The Reduced Hiding Function.....	164
Figure 6.20 Comparison of Measured and Computed Size Fraction Transport Value For Experiment No.4 At Time 190, 599 and 2405 Minutes.....	165
Figure 6.21 Numerical Results of Bed Material Composition In Active Layer For Experiment No.4 .....	166
Figure 6.22 $D_{16}$ , $D_{50}$ and $D_{84}$ Varying With Time For Experiment No.4.....	166

Figure 6.23 Comparisons of Composition of Armour layer and Transported Material Between Computed and Observed Values For Experiment No.4 .....	167
Figure 7.1 Cross Section No.9 In Goodwin Creek.....	183
Figure 7.2 Grading Curves of Bed Material In Surface and Subsurface Layer In Goodwin Creek.....	183
Figure 7.3a Discharge and Water Depth Varying With Time For Event 18/11/84 In Goodwin Creek.....	184
Figure 7.3b Comparison of Total Bedload Rates Between Observed and Calculated Values For Event 18/11/84.....	184
Figure 7.4a Discharge and Water Depth Varying With Time For Event 06/06/86 In Goodwin Creek.....	185
Figure 7.4b Comparison of Total Bedload Rates Between Observed and Calculated Values For Event 06/06/86.....	185
Figure 7.5a Discharge and Water Depth Varying With Time For Event 08/11/86 In Goodwin Creek.....	186
Figure 7.5b Comparison of Total Bedload Rates Between Observed and Calculated Values For Event 08/11/86.....	186
Figure 7.6a Discharge and Water Depth Varying With Time For Event 16/11/87 In Goodwin Creek.....	187
Figure 7.6b Comparison of Total Bedload Rates Between Observed and Calculated Values For Event 11/18/87.....	187
Figure 7.7 Plots of $\omega_0$ and $\sigma_{\phi 0}$ versus $\Phi_{sg0}$ .....	188
Figure 7.8 Predictions of Bedload Rates Using Parker's Formula For Event 18/11/84.....	188
Figure 7.9 Predictions of Bedload Rates Using Parker's Formula For Event 06/06/86.....	189
Figure 7.10 Predictions of Bedload Rates Using Parker's Formula For Event 08/11/86.....	189
Figure 7.11 Predictions of Bedload Rates Using Parker's Formula For Event 16/11/87.....	190
Figure 7.12 Predictions of Bedload Rates Using Equal Mobility For Event 18/11/84.....	190
Figure 7.13 Predictions of Bedload Rates Using Equal Mobility For Event 06/06/86.....	191

Figure 7.14 Predictions of Bedload Rates Using Equal Mobility For Event 08/11/86.....	191
Figure 7.15 Predictions of Bedload Rates Using Equal Mobility For Event 16/11/87.....	192
Figure 7.16 Predictions of Bedload Rates Using van Rijn's Formulae and Subsurface Layer For Event 18/11/84.....	192
Figure 7.17 Predictions of Bedload Rates Using van Rijn's Formulae and Subsurface Layer For Event 08/11/86.....	193
Figure 7.18 Comparison of Bedload Between Equilibrium and Non-equilibrium Upstream Boundary Conditions For Event 08/11/86.....	193
Figure 7.19 Comparison of D <sub>50</sub> in Bedload For Event 18/11/84.....	194
Figure 7.20 Comparison of D <sub>50</sub> in Bedload For Event 06/06/86.....	194
Figure 7.21 Comparison of D <sub>50</sub> in Bedload For Event 08/11/86.....	195
Figure 7.22 Comparison of D <sub>50</sub> in Bedload For Event 16/11/87.....	195
Figure 8.1 General Plan and Key Locations In The River Clyde.....	196
Figure 8.2 Estimated Ultimate and Intermediate Bed Profiles By Regime Method.....	221
Figure 8.3 Tidal Variation at Broomielaw for Present and Regime Conditions (spring tide/100 year flood).....	221
Figure 8.4 Key Locations and Chainage In The River Clyde.....	222
Figure 8.5 Cross-Section at Broomielaw.....	223
Figure 8.6 Cross-Section at Rothesay Dock.....	223
Figure 8.7 Cross-Section at Dumbarton.....	224
Figure 8.8 Cross-Section at Greenock.....	224
Figure 8.9 Grading Curve of Bed Material In The River Clyde.....	225
Figure 8.10 Tidal Record For Greenock, Rothesay Dock and Broomielaw in 16/8/89.....	225
Figure 8.11 Predicted Water Level For Manning's Coefficient 0.015, 0.02 and 0.025 at Rothesay Dock.....	226
Figure 8.12 Predicted Water Level For Manning's Coefficient 0.015, 0.02 and 0.025 at Broomielaw.....	226
Figure 8.13 Predicted and Observed Water Level at Rothesay Dock.....	227

Figure 8.14 Predicted and Observed Water Level at Broomielaw.....	227
Figure 8.15 Predicted Water Level at Rothesay Dock Using Time Increment 300 s and 60 s .....	228
Figure 8.16 Predicted Water Level at Broomielaw Using Time Increment 300 s and 60 s.	228
Figure 8.17 Verification of Model For Tidal Event of August 15, 1989 at Rothesay Dock	229
Figure 8.18 Verification of Model For Tidal Event of August 15, 1989 at Broomielaw.....	229
Figure 8.19 Verification of Model For Tidal Event of January 5, 1991 at Rothesay Dock.	230
Figure 8.20 Verification of Model For Tidal Event of January 5, 1991 at Broomielaw.....	230
Figure 8.21 Verification of Model For Tidal Event of August 13, 1989 at Rothesay Dock	231
Figure 8.22 Verification of Model For Tidal Event of August 13, 1989 at Broomielaw.....	231
Figure 8.23 100 Year Tide at Greenock .....	232
Figure 8.24 Prediction of Water Level For 100 Year Tide at Greenock and 100 Year Flood at Tidal Weir.....	232
Figure 8.25 Estimated Ultimate and Intermediate Bed Profile After Cessation of Dredging In The River Clyde.....	233
Figure 8.26 Comparison of Bed Profile At Regime Conditions Between Model and Regime Method.....	233
Figure 8.27 Estimated Cross-Section Shape In Final Regime Condition at Broomielaw....	234
Figure 8.28 Estimated Cross-Section Shape In Final Regime Condition at Yorkhill.....	234
Figure 8.29 Estimated Cross-Section Shape In Final Regime Condition at Shieldhall.....	235
Figure 8.30 Estimated Cross-Section Shape In Final Regime Condition at Scotstoun.....	235
Figure 8.31 Estimated Cross-Section Shape In Final Regime Condition at Chainage 10 km	236
Figure 8.32 Estimated Cross-Section Shape In Final Regime Condition at Rothesay Dock	236
Figure 8.33 Estimated Cross-Section Shape In Final Regime Condition at Chainage 15 km	237
Figure 8.34 Estimated Cross-Section Shape In Final Regime Condition at Erskine.....	237
Figure 8.35 Estimated Cross-Section Shape In Final Regime Condition at Dumbarton.....	238
Figure 8.36 Estimated Cross-Section Shape In Final Regime Condition at Chainage 30.2 km .....	238

Figure 8.37 Comparison of Bed Profile After 10 Years of Cessation Between Model and Regime Method .....	239
Figure 8.38 Comparison of Bed Profile After 20 Years of Cessation Between Model and Regime Method .....	239
Figure 8.39 Comparison of Bed Profile After 40 Years of Cessation Between Model and Regime Method .....	240
Figure 8.40 Daft Layout of A New Tidal Weir At Confluence of River Kelvin in River Clyde .....	240
Figure 8.41 Estimated Ultimate and Intermediate Bed Profile After Cessation of Dredging In The River Clyde With A New Tidal Weir.....	241

## LIST OF TABLES

Table	Page
Table 3.1 Characters of Bed Material In H R Wallingford Data.....	62
Table 3.2 Hydraulic Conditions and Sediment Transport Rates In H R Wallingford Data...	63
Table 3.3 Characters of Bed Material In USWES Data.....	64
Table 3.4 Hydraulic Conditions and Sediment Transport Rates In USWES Data.....	64
Table 3.5 Characters of Bed Material In Gibbs&Neill Data.....	65
Table 3.6 Hydraulic Conditions and Sediment Transport Rates In Gibbs&Neill Data.....	66
Table 3.7 Grain Size Distribution In Bed Materials.....	67
Table 3.8 Verification For $\Phi$ Value.....	75
Table 3.9 Comparison of Results Between Using Reduced Hiding Function and Single Size Assumption.....	76
Table 3.10 The Percentage of Correct Predicted Value in Total.....	77
Table 4.1 Space and Time Weighting Parameters In The Peissmann Scheme For The Application .....	112
Table 4.2 The Initial Values For All Variables .....	113
Table 5.1 Space and Time Weighting Factors Used In Simulation of Erosion Process.....	129
Table 5.2 Initial Grain Size Distribution.....	130
Table 5.3 Boundary Conditions For Armouring Process .....	131
Table 6.1 Grain Size Distribution By Weight For All Four Mixtures In Aberdeen University .....	146
Table 6.2 Summary of Experimental Conditions In Aberdeen University.....	146
Table 7.1 Summary of Hydraulic Information In Goodwin Creek.....	170
Table 7.2 Cross Sectional Information In Goodwin Creek.....	171
Table 7.3 Details of Bed Matèrial Composition In Goodwin Creek.....	172
Table 7.4 Characteristics of Bed Material In Goodwin Creek.....	173

Table 7.5 Comparison of Velocity Between Observed and Computed Values For Four Events .....	182
Table 8.1 Bed Level at Regime Condition in River Clyde.....	199
Table 8.2 Typical Bed Level Rising Rate.....	200
Table 8.3 Catchment Area and Long Term Average Discharge.....	202
Table 8.4 Summary of Hydrographic Survey Drawings In The River Clyde.....	204
Table 8.5 Sieve Analysis For Bed Material of The River Clyde.....	205
Table 8.6 Properties of Bed Material In The River Clyde.....	205
Table 8.7 River Flow Data.....	206
Table 8.8 Tidal Data for Greenock, Rothesay Dock and Broomielaw.....	208
Table 8.9 Parameters Used in Model After Calibration.....	210
Table 8.10 Mean Annual Flood In The River Clyde and Its Tributaries.....	212
Table 8.11 Boundary Conditions For Regime Simulation of The River Clyde.....	214
Table 8.12 Physical Parameters For The Tidal Weir.....	219
Table 8.13 Boundary Conditions For Regime Simulation of The River Clyde With A Internal Tidal Weir.....	219

## NOTATION

$A$	cross sectional area
$A_m$	cross sectional area in the active layer
$A_Z$	cross sectional area of bed material above datum
$B$	top width of cross section
$B_e$	effective width of cross section
$C$	Chezy coefficient
$C_j$	suspended-load concentration of size fraction $j$
$C_j^*$	equilibrium suspended-load concentration of size fraction $j$
$Cr$	Courant number
$C_{sj}$	lateral suspended-load concentration of inflow or outflow for size fraction $j$
$D$	dispersion coefficient
$D_{16}$	particle diameter for which 16% is finer
$D_{50}$	particle diameter for which 50% is finer
$D_{84}$	particle diameter for which 84% is finer
$D_a$	scalling size
$D_g$	geometric mean diameter
$D_j$	particle diameter of size fraction $j$
$D^*$	dimensionless particle diameter
$Fr$	Froude number
$G_j$	bedload transport rate for size fraction $j$
$G_j^*$	bedload transport capacity for size fraction $j$
$g$	gravity acceleration

$g_j$	reduced hiding function
$g_{sj}$	lateral unit bedload inflow or outflow rate for size fraction $j$
$H_e$	effective depth of cross section
$h$	water depth
$K$	cross sectional conveyance
$L_j^*$	characteristic length of suspended-load for size fraction $j$
$n$	Manning's coefficient
$p$	porosity of bed material
$Q$	discharge
$q$	lateral inflow or outflow
$R$	hydraulic radius
$Re$	Reynolds number
$S$	friction slope
$t$	time
$u_{bj}$	bedload velocity
$u_{cr}$	critical velocity
$u_{cr,j}$	critical velocity for size fraction $j$
$u_{sh}$	critical Shields velocity
$u_{sh,j}$	critical Shields velocity for size fraction $j$
$u^*$	shear velocity
$u[.]$	unit function
$V$	Vedernikov number
$W_j$	suspended-load concentration gradient for size fraction $j$
$X = \sqrt{D_{84}/D_{16}}$	deviation of grain size distribution
$x$	streamwise coordinate

$Y$	water surface level
$\alpha$	relaxation parameter
$\beta_j$	fractional proportion of size fraction $j$ in the active layer
$\beta_{0j}$	fractional proportion of size fraction $j$ in the subsurface layer
$\Delta$	specific submerged density
$\Delta t$	time increment
$\Delta x$	space increment
$\varepsilon$	criterion corresponding to the accuracy
$\varepsilon_j$	hiding function
$\lambda_j$	travel length of bedload for size fraction $j$
$\nu$	viscosity of water
$\theta$	time weighting factor in the Preissmann scheme
$\rho$	water density
$\rho_s$	sediment density
$\sigma_g$	standard geometric deviation
$\tau_{cr,j}$	critical shear stress for size fraction $j$
$\tau_{sh,j}$	critical Shields shear stress for size fraction $j$
$\omega_j$	fall velocity for size fraction $j$
$\psi$	space weighting factor in the Preissmann scheme
$\psi_{cr,j}$	mobility parameter for size fraction $j$
$\psi_{sh,j}$	Shields mobility parameter for size fraction $j$

# CHAPTER 1 Introduction

## 1.1 Introduction

The physical processes dominant in determining the global evolution of mobile bed rivers are shown diagrammatically in Figure 1.1. If one assumes that flow conditions are one-dimensional these processes can be described mathematically by a set of partial differential equations. Numerical techniques exist for solving these equations, which means that it is perfectly feasible to develop a computer code for simulating one-dimensional dynamic changes in mobile bed channels. Figure 1.1 also shows other physical processes that depend on small scale fluid/sediment interaction and how they influence the global equations. The highly complex nature of these small scale processes means that they can only be defined using semi-empirical equations. The success of any numerical model in reproducing or predicting actual global mobile bed behaviour is highly dependent on how well the semi-empirical equations match the behaviour of the small scale physical processes. These semi-empirical equations are often highly site specific and difficult to define in a general form. This has resulted in mobile bed models failing to reach the same level of generality, reliability and robustness that fixed bed hydrodynamic models have achieved.

Recent research publications have discussed the feasibility of developing a general one-dimensional mobile bed computer model applicable to a wide range of circumstances, Holly and Rahuel (1990), Armanini and Silvio (1988) and Rahuel et al (1989). Given the continued increasing availability of low cost high powered

computing facilities the author agrees that this is the way forward for computer simulation in mobile bed problems. This project will therefore take the first steps towards developing a comprehensive mobile bed model at Glasgow University. It is envisaged that this research project will be the first in a number of three year programmes necessary to complete the project. Software development will therefore be undertaken with future expansion in mind.

## 1.2 Aims of The Project

The main aim of this project was therefore to begin the development of a comprehensive numerical model for predicting sediment transport in unsteady flows. There were a number of reasons for choosing this topic:

1. Glasgow University is actively engaged in physical modelling research of graded sediment transport in gravel bed rivers. It was thought appropriate that a parallel numerical modelling project should be undertaken to provide cross fertilisation between the two disciplines. Unfortunately, due to delays in the start of the physical modelling programme the interaction between the two projects has been less than was originally intended.
2. Throughout the developed world the topic of river rehabilitation is becoming popular. This is where rivers that have suffered environmental degradation are reinstated to a more natural condition. Invariably this requires the reinstatement of a gravel bed which must be designed to be stable under the design flood flow. This calculation often requires the use of a numerical model similar to that presented here.
3. Advances in computing hardware mean that it is now possible to run fully coupled sediment transport models on desk top computing facilities. An important factor is that one is concerned with undertaking practical research of relevance to industry.

4. Sediment transport is a major problem in The People's Republic of China, the author's home country. The numerical model will be relevant to engineering problems in this country.

### **1.3 Main Areas of Research**

Achieving objectives 1, 2 and 4 requires that the model be able to accurately simulate graded sediment transport, taking account of both bed and suspended load. This requires that the model is capable of evaluating each of these transport components. To achieve this it was decided to employ van Rijn's sediment transport formulae (1984). This choice of sediment transport formulae necessitated the development of a hiding function to enable the influence of size fraction interaction to be simulated. A large part of the thesis is therefore devoted to the development and testing of this hiding function.

The range of applicability of numerical models for sediment transport predictions can be enhanced if a fully coupled solution using the Preissmann finite difference scheme is employed. This requires special treatment of the finite difference formulation of the advection-dispersion equation. A two point scheme has been developed here and its performance compared with other finite difference schemes such as QUICK.

In addition, the effects of other sediment relationships on graded sediment transport are also discussed such as the resistance factor and the thickness of the active layer. The performance of a fully coupled solution technique, the block double sweep method, is examined through the applications of model to the experiments and field investigations.

### **1.4 Brief Literature Review**

The interaction of size fractions in graded sediment transport results in transport rates which differ considerably from that obtained using single-sized material. In the latter case bed material behaves as a uniform material and the only change with time

is the bed elevation in response to deposition or erosion. When a single size assumption is appropriate the concepts involved in modelling morphological changes are relatively simple, and a continuity law provides all information necessary to predict geomorphological changes. However, when graded material is used a number of additional features are required of models such as the dynamic response of the bed material composition to the local non-equilibrium sediment transport, hiding effects, armouring, and exchanges of particles between different layers.

The study of graded sediment transport dates back to 1950 when Einstein (1950) tried to extend his single-sized bedload predictor to graded sediment transport by introducing a hiding function which took into account the hiding effect for fine material and the exposure effect for coarse material in the bed. This enabled him to adjust the tractive force for each size fraction and then to calculate the fractional sediment transport capacity. At that time equilibrium of graded sediment transport was assumed and therefore estimation of bed evolution was relatively simple.

To evaluate the changes of bed material composition, Hirano (1971) derived an Exner equation to deal with the vertical exchanges of particles in the active layer. Implicit in this equation was the assumption of equilibrium sediment transport and equal transport mobility. This equation allowed bed material to become finer or coarser due to deposition or erosion, therefore enabling armouring to be predicted. The key parameter in this equation is the thickness of the active layer.

Borah (1982) developed a mathematical model to deal with graded sediment transport in streams where the exchanges of particles between the bottom and the active layers is taken into account using the concept of residual transport capacity. Then noting that different size fractions were transported at different rates, he computed fractional residual transport capacity, which was used to form a time invariant volume entrainment matrix, with the help of an entrainment frequency matrix. The actual entrained volume was calculated by introducing an erodibility parameter. Therefore the response of a stream to the graded sediment transport process

is to adjust its bed material composition and cross sections to reduce the residual transport capacity. When erosion takes place the bed material in the active layer eventually becomes coarser. Recognising the fact that some of the size fractions in the active layer cannot be eroded during armour development Borah (1982) proposed an expression for evaluating the thickness of active layer in which the upper bound was adopted for flow to transport all fractions. When an armour layer is formed no erosion can occur until the flow develops the necessary residual transport capacity to break this up. In his model the full St. Venant equations were employed so that it is possible to simulate unsteady flow and sediment transport. A partly coupled solution technique was adopted to compute the hydrodynamic and sediment components separately.

Willets et al (1987) carried out simulations of armour layer development and its consequences. They proposed a procedure for calculating graded sediment transport and changes of bed material composition. In their method, the concept of non-equilibrium graded sediment transport was adopted and the calculations based on the difference between the real transport rate and the transport capacity. When the real transport rate is greater than the transport capacity deposition takes place until equilibrium conditions are satisfied. Conversely erosion takes place when the predicted transport rate is less than the transport capacity and consequently bed material becomes coarser. Because the evaluation of the active layer thickness is critical for static armour development, a two-layer active depth was employed in this model, each layer being a half of the total thickness of the active layer. The active layer thickness was taken to be equal to coarsest particle diameter. Numerical solution was based on the separation of hydraulic parameters and sediment transport, and hydrodynamic components were computed from a backwater calculation.

Han et al (1987) developed a mathematical model for non-equilibrium graded sediment transport in which a distribution function for bed material composition was adopted. A parameter in this function can be adjusted according to deposition or erosion and consequently bed material becomes finer or coarser. This parameter is

directly related to the residual transport capacity. This model can therefore predict the change of bed material composition. Numerical simulation was carried out using an uncoupled solution method. Hydraulic information was computed using a backwater calculation.

By recognition of the fact that spatial and temporal lags occur between transport rates and transport capacity, Armanini and Silvio (1988) developed an one-dimensional model for graded sediment transport. The local equilibrium hypothesis was removed and full non-equilibrium sediment transport was introduced in both the suspended-load equation and the bedload equation for each size fraction in <sup>the</sup> mixture. The bed material conservation was derived based on the concept of bed material displacement. The exchanges of particles between different layers were first proposed to be directly proportional to the residual transport capacity. The concept of characteristic length for suspended-load and travel length for bedload were introduced to evaluate the source term. Equal transport mobility was implicitly assumed in the calculation of the fractional sediment transport capacity. The hiding effect was considered using the procedure suggested by Ranga Raju (1985) to modify real shear stress to effective shear stress according to grain size distribution of bed material and flow strength. In this model the physics of graded sediment transport was analysed systematically and then the fundamental principles were formed for model development. However, a fully coupled solution technique was not adopted even although the physical coupling relationship between flow and graded sediment transport was described and highlighted.

Rahuel et al (1989) developed a computer model to simulate unsteady and non-equilibrium graded sediment transport in mobile bed rivers with sorting and hiding effects. The physics of graded sediment transport in this model is similar to that of the Armanini and Silvio (1988) model, although the treatment of the hiding effect, evaluation of the fractional transport capacity and the thickness of active layer were different. This model was the first to solve the system of equations using a fully

coupled implicit solution technique, called the block double sweep method. The Preissmann scheme was used and the Newton-Raphson method was employed to obtain a fast convergence. Numerical tests proved that this solution technique is robust, flexible and stable.

Holly and Rahuel (1990) published papers giving the framework of mobile bed modelling and details of a fully coupled solution technique. The model was based on the full unsteady St. Venant equations including non-equilibrium graded sediment transport. The full set of governing equations for graded sediment transport were described with the physical concepts involved highlighted. They assumed that all size fractions were transported under a non-equilibrium situation and exchanges of particles between different layers were proportional to the residual transport capacity. The fractional sediment transport capacity was computed using an appropriate graded sediment transport formula including hiding. The sorting equation was given from a conservation law in the active layer for each size fraction by considering bed material displacement. Holly and Rahuel (1990) claimed that the governing equations with a set of appropriate empirical sediment relationships are able to simulate the features of graded sediment transport in mobile bed rivers. These include armouring due to selective erosion, downstream fining and any dynamic geomorphological changes. The basic governing equations are general although it is difficult to obtain a general form for the empirical sediment relationships. They also discussed the numerical dissipation associated with time and space weighting parameters in the Preissmann scheme. They claimed that the objective of establishing a complete framework is to provide a useful standard against which other models employing techniques such as uncoupled solutions and total load approaches can be evaluated.

Parker and Sutherland (1990) published work for the prediction of bed material composition in the static armour layer under certain hydraulic conditions by applying the modified Exner equation which was originally derived by Hirano (1971). In their work Parker's bedload predictor with his reduced hiding function was used. They

implicitly assumed that the equilibrium fractional sediment transport and equal transport mobility hold under the situation considered.

Silvio (1992) suggested a four-layer model for graded sediment transport in which the vertical material sorting was defined and expressed by applying the conservation law for each size fraction. As vertical exchanges of particles between surface and subsurface layers are included this model can predict formation and evolution of the subsurface layer. In addition, the model is able to simulate armouring and evolution of bed material composition when sediment inflow is reduced. Again a semi-theoretical solution technique was adopted with the separation of the hydrodynamic component and graded sediment transport component.

Niekerk et al (1992) published their work of sediment routing modelling. In this model Bagnold's sediment transport formula, see Bagnold (1973), was used in combination with grain protrusion and hiding. Equilibrium sediment transport was assumed and the bed material sorting process described by an Exner equation. The active layer thickness was assumed to increase with the excess shear stress. This model is therefore able to simulate the features of graded sediment transport such as armouring, downstream fining and bed material sorting. The Preissmann scheme was applied and an uncoupled solution technique was adopted. The advantages of this model are a treatment of turbulent fluctuations of bed shear stress, minimisation of calibration factors, and explicit consideration of size fractions. This model was verified against field data from the San Luis canal, Colorado and the East Fork Rivers, Wyoming for a large variety of flow conditions and a good range of bed material. Since the active layer thickness is quite sensitive to the numerical results, the authors claimed that the active layer thickness must be calibrated.

The theoretical consideration of graded sediment transport equations based on the long term morphological processes was given by Silvio in 1993. By adopting the long term response of the averaging quantities he presented the equations for an one and two dimensional model where the averaging was made to remove turbulent

fluctuations. He also discussed non-equilibrium sediment transport and a source term to represent the upward or downward motion of the particles.

Hoey (1994) developed a computer model to simulate downstream fining by selective transport in gravel bed rivers. The bed material sorting process was defined by a modified Exner equation which contains the exchanges of sediment between surface and subsurface layers and is certainly able to reflect finer or coarser processes of bed material during deposition or erosion. Implicit in this model is the assumption of equilibrium graded sediment transport. The bedload formula of Parker (1990) with his reduced hiding function was used in which interaction of size fractions was taken into account. In his model the hydraulic parameters were solved using a backwater calculation. Again an uncoupled solution technique was adopted. Because an explicit scheme was used the time increment was limited by a stability condition.

### **1.5 State of The Art Survey**

Today graded sediment transport research and modelling is becoming very popular. The efforts made in laboratory and field investigations can provide direct guidance for model development. In return mathematical modelling can provide a useful tool to judge the validity of empirical sediment relationships.

To date there are several concepts accepted in graded sediment transport. Some of these concepts have been translated into mathematical language, some are still being investigated. The following concepts are of note

1. The flow and graded sediment transport in a mobile bed river system is generally unsteady. This implies that all independent variables are time dependent and the whole system trends to adjust itself to reach a steady state condition. Any imposed disturbance, such as a change of boundary conditions, results in dynamic changes to the system and consequently a new steady state will be reached.

2. Graded sediment transport is regarded as a non-equilibrium transport process in which transport rate is generally not equal to the transport capacity. Under some circumstances the equilibrium situation can be reached by adjusting channel geometry and bed material characteristics. Non-equilibrium transport implies that graded sediment transport is space and time dependent. Non-equilibrium transport can be simulated using the residual transport capacity. The residual transport capacity provides a measure of force necessary to change the system to the equilibrium situation. Following this the net exchange rates of particles between different layers are assumed to be proportional to the residual transport capacity.
3. Changes of bed material in the active layer occurs in the vertical direction only and bed material displacement must be included. This reflects the fact that during continuous erosion some bed material in the subsurface layer becomes part of the active layer. During deposition, part of bed material in the active layer enters the subsurface layer.
4. Evaluation of fractional sediment transport capacity must include hiding, which reflects the interaction between size fractions. This is crucial for graded sediment transport. Research results indicate qualitatively that the hiding effect is affected by the grain size distribution of bed material in the active layer, channel geometry, turbulent pressure fluctuation and hydraulic parameters. Most hiding functions in the literature are related to grain size distribution only.
5. The separation of suspend and bed load is acceptable for graded sediment transport. This recognises that bedload moves at a relatively slow kinematic wave type propagation velocity and suspended-load moves at an order-of-magnitude-greater. This statement implies that suspended-load should be described by an advection-dispersion equation in which the suspended-load is advected at same velocity as the water particles, and bedload should be described by an advection equation.

6. A four-layer concept forms a basis for model development though this assumption is questionable, instead the multi-layer concept should be used. The stream layer is for suspended-load, the bottom layer for bedload, sorting takes place only in the active or surface layer, and the subsurface layer serves to provide additional material.
7. Finally, the fractional transport capacity must be modulated to reflect the fact that some of the fractions may not be transported as bedload but rather as suspended-load.

All concepts above should be reflected in the model development. In addition, a numerical scheme should reflect all aspects of graded sediment transport. Following the work of Holly and Rahuel (1990) it was decided that the Preissmann scheme should be adopted for simulating unsteady non-equilibrium graded sediment transport. Three main advantages of the Preissmann scheme are that it is robust, flexible and stable. The Preissmann scheme is an implicit finite difference scheme and therefore provides a safety margin for stability even when the Courant number is greater than unity. This is important especially for long term simulations. The time and space weighting parameters in the Preissmann scheme can be adjusted to suit different physical problems. This provides a flexible way of dealing with different problems. Secondly, the resulting algebraic system of the Preissmann scheme has a very compact form. This compactness is useful not only for treating matrices but also for the boundary conditions. Thirdly, there exists an efficient solution technique, the block double sweep method, for solving the resulting finite difference equations. This method replaced the traditional uncoupled method and can provide a fully coupled solution within each time increment, reflecting the physically strong coupling between hydrodynamic and graded sediment transport components. This method can suppress computer errors and divergence of the numerical solution.

There are four main empirical sediment relationships to which the numerical results are sensitive. Without an adequate description of these relationships there is no guarantee of obtaining sensible numerical results.

The resistance factor, such as Chezy or Manning's coefficient, is a very important parameter. Most sediment transport formulae are linked with hydraulic resistance directly or indirectly. Any inaccuracy in estimating resistance will affect not only the hydrodynamic component but also the evaluation of the fractional transport capacity. There are a number of factors which influence resistance factor such as grain roughness, skin roughness, pools and riffles, vegetation and river bends. It is difficult to obtain a general form for resistance factor. It is suggested that for sand the skin roughness should be taken into account, but for gravel the skin roughness can be neglected compared with the grain roughness. However, it is strongly advised that the resistance factor should be calibrated before it is used in the model for predictive purposes.

Interaction of size fractions is still not fully understood although there are currently a number of laboratory investigations being carried out to deal with it. The most acceptable method for use in a computer model is to employ a hiding function, which is related solely to grain size distribution, and can evaluate the threshold condition for each size fraction in the graded sediment.

The choice of sediment transport formulae is always difficult. There exists a number of formulae in the literature. A good selection really needs a good background of sediment transport knowledge, because different formulae have different degrees of accuracy in different circumstance and it is often difficult to judge which is best in a given situation. In addition, as most of the formulae were developed based on single-sized material, in which only total transport capacity can be predicted, the situation is even more complicated in graded sediment transport.

The thickness of the active layer is another important factor which affects the bed material sorting process. A number of suggestions have been proposed some of

which are related to a representative particle diameter. This parameter needs to be carefully defined because it is critical for sorting especially during armouring. Numerical instability may be caused if it is too small.

## 1.6 Layout of The Thesis

The thesis contains nine chapters the contents of which are summarised below.

**Chapter 1** - Introduction and general statement of research aims.

**Chapter 2** - This presents the governing equations solved in the numerical model. In addition, all semi-empirical relationships employed in the model are stated, together with some discussion of their limitations.

**Chapter 3** - Here two alternative hiding functions for use with van Rijn's sediment transport equations are developed and evaluated. The fundamental difference between the two formulations is discussed.

**Chapter 4** - The algorithmic structure of the numerical model is presented, including the fully coupled solution of the governing equations using the Preissmann scheme with Newton-Raphson iteration. Aspects of numerical stability and accuracy are discussed.

**Chapter 5** - Here the results of some standard numerical tests of model performance are presented. In particular the behaviour of the two point scheme for simulating suspended load sediment transport is evaluated.

**Chapter 6** - In this chapter the model is used to simulate steady flow bed armouring experiments conducted at the University of Aberdeen. The alternative formulations of the hiding functions developed in chapter 3 are evaluated.

**Chapter 7** - In this chapter the model is used to simulate graded sediment transport during unsteady flows, using data obtained from Goodwin Creek in the USA. The performance of the numerical model and hiding function is compared with results obtained using the equal mobility assumption and Parker's bed load equation, Parker (1990).

**Chapter 8** - To illustrate the models applicability to large rivers (on a UK scale) the model is used to predict the return to regime conditions of the River Clyde following the cessation of dredging. The effect of a proposed tidal weir on the regime bed profile is also predicted.

**Chapter 9** - Conclusions and recommendations for future work are presented.

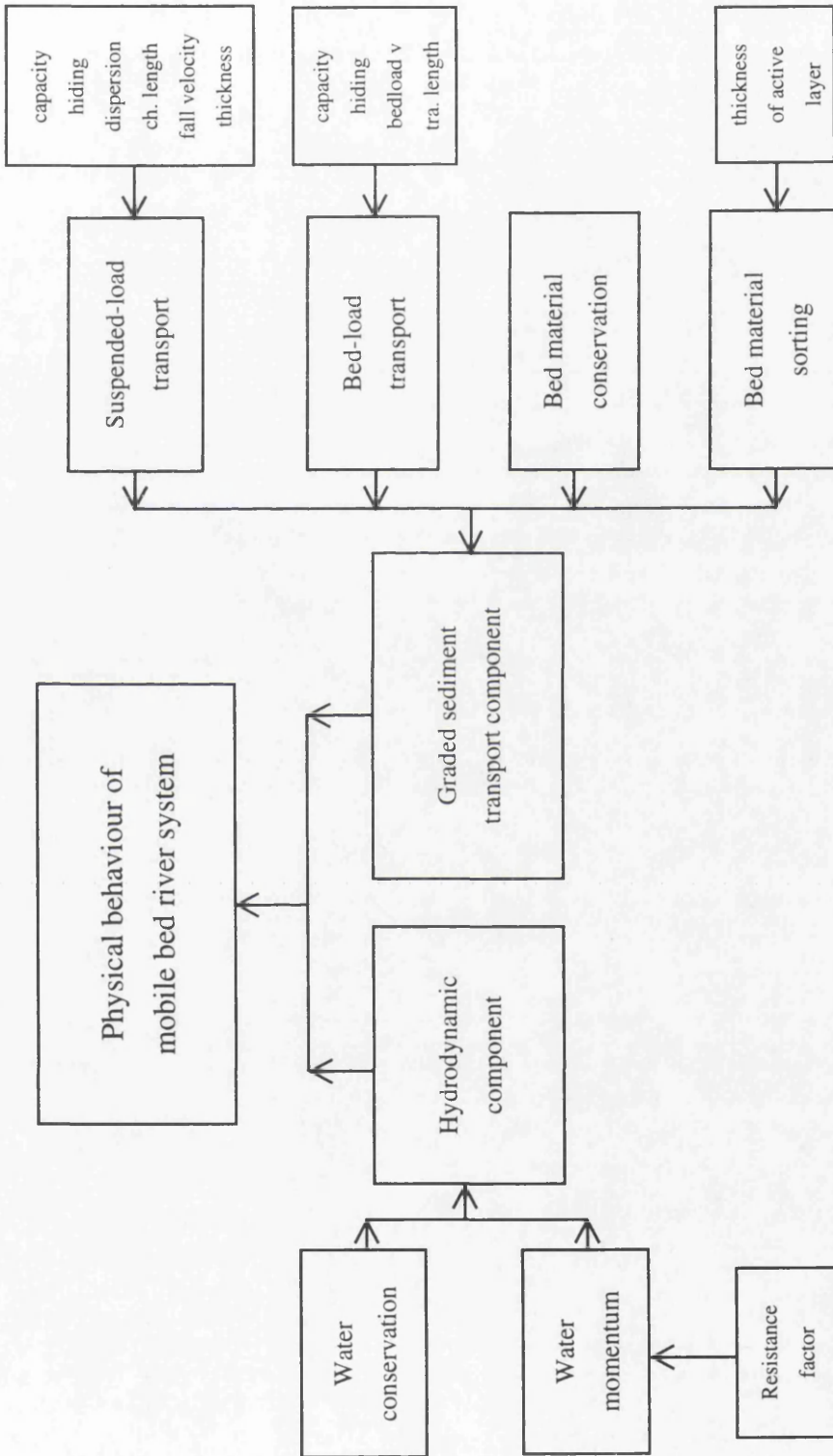


Figure 1.1 Physical Processes of Mobile Bed River System

## CHAPTER 2

### Theory of Non-equilibrium Graded Sediment Transport

#### 2.1 Introduction

A river flowing through mobile bed transports not only water but also sediment. When water flow increases the sediment transport rate will increase and as a result erosion may take place. Deposition is likely as discharge decreases. Erosion or deposition will cause changes in the bed elevation, channel geometry and composition of the bed material. Flow characteristics are affected significantly by these changes. Therefore the simulation of the behaviour of an mobile bed river system must include the processes describing both hydrodynamic and mobile bed behaviour.

An mobile bed river system can be subdivided into three components; hydrodynamics, sediment transport and boundary behaviour. Each of these components has a strong influence on the other two. For a modelling system to be predictive the physics of each of these components must be adequately simulated and their interdependence represented in the model formulation.

The hydrodynamic component simulates the transport of water and is characterised by the dependent variables of flow 'Q' and water surface elevation 'Y'. In a fixed bed river hydraulics the unsteady water flow is commonly simulated using the St. Venant equations. However, in mobile bed river hydraulics the simulation is complicated by the need to link the hydrodynamic behaviour to changing bed geometry and resistance.

## 2.2 Framework of Sediment Transport of Non-Uniform Material

Six equations are necessary to adequately model unsteady, non-equilibrium, graded sediment transport. These are

- i. Water continuity;
- ii. Water momentum;
- iii. Suspended-load transport;
- iv. Bedload transport;
- v. Bed material conservation;
- vi. Bed material sorting;

### 2.2.1 Hydrodynamic Equations

The one-dimensional form of the shallow wave equations is developed following the standard St. Venant hypothesis of;

- i. a hydrostatic pressure distribution with water depth;
- ii. the uniform distribution of pressure on the free water surface;
- iii. cross-sectional averaged variables;
- iv. the influence of alterations in the plan of a river is ignored;

In addition it is assumed that;

- i. the concentration of sediment material in the water body is small enough (less than 10%). The change in water density caused by concentration variations is not significant;
- ii. the graded sediment transport in this model is ranging from sand to gravel. Therefore the cohesiveness of sediment is not important;
- iii. the characteristic particle size is generally small compared with the water depth;

The resulting equations for fixed bed models are presented extensively in the literature, see for example Abbott (1979), Cunge et al (1980) and Pender (1992). They are

$$\frac{\partial A}{\partial t} + \frac{\partial Q}{\partial x} = q \tag{2.1}$$

$$\frac{\partial Q}{\partial t} + \frac{\partial(\beta Q^2/A)}{\partial x} + gA \frac{\partial Y}{\partial x} + gA \frac{Q|Q|}{K^2} = 0 \tag{2.2}$$

in which  $g$  = the gravitational acceleration;  $A$  = the cross sectional area;  $Q$  = the discharge;  $Y$  = the water surface level;  $K$  = the cross sectional conveyance;  $q$  = the lateral inflow or outflow;  $\beta$  = the momentum coefficient.

For mobile bed models the momentum equation remains unchanged, however the water continuity equation requires to be modified to include changes in cross-sectional area arising from erosion and deposition, see Figure 2.1.

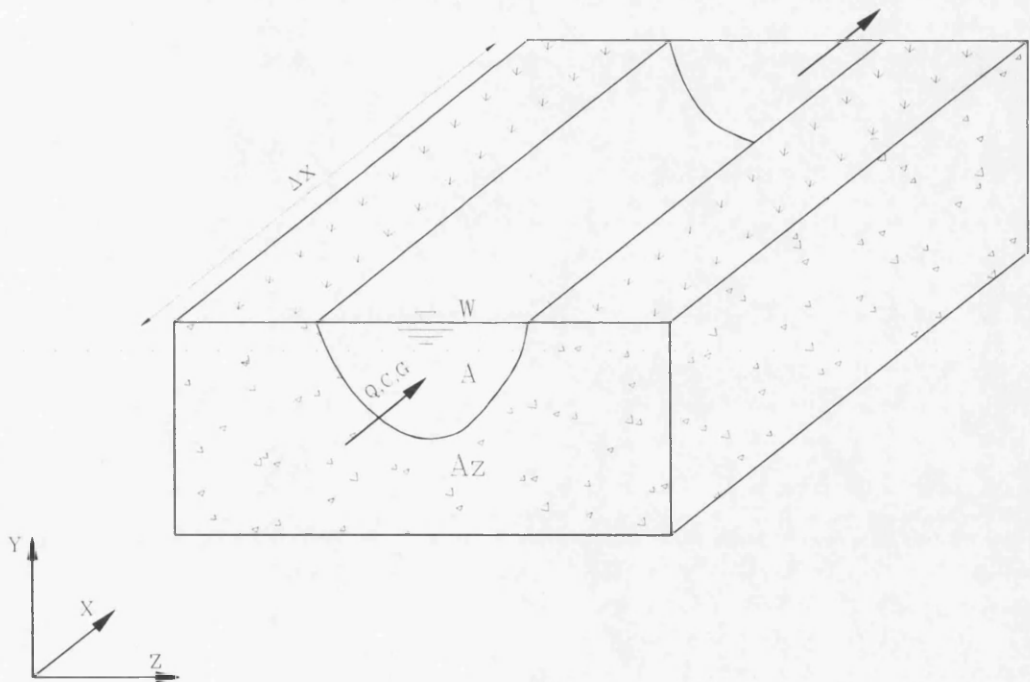


**Figure 2.1 Water and Sediment Transport In An Mobile Bed River**

The top width of the cross section is defined as

$$B = \frac{\partial(A + Az)}{\partial Y} \tag{2.3}$$

This enables first term in (2.1) to be rewritten as

$$\begin{aligned}
 \frac{\partial A}{\partial t} &= \frac{\partial(A + Az)}{\partial t} - \frac{\partial Az}{\partial t} \\
 &= \frac{\partial(A + Az)}{\partial Y} \frac{\partial Y}{\partial t} - \frac{\partial Az}{\partial t} \\
 &= B \frac{\partial Y}{\partial t} - \frac{\partial Az}{\partial t}
 \end{aligned} \tag{2.4}$$

Substitution of (2.4) into (2.1) results in the equation of water continuity.

$$B \frac{\partial Y}{\partial t} + \frac{\partial Q}{\partial x} - \frac{\partial Az}{\partial t} = q \tag{2.5}$$

### 2.2.2 Mechanisms of Sediment Transport

When the shear stress applied on the mobile bed material exceeds the threshold condition of motion, the bed material moves downstream. The transport of material is normally subdivided into suspended-load and bedload according to the different transport processes controlling the movement. To aid with conceptualisation it is necessary to identify four different layers, as shown in Figure 2.2. It is assumed that the transport processes acting in each layer are different, although it must be remembered that sediment is moving continuously between layers.

In the water stream, sediments are conveyed in suspension. The longitudinal motion of the sediment prevails over the threshold condition, so that the average travel length of the suspended grains is large compared with the water depth. In this layer the sediment is maintained in suspension by bed generated turbulence. According to Celik and Rodi (1988) this requires the vertical turbulent component  $v^* = \sqrt{(v'^2)}$  to be equal to or greater than the particle fall velocity. The movement of suspended-load in water stream is caused by either dispersion through turbulent mixing or diffusion through the random molecular motion of the fluid. Since the suspension is transported at approximately the velocity of flow, particle movement is similar to the advection and dispersion process.

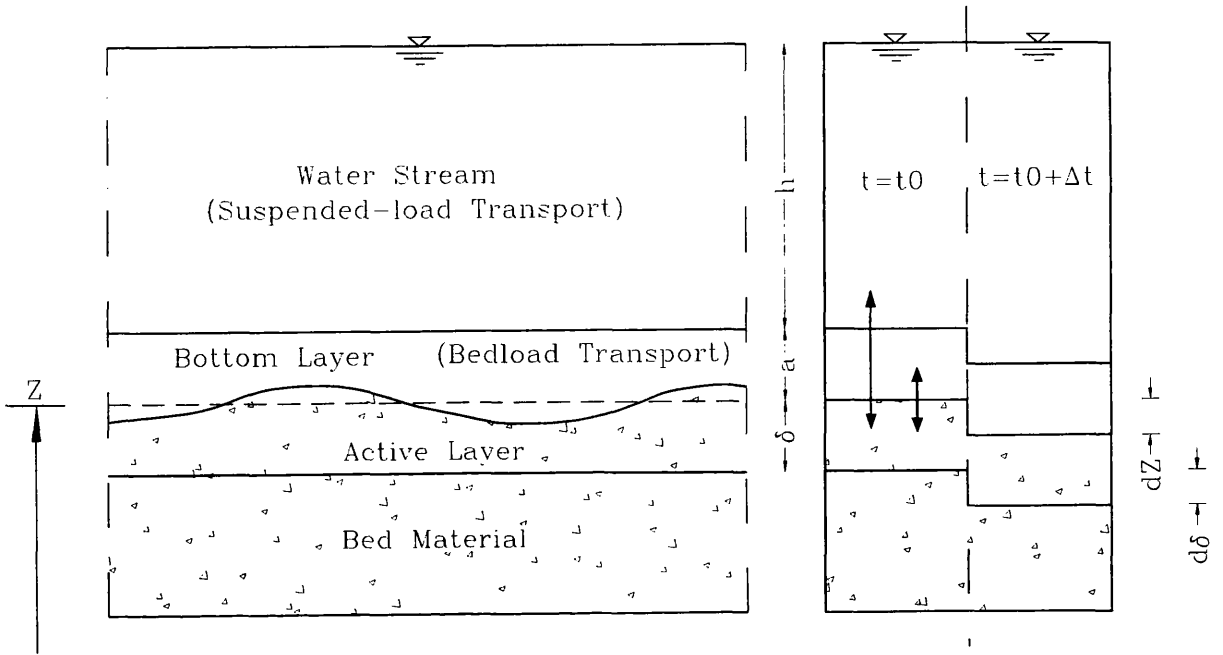


Figure 2.2 Conceptualisation of Sediment Transport Layers

### 2.2.2.1 Suspended-load transport

The continuity hypothesis for suspended-load can be combined from Fick's law to give

$$\frac{\partial c}{\partial t} + \bar{V} \cdot \nabla c = \nabla(D \nabla c) \tag{2.6}$$

In turbulent flow  $c = \bar{c} + c'$  and  $u = \bar{u} + u'$ , etc. Thus, using the analogy to molecular motion and substituting for  $c$  and  $u$ , (2.6) can be written for turbulent flow as

$$\frac{\partial \bar{c}}{\partial t} + u_i \frac{\partial \bar{c}}{\partial x_i} = - \frac{\partial}{\partial x_i} (\overline{c' u_i}) + D \frac{\partial^2 \bar{c}}{\partial x_i \partial x_i} \tag{2.7}$$

by the diffusion analogy

$$\overline{c' u_i} = -D_{ij} \frac{\partial \bar{c}}{\partial x_j} \tag{2.8}$$

which on substitution and addition of the gravitational fall velocity term leads to

$$\frac{\partial \bar{c}}{\partial t} + u_i \frac{\partial \bar{c}}{\partial x_i} = \frac{\partial}{\partial x_i} \left[ D_{ij} \frac{\partial \bar{c}}{\partial x_j} + D_m \frac{\partial \bar{c}}{\partial x_i} \right] + \frac{\partial}{\partial x_i} (\omega_s \bar{c}) \quad (2.9)$$

where  $D_m$  = the molecular diffusion;  $D_{ij}$  = the turbulent diffusivity tensor or the eddy diffusivity tensor;  $\omega_s$  = the fall velocity. Generally,  $D_{ij}$  is much larger than  $D_m$  so that  $D_m$  can be neglected. If the turbulence is homogeneous,  $D_{ij}$  reduces to  $D_{ii}$  and if the turbulence is isotropic,  $D_{ij}$  reduces to a scalar  $D_t$ . In rivers where flow is predominantly aligned to the river bank, an equation of one dimensional advection and dispersion for suspended-load may be obtained from (2.9) as

$$\frac{\partial CA}{\partial t} + \frac{\partial CQ}{\partial x} = \frac{\partial}{\partial x} \left( AD \frac{\partial C}{\partial x} \right) + \Phi_s \quad (2.10)$$

where  $C = \frac{1}{A} \iint_A \bar{c} dA$  = the average concentration of cross section;  $D$  = the dispersion coefficient;  $\Phi_s$  = the source term reflecting the exchange of particles between the water stream and the active layer. Implicit in (2.10) is the assumption that the grains in suspension are advected in the direction of the water velocity. To apply this equation to graded sediment it is necessary to employ a suspended-load transport equation for each size fraction. This can be written as

$$\frac{\partial C_j A}{\partial t} + \frac{\partial C_j Q}{\partial x} = \frac{\partial}{\partial x} \left( A D_j \frac{\partial C_j}{\partial x} \right) + \Phi_{s,j} \quad (2.11)$$

in which  $C_j$  = the average volume concentration of the  $j$ -th size fraction of suspended-load;  $D_j$  = the dispersion coefficient of the  $j$ -th size fraction;  $\Phi_{s,j}$  = the source term reflecting the net flux of  $j$ -th size fraction of suspended-load from the active layer to the water stream.

The difference between the transport capacity and the transport rate of suspended-load has been defined as the residual transport capacity of suspended-load. The exchange rate of particles is assumed to be directly proportional to the residual

transport capacity, see Armanini and Silvio (1988), Rahuel et al (1989) and Holly and Rahuel (1990). This may be described mathematically as

$$\Phi_{s,j} = \frac{Q}{L_j^*} (\beta_j C_j^* - C_j) \quad (2.12)$$

where  $C_j^*$  = the transport capacity of  $j$ -th size fraction of suspended-load;  $\beta_j$  = the fractional proportion of size fraction  $j$  in the active layer;  $L_j^*$  = the characteristic length of  $j$ -th size fraction for suspended-load. Characteristic length is the distance required for particles of  $j$ -th size fraction to achieve the equilibrium transport rate. Substitution of (2.12) into (2.11) gives

$$\frac{\partial C_j A}{\partial t} + \frac{\partial C_j Q}{\partial x} = \frac{\partial}{\partial x} \left( A D_j \frac{\partial C_j}{\partial x} \right) + \frac{Q}{L_j^*} (\beta_j C_j^* - C_j) \quad (2.13)$$

### 2.2.2.2 Bedload transport

In the bottom layer, the conservation equation for  $j$ -th size fraction of bedload can be described as an advective process by

$$\frac{\partial G_j}{\partial t} + u_{bj} \frac{\partial G_j}{\partial x} = u_{bj} \Phi_{b,j} \quad (2.14)$$

where  $G_j$  = the bedload transport rate of  $j$ -th size fraction;  $u_{bj}$  = the average velocity of bed load belonging to  $j$ -th size fraction;  $\Phi_{b,j}$  = the source term reflecting the exchange of  $j$ -th size fraction between the bottom layer and the active layer. The source term  $\Phi_{b,j}$  can be evaluated using the concept of residual transport capacity of bedload. Assuming the exchange rate of particles between bedload and bed material to be directly proportional to the residual transport capacity for that size fraction,  $\Phi_{b,j}$  can be estimated from, see Bell and Sutherland (1983)

$$\Phi_{b,j} = \frac{1}{\lambda_j} (\beta_j G_j^* - G_j) \quad (2.15)$$

in which  $\lambda_j$  = the travel length for j-th size fraction of bedload which is the distance required for bedload transport to reach the equilibrium condition;  $G_j^*$  = the bedload transport capacity of j-th size fraction. Substitution of (2.15) into (2.14) yields

$$\frac{\partial G_j}{\partial t} + u_{bj} \frac{\partial G_j}{\partial x} = \frac{u_{bj}}{\lambda_j} (\beta_j G_j^* - G_j) \quad (2.16)$$

### 2.2.2.3 Bed Material Conservation

The conservation of bed material can be expressed as

$$(1-p) \frac{\partial Az}{\partial t} + \sum \Phi_{s,j} + \sum \Phi_{b,j} = 0 \quad (2.17)$$

where  $p$  = the porosity of bed material. Substitution of (2.12) and (2.15) into (2.17) results in

$$(1-p) \frac{\partial Az}{\partial t} + \sum \frac{Q}{L_j^*} (\beta_j C_j^* - C_j) + \sum \frac{1}{\lambda_j} (\beta_j G_j^* - G_j) = 0 \quad (2.18)$$

### 2.2.2.4 Bed Material Sorting

The process of exchange of grains between the water stream, active layer and bottom layer causes the changes of river geometry by erosion or deposition. As the transport rate differs for each size fraction, the composition of the bed material in the active layer also changes due to selective transport. In the active layer, the conservation law for j-th size fraction results in an equation of bed material sorting as

$$(1-p) \frac{\partial}{\partial t} (Am\beta_j) + (1-p)\beta_j \Phi_0 u[\Phi_0] + (1-p)\beta_{0j} \Phi_0 u[-\Phi_0] + \Phi_{s,j} + \Phi_{b,j} = 0 \quad (2.19)$$

where  $u[\Phi_0]$  = the unit function as

$$u[\Phi_0] = \begin{cases} 1 & \Phi_0 \geq 0 \\ 0 & \Phi_0 < 0 \end{cases} \quad (2.20)$$

$A_m$  = the cross sectional area of active layer;  $\beta_j$  = the fractional proportion of size fraction  $j$  in the active layer;  $\beta_{0j}$  = the fractional proportion of size fraction  $j$  in the subsurface layer which is underlying the active layer.  $\Phi_0$  is written as

$$\Phi_0 = \frac{\partial A_z}{\partial t} - \frac{\partial A_m}{\partial t} \quad (2.21)$$

$\partial A_m / \partial t$  = the variation of area of active layer;  $\partial A_z / \partial t$  = the variation of area of bed material. A negative  $\Phi_0$  means that some of the material in the subsurface layer is entering the active layer due to downward displacement of the bed i.e. erosion. Conversely, a positive  $\Phi_0$  means an upward displacement of the bed, i.e. deposition. Noting the fact that  $\sum \beta_j = 1$  and  $\sum \beta_{0j} = 1$ , and summing (2.19) for all size fractions yields (2.17). Substitution of (2.12), (2.15) and (2.21) into (2.19) yields the material sorting equation

$$\begin{aligned} & (1-p) \frac{\partial}{\partial t} (A_m \beta_j) + (1-p) \beta_j \left( \frac{\partial A_z}{\partial t} - \frac{\partial A_m}{\partial t} \right) u \left[ \frac{\partial A_z}{\partial t} - \frac{\partial A_m}{\partial t} \right] + \\ & (1-p) \beta_{0j} \left( \frac{\partial A_z}{\partial t} - \frac{\partial A_m}{\partial t} \right) u \left[ -\frac{\partial A_z}{\partial t} + \frac{\partial A_m}{\partial t} \right] + \\ & \frac{Q}{L_j^*} (\beta_j C_j^* - C_j) + \frac{1}{\lambda_j} (\beta_j G_j^* - G_j) = 0 \end{aligned} \quad (2.22)$$

## 2.3 Empirical Sediment Relationships

### 2.3.1 Hydraulic Resistance

Hydraulic resistance concerns the prediction of resistance to water flow along the river channel. Several classical formulae of hydraulic resistance exist all of which account for the resistance process with a single coefficient to quantify bed roughness such as Manning's, Chezy and Darcy-Weisbach coefficients. These coefficients are related by

$$\sqrt{\frac{8}{f}} = \frac{R^{1/6}}{n\sqrt{g}} = \frac{C}{\sqrt{g}} \quad (2.23)$$

where  $g$  = the acceleration due to gravity;  $f$  = the Darcy-Weisbach coefficient;  $C$  = the Chezy coefficient;  $n$  = the Manning's coefficient;  $R$  = the hydraulic radius. Although these coefficients can be evaluated for uniform flow situations they are commonly employed to evaluate the friction gradient  $S_f$  in unsteady fixed bed models. If, for example, we replace  $S_0$  by  $S_f$  in Manning's equation it can be rearranged to obtain

$$S_f = \frac{Q|Q|}{K^2} \quad (2.24)$$

where  $K$  = the conveyance which can be evaluated from

$$K = \frac{AR^{2/3}}{n} \quad (2.25)$$

For fixed bed models Manning's  $n$  is then estimated to give a satisfactory comparison between observed and computed results. Here Manning's  $n$  is no longer related solely to bed roughness, but also includes the effect of other energy losses such as plan geometry, pool-riffle sequence, secondary current etc.

Such a simplistic formulation is not suitable for mobile bed models where bed geometry, forms and composition are changing with time. The most common method to improve the formulation is to split bed friction into two components. The first, grain roughness can be quantified using a representative grain diameter. The second, skin roughness accounts for the influence of bed forms such as ripples and dunes. Employing this concept enables the total flow resistance to be evaluated by a combination of grain and skin roughness.

For gravel-bed rivers where the mean diameter of bed material is larger than 2 mm it has been found that the flow resistance can be determined by a representative grain size such as  $D_{50}$ ,  $D_{65}$ ,  $D_{84}$  or  $D_{90}$ . The dominant factor to the flow resistance is the grain size and the composition of bed material. Most equations use only one characteristic size taken from the bed material. For example, the Strickler equation for estimating Manning's  $n$  as reported by Chow (1959) is

$$n = 0.041D_{50}^{1/6} \quad (2.26)$$

and Henderson (1966) is

$$n = 0.038D_{90}^{1/6} \quad (2.27)$$

Limerinos (1970) analysed the gravel-bed river data from California and related Manning's  $n$  to the  $D_{84}$  and hydraulic radius  $R$ . His equation is written as

$$n = \frac{0.113R^{1/6}}{1.16 + 2.00 \log(R/D_{84})} \quad (2.28)$$

The comparisons of the performance for different equations carried out by Bray (1982) indicated that of the available formulae, Limerinos's equation performs best over a range of flows and bed compositions. Limerinos's equation has therefore been employed in the current computer model.

For sand bed rivers where the mean diameter of bed material is less than 2 mm the total resistance consists of grain roughness and skin roughness. The skin roughness is much greater than that of a flat bed and the corresponding friction factor is also much larger. The predicting methods for the roughness of an mobile bed stream divide the total stress  $\tau$  or friction factor ( $C$  or  $f$ ) into grain roughness denoted by  $\tau'$  or  $C'$ ,  $f'$  and skin roughness  $\tau''$  or  $C''$ ,  $f''$ . By definition, it gives

$$\tau = \tau' + \tau'' \quad (2.29)$$

$$\frac{1}{C^2} = \frac{1}{C'^2} + \frac{1}{C''^2} \quad (2.30)$$

$$f = f' + f'' \quad (2.31)$$

Einstein and Barbarossa (1952) suggested that total flow resistance could be evaluated by dividing the hydraulic radius into two parts each of which represents the contributions of grain and skin roughness respectively; where

$$R = R' + R'' \quad (2.32)$$

$$\frac{R'}{R''} = \frac{\tau'}{\tau''} = \frac{u^{*'}^2}{u^{*''2}} \tag{2.33}$$

where  $u^{*'}$  can be calculated by taking  $k_s = D_{65}$  in the Chezy formula

$$C' = 18 \log \left( \frac{12R'}{k_s} \right) \tag{2.34}$$

$$u^{*'} = \sqrt{g} \frac{u}{C'} \tag{2.35}$$

in (2.35)  $u$  = the mean cross sectional velocity. Another parameter  $\beta'_{35}$  is given by, see Einstein and Barbarossa (1952),

$$\beta'_{35} = \frac{\Delta g D_{35}}{(u^{*'})^2} \tag{2.36}$$

The relationship between  $\beta'_{35}$  and  $u/u^{*''}$  has been given empirically as shown in Figure 2.3 where  $u/u^{*''}$  may be found by trial and error. The combination of two contributions results in the prediction of total flow resistance.

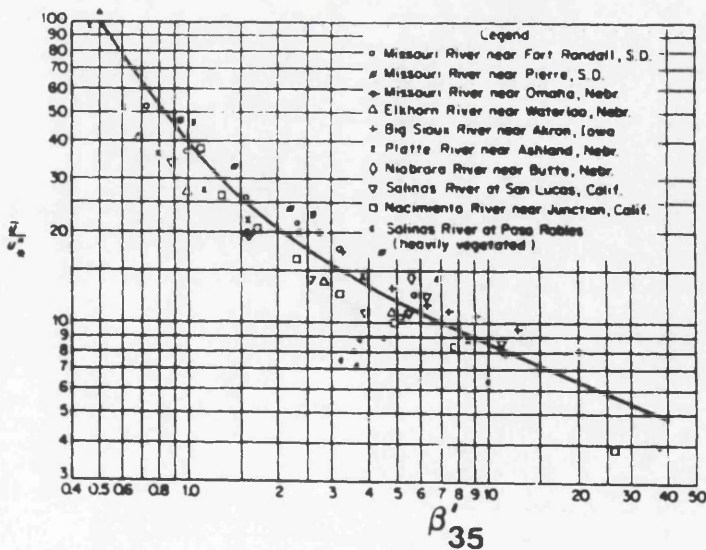


Figure 2.3 Flow Resistance Due To Bedforms (Einstein et al, 1952)

Following the same idea, Engelund and Hanson (1967) developed an equation to set up a relationship between grain and skin resistance by dividing the total water depth into two parts belonging to the contribution of grain and skin roughness separately. Two dimensionless parameters were introduced to reflect the total resistance and grain roughness respectively.

$$\psi = \frac{\tau}{\rho g \Delta D_{50}} \tag{2.37}$$

$$\psi' = \frac{\tau'}{\rho g \Delta D_{50}}$$

Engelund and Hanson concluded that  $\psi$  is a function of  $\psi'$  only, which is shown in Figure 2.4. This function can be formulated by statistical regression as

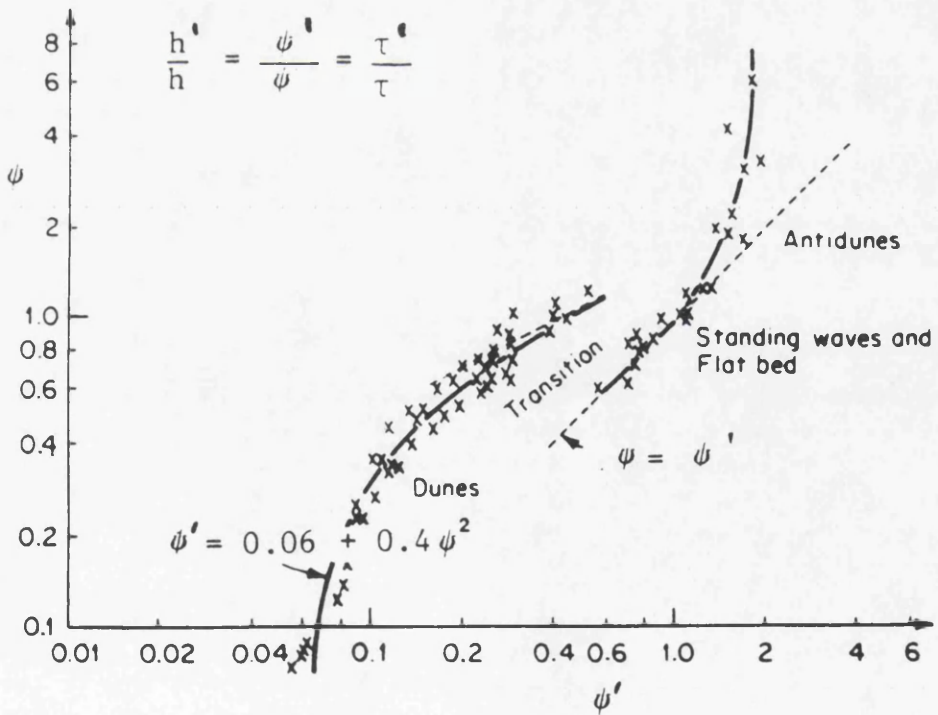


Figure 2.4 Flow Resistance From Grain Roughness and Bed Form Roughness (Engelund and Hanson, 1967)

$$\begin{aligned}
 \psi &= \psi'^{0.838} & \psi' < 0.064 \\
 \psi &= 2.5\sqrt{\psi' - 0.06} & 0.064 \leq \psi' \leq 0.6 \\
 \psi &= \psi' & \psi' > 0.6
 \end{aligned}
 \tag{2.38}$$

The following relationships were also adopted by Engelund and Hanson

$$\frac{u}{u^{*'}} = 5.75 \log \left( \frac{4.8h'}{D_{50}} \right)
 \tag{2.39}$$

$$\frac{h'}{h} = \frac{\psi'}{\psi}
 \tag{2.40}$$

The total resistance can therefore be evaluated by trial and error. Implicit in the Einstein and Barbarossa and the Engelund and Hanson methods is the assumption that the skin roughness depends on not only the grain size and the composition of bed material but also on the flow conditions. The reason is that the bedforms are strongly controlled by the flow. In an mobile bed river, the wake eddies from bedforms depends on the absolute size of the bedforms. Therefore, only if the bedforms and their eddies are small compared with the flow depth is the effect of variable eddy size on the overall flow resistance likely to be insignificant. Under these conditions, the effects of the slight variables such as the roughness size distribution and the shape may be subdued.

White, Paris and Bettess (1980) developed an empirical relationship between the following three parameters

$$\begin{aligned}
 F_{fg} &= \frac{u^*}{\sqrt{\Delta g D}} \\
 D_{gr} &= D \cdot \left( \frac{\Delta g}{v^2} \right)^{1/3} \\
 F_{gr} &= \frac{u^{*n}}{\sqrt{\Delta g D}} \left( \frac{u}{5.64 \log(10h/D)} \right)^{1-n}
 \end{aligned}
 \tag{2.41}$$

where the characteristic diameter is  $D_{35}$ . The relationship was given as shown in Figure 2.5, and described mathematically by equation (2.42)

$$\frac{F_{gr} - A}{F_{fg} - A} = 1.0 - 0.76 \left\{ 1.0 - e^{[-\log(D_{gr})]^{1.7}} \right\} \tag{2.42}$$

where the parameters  $n$  and  $A$  are functions of  $D_{gr}$ .

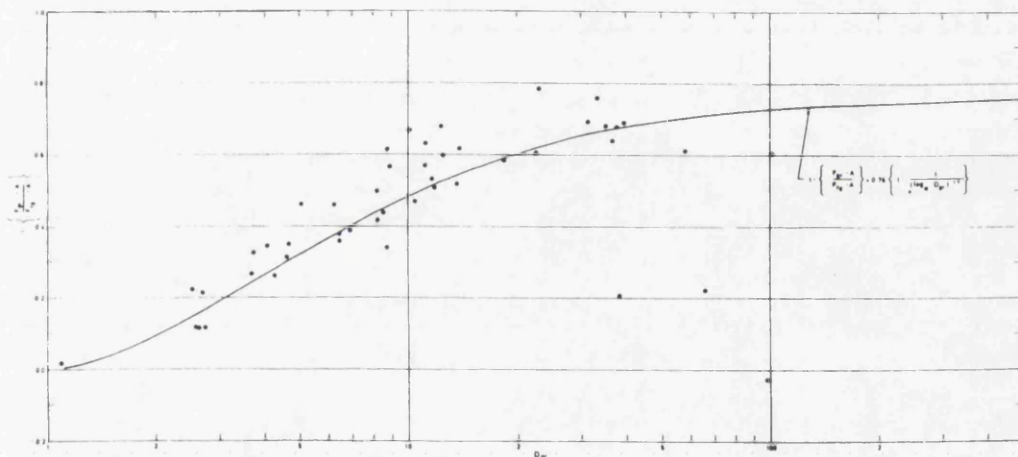


**Figure 2.5 Shear Relationship Based On  $D_{35}$  of The Parent Material (White, Paris and Bettess, 1980)**

Van Rijn (1984) has analysed a large number of data on bed form dimensions and roughness, mainly for dunes. He suggests that the total roughness is dependent on a representative size in bed material, dune height and dune length. The relationship was given as

$$k_s = 3D_{90} + 1.1Hr_d \left( 1 - e^{-25H/\lambda} \right) \tag{2.43}$$

where  $H$  = the dune height;  $\lambda$  = the dune length;  $r_d$  = a parameter related to the property of bed material.

The comparisons carried out by van Rijn have demonstrated that Engelund and Hanson (1967), White, Paris and Bettess (1980) and van Rijn (1984) methods all appear to give reasonable results for both river and flume data. Of the three methods, van Rijn's method (1984) applies only where dune bed forms exist. The technique of Engelund & Hanson and White et al cover the full range flow conditions of interests in this work. Of these the Engelund and Hanson method has proved popular with a larger number researchers. This method has therefore been adopted in this model.

### 2.3.2 Fractional Sediment Transport Capacity

Van Rijn (1984) made a comparison of the performance of the sediment transport formulae of van Rijn (1984), Ackers and White (1973) and Einstein (1942) with 840 set of flume data and 260 field experiments. If the percentage of all data with a ratio  $R$  of calculated to observed transport in the range  $1/2 < R < 2$  is taken, the following results are obtained

Van Rijn	77%
Ackers and White	68%
Einstein	46%

From these results there appears to be little to choose between the van Rijn and Ackers and White formulae, however the van Rijn formula has the additional advantage that suspended and bed load are calculated separately. The van Rijn formula was therefore adopted for use in the current model.

Van Rijn (1984) developed an analytical model for both bedload and suspended-load in terms of the saltation height, particle velocity and bedload concentration. The saltation height and particle velocity were calculated using a computer model which was calibrated against laboratory data. The suspended-load and bedload capacity can be evaluated from knowledge of the mean velocity, flow depth and particle size.

$$\frac{G_s^*}{ubh} = 0.012 \left( \frac{u - u_{cr}}{\sqrt{\Delta g D}} \right)^{2.4} \left( \frac{D}{h} \right) D_*^{-0.6} \quad (2.44)$$

$$\frac{G_b^*}{ubh} = 0.005 \left( \frac{u - u_{cr}}{\sqrt{\Delta g D}} \right)^{2.4} \left( \frac{D}{h} \right)^{1.2} \quad (2.45)$$

where  $G_s^*$ ,  $G_b^*$  = the suspended-load and bedload transport capacity respectively;  $u$  = the mean velocity of the cross section;  $b$  = the width of the channel;  $h$  = the flow depth;  $g$  = the acceleration due to gravity;  $D$  = the particle size;  $u_{cr}$  = the critical velocity at which particles begin to move;  $D_* = D \sqrt[3]{\frac{\Delta g}{\nu^2}}$  the dimensionless particle size in which  $\nu$  = the fluid viscosity.

Implicit in the van Rijn formulae is the assumption of a uniform material. However, the physics of graded sediment transport is more complex due to the interaction of size fractions. Parker et al (1982) suggests the concept of equal mobility to calculate the fractional transport capacity. There are two ideas in the equal mobility hypothesis. One is that all size fractions in a mixture move at the same threshold condition. Second is the equal entrainment hypothesis, which assumes that the transport capacity of any size fraction is directly proportional to its presence in the active layer. The equal mobility hypothesis can be written as

$$G_j^* = \beta_j f(\tau - \tau_c) \quad (2.46)$$

where  $G_j^*$  = the transport capacity of  $j$ -th class;  $\beta_j$  = the fractional part of  $j$ -th class in active layer;  $f$  = a function for calculating the transport capacity of a uniform material.

Holly and Rahuel (1990) concluded that the calculation of bedload capacity must be modified by  $(1-\lambda_j)$  to reflect the fact that some fraction  $\lambda_j$  of  $j$ -th class may not be transported as bedload, but rather as suspended-load. For example, Van Rijn (1984) suggests that  $\lambda_j = 1$  for  $u^*/\omega_j$  greater than about 10, and  $\lambda_j = 0$  for  $u^*/\omega_j$  less than 0.4, with  $\lambda_j$  varying monotonically but non-linearly between these two extremes. In other words, the term  $(1-\lambda_j)$  would suppress any bedload transport of  $j$ -th class whose diameter dictated that it moves partially or entirely as suspended-load. Therefore bedload transport capacity can be expressed as

$$G_{b,j}^* = (1 - \lambda_j) \beta_j f_b(\tau - \tau_c) \quad (2.47)$$

Kuhnle (1992) has examined the hypothesis of equal mobility with the bimodal bed material from Goodwin Creek and suggests that it breaks down for bimodal bed material and at low flow strengths, where observations indicated that not all of the bed material grains sizes were in motion. Deviations from equal mobility were also found from the laboratory flume experiments of Wilcock and Southard (1988). This demonstrates that in some instances the difference in composition between transported and bed material exists. In other words, the threshold condition for the initiation of individual size fractions in a mixture is different. The correct evaluation of threshold conditions is therefore vital to the calculation of the fractional transport capacity for graded sediment.

Since Einstein (1950) introduced the concept of hiding function, a number of hiding functions have been developed to modify the Shields value by taking account of size fraction interaction. For example, White and Day (1982) developed a hiding function which may be used in the Ackers and White formula. Proffitt and Sutherland (1983) used experimental data to modify the Paintal's transport formula. Most of these hiding functions are only related to size fraction availability. However, experimental tests and field investigation have demonstrated that hiding functions could be affected by a number of other factors such as bed material characteristics, flow parameters, bed geometry and turbulent pressure fluctuation near the bed surface.

The choice of van Rijn's formulae necessitates the development of a hiding function to enable the influence of size fraction interaction to be simulated for these formulae.

### **2.3.3 Characteristic Length For Suspended-load**

Sediment transport in a long uniform channel with steady uniform flow has a unique equilibrium transport rate which equals to the transport capacity. However during unsteady flow transport rates respond to the change of the flow condition with a temporal and spatial lag. This lag also can be observed if the incoming sediment

from upstream boundary differs from the equilibrium condition. For example, in Jobson and Sayre's (1970) experiment, reported by Celik and Rodi (1988), sediment was injected from an upstream source near the free surface at a rate larger than the transport capacity, so that a net deposition occurred until the excess suspended-load was removed, see Figure 2.6. In Ashida and Okabe's (1982) experiment, shown in Figure 2.6, also reported by Celik and Rodi (1988), initially clear water flowed over a fixed bed with a sand source and picked up sediment until the full transport capacity was reached.

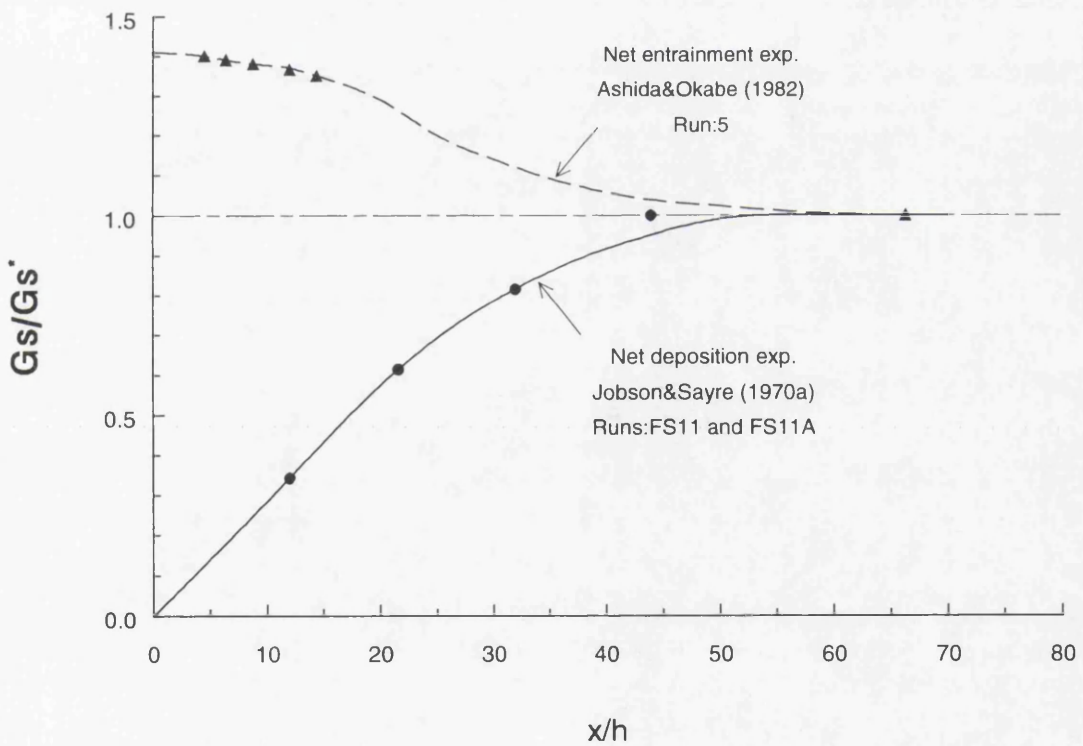


**Figure 2.6 Measured Variations of Suspended-load with Net Deposition and Net Entrainment (from Celik and Rodi, 1988)**

It can be seen from Figure 2.6 that suspended-load transport rate reaches its transport capacity asymptotically in each of these cases. Therefore, with non-equilibrium transport a spatial delay process occurs which must be described by

introducing a parameter called the characteristic length,  $L^*$ , for suspended-load. Celik and Rodi (1988) concluded that the characteristic length is a function of the ratio of the settling velocity to the bed shear velocity for initially clear water flowing over a loose sediment bed.

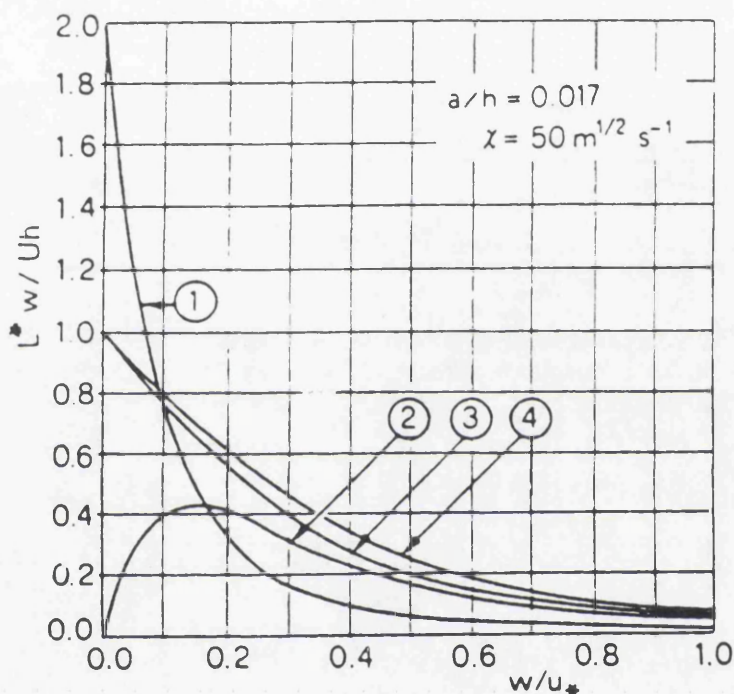


**Figure 2.7 Characteristic Length of Particles Transported in Suspension, Following Different Integration Procedures (from Armanini and Silvio, 1988)**

Armanini and Silvio (1988) obtained an expression of characteristic length for suspended-load from the vertical concentration profile, see Figure 2.7. Here, the dimensionless parameter  $(L^* \omega / uh)$  is given as a function of  $(\omega / u_*)$ . Another expression for  $L^*$ , derived by Galappatti and Vreugdenhil (1985), is shown in curve 2 of Figure 2.7. This was obtained from an approximate analytical integration of the two-dimensional equation describing a concentration boundary condition. Curve 3 in Figure 2.7 has been obtained from the same integration, except that a gradient

boundary condition has been used. A sensitivity analysis of the approximate solution has been made by Armanini and Silvio (1988). This resulted in an expression for the characteristic length shown in curve 4 of Figure 2.7, which can be described mathematically as

$$\frac{L^* \omega}{uh} = \frac{a}{h} + \left(1 - \frac{a}{h}\right) e^{[-1.5(a/h)^{-1/6} \omega/u_*]} \quad (2.48)$$

where  $a$  = the thickness of bottom layer;  $\omega$  = the particle fall velocity;  $u$  = the mean velocity;  $h$  = the water depth;  $u_*$  = the shear velocity. This expression has been adopted in the present model with the modification that  $\omega$  is replaced by  $\omega_j$ , the fall velocity for each size fraction, to give

$$\frac{L_j^* \omega_j}{uh} = \frac{a}{h} + \left(1 - \frac{a}{h}\right) e^{[-1.5(a/h)^{-1/6} \omega_j/u_*]} \quad (2.49)$$

#### 2.3.4 Travel Length of Bedload

Conditions in most mobile bed channels are generally unsteady in either water flow or sediment transport or both. Channels which are in equilibrium over a long period of time may be subject to significant deviations or transients over much shorter time intervals. Transients in mobile bed channels are commonly caused by unsteady flow conditions but they can also occur under steady flow conditions when the upstream sediment transport supply is changed. An increase in the upstream supply will result in deposition and a decrease will lead to erosion of the bed. In other words, a non-equilibrium state exists even under steady flows when the transport rate changes with time so that there is no balance between input and output of sediment.

The spatial delay effect has been found not only in suspended-load transport but also in bedload transport. For example, Bell and Sutherland (1983) examined the response of a gravel bed reach to imposed steady flows under non-equilibrium conditions, where bedload inflow is zero. The difference between actual bedload transport rate and bedload transport capacity was observed in the experimental tests.

The results are shown in Figure 2.8. They concluded that this spatial variation of the transport rate deficit exists because the flow requires a finite length of bed to erode sufficient bed material to satisfy its equilibrium transport capacity. Soni et al (1980) compared local transport rates, derived from bed surface profiles, with equilibrium capacity rates for the case of bed aggradation under steady non uniform flow conditions. They found, in general, that the local transport rate was smaller than the equilibrium rate for any given mean flow velocity. They also presented results of the temporal and spatial delay of the non-equilibrium transport rates.

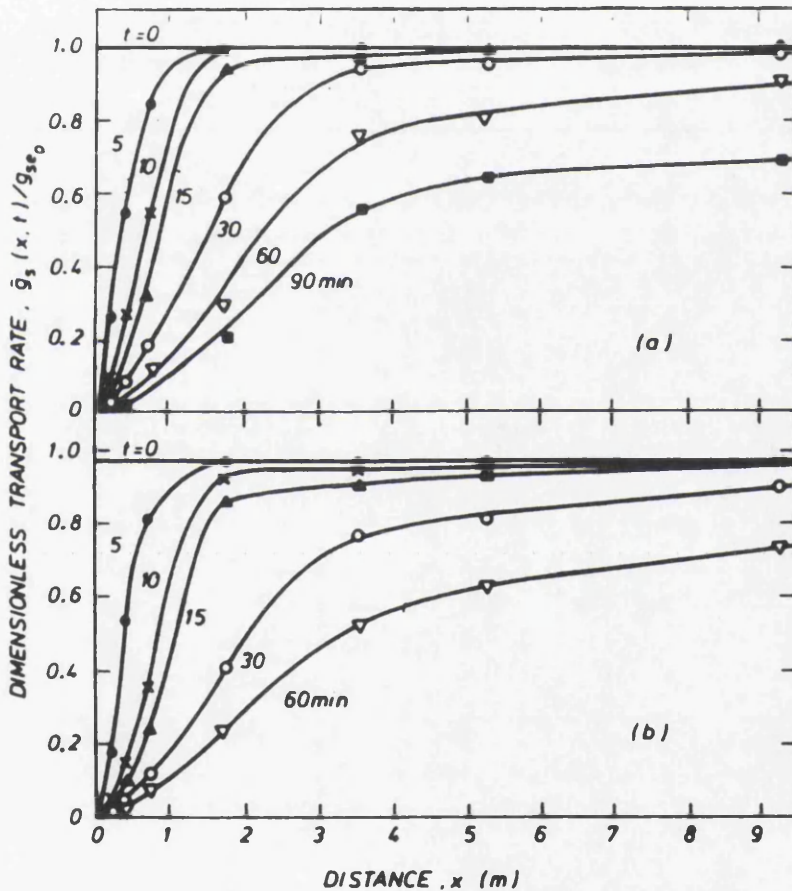


Figure 2.8 Spatial Lag of Bedload in Approaching Equilibrium Condition (From Bell and Sutherland, 1983)

The parameter reflecting the non-equilibrium transport of bedload is referred to as the travel length. Attempts to quantify the travel length have been made by Bell & Sutherland (1983) and Phillips & Sutherland (1985). Here it is assumed that the travel length is equal to the characteristic length.

### 2.3.5 Fall Velocity

Fall velocity of sediment has been studied extensively and defined as a function of size, shape, density and fluid viscosity. In addition, it depends on the extent of fluid in which it falls, on the number of falling particles and on the turbulent intensity.

The basic concept is based on the force balance between gravity and flow resistance.

$$\frac{\pi}{6} D^3 (\rho_s - \rho) g = C_D \frac{1}{2} \rho \omega^2 \frac{\pi}{4} D^2 \quad (2.50)$$

where  $C_D$  = the drag coefficient which depends on grain Reynolds number  $Re = \omega D / \nu$  and the shape of particle;  $\omega$  = the fall velocity;  $\rho_s$  = the density of particle;  $\rho$  = the density of water;  $D$  = the particle diameter. From (2.50), it yields

$$\omega = \sqrt{\frac{4}{3} \frac{gD}{C_D} \Delta} \quad (2.51)$$

where  $\Delta = (\rho_s - \rho) / \rho$ . For spherical particles of diameter  $D$  in a viscous fluid of infinite extent the drag coefficient is fairly well defined for laminar flow. The Stokes solution can only be applied for  $Re$  less than unity.

$$C_D = \frac{24}{Re} \quad (2.52)$$

Substitution of (2.52) into (2.51) yields that in a clear still fluid, the particle fall velocity of a solitary particle can be described by

$$\omega_j = \frac{1}{18} \left( \frac{\Delta g D_j^2}{\nu} \right) \quad (2.53)$$

for  $D < 0.1$  mm (Stokes range)

For higher Reynolds numbers the theoretical treatments have as yet not succeeded in accurately predicting the value of the drag coefficient (Raudkivi, 1991). The difficulties arise mainly from the interaction of the turbulence with the particle. The value of drag coefficient depends strongly on the level of free stream turbulence,

apart from the turbulence caused by the particle itself. The impact of the surface of the particle is also important.

For a sand particle diameter in the range 0.1-1.0 mm, the following type of equation was suggested by van Rijn (1984) as

$$\omega_j = 10 \frac{v}{D_j} \left\{ \sqrt{1 + \frac{0.01 \Delta g D_j^3}{v^2}} - 1 \right\} \quad (2.54)$$

For particles larger than 1.0 mm, the following equation may be used (Van Rijn, 1984)

$$\omega_j = 1.1 \sqrt{\Delta g D_j} \quad (2.55)$$

where  $D_j$  = the particle diameter of j-th class.

It has been found that the presence of a larger number of other particles will decrease the fall velocity, see Yalin (1977). To convert these fall velocities to a river situation with many particles in suspension a correction taking account of concentration should be employed.

$$\omega = \omega_0 (1 - C)^\alpha \quad (2.56)$$

where  $\omega$  = the fall velocity of a particle in a suspension with concentration by volume  $C$ .  $\alpha$  = a function of grain Reynolds number given as

$$\begin{aligned} \alpha &= 4.65 & \text{Re} < 0.2 \\ \alpha &= 4.35 \text{Re}^{-0.03} & 0.2 < \text{Re} < 1 \\ \alpha &= 4.45 \text{Re}^{-0.1} & 1 < \text{Re} < 200 \\ \alpha &= 2.39 & \text{Re} > 500 \end{aligned} \quad (2.57)$$

The drag coefficient is slightly dependent on particle shape but this is normally neglected.

### 2.3.6 Mean Velocity of Bedload

Bagnold (1973) assumed that for steady continuous saltation, the mean velocity causes a mean fluid drag on the particle which is in equilibrium with the mean bed frictional force. The relationship of Bagnold can be represented by the following general expression

$$\frac{u_b}{u_*} = \alpha_1 - \alpha_2 \sqrt{\frac{\theta_{cr}}{\theta}} \quad (2.58)$$

in which  $u_b$  = the mean velocity of bedload;  $\theta = u_*^2 / \Delta g D$  = the particle mobility parameter;  $\theta_{cr}$  = the critical mobility parameter from Shields value;  $\alpha_1, \alpha_2$  = coefficients.

As the saltation height is a function of the sediment size, the coefficients will also be a function of the sediment size. This led Bagnold to suggest the following relationship.

$$\frac{u_b}{u_*} = 9 + 2.6 \log(D_*) - 8 \sqrt{\frac{\theta_{cr}}{\theta}} \quad (2.59)$$

Alternatively, following expression was given by Van Rijn (1984)

$$\frac{u_b}{\sqrt{\Delta g D}} = 1.5 T^{0.6} \quad (2.60)$$

where  $T = \frac{(u_*')^2 - (u_{*,cr})^2}{(u_{*,cr})^2}$ ;  $u_*' = \frac{\sqrt{g} u}{C'}$  = the bed shear velocity related to grains;  $C'$  = the Chezy coefficient due to grain roughness;  $u_{*,cr}$  = the critical bed shear stress from the Shields curve.

The effect of interaction of size fractions on the bedload velocity may be taken into account using a suitable hiding function to adjust the critical shear stress.

Of these two expressions van Rijn's method is based on a statistical regression, whereas Bagnold's expression takes accounts of the physical influence of saltation height. In the Author's opinion it is desirable that, whenever possible, physical processes should be accounted for in numerical models, Bagnold method (2.59) has therefore been adopted.

### 2.3.7 Thickness of Bottom Layer

The bottom layer is defined as the height above the bed surface in which bedload transport takes place. Garcia and Parker (1991) summarised the choices of defining and calculating bottom layer thickness as

- a function of the flow depth, Itakura and Kishi (1980), Celik and Rodi (1988), Akiyama and Fukushima (1986) and Armanini and Silvio (1988);
- proportional to the sediment grain size, Einstein (1953), Engelund and Fresse (1976) and Willetts (1987);
- a function of the bed form height, Van Rijn (1984);
- the elevation of the top of the saltation layer, Smith and Mclean (1977);

Insufficient time was available to undertake a detailed numerical review of above options, for this reason, a flow depth function as demonstrated as adequate by Armanini and Silvio was adopted here.

### 2.3.8 Thickness of Active Layer

The concept of active layer differs for erosion and deposition. For erosion it can be defined as the depth of the bed from which erosion can take place. The active layer thickness is evaluated by an appropriate empirical conceptualisation of the depth of bed material which supplies material for bedload transport (Holly and Rahuel, 1990). In the case of deposition the active layer thickness is the depth of the deposition stratum.

Armanini and Silvio (1988) related the thickness of the active layer equal to one of the bottom layer in their model and employed a minimum limit of  $0.05h$ . They mentioned that when the active layer thickness is too small, there is a tendency for numerical instability when computing the percentages of the different size fractions present in the bed. Borah (1982) utilised the assumption of a homogeneous layer to reflect the active layer thickness as

$$\delta = \frac{100}{\sum_{j=L}^N \beta_j} \frac{d_L}{1 - \lambda_L} \quad (2.61)$$

where  $\delta$  = the thickness of the active layer;  $d_L$  = the particle diameter of L-th class;  $\lambda_L$  = the porosity of fraction L; fraction L is smallest ( $d_L$ ) of the material that the flow cannot transport. Borah's equation (2.61) is a measure of the active layer thickness when some of the fractions in the active layer cannot be eroded by the flow. These fractions will contribute to the formation of an armour layer. At low discharges, only the smaller fractions will be set into motion. Therefore a thinner active layer ( $d_L$  is small and  $\Sigma P_j$  is high) may be predicted. If the discharge is higher, only the coarser fractions will be left on the bed, and a thicker layer ( $d_L$  is high and  $\Sigma P_j$  is small) may be predicted. This behaviour is in agreement with the fact that a greater depth of bed can be sorted by a higher flow during the same period of time. Borah introduced the limit  $L = N$ ; i.e. the immobile particles are only the largest fraction. This limit is adopted here as the upper bound of the active layer thickness when the flow is capable of transporting all the fractions within the active layer. For instance, in a uniform bed material with porosity of 0.5, Borah's equation gives the active layer thickness equal to twice the particle diameter. The sediment contained in the active layer is the only material available for erosion. When the bed is armoured, no erosion can occur until the flow develops the necessary stress to move the smallest size fraction present in the armour layer. When this happens the armouring again becomes an eroding active layer. If deposition of a certain amount of sediment occurs during simulation, this material is added to the bed and a new active layer thickness is computed based on the new mixture composition.

Willets et al (1987) introduced the concept of a two-layer active depth which divided the thickness of the active layer into two, each equal in thickness to half of the largest grain size present. These are called layer 1 and layer 2 as in Figure 2.9. When the bed is scanned for a contribution to the transported load of fraction  $j$  all the material in layer 1 is considered available. As layer 1 is depleted, material from layer 2 gradually becomes available. Layer 2 can be said to be sheltered by the overlying layer 1 material. This sheltering is an intrinsic feature of the numerical procedure

made possible by the adoption of a two-layer active depth. The procedure was based on the observation that armouring stones are swept clean of finer material down to a plane which is very roughly where a horizontal section has maximum area; below that plane material is sheltered. Hence the calculation method simulates what is conceived to occur in nature. This simulation is crude because the thickness of the active layer is based arbitrarily on the  $D_{100}$  size, rather than on the smallest immobile grains in the prevailing flow, which would accord better with the conceptualised process. However, it permits the sheltering effect to be based on the initial bed mixture without empirical adjustment.

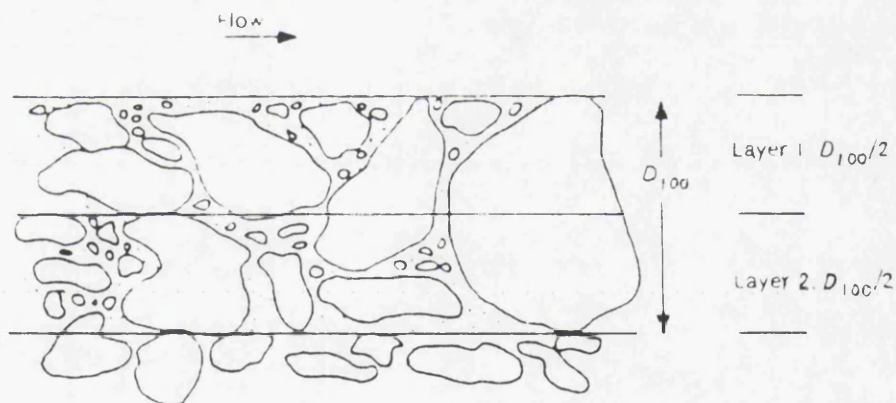


**Figure 2.9 Two-Active Layer Depths Below The Bed-Flow Interface (From Willetts, 1987)**

Vogel et al (1992) suggested the following equation for evaluating the thickness of the active layer.

$$\delta = 2D_{50} \frac{\bar{\tau}}{\tau_{c50}} \quad (2.62)$$

where  $\bar{\tau}$  = the effective temporal mean bed shear stress;  $\tau_{c50}$  = the critical shear stress necessary to entrain the median grain diameter. Equation (2.62) indicates the thickness of the active layer is linearly proportional to the excess shear stress with a minimum of two particle diameters. In their model, the thickness of the active layer is not allowed to vary dynamically because at high flows a dynamic thickness made the numerical model unstable.

Celik and Rodi (1988) suggested an empirical expression to evaluate the thickness of the active layer which is given as

$$\max\left(2D_m \frac{30\nu}{u_*} \frac{2}{3} k_s\right) < \delta_b \leq k_s \quad (2.63)$$

where  $k_s$  = the actual height of any roughness elements;  $D_m$  = the mean particle diameter;  $\nu$  = the viscosity. Hence the reference level is placed outside the bedload layer consisting of rolling particles (for which  $\delta_b = 2D_m$ ), outside the viscous sublayer for smooth walls, and in the case of rough walls, at a level where the velocity goes to zero, which is somewhere between two thirds of the height and full height of the roughness elements.

The expressions given in (2.62) and (2.63) provide a dynamic change of active layer thickness. Armanini and Silvio (1988) indicate that this can lead to instability in the calculation, therefore the model adopts the non dynamic method suggested by Armanini and Silvio (1988).

### 2.3.9 Dispersion Coefficient

Dispersion coefficient values have been investigated for many years. Under the assumption of a logarithmic velocity distribution Elder (1959) presented the following relationship from the research to an infinitely wide two dimensional channel as

$$D = 5.9u_*h \quad (2.64)$$

Fischer (1979) presented

$$D = 0.011 \frac{u^2 w^2}{u_* h} \quad (2.65)$$

Marivoet and Craenenbroeck (1986) modified the Fischer relationship to

$$D = 0.0021 \frac{u^2 w^2}{u_* h} \quad (2.66)$$

in which  $w$  = the top width,  $R$  = the hydraulic radius.

It has been found for suspended sediment transport that the dispersion coefficient also depends on the particle size. Van Rijn (1986) studied the dispersion process of suspended-load transport in open channels and presented a relationship where the dispersion coefficient varied with hydraulic parameters and particle size.

In addition, the distribution of the dispersion coefficient for suspended-load is not uniform over water depth. Most research demonstrates that a parabolic distribution of dispersion coefficient  $\varepsilon_s$  may be assumed. This is equal to the coefficient of momentum exchange  $\varepsilon_m$  as suggested by Van Rijn (1984)

$$\varepsilon_s = \varepsilon_m = \frac{y}{h} \left( 1 - \frac{y}{h} \right) \kappa u_* h \quad (2.67)$$

where  $\kappa$  = the Von Karman constant;  $h$  = the water depth;  $u^*$  = the shear velocity. Equation (2.67) was derived from a logarithmic velocity depth distribution.

The measurements carried out by Coleman (1970) show that a difference between  $\varepsilon_s$  and  $\varepsilon_m$  exists. This difference has been analysed by Van Rijn (1984) who related the dispersion of sediment particles to the diffusion of fluid momentum by

$$\varepsilon_s = \beta \phi \varepsilon_m \quad (2.68)$$

where the  $\beta$  factor describes the difference between the diffusion of a discrete sediment particle and the diffusion of a fluid particle (or small coherent fluid structure), this is assumed to be constant over the flow depth. The  $\phi$  factor expresses the damping of the fluid turbulence by the sediment particles and is assumed to be dependent on the local sediment concentration. Some investigators have concluded that the  $\beta$  factor must be larger than unity, because the sediment particles cannot respond fully to the turbulent velocity fluctuations. Others have reasoned that in a

turbulent flow the centrifugal forces on the sediment particles would be greater than those on the fluid particles, thereby causing the sediment particles to be thrown to the outside of the eddies with a consequent increase in the effective mixing length and diffusion rate, resulting in  $\beta > 1$ . The computed  $\beta$  factor can be described by

$$\beta = 1 + 2 \left( \frac{\omega}{u_*} \right)^2 \tag{2.69}$$

as shown in Figure 2.10. A relationship proposed by Kikkawa and Ishikawa (1980), reported by van Rijn (1984), based on a stochastic approach is also shown in Figure 2.10. According to the result of (2.69),  $\beta$  is always larger than unity, thereby indicating a dominating influence of the centrifugal forces.

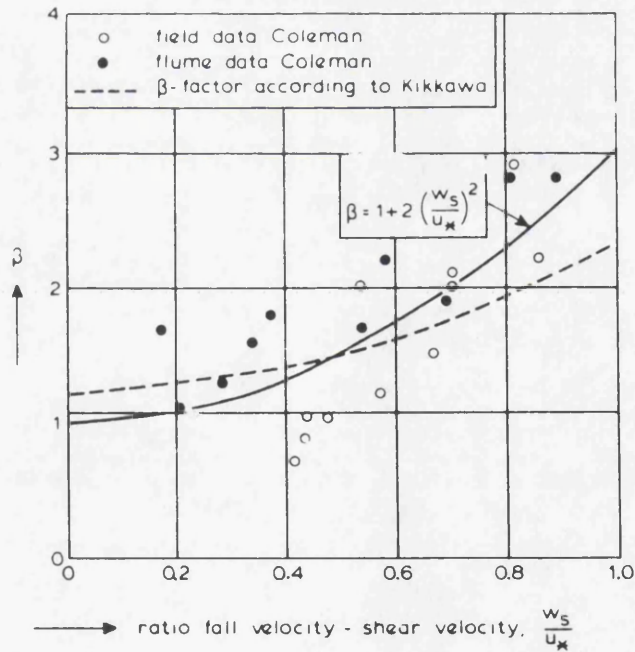


**Figure 2.10 Difference Between Dispersion of Particles and Diffusion of Momentum Exchange (Rijn, 1984)**

Usually the damping effect is taken into account by reducing the Von Karman constant. It has been demonstrated by Einstein and Chien (1953) that the Von Karman

constant becomes less than the value of 0.4 (clear flow) in the case of a heavy sediment-laden flow over a rigid, flat bed. The flow velocities in a layer close to the bed are reduced, while in the remaining part of the flow there are larger flow velocities. Apparently, the mixing is reduced by the presence of a large amount of sediment particles. According to Einstein and Chien (1953), who determined the amount of energy needed to keep the particles in suspension, the Von Karman constant is a function of the depth-averaged concentration, the particles fall velocity and the bed-shear velocity.

Although Ippen (1971) suggested that the Von Karman constant is primarily a function of some concentration near the bed, an investigation of Einstein and Abdel-Aal (1972) showed only a weak correlation between the near-bed concentration and the Von Karman constant. Coleman (1970) questioned the influence of the sediment particles on the Karman constant. He re-analysed the original data of Einstein-Chien (1953) and Vanoni and Brooks (1957) and concluded that they used an erroneous method to determine the Von Karman constant. In view of these contradictions it may be questioned if the concept of an overall Von Karman constant for the entire velocity profile is correct for a heavy sediment-laden flow. Van Rijn (1984) used three sets of data to fit a  $\phi$ -function; the data of Einstein-Chien (1953); Barton and Lin (1955); and Vanoni and Brooks (1957). The following expression has been derived empirically by fitting with measured velocity and concentration profiles.

$$\phi = 1 + \left(\frac{c}{c_0}\right)^{0.8} - \left(\frac{c}{c_0}\right)^{0.4} \quad (2.70)$$

(2.70) was shown in Figure 2.11 which indicates that values are considerably larger (less damping) than those given by Yalin and Finlayson (1972).

This is one dimensional model and there is therefore no need to take account of variation of dispersion coefficient either transversely or with depth. The one dimension equation (2.64) suggested by Elder (1959) is therefore adopted.

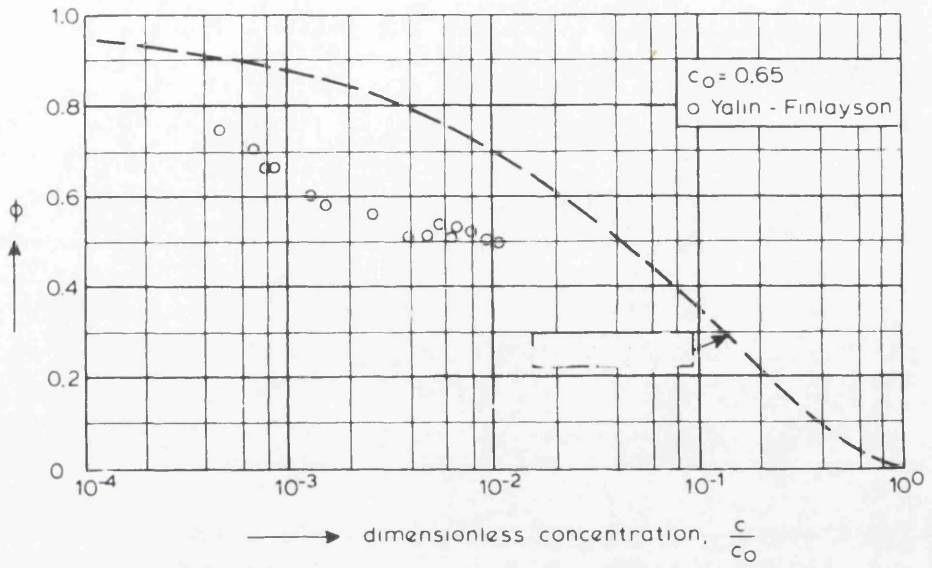


Figure 2.11 Damping Effect To Dispersion Coefficient (Rijn, 1984)

## **CHAPTER 3**

### **Development of Two Hiding Functions For Use With Van Rijn's Sediment Formulae**

#### **3.1 Introduction**

The interaction of size fractions in graded sediment during transport results in the sediment transport rate differing considerably from that computed using a single representative grain diameter. Experimental tests and field investigations, see Einstein (1950), White and Day (1982), Proffitt and Sutherland (1983), Sutherland (1991) and Kunhle (1992), demonstrate that the smaller grains in graded sediment are sheltered by the larger grains and consequently their mobility decreases. Conversely, the larger grains may be more exposed with a resulting increase in mobility. The net effect of this interaction is termed hiding and was first introduced into sediment transport calculations by Einstein (1950). One way of reproducing this phenomenon in calculations is to represent the graded sediment as a number of different size fractions. Calculations for graded sediment transport are then based on the mean size for each size fraction. The threshold condition for each size fraction is evaluated to account for the existence of others using a hiding function, see Einstein (1950), White and Day (1982), Proffitt and Sutherland (1983) and Sutherland (1991). Implicit in this technique is the assumption that all particles in a size fraction have equal entrainment mobility, Kircher et al (1990), and are transported according to their relative proportion in the bed material, see Kunhle (1992). The evaluation of the threshold

condition for each size fraction is critical to estimating graded sediment transport rates.

### 3.2 Background

The first hiding function, introduced by Einstein (1950), was used to extend the application of his statistically based uniform sediment bedload formula to graded sediment. Einstein recognised that finer grains may be hidden between larger grains. From the recirculating flume experiments, Einstein derived an empirical hiding function by matching the computed and measured total load transport rates under graded sediments. For fully rough turbulent flow, this hiding function  $\epsilon_j$  was presented as a function of relative particle size  $D_j/D_{50}$ . The critical stress  $\tau_{cr,j}$  for size fraction  $j$  is obtained from  $\tau_{cr,j} = \epsilon_j \tau_{sh,j}$ , where  $\tau_{sh,j}$  is the Shields critical stress for size fraction  $j$ . When the relative particle size is larger than 1.3, the hiding function is unity, and thus the coarser fractions were considered to be unaffected by hiding. When the relative particle size is less than 1.3, the applied shear stress is reduced. As can be seen from Figure 3.1 the reduction in applied shear stress for the relative particle size less than 0.1 is in excess of 100. Einstein and Chien (1953) reduced the maximum hiding factor to about 40 times by taking account of the wake effects and the measured turbulence associated with the larger grains. They also related hiding to the parameter  $D_{75}/D_{25}$ , thereby making some allowance for the grading curve shape. Later Pemberton (1972) modified the hiding function further based on river data. Figure 3.1 shows Pemberton's results providing significantly less hiding to the smaller grains.

Egiazaroff (1965) investigated threshold conditions in graded sediment and used this to derive his own graded sediment transport theory. The expression for the threshold condition suggested by Egiazaroff shows that the critical shear stress for an individual size fraction depends on its particle size  $D_j$  and the geometric mean  $D_g$  of

the sediment. A fundamental objection to Egiazaroff philosophy is that it employs a parabolic velocity profile at an elevation below the surface of the bed.

White and Day (1982) investigated threshold conditions for size fractions in graded sediment by fitting curves to experimental data of graded sediment transport in a recirculating flume. The results led to the hiding function in Equation (3.1) which is also plotted Figure 3.1.

$$\varepsilon_j = \left[ 0.4(D_j/D_a)^{-0.5} + 0.6 \right]^2 \quad (3.1)$$

where the scaling size  $D_a$  is diameter of particle which possesses the same critical shear stress in the non-uniform bed as it would in a uniform bed of diameter  $D_a$ . The scaling size is given by

$$\frac{D_a}{D_{50}} = 1.6(\sqrt{D_{84}/D_{16}})^{-0.56} \quad (3.2)$$

The range of data is good, although limited for data in the range  $D_j/D_a > 4$ .

Proffitt and Sutherland (1983) used the data obtained from the laboratory investigations of the static armour layers to develop two hiding functions for use with the sediment transport formulae of Paintal (1971) and Ackers & White (1973). The hiding functions were determined by matching predicted rates for each size fraction to measured values.

Ranga Raju (1985) introduced the concept of effective values of shear stress for the calculation of graded sediment transport. The effective values are obtained by applying a correction coefficient  $\xi_{bj}$  to the grain shear stress  $\tau_j$  for bedload and a correction coefficient  $\xi_{sj}$  to the actual shear stress  $\tau$  for suspended load. As expected, these correction coefficients are larger than unity for the coarser particles and smaller than unit for the finer particles. According to Ranga Raju's procedure, the correction for each size fraction depends on flow characteristics and bed composition.

$$\xi_{bj} = f_b \left\{ \frac{\tau_j}{\tau_{sh}}, \frac{\tau_j}{g(\rho_s - \rho)D_j}, M \right\} \quad (3.3)$$

$$\xi_{sj} = f_s \left\{ \frac{\tau}{\tau_{sh}}, \frac{\tau}{g(\rho_s - \rho)D_j}, M \right\} \quad (3.4)$$

where  $\tau_j$  = the grain shear stress of size fraction  $j$  for bedload;  $\tau$  = the actual shear stress of size fraction  $j$  for suspended-load;  $\tau_{sh}$  = the Shields critical shear stress for mean diameter of the mixture;  $D_j$  = the size fraction  $j$ ;  $M$  = the Kramar non-uniformity coefficient. The correction coefficients  $\xi_{bj}$  and  $\xi_{sj}$  are sediment transport formula specific.

Kirchner et al (1990) made the measurements of bed surface topography along streamwise transects of a graded sediment bed, the surface of which has been formed by equilibrium graded sediment transport. The rate and size distribution of the bedload matched those of the imposed bedload supply. The surface generated at the highest transport rate showed marked longitudinal sorting of the bed material to produce the congested and smooth surfaces. The congested zones resembled a static armour containing mainly coarse grains with a few fines. The smooth zones had a finer surface with isolated protruding grains.

Parker (1990) introduced the concept of a reduced hiding function which adjusts the mobility of each size fraction relative to that of the geometric mean size. In principle, the reduced hiding function is similar to the formulation suggested by Einstein, however, the application of the reduced hiding function is slightly different from those discussed previously. The main difference between the two hiding functions is that the reduced hiding function is calculated based on the Shields value of mean particle size, whereas the hiding function is calculated using Shields value for each size fraction. The relationship between the reduced hiding function  $g_j$  and  $D_j/D_{50}$  was obtained by Parker as

$$g_j = \frac{\Psi_{sh,50}}{\Psi_{cr,j}} = 1.048 \left( D_j / D_{50} \right)^{-0.0951} \quad (3.5)$$

see Figure 3.1.

Gessler (1970) presented a method for predicting the grain size distribution of the armour layer. His procedure utilised the armouring phenomenon to determine the probability for a given particle to remain stationary. Gessler defined an average probability of the bed becoming stable due to armouring as

$$\bar{q} = \int_{d_{min}}^{d_{max}} q P_a(y) dy \quad (3.6)$$

$P_a(y)$  = the probability distribution function for the armour layer,  $q$  = the probability that a grains of size  $y$  will remain as part of the stable armour layer. It is assumed by Gessler that if  $\bar{q} > 0.5$ , the bed could be expected to become stable, if  $\bar{q} < 0.5$ , the continuous erosion would occur until stability was reached by a reduction in the energy slope, thus increasing  $\bar{q}$ .

### 3.3 Effects of Surface Characteristics On Hiding

The effects of surface characteristics on hiding lies in the sheltering ability in active layer and the feedback effect of surface geometry on near bed flow structure. The latter occurs through the influence of surface geometry, by eddy shedding and the creation of wakes, on turbulence and in turn its effect on grain motion. The development of methods to describe and quantify the surface characteristics are therefore essential to evaluate the hiding effect.

The effect of surface characteristics on grain transport is apparent in the experimental studies of the static armouring in which significant reductions in transport rates occurs as the armour layer forms, see Proffitt and Sutherland (1983). According to Sutherland (1991), the surface characteristics changes are of two types: those associated with changes in grain size distribution and those associated with the

rearrangement of grains. In the development of armour layers the approach to the final grain size distribution occurs early while the transport rates are still large with the rearrangement phase being dominant throughout middle and later stages.

### **3.4 Equal Mobility and Hiding Function**

The concept of equal mobility for graded sediment transport was proposed by Parker et al (1982). Equal mobility consists of two parts: equal entrainment and equal transport mobility. The equal entrainment is defined as the case when all the sediment sizes in the bed material begin to move at the same flow strength. The equal transport mobility is the case when all sediment sizes are transported according to their relative proportion in the bed material. If one condition of equal mobility is true for a given channel it does not imply the other will also be true. For example, Wilcock & Southard (1988) found that near-perfect equal entrainment occurred in their laboratory flume runs, although the equal transport mobility was approached only at the highest flow strengths.

Several subsequent studies have supported this hypothesis. Wilcock and Southard (1988) have undertaken flume experiments involving bed sediments of mixed sizes and concluded that incipient motion occurs at nearly the same shear stress for all size fractions in a wide range of unimodal and weakly bimodal sediments. For these sediments the critical shear stress for each size fraction is well represented by a value slightly smaller than the Shields value for  $D_{50}$  of the mixture. Material sorting is demonstrated to have no effect on the critical shear stress. A theoretical foundation for the hypothesis has been provided by the analysis of Wilberg and Smith (1989). The collective impact of these studies has been to prove the equal mobility or near-equal mobility of grain entrainment and transport in gravel bed streams.

For strongly bimodal mixtures however, the size independence of the fractional critical shear stress is no longer maintained. The field investigation in Goodwin Creek, see Kunhle (1992), indicates that the larger grains in the graded sediment still

require larger bed shear stresses for movement than smaller ones. The value of critical shear stress for each fraction in strongly bimodal sediments depends on not only the shape of grain size distribution in bed material but also the protrusion present in each mode. Deviations from equal mobility were also found where the equal mobility yields the same composition of bed material as one of transported material and fails to approach the armouring layer. Under equal mobility as flow discharge or bed stress increases, the size fractional sediment transport rates are greater but remain in the same proportions so that the resulting grain size distributions are invariant.

On balance it is concluded that a hiding function related to particle size, grain size distribution and flow conditions will provide better results over a wider range of conditions than equal mobility.

### 3.5 Analysis of Hiding Function and Reduced Hiding Function

#### 3.5.1 Dimension Analysis of Threshold Conditions For Graded Bed Material

The characteristic parameters of the threshold conditions for graded bed material in uniform free surface flow are

- (i). fluid properties,
- (ii). character of bed material,
- (iii) open channel flow,

A fluid is normally defined by its density  $\rho$  ( $\text{kg/m}^3$ ) and viscosity  $\nu$  ( $\text{kg/s,m}$ ).

The characteristics of graded bed material can be determined by its density  $\rho_s$  ( $\text{kg/m}^3$ ), grain size distribution and grain geometry. The representation parameters for grain size distribution can be chosen as the particle diameter  $D_j$  (m) for each size fraction  $j$ , mean size diameter  $\bar{D}$  (m) and standard deviation  $\sigma$  of the grain size distribution. The grain geometry cannot be adequately defined by employing a finite number of quantities (Yalin, 1977), therefore the following analysis does not attempt

to include any parameters for grain geometry. The omission of grain geometry implies that the analysis is valid only for a particular grain geometry.

Uniform flow for a given fluid is determined by its average water depth  $h$  (m), energy slope  $S$  and force of gravity characterised by the gravitational acceleration  $g$  ( $m/s^2$ ).

The threshold conditions of graded bed material in the uniform flow can therefore be defined by a set of nine characteristic parameters:

$$\rho, \nu, \rho_s, D_j, \bar{D}, \sigma, h, S, g$$

Selecting the parameters of  $\bar{D}$ ,  $\rho$  and  $u_* = \sqrt{ghS}$  which obviously have independent dimensions as basic quantities, the following dimensionless variables can be constructed.

- (1) individual grain size Reynolds number  $Re_j$  or mean grain size Reynolds number  $Re_d$ ;

$$Re_j = \frac{u_* D_j}{\nu} \quad \text{or} \quad Re_d = \frac{u_* \bar{D}}{\nu} \quad (3.7)$$

- (2) threshold condition for size fraction  $j$ ,  $\psi_{cr,j}$ ;

$$\psi_{cr,j} = \frac{u_*^2}{\Delta g D_j} \quad (3.8)$$

- (3) relative particle size;

$$\frac{D_j}{\bar{D}} \quad (3.9)$$

- (4) standard deviation of grain size distribution;

$$\sigma \quad (3.10)$$

- (5) Froude number  $Fr$ ;

$$Fr = \frac{u}{\sqrt{gh}} \quad (3.11)$$

- (6) specific submerged density  $\Delta$ ;

$$\Delta = \frac{\rho_s - \rho}{\rho} \quad (3.12)$$

Based on the  $\pi$ -theorem, a dimensionless functional relation for the threshold condition of graded bed material is supposed to exist as

$$\psi_{cr,j} = f(\text{Re}_j, \frac{D_j}{D}, \sigma, \text{Fr}, \Delta) \quad \text{or} \quad (3.13)$$

$$\psi_{cr,j} = f(\text{Re}_d, \frac{D_j}{D}, \sigma, \text{Fr}, \Delta)$$

The significance of each variable in Equation (3.13) cannot be the same. It depends on the nature of the threshold condition of graded bed material and the order of its own numerical value. In order to clarify the significance of each variable, it is necessary to consider their physical meaning and relative importance.

The grain size Reynolds number reflects the influence of fluid viscosity. A decrease in the numerical value of viscosity will increase the grain size Reynolds number and thus approach the condition of an ideal fluid. Even for quite high grain size Reynolds numbers, it is not a sufficient indication that the effect of the variable can be neglected (Yalin, 1977). The grain size Reynolds number is a characteristic parameter of the relative motion of a grain in the fluid, not the motion of the fluid in channel.

The threshold condition for each size fraction  $j$  is, in a sense, a measure of the ratio of the magnitude of the tractive force acting on the size fraction  $j$  to the resistance including the grain weight and interaction between different size fractions. Clearly, the tractive force increases with  $\psi_{cr,j}$ . For uniform material the resistance force has no hiding component and is only the grain weight.

The relative particle size and the standard deviation of grain size distribution reflect the influence of the grain size distribution on the threshold condition. For uniform bed material the threshold condition does not depend on these two

parameters. However they significantly affect the threshold condition for graded bed material.

The Froude number  $Fr$  reflects the influence of flow depth. It has been demonstrated, see Yalin (1977), that sediment transport which is independent on the water depth can only be valid when the sediment transport takes place in the vicinity of the bed surface. For sediment transport including the suspended-load, the effect of the water depth should be included.

The specific submerged density reflects the influence of specific mass  $\rho_s$ . If the density of grains was uniform, then  $\rho_s$  would not be a characteristic parameter and thus specific submerged density  $\Delta$  would not be a variable of the phenomenon (Yalin, 1977). Usually, in engineering practice one is much more interested in the properties of the uniform motion of the grains and accordingly the specific density appears to be least important variable.

Following the above analysis, Equation (3.13) can be simplified to

$$\psi_{cr,j} = f(\text{Re}_j, \frac{D_j}{D}, \sigma, Fr) \quad \text{or} \quad (3.14)$$

$$\psi_{cr,j} = f(\text{Re}_d, \frac{D_j}{D}, \sigma, Fr)$$

### 3.5.2 Form of Hiding Function and Reduced Hiding Function

#### 3.5.2.1 Form of Hiding Function

A hiding function is defined as a modifier of grain threshold conditions. In essence a hiding function modifies the threshold condition of size fractions with respect to their single size threshold condition as determined by the Shields value. There are two definitions of the hiding function available in literature. One was suggested by Einstein (1950) which can be written as:

$$\varepsilon_j = \frac{\psi_{cr,j}}{\psi_{sh,j}} \quad (3.15)$$

where  $\varepsilon_j$  = the hiding function;  $\psi_{cr,j}$  = the threshold condition for size fraction j;  $\psi_{sh,j}$  = the Shields value for size fraction j which can be related solely to the individual grain size Reynolds number through the expression:

$$\psi_{sh,j} = f_{sh}(Re_j) \tag{3.16}$$

It is assumed that (3.14) can be rearranged as

$$\psi_{cr,j} = f_{sh}(Re_j) \cdot f_{\varepsilon} \left( \frac{D_j}{D}, \sigma, Fr \right) \tag{3.17}$$

Substitution of (3.16) into (3.17) leads to following expression

$$\psi_{cr,j} = \psi_{sh,j} \cdot f_{\varepsilon} \left( \frac{D_j}{D}, \sigma, Fr \right) \tag{3.18}$$

By using Einstein's definition (3.15) we have

$$\varepsilon_j = f_{\varepsilon} \left( \frac{D_j}{D}, \sigma, Fr \right) \tag{3.19}$$

Equation (3.19) indicates that a hiding function is dependent on three parameters, the relative particle size, the deviation of the grain size distribution and the Froude number.

### 3.5.2.2 Form of Reduced Hiding Function

The definition of the reduced hiding function was suggested by Parker (1990) which can be written as

$$g_j = \frac{\psi_{sh,g}}{\psi_{cr,j}} \tag{3.20}$$

where  $g_j$  = the reduced hiding function;  $\psi_{cr,j}$  = the threshold condition for size fraction j;  $\psi_{sh,g}$  = the Shields value for geometric mean size  $D_g$  which can be related to the geometric mean size Reynolds number by

$$\Psi_{sh,g} = f_{sh}(Re_g) \quad (3.21)$$

Here it is assumed that (3.14) can be rearranged to

$$\Psi_{cr,j} = \frac{f_{sh}(Re_g)}{f_g\left(\frac{D_j}{D_g}, \sigma_g, Fr\right)} \quad (3.22)$$

Substitution of (3.21) into (3.22) results in

$$\Psi_{cr,j} = \frac{\Psi_{sh,g}}{f_g\left(\frac{D_j}{D_g}, \sigma_g, Fr\right)} \quad (3.23)$$

Employing the definition of the reduced hiding function Equation (3.20), we have

$$g_j = f_g\left(\frac{D_j}{D_g}, \sigma_g, Fr\right) \quad (3.24)$$

Equation (3.24) shows that the reduced hiding function is also dependent on the relative particle size, the geometric standard deviation and the Froude number. Geometric mean and standard geometric deviation in Equation (3.24) can be computed from

$$D_g = \exp\left(\frac{\sum P_j \ln(D_j)}{\sum P_j}\right) \quad (3.25)$$

$$\sigma_\phi^2 = \frac{\sum \left[ \frac{\ln(D_j/D_g)}{\ln(2)} \right]^2 P_j}{\sum P_j} \quad (3.26)$$

$$\sigma_g = 2^{\sigma_\phi}$$

where  $D_j$  = the diameter of size fraction  $j$ ;  $P_j$  = the fractional representation for size fraction  $j$ . For uniform material the standard geometric mean is equal to 1. For graded sediment the standard geometric mean is greater than 1.

### 3.5.3 Relationship Between Hiding Function and Reduced Hiding Function

The reduced hiding function can be related to hiding function through Equations (3.15) and (3.20). From Equation (3.20) we can obtain

$$g_j = \frac{\Psi_{sh,j}}{\Psi_{cr,j}} \cdot \frac{\Psi_{sh,g}}{\Psi_{sh,j}} \quad (3.27)$$

and substitution of Equation (3.15) into Equation (3.27) gives

$$g_j = \frac{1}{\varepsilon_j} \cdot \frac{\Psi_{sh,g}}{\Psi_{sh,j}} \quad (3.28)$$

Using Equation (3.28) the reduced hiding function can be transferred into the hiding function and vice versa. This indicates that the two definitions of hiding function are not independent <sup>&</sup> each other.

## 3.6 Available Experimental Data

The evaluation of the hiding effect requires experimental measurements. The work described uses data from three sources, H.R. Wallingford (Day, 1980), The United States Waterway Experimental Station (1935) and Gibbs and Neill (1972 & 1973). The data covers a range of flow conditions, bed material grading, and mean sediment size. There is some overlap between the data sets.

### 3.6.1 H.R. Wallingford Data

Two series of experiments were undertaken, series A (HRS-A) and series B (HRS-B). For series A, the bed material was a natural mixture obtained from a local gravel pit. It had the advantage of being both widely graded and bimodal. Although its mean size was only 1.75 mm, it contained size fractions ranging from 0.153 to 11.11 mm. The second bed material (HRS-B) was mixed from size fractions extracted from the series A material. Its composition was designed to produce a sediment of similar mean size but narrower grading. The mean size of HRS-B was 1.55 mm with size

fractions ranging from 0.153 to 4.06 mm. The characters of bed material are listed in Table 3.1.

**Table 3.1 Characters of Bed Material In H R Wallingford Data**

Data set	Source	Range of $D_j$ (mm)	$D_{50}$ (mm)	$\sqrt{D_{84}/D_{16}}$	$D_g$ (mm)	$\sigma_g$
1	HRS-A	0.153-14.2	1.75	4.28	1.518	3.414
2	HRS-B	0.153-5.560	1.55	3.24	1.179	2.747

The experiments were conducted in a 2.46 m wide recirculating tilting flume. A sediment return system had been constructed within the flume channel. Any suspended load was transported through the main pumping system whereas the coarser grains were deposited into hoppers at the downstream end of the sediment bed. This coarser sediment was pumped continuously underneath the flume channel through a separate system of pipes to re-enter the main channel through a set of eight nozzles located downstream of the main discharge pump entrances and just at the beginning of the sediment bed.

For all runs a 0.2 m deep sediment bed was laid in the flume and smoothed out by template. After each run in HRS-A the top few centimetres were removed and new sediment added and levelled. In HRS-B, the bed was formed of a 0.1 m thick layer of bed material separated by plywood sheets from an underlying layer of equal thickness of the initial material.

Each run consisted of several tests and each test consisted of measurements of the sediment transport rate, the discharge, the water surface elevation and the flow depth. The sediment load was measured as it was returned to the upstream end of the flume. All sediment samples used in the subsequent analysis were taken at least 2 hours after the beginning of the experiment.

A total of 20 runs were completed, eleven for series A and nine for series B. Summaries of hydraulic and sediment transport measurements are listed in Table 3.2.

The mean velocities were determined from the continuity equation. The water surface slope was determined from a regression analysis of the five point gauge readings. The sediment concentrations are given as parts per million by weight (PPM).

**Table 3.2 Hydraulic Conditions and Sediment Transport Rates In H R Wallingford Data**

Source	No. of runs	Mean depth (m)	Mean velocity (m/s)	Shear velocity (m/s)	Transport rate <sup>a</sup> (kg/s)	Concentration (PPM)
HRS-A	11	0.107~0.169	0.479~0.745	0.033~0.062	0.00175~0.16100	8.90~834.85
HRS-B	9	0.115~0.189	0.189~0.722	0.029~0.058	0.00033~0.22218	1.62~1089.95

<sup>a</sup> Dry weights used in all calculations

The precision of the discharge and depth measurements ranged from 0.3 to 3% over both series. The water surface slope are the least precise with coefficients of variation ranging from 3 to 32% and an average of approximately 10%. The precision of the sediment transport measurements varies from 6.5 to 41% with no clear tendency to change with different sediment transport rates. On average the series B experiments were slightly more accurate with an average coefficient of variation of 20% compared to 25% for series A.

### 3.6.2 USWES Data

This was an extensive series of experiments into graded sediment transport rates for nine different bed materials. Of these nine series of experiments, three were chosen for use in the present study: sand No.1, 2 and 9 since the full information for these three experiments was provided. No.1 and 2 bed materials were tested at three slopes 0.001, 0.0015 and 0.002. No.9 material, a small gravel, was tested at slopes of 0.003, 0.004 and 0.0045. The characters of bed materials are summarised in Table 3.3

**Table 3.3 Characters of Bed Material In USWES Data**

Data set	Source	Range of $D_j$ (mm)	$D_{50}$ (mm)	$\sqrt{D_{84}/D_{16}}$	$D_g$ (mm)	$\sigma_g$
3	USWES-1	0.153-2.86	0.42	1.82	0.437	1.915
4	USWES-2	0.153-2.03	0.44	1.51	0.466	1.654
5	USWES-9	0.925-5.56	4.10	1.45	3.942	1.452

The experiments were conducted in a tilting flume 18.89 m long and 0.9 m wide. At the lower end of the flume a sand trap was installed to measure the transport rate. An automatic sandfeed was used to discharge the sand into the flume at approximately the same rate at which it was leaving at the lower end.

**Table 3.4 Hydraulic Conditions and Sediment Transport Rates In USWES Data**

Source	No. of runs	Mean depth (m)	Mean velocity (m/s)	Shear velocity (m/s)	Transport rate <sup>a</sup> (kg/s)	Concentration (PPM)
USWES-1	17	0.019~0.067	0.271~0.549	0.017~0.036	0.00006~ 0.00953	7.14~ 353.74
USWES-2	19	0.022~0.126	0.262~0.555	0.021~0.043	0.00003~ 0.01925	6.91~ 374.44
USWES-9	17	0.074~0.107	0.558~0.732	0.047~0.069	0.00003~ 0.01516	0.98~ 274.82

<sup>a</sup> Dry weights used in all calculations

The water surface and bed elevation were determined by means of a needle-gauge, which was mounted to slide along the rails on the side of the flume. The elevation of the water surface at the lower end of the flume was controlled by the manipulation of a vertical, sliding tailgate. The flow discharge was supplied at the constant rate from the inlet. Mean velocities were computed from the discharge and cross-sectional area. The transported sand was trapped at the lower end of the flume. The intensity of sand movement and the bed forms were classified by a visual method. During the period of experimental tests, the air temperature remained fairly constant between 20°C to 22°C. The temperature of water was assumed to be the same as the

air. A total of 53 runs were completed, 17 for No.1 and No.9 and 19 for No.2. The range of size fractions in the bed material, the range of velocity and the details of each run are considerable. For each run only one measurement of sediment transport was made so that the precision of measured data cannot be assessed. The summary of hydraulic and transport measurements are listed in Table 3.4.

### 3.6.3 Gibbs & Neill Data

In their evaluation of the efficiency of basket-type bed-load samplers the Gibbs & Neill (1972&1973) presented the graded sediment transport measurements from two sets of experiments. A common bed material with a median size similar to that of USWES No.9 but with a wider grading and range of size fractions was used for all runs. The characters of bed material are summarised in Table 3.5.

**Table 3.5 Characters of Bed Material In Gibbs&Neill Data**

Data set	Source	Range of $D_j$ (mm)	$D_{50}$ (mm)	$\sqrt{D_{84}/D_{16}}$	$D_g$ (mm)	$\sigma_g$
6	Gibbs & Neill	1.20-14.2	4.75	2.28	4.251	2.043

**Table 3.6 Hydraulic Conditions and Sediment Transport Rates In Gibbs&Neill Data**

Source	No. of runs	Mean depth (m)	Mean velocity (m/s)	Shear velocity (m/s)	Transport rate <sup>a</sup> (kg/s)	Concentration (PPM)
Gibbs & Neill	6	0.165~0.177	0.810~1.088	0.057~0.091	0.03330~0.25197	234.51~1483.10

<sup>a</sup> Dry weights used in all calculations

The experiments were performed with a nearly constant flow depth and a narrow range of mean velocity. The shear stress was increased by varying the flume slope. Although only six measurements are available, they represent average values of detailed studies into the variation of transport rates. In each run 50 test measurements

of bedload were taken from a slot sampler located in the flume bed. The length of sampling period was variable while the interval between tests in a specific run was kept constant. A summary of these results are listed in Table 3.6.

**3.6.4 Grain Size Distributions For All Bed Materials**

The grain size distributions for all bed materials in H.R. Wallingford, USWES and Gibbs&Neill data are shown in Figure 3.2 and Table 3.7.

**Table 3.7 Grain Size Distribution In Bed Materials**

intermediate size (mm) <sup>a</sup>	Percentage by weight					
	HRS-A	HRS-B	USWES No.1	USWES No.2	USWES No.9	Gibbs & Neill
0.153	1.30	2.13	8.0	1.6		
0.215	4.16	4.70	12.0	7.5		
0.275	—	5.67	—	—		
0.303	11.00	—	16.0	21.5		
0.328	—	6.10	—	—		
0.390	5.68	5.03	11.2	12.5		
0.463	5.75	4.27	10.3	16.5		
0.550	4.31	2.77	11.5	14.0		
0.655	2.69	2.33	7.5	8.5		
0.780	2.56	3.07	7.7	7.0		
0.925	2.21	3.07	2.6	2.7	0.1	
1.200	4.98	6.97	2.9	4.5	1.6	10.0
1.550	3.10	4.90	1.8	2.3	1.7	5.8
2.030	6.96	16.93	1.0	0.7	6.3	9.2
2.860	10.10	13.47	2.5	0.3	18.5	11.3
4.060	9.88	15.00			38.0	12.0
5.560	10.75	1.47			28.0	13.7
7.180	6.87				5.0	16.0
8.730	3.35					9.5
11.110	2.27					9.7
14.200	0.36					1.8

<sup>a</sup> Intermediate particle size determined as size half way between bracketing sieve size

### 3.7 Van Rijn's Sediment Transport Formula

Sediment transport may be subdivided into the bedload and suspended-load depending on the manner in which the particles are transported. In the literature many formulae have been suggested and developed by various authors. For example Einstein's bedload transport formula (1942), Engelund and Hanson's total load transport formulae (1967), Ackers and White's total load transport formula (1973) and Van Rijn's sediment transport formula (1984). A comparison of the performance of the different formulae made by Van Rijn (1984) suggested that his own sediment transport formula gives more reliable predictions. This formula has therefore been adopted in the following. The formula calculates the bedload and suspended-load transport rate separately using

$$\frac{G_s}{uhb} = 0.012 \left( \frac{u - u_{cr}}{\sqrt{g \Delta D}} \right)^{2.4} \left( \frac{D}{h} \right) D_*^{-0.6} \quad (3.29)$$

$$\frac{G_b}{uhb} = 0.005 \left( \frac{u - u_{cr}}{\sqrt{g \Delta D}} \right)^{2.4} \left( \frac{D}{h} \right)^{1.2} \quad (3.30)$$

where  $G_s$  = the suspended-load transport rate;  $G_b$  = the bed load transport rate;  $u$  = the mean water velocity over the cross-section;  $h$  = the water depth;  $b$  = the cross-section width;  $u_{cr}$  = the critical velocity;  $D$  = the particle size;  $g$  = the acceleration due to gravity;  $D_* = D \sqrt[3]{\frac{g \Delta}{\nu^2}}$  = the dimensionless particle size and  $\nu$  = the viscosity of water.

For graded sediment transport calculations it is necessary to compute the suspended and bedload transport rates for each size fraction, then summate these to obtain the net values.

### 3.8 Hiding Function Development

Following Sutherland (1991), it was assumed that the hiding function Equation (3.19) can be subdivided into two parts by introducing a scaling size. The first part is

to obtain the relationship between the hiding function and the scaling size which can be written as,

$$\varepsilon_j = f_\varepsilon \left( \frac{D_j}{D_a} \right) \quad (3.31)$$

The second part is to relate the scaling size  $D_a$  to the mean particle size  $D_{50}$ , grain size deviation  $\sqrt{D_{84}/D_{16}}$  and Froude number  $Fr$  through the following expression,

$$\frac{D_a}{D_{50}} = f_a(\sqrt{D_{84}/D_{16}}, Fr) \quad (3.32)$$

As discussed previously the scaling size  $D_a$  is the diameter of particle which possesses the same critical shear stress in the non-uniform bed as it would in a uniform bed of diameter  $D_a$ . If a particle size in the graded sediment is equal to the scaling size, then the value of the hiding function for this particle size is one. Hence, one could expect that for  $D_j = D_a$ , then  $\tau_{cr,j} = \tau_{sh,j}$ ; for  $D_j < D_a$ , then  $\tau_{cr,j} < \tau_{sh,j}$  and for  $D_j > D_a$ , then  $\tau_{cr,j} < \tau_{sh,j}$ .

### 3.8.1 Scaling Size

The physics of hiding suggests that when the bed material is uniform, the hiding effect should vanish giving a hiding function equal to one. As a result, Equation (3.32) should also be equal to one for uniform sediment. Therefore Equation (3.32) is proposed as a power law of  $\sqrt{D_{84}/D_{16}}$  with the value of the power depending on both the grading curve shape and the flow conditions characterised by the Froude number. The parameters in Equation (3.33) were obtained by a non-linear optimisation on the data from Day (1980) and USWES (1935) giving

$$\frac{D_a}{D_{50}} = \sigma^{7.024 - 2.353\sigma + 0.054\sigma^2 - 7.566Fr - 4.579Fr^2 + 3.241\sigma Fr} \quad (3.33)$$

where  $\sigma = \sqrt{D_{84}/D_{16}}$ . This relationship is shown in Figure 3.3.

The statistical fit between this curve and the available data is good, however, it must be recognised that the data set is limited in size.

### 3.8.2 Hiding Function

Following the work of Andrews (1983) and Ferguson et al (1989), Equation (3.31) is presented in the form

$$\varepsilon_j = \left( \frac{D_j}{D_a} \right)^{-b} \quad (3.34)$$

where, as suggested by Sutherland (1991), parameter  $b$  varies with the relative particle size  $D_j/D_a$ . Here a linear relationship between  $b$  and  $D_j/D_a$  is assumed.

This hiding function was evaluated in the following way. First Equations (3.29) and (3.30) were combined to obtain a total load Equation (3.35).

$$\frac{G}{uhb} = \left( 0.012D_*^{-0.6} + 0.005(D/h)^{0.2} \right) \left( \frac{u - u_{cr}}{\sqrt{g(\Delta - 1)D}} \right)^{2.4} \left( \frac{D}{h} \right) \quad (3.35)$$

This was rearranged to provide an expression for the critical velocity. From this, the critical velocity for each size fraction in the data can be calculated in Equation (3.36).

$$u_{cr,j} = u - \sqrt{g(\Delta - 1)D_j} \sqrt[2.4]{\frac{G}{uhb} \frac{h/D_j}{[0.012D_*^{-0.6} + 0.005(D_j/h)^{0.2}]}} \quad (3.36)$$

Then the critical shear stress for each size fraction can be obtained from the critical velocity  $u_{cr,j}$ . The Shields critical shear stress for each size fraction can then be obtained directly from Shields curve. Based on the definition of a hiding function as the ratio of the true critical shear stress to the Shields critical shear stress the hiding function can be obtained and plotted against particle size. The parameters in the relationship were determined using a regression analysis. This hiding function is given in Equation (3.37) and is shown graphically in Figure 3.4.

$$\varepsilon_j = \left( \frac{D_j}{D_a} \right)^{-0.789 + 0.143 \log(D_j/D_a)} \quad (3.37)$$

To quantify the goodness of a fit to the data a two parameter Me and Ad statistical analysis as suggested by Garcia and Parker (1991) was undertaken.

$$Me = 10^{\frac{1}{n} \sum \log(G_{ca,j}/G_{ob,j})} \quad (3.38)$$

$$Ad = 10^{\frac{1}{n} \sum |\log(G_{ca,j}/G_{ob,j}) - \log(Me)|} \quad (3.39)$$

where  $G_{ca,j}$  = the calculated value;  $G_{ob,j}$  = the observed value. For perfect agreement the correlation parameters Me and Ad would be equal to one. For Equations (3.33) and (3.37) we obtained Me of 1.002 and Ad of 2.261 for HRS and USWES data.

### 3.8.3 Verification of The Hiding Function

The hiding function in Equation (3.37) was tested using the independent data available in Gibbs and Neill (1972&1973). Results with and without the hiding function are shown in Figures 3.5 and 3.6 respectively. It can be seen from Figures 3.5 and 3.6 that the significant improvements are achieved by using the hiding function with Me increasing from 0.307 to 0.721 and Ad decreasing from 6.274 to 2.147.

## 3.9 Development of The Reduced Hiding Function

### 3.9.1 Reduced Hiding Function

Van Rijn's formulae were derived empirically based on the single size assumption. When the formulae are used to predict total transport rates, a representative grain size in a mixture, for example the median size, must be chosen. This is used to compute the critical velocity required in Equation (3.29) and (3.30). However, the representative grain size may vary with grading curve shape and flow conditions. This makes it difficult to estimate the total transport rate correctly over a range of sediment types and flow conditions.

One way of improving this is to introduce an additional parameter to adjust the representative grain size to take account of the grain size distribution characterised by  $\sigma_g$  and flow conditions characterised by Fr. This parameter may be defined as

$$\Phi = \frac{u_{cr}^2}{u_{sh,g}^2} = \Phi(\sigma_g, Fr) \quad (3.40)$$

where  $u_{cr}$  = the critical velocity used in Equations (3.29) and (3.30);  $u_{sh,g}$  = the Shields critical velocity based on the geometric mean size  $D_g$ ;  $\sigma_g$  = the standard geometric deviation, and  $Fr$  = the Froude number. For given flow conditions and grain size distribution,  $\Phi$  can be estimated from Equation (3.40) and the critical velocity for use with the calculation of total load transport capacity obtained from  $u_{cr} = u_{sh,g} \sqrt{\Phi}$ . As with the previous hiding function  $\Phi$  must be unity for uniform bed material. This suggests that a power function of  $\sigma_g$  will be appropriate. The following expression has therefore been adopted,

$$\Phi = \sigma_g^{a_0 + a_1(\sigma_g) + a_2(\sigma_g^2) + b_0 + b_1(Fr) + b_2(Fr^2) + c_0(\sigma_g Fr)} \quad (3.41)$$

Applying the non-linear optimisation technique on the data taken from Day (1980) and USWES (1935) enabled the evaluation of all parameters in Equation (3.41) as  $a_0 = 4.198$ ,  $a_1 = -2.548$ ,  $a_2 = 0.192$ ,  $b_0 = 0$ ,  $b_1 = 0.275$ ,  $b_2 = -7.488$ ,  $c_0 = 2.490$ .

So far account has only been taken of the effect of grading curve shape and flow conditions on the representative grain size. The hiding effect where the threshold condition of each size fraction in the sediment is modified to account for the existence of others requires to be included. Following Parker (1990), a parameter  $\omega_j$  to reflect the hiding effect for each size fraction is defined as

$$\omega_j = \omega_j(D_j/D_g) = \frac{u_{cr}^2}{u_{cr,j}^2} \quad (3.42)$$

where  $u_{cr}$  = the critical velocity used for estimation of total transport rate;  $u_{cr,j}$  = the actual critical velocity of size fraction  $j$  which can be used to calculate the transport rate of size fraction  $j$ . Using the experimental data from Day (1980) and USWES (1935) and a regression analysis, Equation (3.43) is obtained

$$\omega_j = \left( \frac{D_j}{D_g} \right)^{-0.105} \quad (3.43)$$

$\omega_j$  value against relative size  $D_j/D_g$  is shown in Figure 3.8.

Therefore from the definition of a reduced hiding function in Equation (3.20), we obtain

$$g_j = \frac{u_{sh,g}^2}{u_{cr,j}^2} = \frac{\omega_j}{\Phi} \quad (3.44)$$

where  $g_j$  = a reduced hiding function relative to the geometric mean size. Substitution of Equations (3.41) and (3.43) into Equation (3.44) yields the expression

$$g_j = \frac{\left( D_j/D_g \right)^{-0.105}}{\sigma_g^{4.198-2.548(\sigma_g)+0.192(\sigma_g^2)+0.275(Fr)-7.488(Fr^2)+2.490(\sigma_g Fr)}} \quad (3.45)$$

This reduced hiding function varies with the relative size and the standard geometric deviation at different  $Fr$  values of 0.3, 0.5 and 0.7 is shown in Figures 3.9, 3.10 and 3.11.

For given flow conditions and grain size distribution,  $g_j$  can be evaluated using Equation (3.45) and  $u_{sh,g}$  can be obtained from

$$\frac{u_{scr,g}^2}{\Delta g D_g} = 2.89 \left( \frac{h}{D_g} \right)^{0.19} \quad (3.46)$$

where  $h$  = the water depth;  $D_g$  = the geometric mean size which can be given by Equation (3.25). The standard geometric deviation  $\sigma_g$  is given by Equation (3.26). Then the critical velocity for each size fraction can be evaluated through Equation (3.44) and used to calculate the transport capacity for this size fraction by applying Equations (3.29) and (3.30). The total transport capacity is obtained by summing over all the size fractions.

The goodness of fit of the reduced hiding function to the HRS and USWES data is given with  $Me$  of 1.291 and  $Ad$  of 2.026.

### 3.9.2 Reduced Hiding Function Verification

The verification of the hiding function was undertaken in two steps. Firstly, the calculated and observed  $\Phi$  values were compared, and secondly, the behaviour of the hiding function was evaluated.

The results of verification for  $\Phi$  are shown in Table 3.8 where  $\Phi$  is the observed value and  $\Phi_c$  is the calculated value from Equation (3.41). The overall mean percentage error is 10.6%. The extent of the data implies that Equation (3.41) can be only used for Froude numbers between 0.2 and 0.8 and for  $\sigma_g$  between 1.0 and 3.5.

The performance of the reduced hiding function was tested by predicting the size fractional transport rate for the experimental data of Day (1980) and USWES (1935). As before the statistical correlation parameters of Garcia and Parker (1991) have been employed. The results are shown in Table 3.9 and Figure 3.12. Comparisons between the calculated and observed value are made using the ratio of the observed and calculated value. Four methods are used for the evaluation. Firstly, the median size in a mixture is used directly in Equations (3.29) and (3.30) and then the transport rate of a size fraction is calculated in proportion to its presence in the active layer. Secondly, the geometric mean size is employed instead of using the median size in the first method. Thirdly, the geometric mean size and  $\Phi$  value in Equation (3.41) are utilised to calculate the total transport rate and then the transport rate of a size fraction is assumed to be proportional to its percentage in the active layer. Finally, the reduced hiding function, see Equation (3.45), is used to estimate the critical velocity of a size fraction in the graded sediment and then the transport rate of a size fraction is evaluated based on the Equations (3.29) and (3.30) and its availability of this size fraction in the active layer. Clearly, a good improvement is achieved if the reduced hiding function is employed.

Table 3.8 Verification For  $\Phi$  Value

Source of data	$\sigma_g$	Fr	$\Phi$	$\Phi_c$	$(\Phi - \Phi_c)/\Phi * 100$
HRS-A	3.414	0.372	0.988	0.958	3.0
	3.414	0.386	0.997	1.011	-1.4
	3.414	0.413	1.083	1.109	-2.4
	3.414	0.456	1.228	1.250	-1.8
	3.414	0.474	1.406	1.301	7.5
	3.414	0.532	1.591	1.421	10.6
	3.414	0.548	1.389	1.441	-3.7
	3.414	0.601	1.600	1.457	8.9
	3.414	0.611	1.453	1.452	0.1
	3.414	0.697	1.350	1.304	3.4
	3.414	0.727	1.231	1.216	1.2
HRS-B	2.747	0.409	1.338	1.361	-1.7
	2.747	0.439	1.397	1.393	0.3
	2.747	0.475	1.336	1.407	-5.3
	2.747	0.614	0.962	1.216	-26.3
	2.747	0.645	1.026	1.131	-10.2
	2.747	0.653	0.978	1.107	-13.2
USWES-1	1.915	0.509	1.433	1.525	-6.4
	1.915	0.539	1.488	1.444	2.9
	1.915	0.541	1.635	1.438	12.0
	1.915	0.545	1.511	1.427	5.6
	1.915	0.546	1.601	1.424	11.1
	1.915	0.594	1.363	1.277	6.3
	1.915	0.603	1.528	1.248	18.3
	1.915	0.606	1.302	1.238	4.9
	1.915	0.628	1.425	1.166	18.2
	1.915	0.641	1.357	1.123	17.2
	1.915	0.643	1.288	1.117	13.3
	1.915	0.652	1.548	1.087	29.8
	1.915	0.697	1.437	0.937	34.8
1.915	0.706	1.136	0.908	20.1	
USWES-2	1.654	0.471	1.697	1.586	6.5
	1.654	0.472	1.595	1.584	0.7
	1.654	0.481	1.419	1.565	-10.3
	1.654	0.540	2.073	1.421	31.5
	1.654	0.564	1.307	1.356	-3.7
	1.654	0.580	0.941	1.311	-39.3
USWES-9	1.452	0.640	1.118	1.129	-1.0
	1.452	0.649	1.046	1.108	-5.9
	1.452	0.651	0.997	1.103	-10.6
	1.452	0.664	0.931	1.071	-15.1
	1.452	0.677	0.985	1.040	-5.6
	1.452	0.694	0.863	0.999	-15.7
	1.452	0.731	0.764	0.910	-19.0
			average	error	10.6

**Table 3.9 Comparison of Results Between Using Reduced Hiding Function and Single Size Assumption**

Sources of data	using $D_{50}$		using $D_g$		using $D_g$ & $\Phi$		Hiding function	
	$A_d$	$M_e$	$A_d$	$M_e$	$A_d$	$M_e$	$A_d$	$M_e$
HRS USWES	2.380	2.477	2.502	2.291	1.189	2.182	1.291	2.026
Gibbs&Neill	0.324	2.057	0.317	2.057	1.078	2.080	1.067	2.014

The performance of the reduced hiding function is also shown in Figures 3.13 and 3.14. Figure 3.13 shows the comparison of observed and computed sediment transport capacity without the hiding function. Figure 3.14 shows the comparison of observed and computed sediment transport capacity when a reduced hiding function is employed. A clear improvement is obtained by using the reduced hiding function. Figure 3.15 shows the predicted transport capacity when the reduced hiding function and  $D_{50}$  are applied for data of HRS and USWES. In Figure 3.15 the ratio of calculated and observed values is chosen as 1/2 to 2, 1/3 to 3, 1/4 to 4 and 1/8 to 8. The percentage of correct predicted value in total is shown in the same figure. The detail information can be found in Table 3.10 which includes the percentage of correctly predicted values in total when four methods are used.

For the purpose of verification, the reduced hiding function was also tested using the independent data available in Gibbs and Neill (1972 & 1973). Results with and without the reduced hiding function are shown in Figures 3.16 and 3.17 respectively. Figures 3.16 and 3.17 show that the good improvements are achieved by using the reduced hiding function with  $M_e$  increasing from 0.324 to 0.598 and  $A_d$  decreasing from 2.057 to 1.955.

**Table 3.10 The Percentage of Correct Predicted Value in Total**

Sources of data	threshold	percentage of data in total			
		1/2 — 2	1/3 — 3	1/4 — 4	1/8 — 8
HRS USWES	$D_{50}$	42.3	62.1	69.3	84.8
	$D_g$	40.2	64.0	72.7	84.5
	$D_g$ and $\Phi$	63.5	77.1	82.4	90.0
	$\epsilon_j$	65.4	79.4	83.4	91.0
Gibbs & Neill	$D_{50}$	20.0	31.7	53.3	86.7
	$D_g$	20.0	31.7	53.3	86.7
	$D_g$ and $\Phi$	36.7	60.0	85.0	98.3
	$\epsilon_j$	38.3	68.3	86.6	98.3

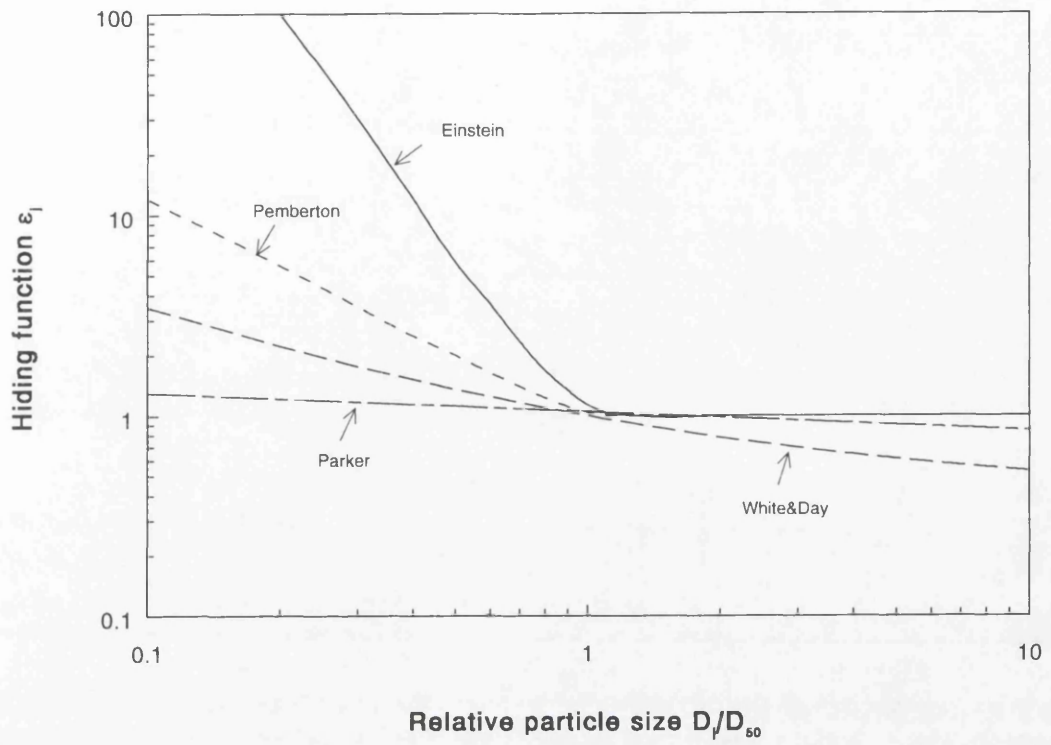


Figure 3.1 Hiding Functions: (i) Einstein; (ii) Pemberton; (iii) White and Day; (iv) Parker

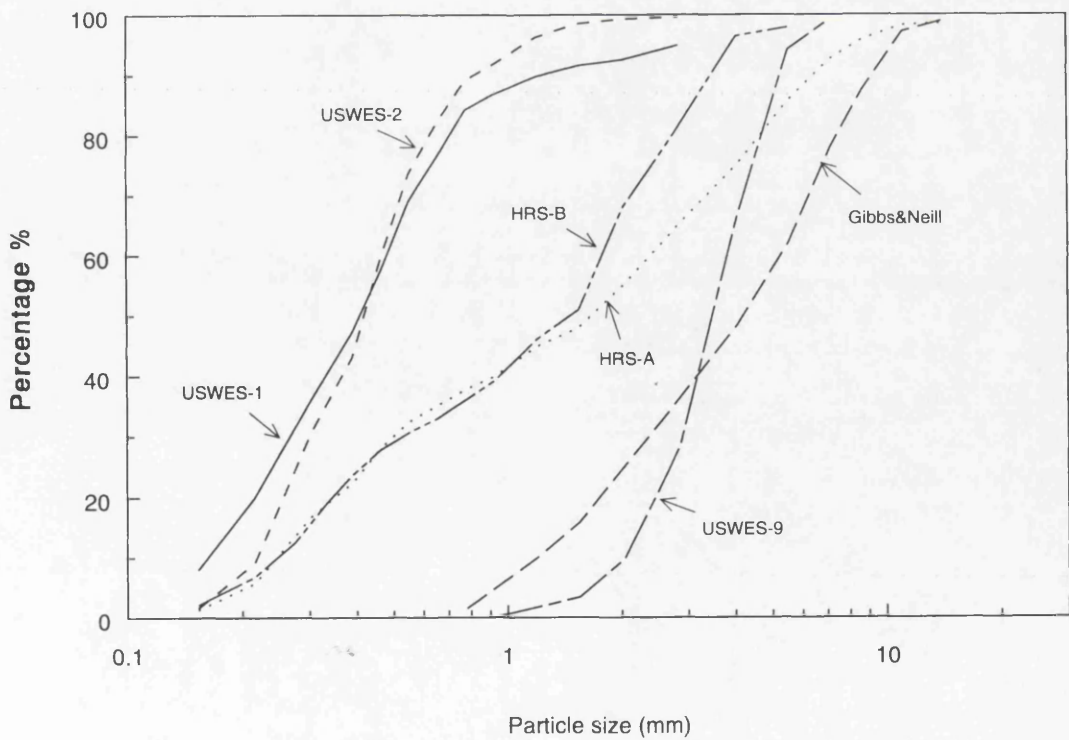


Figure 3.2 Grain Size Distributions For All Bed Material

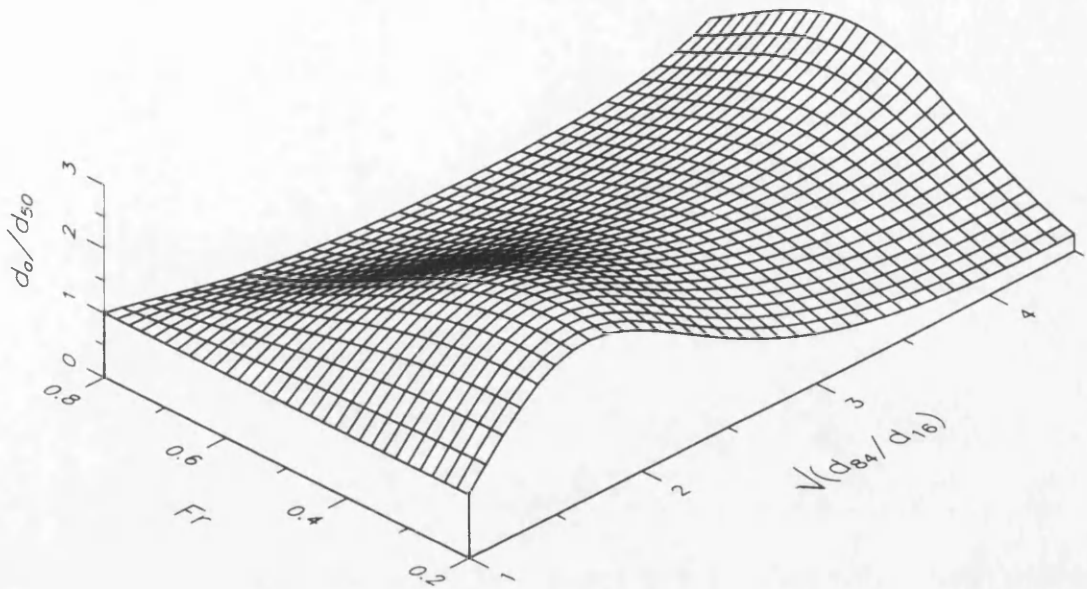


Figure 3.3 Scaling Size  $D_a$  Verse  $\sqrt{D_{84}/D_{16}}$  and  $Fr$

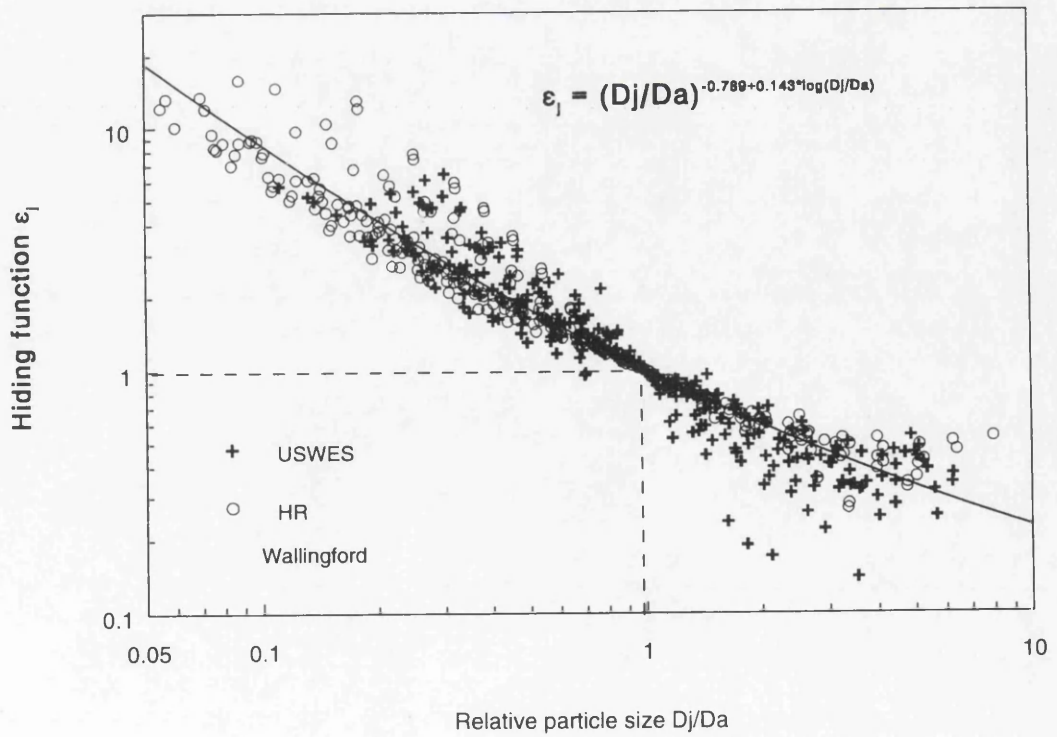


Figure 3.4 Hiding Function  $\epsilon_j$  Against Relative Particle Size  $D_j/D_a$

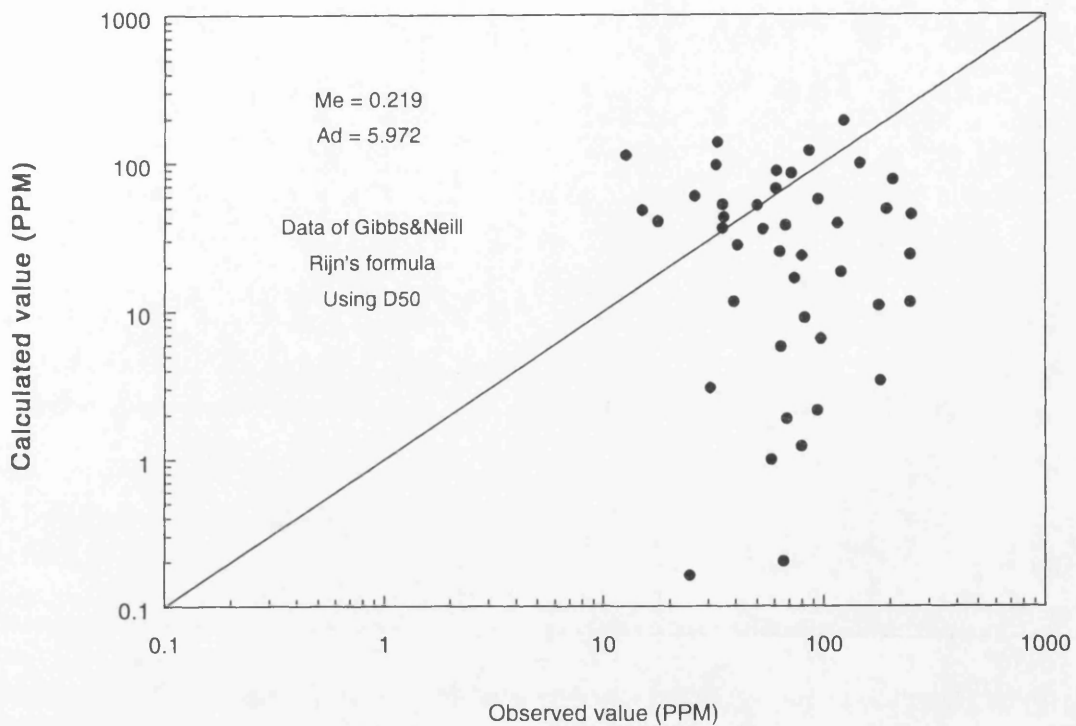


Figure 3.5 Comparison of Transport Capacity Between Calculated and Observed Values Without Hiding Function

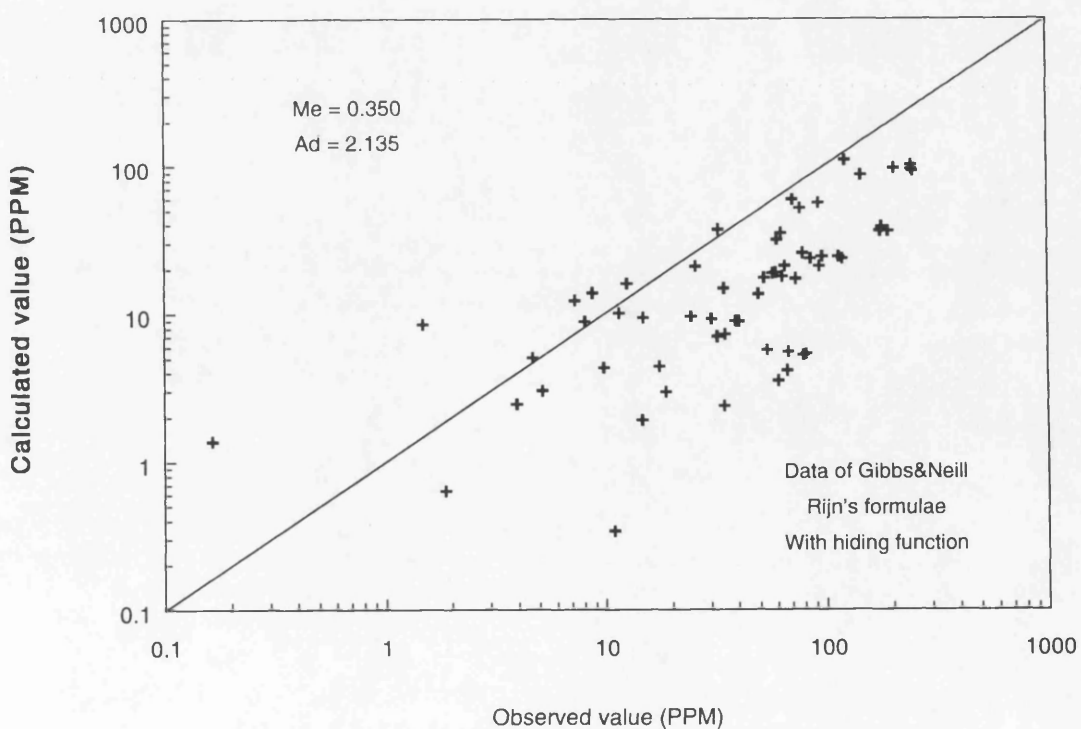


Figure 3.6 Comparison of Transport Capacity Between Calculated and Observed Values With Hiding Function

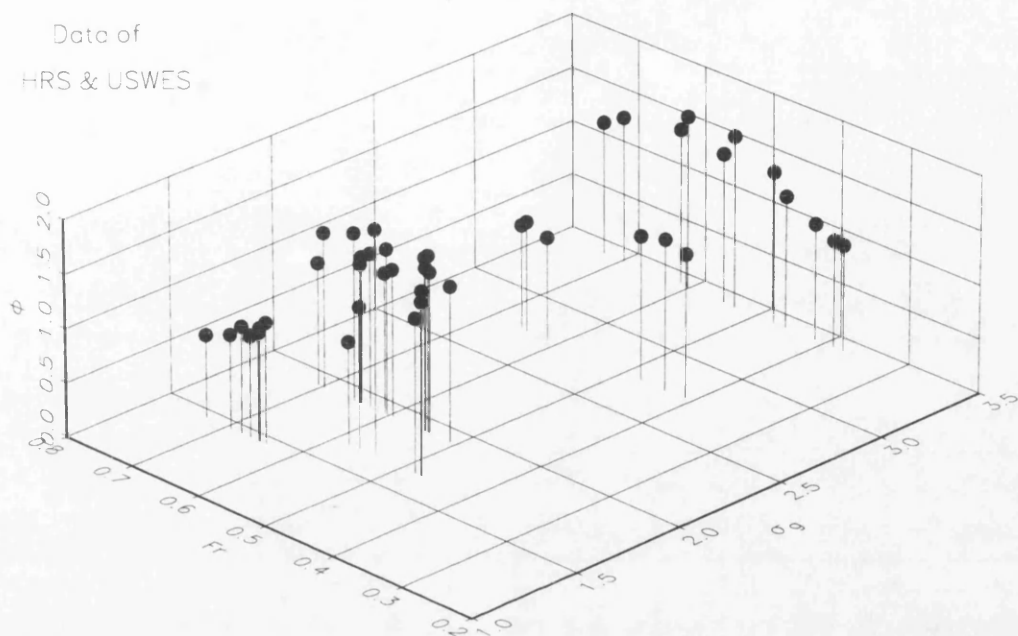


Figure 3.7  $\Phi$  Value Against  $\sigma_g$  and  $Fr$  From Data of Day and USWES

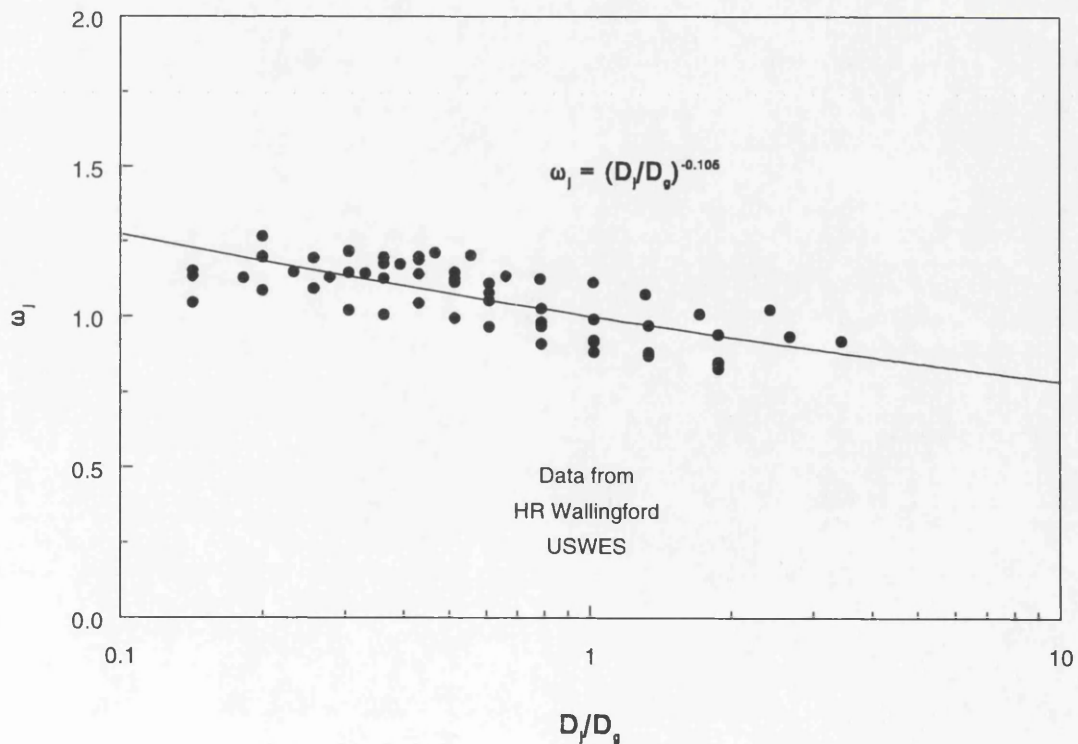


Figure 3.8  $\omega_j$  Value Against Relative Size  $D_j/D_g$

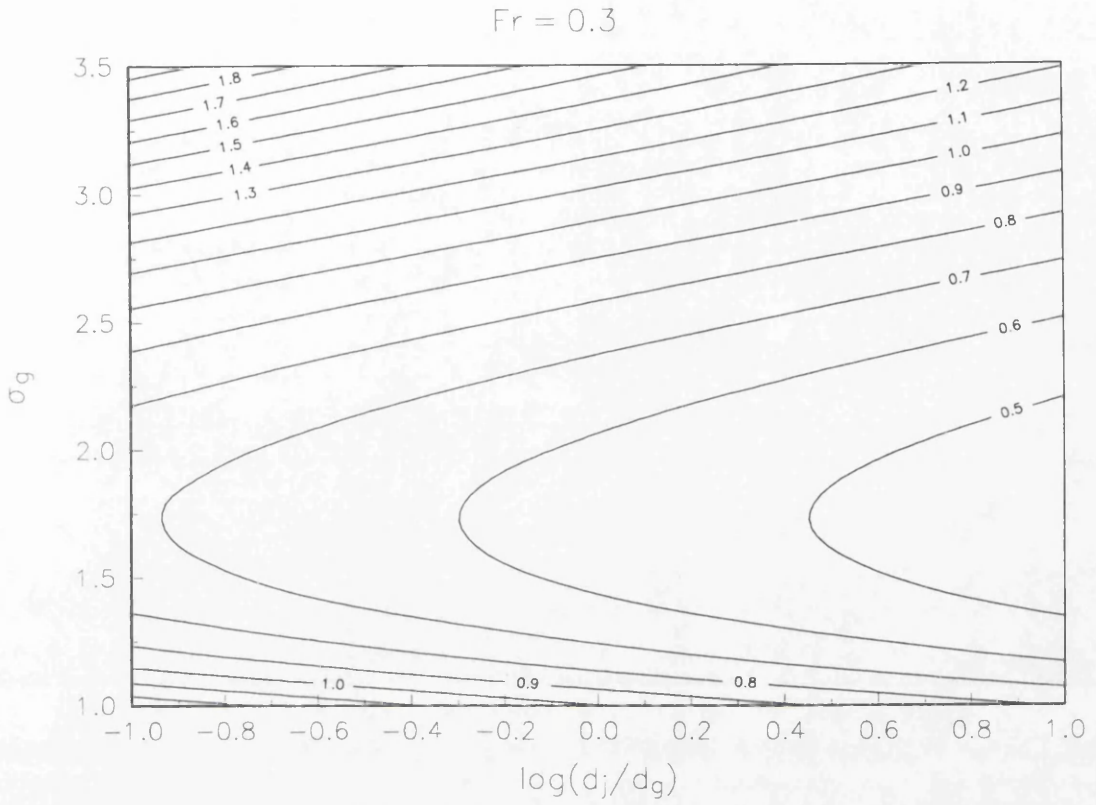


Figure 3.9  $g_j$  Against  $D_j/D_g$  and  $\sigma_g$  For  $Fr = 0.3$

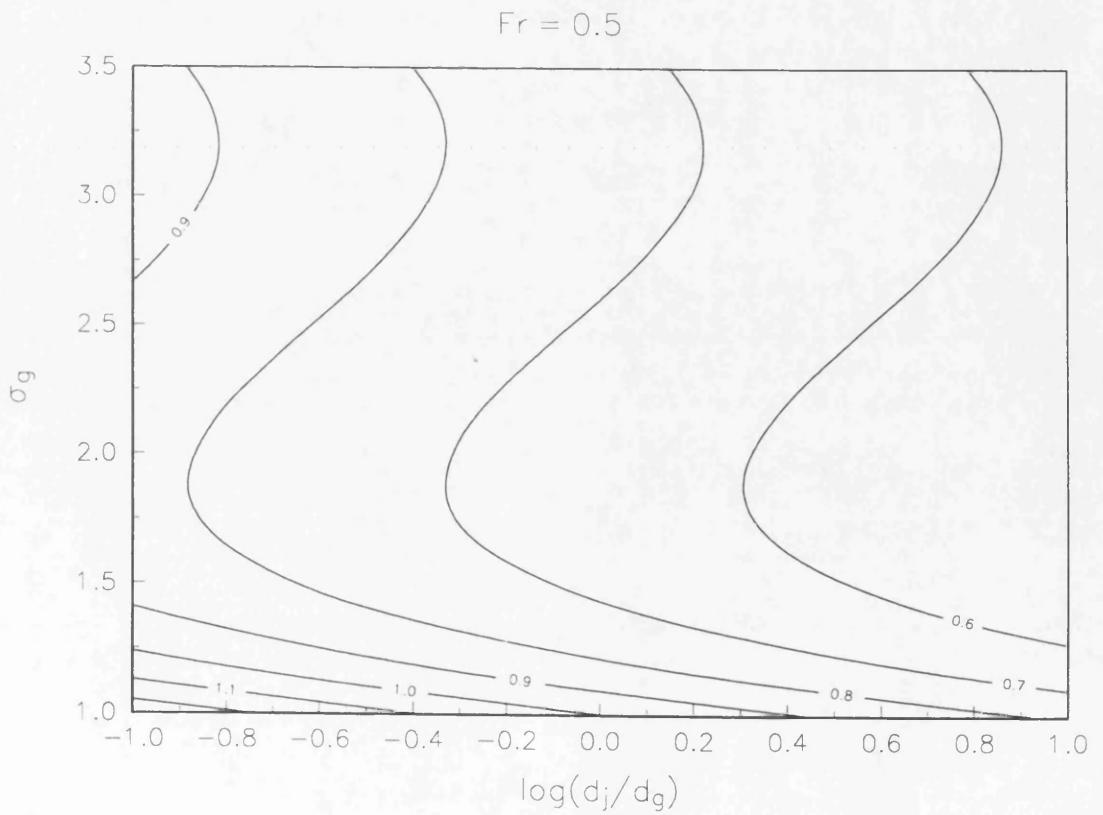


Figure 3.10  $g_j$  Against  $D_j/D_g$  and  $\sigma_g$  For  $Fr = 0.5$

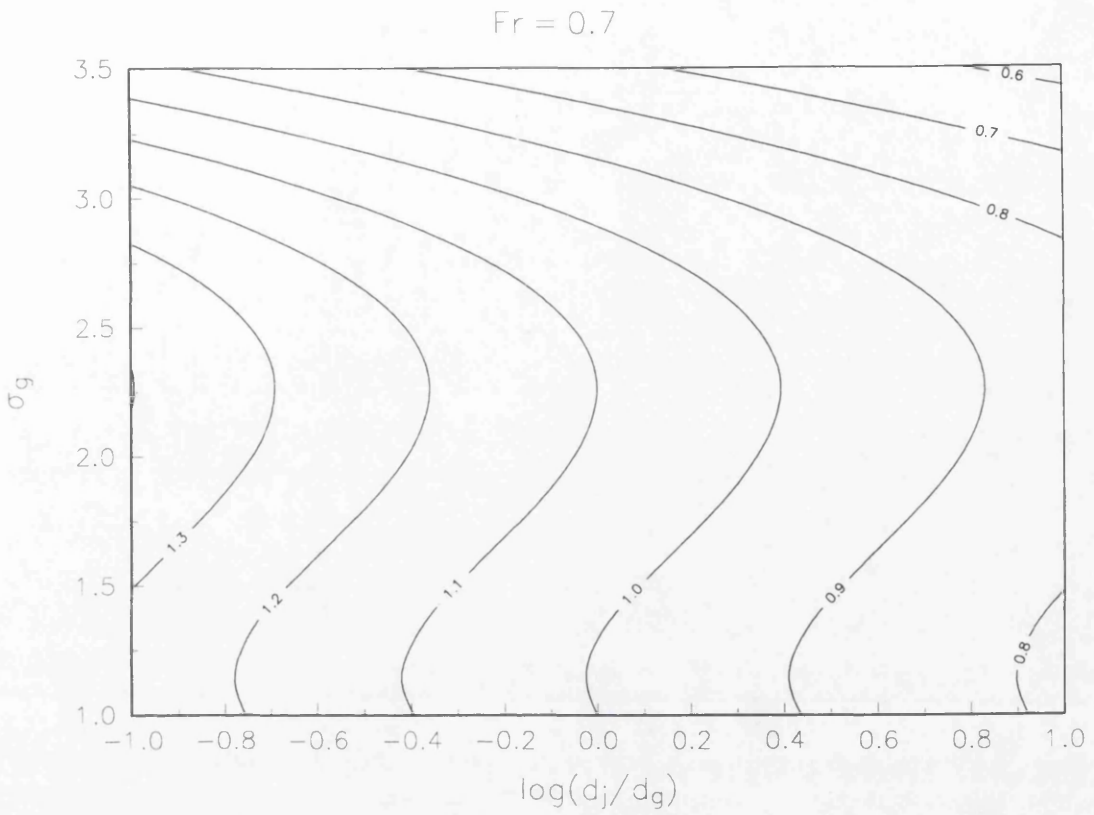


Figure 3.11  $g_j$  Against  $D_j/D_g$  and  $\sigma_g$  For  $Fr = 0.7$

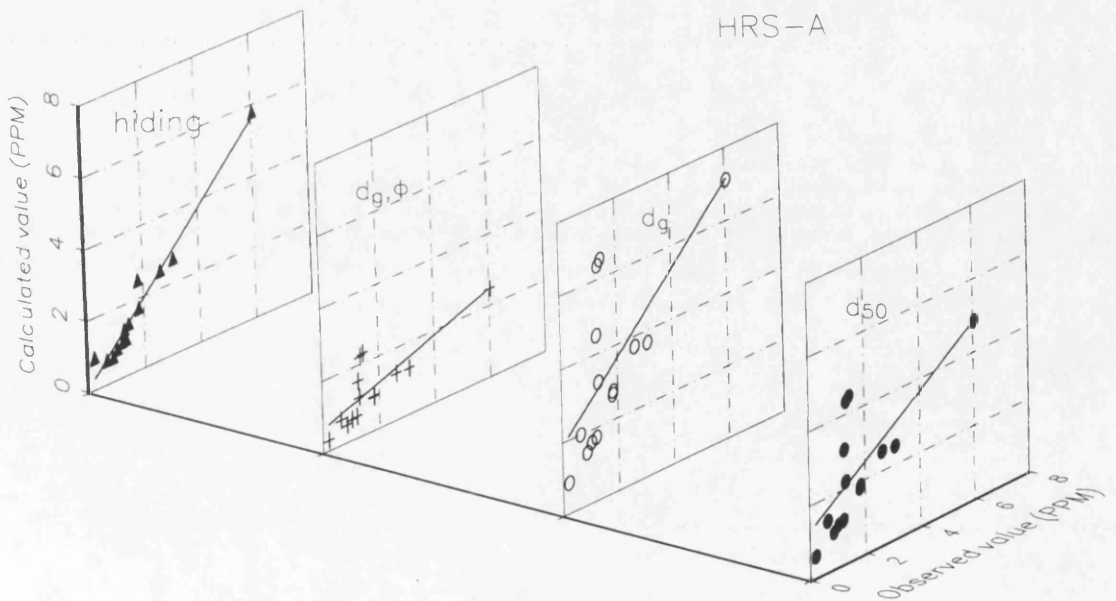


Figure 3.12 Comparison of Results Between Using Reduced Hiding Function and Single Size Assumption

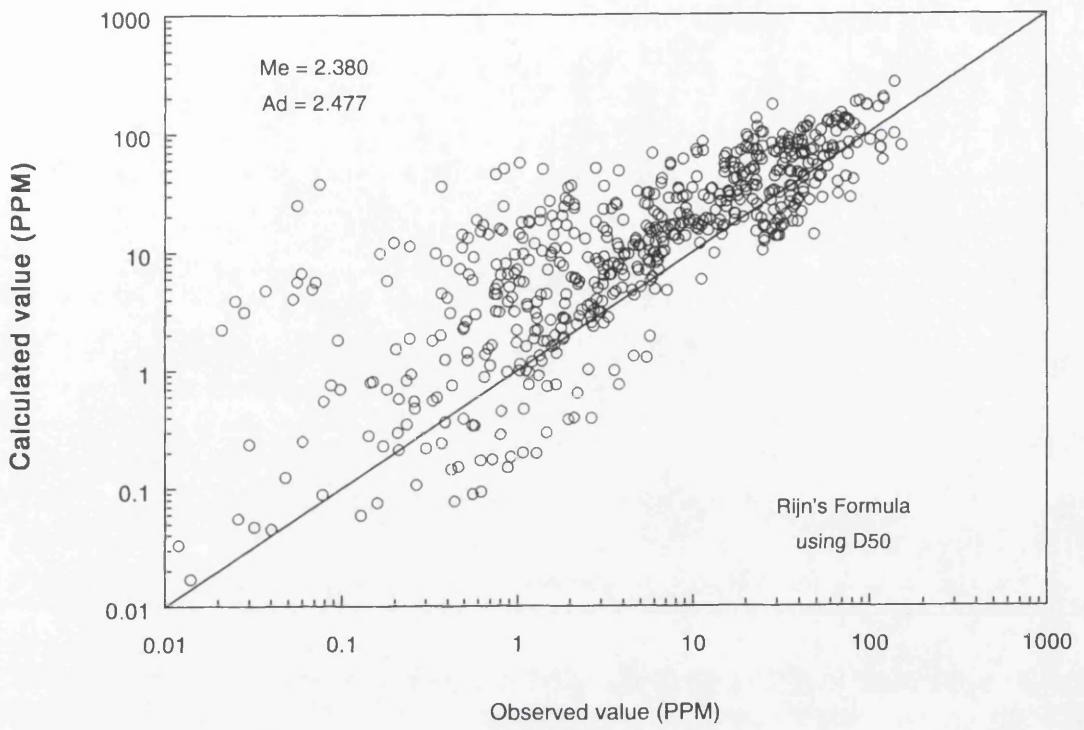


Figure 3.13 Comparison Between Observed and Calculated Transport Capacity For HRS and USWES Data Without Hiding Function

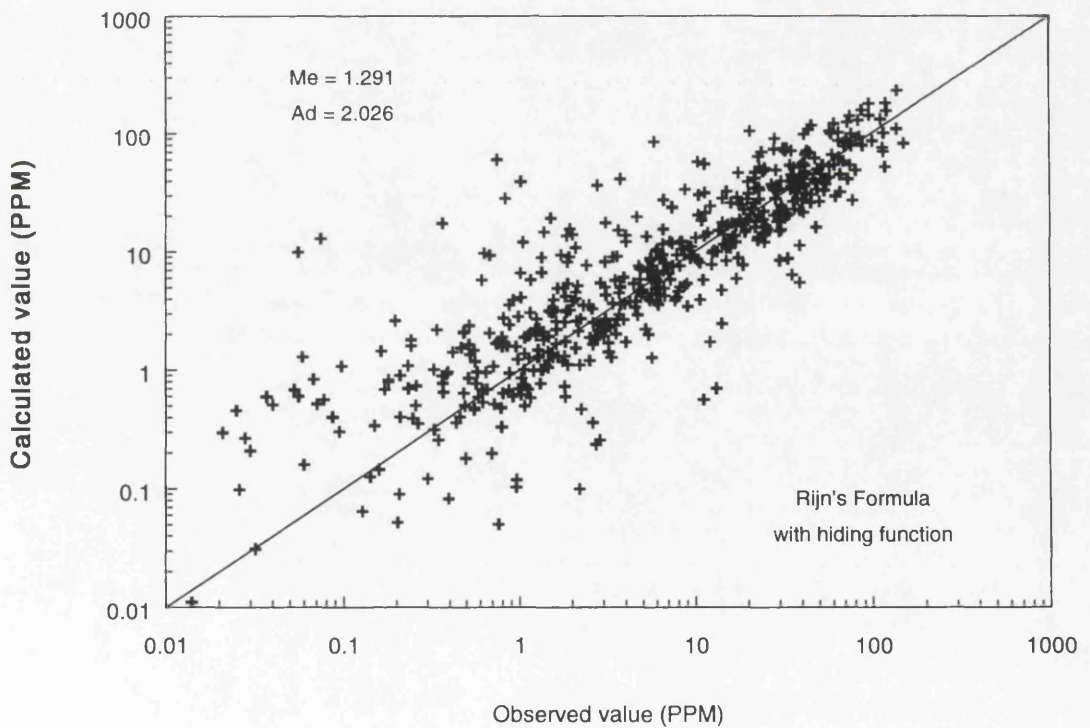


Figure 3.14 Comparison Between Observed and Calculated Transport Capacity For HRS and USWES Data With Reduced Hiding Function

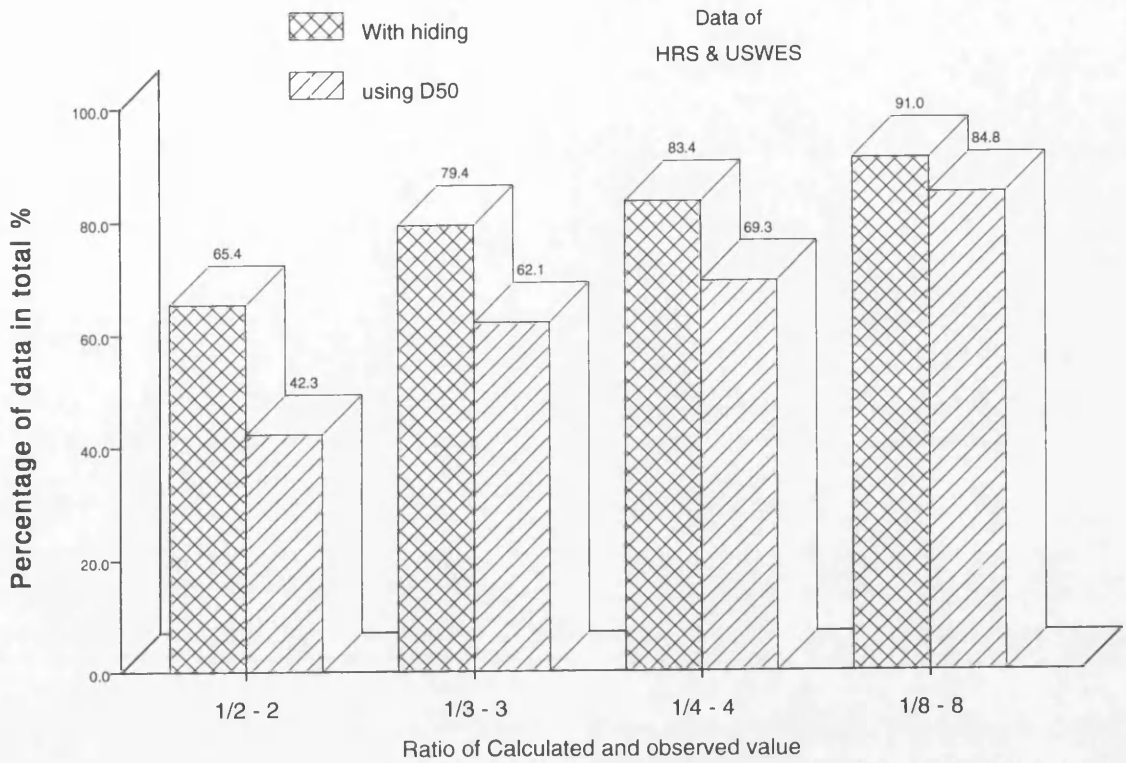


Figure 3.15 Transport Capacity Results of Using Reduced Hiding Function and D<sub>50</sub> For HRS and USWES Data

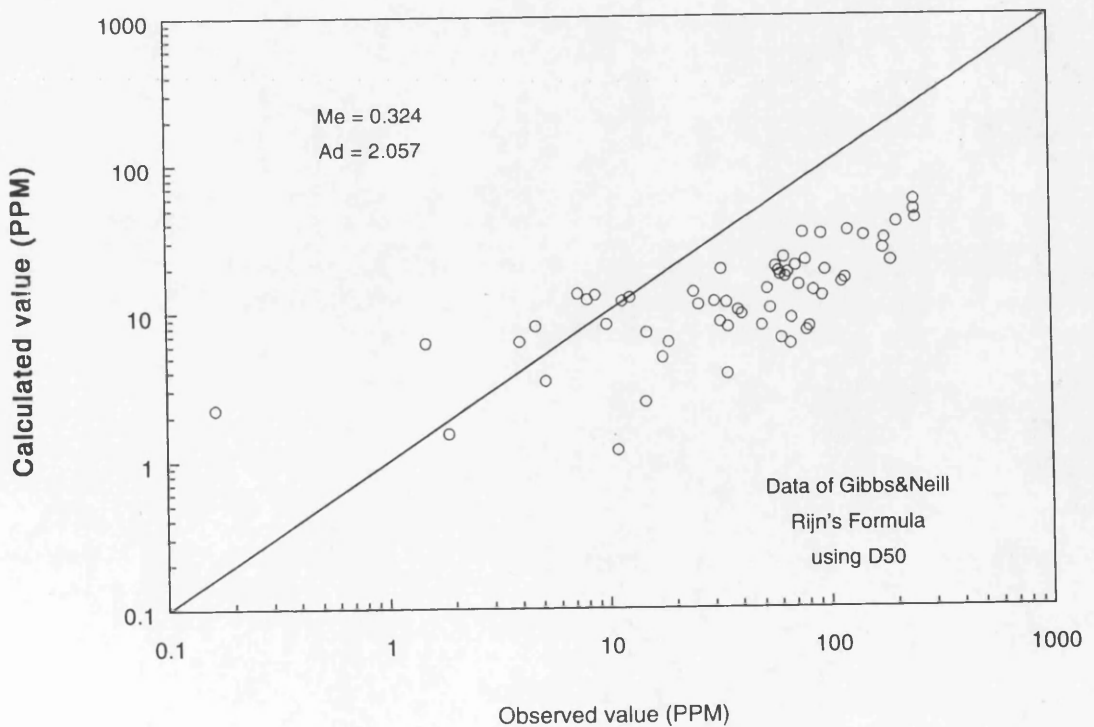


Figure 3.16 Comparison Between Observed and Calculated Transport Capacity For Gibbs & Neill Data Without Hiding Function

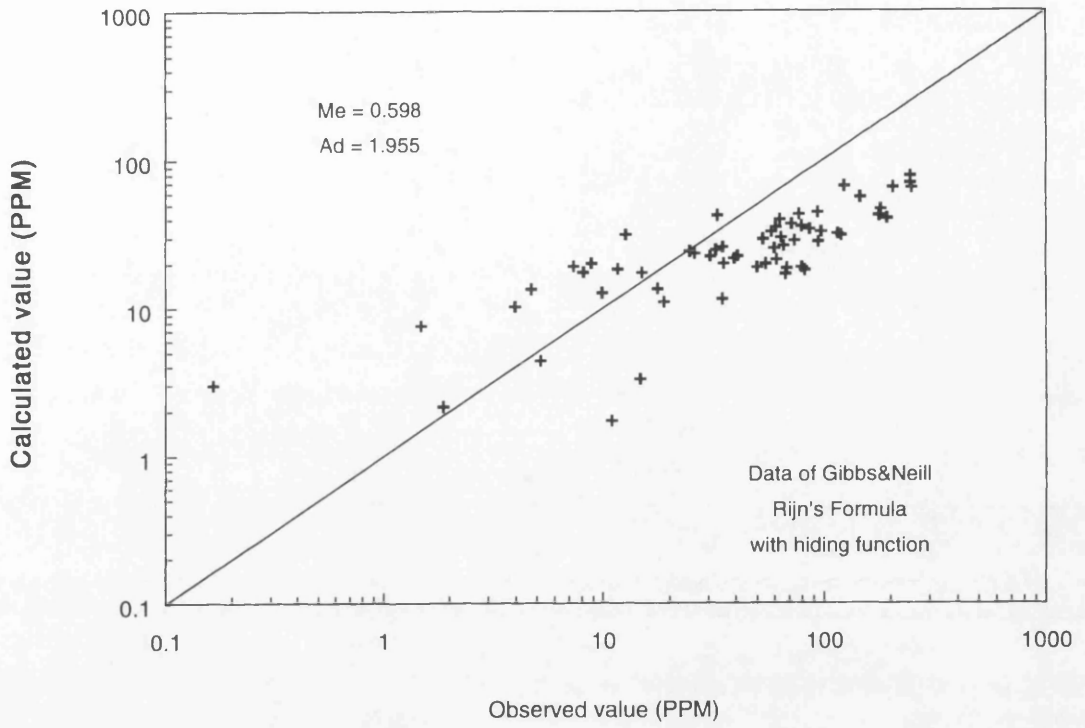


Figure 3.17 Comparison Between Observed and Calculated Transport Capacity For Gibbs&Neill Data With Reduced Hiding Function

## CHAPTER 4

### Numerical Model Development

#### 4.1 Equations For Graded Sediment Transport

The full details of the equations for the unsteady non-equilibrium graded sediment transport mathematical model have been described in Chapter 2. These include the water continuity, the water momentum, the conservation of suspended-load for each size fraction  $j$ , the conservation of bedload for each size fraction  $j$ , the bed material conservation and the bed material sorting.

$$B \frac{\partial Y}{\partial t} + \frac{\partial Q}{\partial x} - \frac{\partial Az}{\partial t} = q \quad (4.1)$$

$$\frac{\partial Q}{\partial t} + \frac{\partial(\beta Q^2/A)}{\partial x} + gA \frac{\partial Y}{\partial x} + gA \frac{Q|Q|}{K^2} = 0 \quad (4.2)$$

$$\frac{\partial C_j A}{\partial t} + \frac{\partial C_j Q}{\partial x} = \frac{\partial}{\partial x} (A D_j W_j) + \frac{Q}{L_j^*} (\beta_j C_j^* - C_j) + q C_{sj} \quad (4.3)$$

$$W_j = \frac{\partial C_j}{\partial x} \quad (4.4)$$

$$\frac{\partial G_j}{\partial t} + u_{bj} \frac{\partial G_j}{\partial x} = \frac{u_{bj}}{\lambda_j} (\beta_j G_j^* - G_j) + u_{bj} g_{sj} \quad (4.5)$$

$$(1-p) \frac{\partial Az}{\partial t} + \sum \frac{Q}{L_j^*} (\beta_j C_j^* - C_j) + \sum \frac{1}{\lambda_j} (\beta_j G_j^* - G_j) = 0 \quad (4.6)$$

$$\begin{aligned}
& (1-p)\frac{\partial}{\partial t}(Am\beta_j) + (1-p)\beta_j\left(\frac{\partial Az}{\partial t} - \frac{\partial Am}{\partial t}\right)u\left[\frac{\partial Az}{\partial t} - \frac{\partial Am}{\partial t}\right] + \\
& (1-p)\beta_{0j}\left(\frac{\partial Az}{\partial t} - \frac{\partial Am}{\partial t}\right)u\left[-\frac{\partial Az}{\partial t} + \frac{\partial Am}{\partial t}\right] + \\
& \frac{Q}{L_j^*}(\beta_j C_j^* - C_j) + \frac{1}{\lambda_j}(\beta_j G_j^* - G_j) = 0
\end{aligned} \tag{4.7}$$

where  $C_{sj}$  = the suspended-load concentration of lateral inflow or outflow for size fraction  $j$ ;  $g_{sj}$  = the unit bedload rate of lateral inflow or outflow for size fraction  $j$ ;  $W_j$  is defined as the gradient of the suspended-load concentration for size fraction  $j$  with respect to space. Hence the advection and dispersion equation of suspended-load transport is divided into two equations (4.3) and (4.4) each of which only contains the first derivative. Therefore all equations in the system contain the first derivative with respect to space and time. The reason for doing this will be explained in following sections. The reference of other variables can be found in Chapter 2. Total number of equations  $N$  can be calculated from

$$N = 3 + 4J \tag{4.8}$$

where  $J$  = the number of size fractions to represent whole graded material.

## 4.2 Brief Review of One-Dimensional Mobile Bed Model

The limitations of one-dimensional mobile bed models have been defined, by Bettess and White (1981), as

- i. All variables are averaged over a cross-section, and it is therefore not possible to determine how the values of variables change across the river width;
- ii. No account is taken of bends or any effects caused by bends;
- iii. A one-dimensional model cannot directly predict changes in the plan of a river;
- iv. Alternations in the plan of a river do not influence a one-dimensional model provided the overall length of the river under consideration does not change.

In certain circumstances, it is possible to reduce the number of equations. For example, where one is interested in the evolution of the river profile over a long period of time, and no flow reversal takes place, a quasi-steady flow assumption can be employed, see Cunge et al (1973), De Vries (1973), Chang (1976, 1982), Ponce et al (1979), Bettess and White (1981), Lyn (1987), Willetts et al (1987) and Bhallamudi (1991). In these papers the hydrodynamic equations (4.1) and (4.2) are simplified to steady flow equations and solved using a backwater calculation. Hence, the flow through the length of river under consideration is constant at any given time. Unsteady flow can be approximately reproduced by using a flow duration curve to obtain discharges for use in the backwater calculation.

In other circumstances, it is sufficient to simplify one or more of the equations. A common example of this is the assumption that sediment transport is in equilibrium. Here, the computed sediment transport rate at any reach is assumed equal to the transport capacity calculated from a suitable sediment transport formula. This assumption permits simplifications to be made to suspended-load, bedload transport and bed material conservation. Many examples of models using this assumption are described in the literature. Probably the most widely used the HEC-6 model developed by the US Corps of Engineers.

Models that are not based on the full set of governing equations are limited in their applications. The uni-directional quasi-steady flow simplification prevents such models being employed where one wishes to simulate the sudden release of water and sediment into a river, such as occurs with a reservoir flushing operation. In addition in circumstances where flow reversal takes place, such as in a tidal river reach, the simplifications make the model invalid. Models using the equilibrium sediment transport assumption give poor results where the sediment inflow through the upstream boundary differs greatly from the equilibrium value, or where one wishes to use the model to simulate the results of abstracting water or sediment from a river.

Recent publications have discussed the feasibility of developing a general one-dimensional mobile bed computer model, applicable to a wide range of circumstances, see Armanini and Silvio (1988), Rahuel (1989) and Holly and Rahuel (1990). Given the continued increasing availability of low cost high power computing facilities this is the way forward for computer simulation in mobile bed problems. Therefore the work described will focus on the development of such a numerical model.

### 4.3 Numerical Scheme

To date no analytical solution to equations (4.1) to (4.7) is available, however, numerical techniques exist for solving these equations, which means that it is feasible to develop a computer code for simulating graded sediment transport. The success of any numerical model in producing or predicting actual mobile bed behaviour requires (i) a good mathematical conceptualisation based on sound physical principles, (ii) some empirical sediment relationships, and (iii) a stable and convergent numerical scheme.

It was decided to use the Peissmann scheme in the development of the current model. The Preissmann scheme is an implicit finite difference scheme by which the unknown values at the future time level can be determined by a system of simultaneous algebraic equations that include statements of the boundary conditions. The Preissmann scheme is also referred to as the box or four point scheme. The reasons for this choice are explained as follows.

The Peissmann scheme is considered to be robust, flexible and user-friendly, see Abbott (1989). The greatest advantage of the Preissmann scheme is that should unforeseen conditions cause the value of the Courant number to exceed one locally during the computation, the overall computation will still remain stable. Unlike explicit schemes in which some safety margin is needed to ensure a Courant number less than one and prevent the computation from becoming unstable. However, the

uncontrolled use of a Courant number greater than one is not recommended as phase errors are introduced which can be excessive. Control has therefore to be kept on Courant number in practical computations. So long as this control is kept, the Preissmann scheme is ideal for use in a general purpose modelling system.

Another advantage of the Preissmann scheme is that it is fully compact so that all variables are computed at each grid point at every time step. This compactness has many advantages, especially at the boundaries. It has been found that the Preissmann scheme can be used to treat different type of boundaries and internal boundaries such as the multiply-connected system, and different types of flows such as sub- and supercritical flows and mixed type flows, see Abbott (1989).

The Preissmann scheme is sensitive to boundary and internal data structures that are in turn transmitted through the solution domain to appear at all points within the solution. Therefore the appropriate algorithmic procedure is needed to suppress computer errors and divergence of the numerical algorithm.

The time and space weighting parameters in the Preissmann scheme can be adjusted to satisfy the numerical requirements. For example, a small value 0.55 of the time weighting parameter can be used to provide a good resolution for flood or tidal simulations. But for the long term simulation of bed evolution in the mobile bed river, it is possible to employ a larger value such as unity so that a larger time increment such as a few days can be applied.

US Government Agencies such as the National Weather Service and Geological Survey are making extensive practical use of the Preissmann scheme for open channel flow problems, apparently to the exclusion of almost all other methods, see Fread (1980) and Schaffranek et al (1981). The reference books by Abbott (1979, 1989) and Cunge et al (1980) give extensive coverage to the method.

#### **4.4 Preissmann Scheme**

A schematic representation of the Preissmann operator is shown in Figure 4.1.

Let  $f(x,t)$  be any one dependent variable. Then the Preissmann scheme is

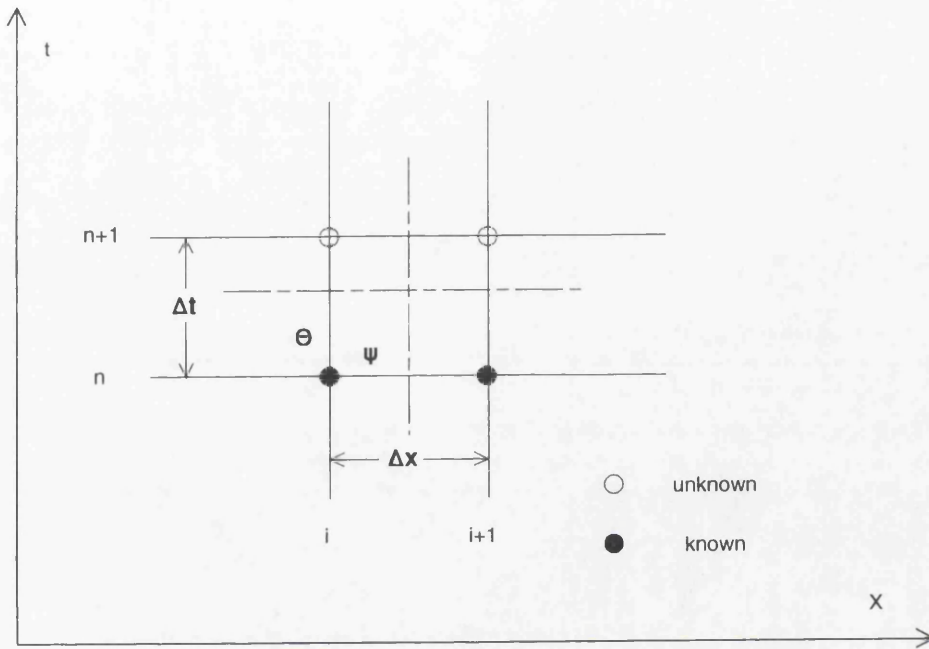


Figure 4.1 Preissmann Scheme

$$\frac{\partial f}{\partial t} \approx (1-\psi) \frac{f_i^{n+1} - f_i^n}{\Delta t} + \psi \frac{f_{i+1}^{n+1} - f_{i+1}^n}{\Delta t} \quad (4.9)$$

$$\frac{\partial f}{\partial x} \approx (1-\theta) \frac{f_{i+1}^n - f_i^n}{\Delta x} + \theta \frac{f_{i+1}^{n+1} - f_i^{n+1}}{\Delta x} \quad (4.10)$$

$$f \approx (1-\psi)(1-\theta)f_i^n + \psi(1-\theta)f_{i+1}^n + (1-\psi)\theta f_i^{n+1} + \psi\theta f_{i+1}^{n+1} \quad (4.11)$$

where  $\psi$  is a space weighting factor ( $0 \leq \psi \leq 1$ ) and  $\theta$  is a time weighting factor ( $0 \leq \theta \leq 1$ ). Taking  $\theta > 0.5$  introduces a truncation error that produces numerical dissipation. It is normal practice to take  $\psi = 0.5$ , see Abbott (1989).

Equations (4.9), (4.10) and (4.11) can be rewritten in compact form as

$$\tau[f] = (1 - \psi) \frac{f_i^{n+1} - f_i^n}{\Delta t} + \psi \frac{f_{i+1}^{n+1} - f_{i+1}^n}{\Delta t} \quad (4.12)$$

$$\delta[f] = (1 - \theta) \frac{f_{i+1}^n - f_i^n}{\Delta x} + \theta \frac{f_{i+1}^{n+1} - f_i^{n+1}}{\Delta x} \quad (4.13)$$

$$\mu[f] = (1 - \psi)(1 - \theta)f_i^n + \psi(1 - \theta)f_{i+1}^n + (1 - \psi)\theta f_i^{n+1} + \psi\theta f_{i+1}^{n+1} \quad (4.14)$$

Equations (4.12), (4.13) and (4.14) can be used to discretise the system (4.1) to (4.7) into non-linear equations as follows

$$F_1 = \mu[B] \tau[Y] + \delta[Q] - \tau[Az] - \mu[q] = 0 \quad (4.15)$$

$$F_2 = \tau[Q] + \delta\left[\beta \frac{Q^2}{A}\right] + g\mu[A] \delta[Y] + g\mu\left[\frac{AQ|Q|}{K^2}\right] = 0 \quad (4.16)$$

$$F_{3j} = \tau[C_j A] + \delta[C_j Q] - \delta[AD_j W_j] - \mu\left[\frac{Q}{L_j^*}(\beta_j C_j^* - C_j) + qC_{sj}\right] = 0 \quad (4.17)$$

$$F_{4j} = \mu[W_j] - \delta[C_j] = 0 \quad (4.18)$$

$$F_{5j} = \tau[G_j] + \mu[u_{bj}] \delta[G_j] - \mu\left[\frac{u_{bj}}{\lambda_j}(\beta_j G_j^* - G_j) + u_{bj} q_{sj}\right] = 0 \quad (4.19)$$

$$F_6 = (1 - p) \tau[Az] + \sum \mu\left[\frac{Q}{L_j^*}(\beta_j C_j^* - C_j)\right] + \sum \mu\left[\frac{1}{\lambda_j}(\beta_j G_j^* - G_j)\right] = 0 \quad (4.20)$$

$$\begin{aligned} F_{7j} &= (1 - p) \tau[Am\beta_j] + (1 - p) \mu[\beta_j] \{\tau[Az] - \tau[Am]\} u[\tau[Az] - \tau[Am]] \\ &\quad + (1 - p) \mu[\beta_{0j}] \{\tau[Az] - \tau[Am]\} u[-\tau[Az] + \tau[Am]] \\ &\quad + \mu\left[\frac{Q}{L_j^*}(\beta_j C_j^* - C_j)\right] + \mu\left[\frac{1}{\lambda_j}(\beta_j G_j^* - G_j)\right] = 0 \end{aligned} \quad (4.21)$$

### 4.5 Newton-Raphson Method

The algebraic equations from (4.15) to (4.21) can now be linearized within a time increment by using the Newton-Raphson method. After linearization of all equations, the new linear system can be solved to obtain estimates for all variables at the future time level. This process must be iterated until some convergence criterion is satisfied, such as one corresponding to the required accuracy.

The Newton-Raphson method for multi variables can be written as

$$F(X_{i,j}, X_{i+1,j}) = 0, \quad j = 1, 2, \dots, N$$

$$\sum_{j=1}^N \frac{\partial F(X_{i,j}^m, X_{i+1,j}^m)}{\partial X_{i,j}^m} \Delta X_{i,j}^{m+1} + \sum_{j=1}^N \frac{\partial F(X_{i,j}^m, X_{i+1,j}^m)}{\partial X_{i+1,j}^m} \Delta X_{i+1,j}^{m+1} + F(X_{i,j}^m, X_{i+1,j}^m) = 0$$

$$\Delta X_{i,j}^{m+1} = X_{i,j}^{m+1} - X_{i,j}^m, \quad \Delta X_{i+1,j}^{m+1} = X_{i+1,j}^{m+1} - X_{i+1,j}^m$$

(4.22)

where  $F$  = the any equation from (4.15) to (4.21);  $i$  = the grid point,  $i = 1, 2, \dots, I$ ;  $m$  = the number of iterations;  $X_{i,j}$  and  $X_{i+1,j}$  = the independent variables which are expressed as

$$\{X_i\}^{-1} = \{Q_i, Y_i, C_{1,i}, C_{2,i}, \dots, C_{J,i}, W_{1,i}, W_{2,i}, \dots, W_{J,i}, G_{1,i}, G_{2,i}, \dots, G_{J,i}, Az, \beta_{1,i}, \beta_{2,i}, \dots, \beta_{J,i}\} \quad (4.23)$$

$$\{X_{i+1}\}^{-1} = \{Q_{i+1}, Y_{i+1}, C_{1,i+1}, C_{2,i+1}, \dots, C_{J,i+1}, W_{1,i+1}, W_{2,i+1}, \dots, W_{J,i+1}, G_{1,i+1}, G_{2,i+1}, \dots, G_{J,i+1}, Az, \beta_{1,i+1}, \beta_{2,i+1}, \dots, \beta_{J,i+1}\} \quad (4.24)$$

Equation (4.22) can be rewritten in the form of

$$[L_i]\{\Delta X_i\} + [R_i]\{\Delta X_{i+1}\} + \{S_i\} = 0 \quad (4.25)$$

where  $[L_i]$ ,  $[R_i]$  are  $N \times N$  matrix;  $\{S_i\} = 1 \times N$  matrix.

$$[L_i] = \left[ \frac{\partial F_{k,i}^m}{\partial \{X_i\}^m} \right]_{N \times N} = \begin{bmatrix} L_{i,11} & L_{i,12} & L_{i,13} & \cdots & L_{i,1N} \\ L_{i,21} & L_{i,22} & L_{i,23} & \cdots & L_{i,2N} \\ \vdots & & & & \\ \vdots & & & & \\ L_{i,N1} & L_{i,N2} & L_{i,N3} & \cdots & L_{i,NN} \end{bmatrix} \quad (4.26)$$

$$[R_i] = \left[ \frac{\partial F_{k,i}^m}{\partial \{X_{i+1}\}^m} \right]_{N \times N} = \begin{bmatrix} R_{i,11} & R_{i,12} & R_{i,13} & \cdots & R_{i,1N} \\ R_{i,21} & R_{i,22} & R_{i,23} & \cdots & R_{i,2N} \\ \vdots & & & & \\ \vdots & & & & \\ R_{i,N1} & R_{i,N2} & R_{i,N3} & \cdots & R_{i,NN} \end{bmatrix} \quad (4.27)$$

$$\{S_i\}^{-1} = \{F_{1,i}^m, F_{2,i}^m, \dots, F_{N,i}^m\} = \{S_{i,1}, S_{i,2}, \dots, S_{i,N}\} \quad (4.28)$$

The speed of convergence for successive solutions of the linearized systems to the non-linear solution depends on the definition of the coefficients, see Abbott (1989). The Newton-Raphson method is one in which the coefficients are defined as derivatives of the updated functions with respect to the dependent variables, and the rate of convergence is of second or high order. This necessitates rewriting (4.25) in terms of differential changes in variables and a subsequent redefinition of all coefficients.

It has been found that for strong non-linear system, the Newton-Raphson method can produce divergence. This divergence can be prevented by using a tolerance coefficient or relaxation parameter  $\alpha$  the value of which is between 0 to 1. Therefore a new value in  $m+1$  iteration is calculated using  $\{X_i\}^{m+1} = \{X_i\}^m + \alpha\{\Delta X_i\}^{m+1}$ .

The Preissmann scheme as used for general purpose modelling systems is built upon this principle, see Liggett and Cunge (1975), Cunge et al (1980) and Holly and Rahuel (1990). Applying Newton-Raphson (4.22) to equations (4.15) to (4.21) results in the coefficients in equation (4.25), developed in the sections 4.5.1 to 4.5.6.

### 4.5.1 Discretion of Water Continuity Equation

The water continuity equation (4.15) can be discretised as

$$L_{i,11} = \frac{\partial F_{1,i}^m}{\partial (Q_i^{n+1})^m} = -\frac{\theta}{\Delta x}$$

$$L_{i,12} = \frac{\partial F_{1,i}^m}{\partial (Y_i^{n+1})^m} = \mu[B] \frac{1-\psi}{\Delta t}$$

$$L_{i,1,3+3J} = \frac{\partial F_{1,i}^m}{\partial (Az_i^{n+1})^m} = -\frac{1-\psi}{\Delta t}$$

$$R_{i,11} = \frac{\partial F_{1,i}^m}{\partial (Q_{i+1}^{n+1})^m} = \frac{\theta}{\Delta x}$$

$$R_{i,12} = \frac{\partial F_{1,i}^m}{\partial (Y_{i+1}^{n+1})^m} = \mu[B] \frac{\psi}{\Delta t}$$

$$R_{i,1,3+3J} = \frac{\partial F_{1,i}^m}{\partial (Az_{i+1}^{n+1})^m} = -\frac{\psi}{\Delta t}$$

$$S_{i,1} = F_{1,i}^m$$

$$= \left( (1-\psi)(1-\theta)B_i^n + \psi(1-\theta)B_{i+1}^n + (1-\psi)\theta(B_i^{n+1})^m + \psi\theta(B_{i+1}^{n+1})^m \right).$$

$$\left( (1-\psi) \frac{(Y_i^{n+1})^m - Y_i^n}{\Delta t} + \psi \frac{(Y_{i+1}^{n+1})^m - Y_i^n}{\Delta t} \right) -$$

$$\left( (1-\theta) \frac{Y_{i+1}^n - Y_i^n}{\Delta x} + \theta \frac{(Y_{i+1}^{n+1})^m - (Y_i^{n+1})^m}{\Delta x} \right) -$$

$$\left( (1-\psi)(1-\theta)q_i^n + \psi(1-\theta)q_{i+1}^n + (1-\psi)\theta(q_i^{n+1})^m + \psi\theta(q_{i+1}^{n+1})^m \right)$$

#### 4.5.2 Discretion of Water Momentum Equation

The water momentum equation (4.16) can be discretised as

$$L_{i,21} = \frac{\partial F_{2,i}^m}{\partial (Q_i^{n+1})^m} = \frac{1-\psi}{\Delta t} - 2\beta \frac{\theta}{\Delta x} \left( \frac{Q_i^{n+1}}{A_i^{n+1}} \right)^m + 2g\theta(1-\psi) \left( \frac{A_i^{n+1}|Q_i^{n+1}|}{(K_i^{n+1})^2} \right)^m$$

$$L_{i,22} = \frac{\partial F_{2,i}^m}{\partial (Y_i^{n+1})^m} = -g\mu[A] \frac{\theta}{\Delta x}$$

$$R_{i,21} = \frac{\partial F_{2,i}^m}{\partial (Q_{i+1}^{n+1})^m} = \frac{\psi}{\Delta t} + 2\beta \frac{\theta}{\Delta x} \left( \frac{Q_{i+1}^{n+1}}{A_{i+1}^{n+1}} \right)^m + 2g\theta\psi \left( \frac{A_{i+1}^{n+1}|Q_{i+1}^{n+1}|}{(K_{i+1}^{n+1})^2} \right)^m$$

$$R_{i,22} = \frac{\partial F_{2,i}^m}{\partial (Y_{i+1}^{n+1})^m} = g\mu[A] \frac{\theta}{\Delta x}$$

$$S_{i,2} = F_{2,i}^m = (1-\psi) \frac{(Q_i^{n+1})^m - Q_i^n}{\Delta t} + \psi \frac{(Q_{i+1}^{n+1})^m - Q_{i+1}^n}{\Delta t} +$$

$$(1-\theta)\beta \frac{(Q_{i+1}^n)^2/A_{i+1}^n - (Q_i^n)^2/A_i^n}{\Delta x} +$$

$$\theta\beta \frac{\left( (Q_{i+1}^n)^2/A_{i+1}^n \right)^m - \left( (Q_i^n)^2/A_i^n \right)^m}{\Delta x}$$

$$g \left\{ (1-\psi)(1-\theta)A_i^n + \psi(1-\theta)A_{i+1}^n + (1-\psi)\theta(A_i^{n+1})^m + \psi\theta(A_{i+1}^{n+1})^m \right\}.$$

$$\left\{ (1-\theta) \frac{Y_{i+1}^n - Y_i^n}{\Delta x} + \theta \frac{(Y_{i+1}^{n+1})^m - (Y_i^{n+1})^m}{\Delta x} \right\} +$$

$$g \left\{ (1-\psi)(1-\theta) \frac{A_i^n Q_i^n |Q_i^n|}{(K_i^n)^2} + \psi(1-\theta) \frac{A_{i+1}^n Q_{i+1}^n |Q_{i+1}^n|}{(K_{i+1}^n)^2} + \right. \\ \left. (1-\psi)\theta \left( \frac{A_i^{n+1} Q_i^{n+1} |Q_i^{n+1}|}{(K_i^{n+1})^2} \right)^m + \psi\theta \left( \frac{A_{i+1}^{n+1} Q_{i+1}^{n+1} |Q_{i+1}^{n+1}|}{(K_{i+1}^{n+1})^2} \right)^m \right\}$$

### 4.5.3 Discretion of Suspended-load Transport Equations

Equation (4.17) can be discretised as

$$L_{i,3j,1} = \frac{\partial F_{3j,i}^m}{\partial (Q_i^{n+1})^m} = -\frac{\theta}{\Delta x} (C_{j,i}^{n+1})^m - \theta(1-\psi) \left( \frac{\beta_{j,i}^{n+1} C_{j,i}^{*,n+1} - C_{j,i}^{n+1}}{L_{j,i}^{*,n+1}} \right)^m$$

$$L_{i,3j,2+j} = \frac{\partial F_{3j,i}^m}{\partial (C_{j,i}^{n+1})^m} = \frac{1-\psi}{\Delta t} (A_i^{n+1})^m - \frac{\theta}{\Delta x} (Q_i^{n+1})^m + \theta(1-\psi) \left( \frac{Q_i^{n+1}}{L_{j,i}^{*,n+1}} \right)^m$$

$$L_{i,3j,2+J+j} = \frac{\partial F_{3j,i}^m}{\partial (W_{j,i}^{n+1})^m} = \frac{\theta}{\Delta x} (A_i^{n+1} D_{j,i}^{n+1})^m$$

$$L_{i,3j,3+3J+j} = \frac{\partial F_{3j,i}^m}{\partial (\beta_{j,i}^{n+1})^m} = -\theta(1-\psi) \left( \frac{Q_i^{n+1} C_{j,i}^{*,n+1}}{L_{j,i}^{*,n+1}} \right)^m$$

$$R_{i,3j,1} = \frac{\partial F_{3j,i}^m}{\partial (Q_{i+1}^{n+1})^m} = \frac{\theta}{\Delta x} (C_{j,i+1}^{n+1})^m - \theta\psi \left( \frac{\beta_{j,i+1}^{n+1} C_{j,i+1}^{*,n+1} - C_{j,i+1}^{n+1}}{L_{j,i+1}^{*,n+1}} \right)^m$$

$$R_{i,3j,2+j} = \frac{\partial F_{3j,i}^m}{\partial (C_{j,i+1}^{n+1})^m} = \frac{\psi}{\Delta t} (A_{i+1}^{n+1})^m + \frac{\theta}{\Delta x} (Q_{i+1}^{n+1})^m + \theta\psi \left( \frac{Q_{i+1}^{n+1}}{L_{j,i+1}^{*,n+1}} \right)^m$$

$$R_{i,3j,2+J+j} = \frac{\partial F_{3j,i}^m}{\partial (W_{j,i+1}^{n+1})^m} = -\frac{\theta}{\Delta x} (A_{i+1}^{n+1} D_{j,i+1}^{n+1})^m$$

$$\begin{aligned}
 R_{i,3j,3+3j} &= \frac{\partial F_{3j,i}^m}{\partial (\beta_{j,i+1}^{n+1})^m} = -\theta \psi \left( \frac{Q_i^{n+1} C_{j,i+1}^{*,n+1}}{L_{j,i+1}^{*,n+1}} \right)^m \\
 S_{i,3j} &= F_{3j,i}^m = (1-\psi) \frac{(C_{j,i}^{n+1} A_i^{n+1})^m - C_{j,i}^n A_i^n}{\Delta t} + \psi \frac{(C_{j,i+1}^{n+1} A_{i+1}^{n+1})^m - C_{j,i+1}^n A_{i+1}^n}{\Delta t} + \\
 & (1-\theta) \frac{C_{j,i+1}^n Q_{i+1}^n - C_{j,i}^n Q_i^n}{\Delta x} + \theta \frac{(C_{j,i+1}^{n+1} Q_{i+1}^{n+1})^m - (C_{j,i}^{n+1} Q_i^{n+1})^m}{\Delta x} - \\
 & \left\{ (1-\theta) \frac{A_{i+1}^n D_{j,i+1}^n W_{j,i+1}^n - A_i^n D_{j,i}^n W_{j,i}^n}{\Delta x} + \right. \\
 & \left. + \theta \frac{(A_{i+1}^{n+1} D_{j,i+1}^{n+1} W_{j,i+1}^{n+1})^m - (A_i^{n+1} D_{j,i}^{n+1} W_{j,i}^{n+1})^m}{\Delta x} \right\} - \\
 & \left\{ (1-\psi)(1-\theta) \left[ \frac{Q_i^n (\beta_{j,i}^n C_{j,i}^{*,n} - C_{j,i}^n)}{L_{j,i}^{*,n}} + q_i^n C_{s,j,i}^n \right] + \right. \\
 & \left. \psi(1-\theta) \left[ \frac{Q_{i+1}^n (\beta_{j,i+1}^n C_{j,i+1}^{*,n} - C_{j,i+1}^n)}{L_{j,i+1}^{*,n}} + q_{i+1}^n C_{s,j,i+1}^n \right] + \right. \\
 & \left. (1-\psi)\theta \left[ \frac{Q_i^{n+1} (\beta_{j,i}^{n+1} C_{j,i}^{*,n+1} - C_{j,i}^{n+1})}{L_{j,i}^{*,n+1}} + q_i^{n+1} C_{s,j,i}^{n+1} \right]^m + \right. \\
 & \left. \psi\theta \left[ \frac{Q_{i+1}^{n+1} (\beta_{j,i+1}^{n+1} C_{j,i+1}^{*,n+1} - C_{j,i+1}^{n+1})}{L_{j,i+1}^{*,n+1}} + q_{i+1}^{n+1} C_{s,j,i+1}^{n+1} \right]^m \right\}
 \end{aligned}$$

Equation (4.18) can be discretised as

$$L_{i,4j,2+j} = \frac{\partial F_{4j,i}^m}{\partial (C_{j,i}^{n+1})^m} = \frac{\theta}{\Delta x}$$

$$L_{i,4j,2+J+j} = \frac{\partial F_{4j,i}^m}{\partial (W_{j,i}^{n+1})^m} = \theta(1-\psi)$$

$$R_{i,4j,2+j} = \frac{\partial F_{4j,i}^m}{\partial (C_{j,i+1}^{n+1})^m} = -\frac{\theta}{\Delta x}$$

$$R_{i,4j,2+J+j} = \frac{\partial F_{4j,i}^m}{\partial (W_{j,i+1}^{n+1})^m} = \theta\psi$$

$$S_{i,4j} = F_{4j,i}^m$$

$$\begin{aligned} &= (1-\psi)(1-\theta)W_{j,i}^n + \psi(1-\theta)W_{j,i+1}^n + (1-\psi)\theta(W_{j,i}^{n+1})^m + \psi\theta(W_{j,i+1}^{n+1})^m \\ &\quad - \left\{ (1-\theta)\frac{C_{j,i+1}^n - C_{j,i}^n}{\Delta x} + \theta\frac{(C_{j,i+1}^{n+1})^m - (C_{j,i}^{n+1})^m}{\Delta x} \right\} \end{aligned}$$

#### 4.5.4 Discretion of Bedload Transport Equation

The bedload transport equation (4.19) can be discretised as

$$L_{i,5j,2+2J+j} = \frac{\partial F_{5j,i}^m}{\partial (G_{j,i}^{n+1})^m} = \frac{1-\psi}{\Delta t} - \mu[u_{bj,i}]^m \frac{\theta}{\Delta x} + \theta(1-\psi)\left(\frac{u_{bj,i}^{n+1}}{\lambda_{j,i}^{n+1}}\right)^m$$

$$L_{i,5j,3+3J+j} = \frac{\partial F_{5j,i}^m}{\partial (\beta_{j,i}^{n+1})^m} = -\theta(1-\psi)\left(\frac{u_{bj,i}^{n+1}}{\lambda_{j,i}^{n+1}}G_{j,i}^{*,n+1}\right)^m$$

$$R_{i,5j,2+2J+j} = \frac{\partial F_{5j,i}^m}{\partial (G_{j,i+1}^{n+1})^m} = \frac{\psi}{\Delta t} + \mu[u_{bj,i}]^m \frac{\theta}{\Delta x} + \theta\psi\left(\frac{u_{bj,i+1}^{n+1}}{\lambda_{j,i+1}^{n+1}}\right)^m$$

$$R_{i,5j,3+3J+j} = \frac{\partial F_{5j,i}^m}{\partial (\beta_{j,i+1}^{n+1})^m} = -\theta\psi\left(\frac{u_{bj,i+1}^{n+1}}{\lambda_{j,i+1}^{n+1}}G_{j,i+1}^{*,n+1}\right)^m$$

$$\begin{aligned}
 S_{i,5j} = F_{5j,i}^m &= (1-\psi) \frac{(G_{j,i}^{n+1})^m - G_{j,i}^n}{\Delta t} + \psi \frac{(G_{j,i+1}^{n+1})^m - G_{j,i+1}^n}{\Delta t} + \\
 &\left\{ (1-\psi)(1-\theta)u_{bj,i}^n + \psi(1-\theta)u_{bj,i+1}^n + (1-\psi)\theta(u_{bj,i}^{n+1})^m + \psi\theta(u_{bj,i+1}^{n+1})^m \right\} \cdot \\
 &\left\{ (1-\theta) \frac{G_{j,i+1}^n - G_{j,i}^n}{\Delta x} + \theta \frac{(G_{j,i+1}^{n+1})^m - (G_{j,i}^{n+1})^m}{\Delta x} \right\} - \\
 &\left\{ (1-\psi)(1-\theta) \left[ \frac{(\beta_{j,i}^n G_{j,i}^{*,n} - G_{j,i}^n)}{\lambda_{j,i}^n} + q_{sj,i}^n \right] + \right. \\
 &\left. \psi(1-\theta) \left[ \frac{(\beta_{j,i+1}^n G_{j,i+1}^{*,n} - G_{j,i+1}^n)}{\lambda_{j,i+1}^n} + q_{sj,i+1}^n \right] \right. \\
 &\left. (1-\psi)\theta \left[ \frac{(\beta_{j,i}^{n+1} G_{j,i}^{*,n+1} - G_{j,i}^{n+1})}{\lambda_{j,i}^{n+1}} + q_{sj,i}^{n+1} \right]^m + \right. \\
 &\left. \psi\theta \left[ \frac{(\beta_{j,i+1}^{n+1} G_{j,i+1}^{*,n+1} - G_{j,i+1}^{n+1})}{\lambda_{j,i+1}^{n+1}} + q_{sj,i+1}^{n+1} \right]^m \right\}
 \end{aligned}$$

#### 4.5.5 Discretion of Bed Material Conservation Equation

The bed material conservation equation (4.20) can be discretised as

$$R_{i,61} = \frac{\partial F_{6,i}^m}{\partial (Q_{i+1}^{n+1})^m} = \theta \sum_{j=1}^J \left( \frac{\beta_{j,i+1}^{n+1} C_{j,i+1}^{*,n+1} - C_{j,i+1}^{n+1}}{L_{j,i+1}^{*,n+1}} \right)^m$$

$$R_{i,6,2+j} = \frac{\partial F_{6,i}^m}{\partial (C_{j,i+1}^{n+1})^m} = -\theta \left( \frac{Q_{i+1}^{n+1}}{L_{j,i+1}^{*,n+1}} \right)^m$$

$$R_{i,6,2+2J+j} = \frac{\partial F_{6,i}^m}{\partial (C_{j,i+1}^{n+1})^m} = -\theta \left( \frac{1}{\lambda_{j,i+1}^{n+1}} \right)^m$$

$$R_{i,6,2+3J} = \frac{\partial F_{6,i}^m}{\partial (Az_{j,i+1}^{n+1})^m} = (1-p) \frac{1}{\Delta t}$$

$$R_{i,6,2+3J+j} = \frac{\partial F_{6,i}^m}{\partial (\beta_{j,i+1}^{n+1})^m} = \theta \left( \frac{Q_{i+1}^{n+1} C_{j,i+1}^{*,n+1}}{L_{j,i+1}^{*,n+1}} \right)^m + \theta \left( \frac{G_{j,i+1}^{*,n+1}}{\lambda_{j,i+1}^{n+1}} \right)^m$$

$$S_{i,6} = F_{6,i}^m = (1-p) \left\{ \frac{(Az_{i+1}^{n+1})^m - Az_{i+1}^n}{\Delta t} \right\} +$$

$$\sum \left\{ (1-\theta) \left[ \frac{Q_{i+1}^n (\beta_{j,i+1}^n C_{j,i+1}^{*,n} - C_{j,i+1}^n)}{L_{j,i+1}^{*,n}} \right] + \theta \left[ \frac{Q_{i+1}^{n+1} (\beta_{j,i+1}^{n+1} C_{j,i+1}^{*,n+1} - C_{j,i+1}^{n+1})}{L_{j,i+1}^{*,n+1}} \right] \right\} +$$

$$\sum \left\{ (1-\theta) \left[ \frac{(\beta_{j,i+1}^n G_{j,i+1}^{*,n} - G_{j,i+1}^n)}{\lambda_{j,i+1}^n} \right] + \theta \left[ \frac{(\beta_{j,i+1}^{n+1} G_{j,i+1}^{*,n+1} - G_{j,i+1}^{n+1})}{\lambda_{j,i+1}^{n+1}} \right]^m \right\}$$

#### 4.5.6 Discretion of Bed Material Sorting Equation

The bed material sorting equation (4.21) can be discretised as

$$R_{i,7j,1} = \frac{\partial F_{7j,i}^m}{\partial (Q_{i+1}^{n+1})^m} = \theta \left( \frac{\beta_{j,i+1}^{n+1} C_{j,i+1}^{*,n+1} - C_{j,i+1}^{n+1}}{L_{j,i+1}^{*,n+1}} \right)^m$$

$$R_{i,7j,2+j} = \frac{\partial F_{7j,i}^m}{\partial (C_{j,i+1}^{n+1})^m} = -\theta \left( \frac{Q_{i+1}^{n+1}}{L_{j,i+1}^{*,n+1}} \right)^m$$

$$R_{i,7j,2+2J+j} = \frac{\partial F_{7j,i}^m}{\partial (G_{j,i+1}^{n+1})^m} = -\theta \left( \frac{1}{\lambda_{j,i+1}^{n+1}} \right)^m$$

$$R_{i,7j,2+3J} = \frac{\partial F_{7j,i}^m}{\partial (Az_{i+1}^{n+1})^m} = (1-p) \frac{1}{\Delta t} \left\{ (1-\theta) \beta_{j,i+1}^n + \theta [\beta_{j,i+1}^{n+1}]^m \right\}.$$

$$u \left[ \frac{(Az_{i+1}^{n+1})^m - Az_{i+1}^n}{\Delta t} - \frac{(Am_{i+1}^{n+1})^m - Am_{i+1}^n}{\Delta t} \right] +$$

$$(1-p) \frac{1}{\Delta t} \left\{ (1-\theta) \beta_{0j,i+1}^n + \theta [\beta_{0j,i+1}^{n+1}]^m \right\}.$$

$$u \left[ -\frac{(Az_{i+1}^{n+1})^m - Az_{i+1}^n}{\Delta t} + \frac{(Am_{i+1}^{n+1})^m - Am_{i+1}^n}{\Delta t} \right]$$

$$R_{i,7j,3+3J+j} = \frac{\partial F_{7j,i}^m}{\partial (\beta_{j,i+1}^{n+1})^m} = (1-p) \frac{(Am_{i+1}^{n+1})^m}{\Delta t} + \theta(1-p) \cdot$$

$$\left\{ \frac{(Az_{i+1}^{n+1})^m - Az_{i+1}^n}{\Delta t} - \frac{(Am_{i+1}^{n+1})^m - Am_{i+1}^n}{\Delta t} \right\}.$$

$$u \left[ \frac{(Az_{i+1}^{n+1})^m - Az_{i+1}^n}{\Delta t} - \frac{(Am_{i+1}^{n+1})^m - Am_{i+1}^n}{\Delta t} \right] +$$

$$\theta \left( \frac{Q_{i+1}^{n+1} C_{j,i+1}^{*,n+1}}{L_{j,i+1}^{*,n+1}} \right)^m + \theta \left( \frac{G_{j,i+1}^{n+1}}{\lambda_{j,i+1}^{n+1}} \right)^m$$

$$S_{i,7j} = F_{7j,i}^m = (1-p) \left\{ \frac{(Am_{i+1}^{n+1} \beta_{j,i+1}^{n+1})^m - Am_{i+1}^n \beta_{j,i+1}^n}{\Delta t} \right\} +$$

$$(1-p) \left\{ (1-\theta) \beta_{j,i+1}^n + \theta (\beta_{j,i+1}^{n+1})^m \right\}.$$

$$\begin{aligned}
& \left\{ \frac{(Az_{i+1}^{n+1})^m - Az_{i+1}^n}{\Delta t} - \frac{(Am_{i+1}^{n+1})^m - Am_{i+1}^n}{\Delta t} \right\} \\
& u \left[ \frac{(Az_{i+1}^{n+1})^m - Az_{i+1}^n}{\Delta t} - \frac{(Am_{i+1}^{n+1})^m - Am_{i+1}^n}{\Delta t} \right] + \\
& (1-p) \left\{ (1-\theta) \beta_{0,j,i+1}^n + \psi \theta (\beta_{0,j,i+1}^{n+1})^m \right\} \\
& \left\{ \frac{(Az_{i+1}^{n+1})^m - Az_{i+1}^n}{\Delta t} - \frac{(Am_{i+1}^{n+1})^m - Am_{i+1}^n}{\Delta t} \right\} \\
& u \left[ -\frac{(Az_{i+1}^{n+1})^m - Az_{i+1}^n}{\Delta t} + \frac{(Am_{i+1}^{n+1})^m - Am_{i+1}^n}{\Delta t} \right] + \\
& \left\{ (1-\theta) \left[ \frac{Q_{i+1}^n (\beta_{j,i+1}^n C_{j,i+1}^{*,n} - C_{j,i+1}^n)}{L_{j,i+1}^{*,n}} \right] + \theta \left[ \frac{Q_{i+1}^{n+1} (\beta_{j,i+1}^{n+1} C_{j,i+1}^{*,n+1} - C_{j,i+1}^{n+1})}{L_{j,i+1}^{*,n+1}} \right]^m \right\} + \\
& \left\{ (1-\theta) \left[ \frac{(\beta_{j,i+1}^n G_{j,i+1}^{*,n} - G_{j,i+1}^n)}{\lambda_{j,i+1}^n} \right] + \theta \left[ \frac{(\beta_{j,i+1}^{n+1} G_{j,i+1}^{*,n+1} - G_{j,i+1}^{n+1})}{\lambda_{j,i+1}^{n+1}} \right]^m \right\}
\end{aligned}$$

In above formulae,  $i$  = the grid number;  $j$  = the size fraction  $j$  in the graded material;  $m$  = the iterations of the Newton-Raphson method;  $n+1$  = the  $n+1$  time level at which the unknown variables will be computed.

#### 4.5.7 Final Parameter Matrix

The above equations in section 4.5.2 to 4.5.6 can be applied in the computational domain from  $i = 1$  to  $I-1$  to form the parameter matrix as



transforms to the other. This point should be followed in the solution domain, and once again a generalised algorithm can be constructed to facilitate the computation.

The problem of combining different algorithmic structures can be avoided altogether through a technique described by Havno and Brorsen (1986), whereby the influence of the convective terms in the governing equations is reduced by a factor of  $(1-Fr^2)$ , until  $Fr = 1$ , after which this factor remains zero. By these means it is certainly possible to maintain a subcritical flow characteristic structure and data structure while simulating supercritical flows. This can be justified by observing that the amplification factor stays the same and only the phase error is increased during its implementation; since supercritical flows are strongly localised, the influence of the phase error is usually negligible,

#### **4.7 Need For Fully Coupled Solution**

Most numerical models of water flow and sediment transport presented in the literature use an uncoupled solution which isolates the different physical processes and solves these separately. For example, if we consider equations (4.1) to (4.7), solution of the hydrodynamic model is in general a first step to give flow rate and water level. Based on these results, the suspended-load concentration and the bedload process are evaluated independently. The bed elevation and the bed material sorting are then estimated. Such solution procedures are generally acceptable for water quality modelling since changes in solute transport values do not significantly affect water flow. However, this assumption is not always valid in the simulation of graded sediment transport.

The interaction between fluid and sediments provides a strong coupled relationship between water flow and sediment transport in mobile bed rivers. Any change in geometry due to deposition or erosion will directly influence water flow and vice versa. The significance of this effect increases with the magnitude of time

increment. In other word, for uncoupled models the time increment will be limited in size to reduce distortion of flow at the upper time level caused by changes in channel geometry. This is undesirable for long term simulation in which we wish to use a relatively larger time increment to save computer time and costs.

Secondly, the bed material sorting process has the physical requirement that proportion of each size fraction in the active layer must be in the range of 0 to 1. If an uncoupled solution for equation (4.7) is used, it is possible to produce results which violate this condition. For example, if a downward displacement of the bed takes place, equation (4.7) may be rearranged as

$$\frac{\partial \beta_j}{\partial t} + \beta_j \frac{1}{Am} \frac{\partial Az}{\partial t} = \alpha_j \quad (4.30)$$

where  $\alpha_j = -\frac{\Phi_{s,j} + \Phi_{b,j}}{Am(1-p)}$

An analytical solution for (4.30) can be obtained as

$$\beta_j = \left[ \int \alpha_j e^{\int \frac{1}{Am} \frac{\partial Az}{\partial t} dt} dt + C \right] e^{-\int \frac{1}{Am} \frac{\partial Az}{\partial t} dt} \quad (4.31)$$

in which  $C =$  a constant of integration. Considering the condition  $\beta_j(t)|_{t=t_0} = \beta_j(t_0)$ ,

$C$  is obtained from (4.31) as

$$C = \beta_j(t_0) \int_0^{t_0} \frac{1}{Am} \frac{\partial Az}{\partial t} dt - \int_0^{t_0} \alpha_j e^{\int_0^{t_0} \frac{1}{Am} \frac{\partial Az}{\partial t} dt} dt \quad (4.32)$$

Substitution of (4.32) into (4.31) gives

$$\beta_j(t) = \left\{ \int_0^t \alpha_j e^{\int_0^t \frac{1}{Am} \frac{\partial Az}{\partial t} dt} dt + \beta_j(t_0) \int_0^{t_0} \frac{1}{Am} \frac{\partial Az}{\partial t} dt - \int_0^{t_0} \alpha_j e^{\int_0^{t_0} \frac{1}{Am} \frac{\partial Az}{\partial t} dt} dt \right\} e^{-\int_0^t \frac{1}{Am} \frac{\partial Az}{\partial t} dt} \quad (4.33)$$

As far as time level  $t_0 + \Delta t$  is considered, the following expression is obtained from (4.33) as

$$\beta_j(t_0 + \Delta t) = \{\gamma_j + \beta_j(t_0)\} e^{-\int_{t_0}^{t_0+\Delta t} \frac{1}{A_m} \frac{\partial A_z}{\partial t} dt} \quad (4.34)$$

where

$$\gamma_j = \left( \int_0^{t_0} \alpha_j e^{\int_{t_0}^{t_0+\Delta t} \frac{1}{A_m} \frac{\partial A_z}{\partial t} dt} dt + \int_{t_0}^{t_0+\Delta t} \alpha_j e^{\int_0^{t_0+\Delta t} \frac{1}{A_m} \frac{\partial A_z}{\partial t} dt} dt \right) \cdot e^{-\int_0^{t_0} \frac{1}{A_m} \frac{\partial A_z}{\partial t} dt} \quad (4.35)$$

If the following relationship is defined

$$\frac{1}{\tau} = -\frac{1}{A_m} \frac{\partial A_z}{\partial t} \quad (4.36)$$

and the linear relationship of (4.36) within the time increment  $\Delta t$  is assumed, (4.34) can be simplified as

$$\beta_j(t_0 + \Delta t) = \{\gamma_j + \beta_j(t_0)\} e^{\Delta t / \tau} \quad (4.37)$$

The definition of the fractional part of  $j$ -th class in a graded sediment gives  $0 \leq \beta_j(t_0 + \Delta t) \leq 1$ . Therefore (4.37) is written as

$$0 \leq \{\gamma_j + \beta_j(t_0)\} e^{\Delta t / \tau} \leq 1 \quad (4.38)$$

By rearrangement of (4.38), we obtain

$$0 \leq \Delta t \leq \tau \ln \left( \frac{1}{\gamma_j + \beta_j(t_0)} \right) \quad (4.39)$$

Equation (4.39) shows that the time increment must be limited so that the reasonable numerical solutions can be obtained. Otherwise, it may result in a fractional value larger than unity or less than zero for any given size fraction. For example, if  $\partial A_z / \partial t$  is taken as  $0.001 \text{ m}^2/\text{s}$ , the area of the active layer is  $0.1 \text{ m}^2$  and

$\gamma_j + \beta_j(t_0)$  is taken to be 0.1, then from (4.39) time increment at time layer  $t_0$  should be less than 230 seconds.

Equation (4.39) also demonstrates that the time increment varies with the time level, the fractional proportion of each class and the parameter  $\tau$  for simulation of the bed material sorting process. This makes it difficult to select the suitable time increment at outset.

As a result a fully coupled solution is needed to reflect the strong physical relationship between water flow and graded sediment transport, and to suppress computer error and divergence.

#### 4.8 Block Double Sweep Method

Computations of the mobile bed river systems often contain hundreds, and sometime thousands of equations. The advantages of the Preissmann scheme can be negated if inefficient solution techniques are employed. This is especially true for this model where a fully coupled solution technique is adopted. Therefore an efficient solution technique is a prerequisite to the practical implementation of a fully coupled solution algorithm.

Such a solution technique, called the block double sweep method, has been suggested by Holly and Rahuel (1990) for the Preissmann scheme. The main advantage of this method is that it takes advantage of the compact matrix from the finite difference equations without using other zero elements. The idea is that a recurrent relation is introduced and used to transfer downstream boundary conditions into pseudo upstream boundary conditions which can be merged with upstream boundary conditions to form full boundary conditions. Under these full boundary conditions unknown variables at the future time step and at the upstream boundary can be obtained. Then equation (4.25) can be used directly to give a solution to all unknown variables at each grid point. Following Holly and Rahuel (1990) the upstream boundary condition is written as

$$[E_i^u]\{\Delta X_i\} + \{F_i^u\} = 0 \quad (4.40)$$

and downstream boundary conditions

$$[E_i^d]\{\Delta X_i\} + \{F_i^d\} = 0 \quad (4.41)$$

Now a recurrent relation is introduced as

$$[E_i]\{\Delta X_i\} + \{F_i\} = 0 \quad (4.42)$$

Multiplying by  $[R_i]^{-1}$ , equation (4.25) can be rearranged into

$$[R_i]^{-1}[L_i]\{\Delta X_i\} + \{\Delta X_{i+1}\} + [R_i]^{-1}\{S_i\} = 0 \quad (4.43)$$

Multiplying  $[E_{i+1}]$  in equation (4.43) results in

$$[E_{i+1}][R_i]^{-1}[L_i]\{\Delta X_i\} + [E_{i+1}]\{\Delta X_{i+1}\} + [E_{i+1}][R_i]^{-1}\{S_i\} = 0 \quad (4.44)$$

Substitution of equation (4.42) into (4.44) yields

$$[E_{i+1}][R_i]^{-1}[L_i]\{\Delta X_i\} + [E_{i+1}][R_i]^{-1}\{S_i\} - \{F_{i+1}\} = 0 \quad (4.45)$$

Compared with equation (4.42), one can expect

$$\begin{aligned} [E_i] &= [E_{i+1}][R_i]^{-1}[L_i] \\ \{F_i\} &= [E_{i+1}][R_i]^{-1}\{S_i\} - \{F_{i+1}\} \end{aligned} \quad (4.46)$$

Using equation (4.46) the downstream boundary conditions can be translated into pseudo upstream boundary conditions. At the downstream end, equation (4.46) becomes

$$\begin{aligned} [E_{I-1}] &= [E_I^d][R_{I-1}]^{-1}[L_{I-1}] \\ \{F_{I-1}\} &= [E_I^d][R_{I-1}]^{-1}\{S_{I-1}\} - \{F_I^d\} \end{aligned} \quad (4.47)$$

At the upstream end full boundary conditions are as follows

$$\begin{aligned} [E_i^f] &= [E_i^u] + [E_i] \\ \{F_i^f\} &= \{F_i^d\} + \{F_i\} \end{aligned} \quad (4.48)$$

Substitution of equation (4.48) into equation (4.42) results in

$$[E_i^f]\{\Delta X_i\} + \{F_i^f\} = 0 \quad (4.49)$$

Equation (4.49) can be used to give all values of the unknown variables at the upstream and then equation (4.25) is used to solve all unknown variables from  $i = 2$  to  $I$ .

The recurrence process in the block double sweep method can produce a fast and almost exponential growth of the coefficients in matrix  $[E_i]$  and  $\{F_i\}$ . Therefore the matrix  $[E_i]$  and  $\{F_i\}$  must be bounded and this is done in each step of the recurrence by first computing  $[E_i]$  and  $\{F_i\}$ , then dividing each term by maximum value in  $[E_i]$ . Again the backward sweep needs to be performed carefully, see Holly and Rahuel (1990), because it tends to diverge due to successive rounding errors. This divergence can be obviated by first computing the entire vector  $\{X_i\}$  from equation (4.25), then re-computing  $\Delta Q$  from  $[E_i]$ . Since  $\Delta Q$  has a strong presence throughout the system of equations, its control prevents divergence of the backward sweep.

#### 4.9 Solution Procedure

Solution procedure can be summarised as

1. Whole channel is divided into  $I$  number of cross sections and graded bed material is subdivided into  $J$  size fractions;
2. The space and time weighting parameters in the Preissmann scheme are specified for hydrodynamic component, suspended-load component, bedload component and bed material conservation and sorting component;
3. The time increment is selected, giving consideration to numerical dissipation; The cross sectional and bed material information are defined initially;
4. Initial data  $\{X_i\}^n$  are specified for all grid points for  $i = 1$  to  $i = I$ ;

5. Upstream boundary conditions are defined to form upstream boundary matrices  $[E_i^u]$  and  $\{F_i^u\}$  which includes either water inflow or water surface level, or some combination of these, suspended-load inflows and bedload inflows;
6. Downstream boundary conditions are defined to form downstream boundary matrices  $[E_i^d]$  and  $\{F_i^d\}$  which includes again either water outflow or water surface level, or some combination of these and zero flux for suspended-load transport;
7. All coefficients in matrices  $[L_i]$ ,  $[R_i]$  and  $[S_i]$  are calculated using equations in section 4.5 from  $i = 1$  to  $i = I-1$ ;
8. Using equation (4.47) the matrices  $[E_{I-1}]$  and  $\{F_{I-1}\}$  are calculated. This implies that the first sweep is from downstream to upstream because the downstream boundary conditions are generally simpler than the upstream boundary. As a result the CPU time can be saved compared with sweeping from upstream to downstream in the first sweep. However, the choice is up to the modeller;
9. Using equation (4.46) and  $[E_{I-1}]$  and  $\{F_{I-1}\}$  the matrices  $[E_i]$  and  $\{F_i\}$  in the current relation are calculated from  $i = I-2$  to  $i = 1$ . Care should be taken in this procedure due to a fast, almost exponential growth of the coefficients of the matrix  $[E_i]$  and  $\{F_i\}$ . Therefore in the model the matrices  $[E_i]$  and  $\{F_i\}$  are bounded by first computing  $[E_i]$  and  $\{F_i\}$ , then dividing each term with maximum value in  $[E_i]$ ;
10. Using equation (4.48) the full boundary conditions are formed and then from equation (4.49) new estimated values of matrix  $\{\Delta X_1\}$  are computed;
11. Using equation (4.25) all new estimated values of matrix  $\{\Delta X_i\}$  are computed from  $i = 2$  to  $i = I$ ; again the backward sweep should be performed carefully due to successive rounding errors;
12. The new estimated value of matrix  $\{X_i\}$  at upper time level are updated using results from step 11;

13. This process from step 4 to 12 can be continued using new stated values to refine all the needed coefficients until some convergence criterion is satisfied, such as one  $\epsilon$  corresponding to the accuracy that is desired; in the current model the following criterion is used

$$\sqrt{\left[ \max \left| \frac{\Delta Y_i}{H_i} \right| \right]^2 + \left[ 20 \cdot \max \left| \frac{\Delta A z_i}{B e_i} \right| \right]^2} \leq \epsilon \tag{4.50}$$

where  $\Delta Y_i$  = the change of water surface level within an iteration;  $H_i$  = the water depth;  $B e_i$  = the effective width;  $\Delta A z_i$  = the change of deposition or erosion area within an iteration;

14. Go on to the calculations of next time step in the same fashion.

To demonstrate the solution procedure graded sediment transport of two size fractions in a rectangular channel has been undertaken. This channel is 100 m long with a uniform rectangular cross section with the width of 20 m. The initial bed slope is 1/1000 and the channel is initially in equilibrium sediment transport. The water inflow is constant at 30 m<sup>3</sup>/s. The initial water depth along the channel, calculated from the steady flow theory, is 1.15 m at each cross section. The sediment inflow is assumed to be equal to the equilibrium transport capacity at the upstream boundary. The diameter of the two size fractions are 0.5 mm (50%) and 1.0 mm (50%). The parameters employed in the Peissmann scheme are listed in Table 4.1.

**Table 4.1 Space and Time Weighting Parameters In The Peissmann Scheme For The Application**

	Hydrodynamic equations	Suspended-load Transport	Bedload transport	Bed material conservation
Time weighting, $\theta$	0.55	0.55	0.55	0.55
Space weighting, $\psi$	0.5	0.5	0.5	1.0

The time increment used is 120 seconds. The total number of independent variables is 11 from equation (4.8). These variables at cross section  $i$  are written as

$$\{X_i\} = \{Q_i, Y_i, C_{1,i}, C_{2,i}, W_{1,i}, W_{2,i}, G_{1,i}, G_{2,i}, Az_i, \beta_{1,i}, \beta_{2,i}\} \quad (4.51)$$

where  $Q$  = the discharge ( $m^3/s$ );  $Y$  = the water level (m);  $C_1$  and  $C_2$  = the suspended-load concentration for size fraction 1 and 2 ( $m^3/m^3$ );  $W_1$  and  $W_2$  = the suspended-load concentration gradient for size fraction 1 and 2 ( $m^3/m^3, m$ );  $G_1$  and  $G_2$  = the bedload rates for size fraction 1 and 2 ( $m^3/s$ );  $Az$  = the area of deposition or erosion ( $m^2$ );  $\beta_1$  and  $\beta_2$  = the fractional representation for size fraction 1 and 2. The initial values for all variables at each cross section are listed in Table 4.2

**Table 4.2 The Initial Values For All Variables**

	Q	Y-Zb	$C_1$ $\times 10^{-4}$	$C_2$ $\times 10^{-4}$	$W_1$	$W_2$	$G_1$ $\times 10^{-4}$	$G_2$ $\times 10^{-4}$	Az	$\beta_1$	$\beta_2$
1	30	1.15	1.26	1.06	0	0	5.7	9.7	0	0.5	0.5
2	30	1.15	1.26	1.06	0	0	5.7	9.7	0	0.5	0.5
3	30	1.15	1.26	1.06	0	0	5.7	9.7	0	0.5	0.5
4	30	1.15	1.26	1.06	0	0	5.7	9.7	0	0.5	0.5
5	30	1.15	1.26	1.06	0	0	5.7	9.7	0	0.5	0.5

The matrices  $[E_1^u]$  and  $\{F_1^u\}$  can be constructed from the upstream boundary conditions. For example, given the water inflow at the upstream boundary  $\Delta Q_1^2$  within each iteration should be equal to zero. This yields that if an element  $E_{11}$  in the matrix  $[E_1^u]$  is defined to be unity, an element  $F_1$  in the matrix  $\{F_1^u\}$  is zero. The same treatment is also employed for the suspended and bed load inflows. The upstream boundary conditions for the bed material conservation and the bed material sorting can be calculated by applying the equations in the section 4.5.5 and 4.5.6 directly. This results in the full matrices  $[E_1^u]$  and  $\{F_1^u\}$ .



The matrix is  $\{F_5^d\}^{-1} = \{0, 0, 0, 0, 0, 0, 0, 0, 0, 0, 0, 0\}$ .

The values in the matrices  $[L_i]$ ,  $[R_i]$  and  $[S_i]$  are calculated using the equations in section 4.5 from  $i = 1$  to 4. As an example, only the  $[L_1]$ ,  $[R_1]$  and  $[S_1]$  are listed below. The  $[L_1]$  is

	1	2	3	4	5	6	7	8	9	10	11
1	-2.2e-2	-8.3e-2	0	0	0	0	0	0	-4.2e-3	0	0
2	-4.9e-2	-5.0	0	0	0	0	0	0	0	0	0
3	-2.8e-6	0	-5.7e-2	0	0.8	0	0	0	0	-1.3e-3	0
4	-2.3e-6	0	0	-5.6e-2	0	0.8	0	0	0	0	-1.1e-4
5	0	0	2.2e-2	0	0.3	0	0	0	0	0	0
6	0	0	0	2.2e-2	0	0.3	0	0	0	0	0
7	0	0	0	0	0	0	-1.1e-3	0	0	-2.0e-5	0
8	0	0	0	0	0	0	0	-1.2e-3	0	0	-3.5e-5
9	0	0	0	0	0	0	0	0	0	0	0
10	0	0	0	0	0	0	0	0	0	0	0
11	0	0	0	0	0	0	0	0	0	0	0

The matrix  $[R_1]$  is

	1	2	3	4	5	6	7	8	9	10	11
1	2.2e-2	8.3e-2	0	0	0	0	0	0	-4.2e-3	0	0
2	6.6e-2	5.0	0	0	0	0	0	0	0	0	0
3	2.8e-6	0	1.3	0	-0.8	0	0	0	0	-1.2e-4	0
4	0	2.3e-6	0	1.3	0	-0.8	0	0	0	0	-1.1e-4
5	0	0	-2.2e-2	0	0.3	0	0	0	0	0	0
6	0	0	0	-2.2e-2	0	0.3	0	0	0	0	0
7	0	0	0	0	0	0	4.4e-3	0	0	-2.0e-5	0
8	0	0	0	0	0	0	0	4.6e-3	0	0	-3.5e-5
9	-1.2e-8	0	-1.0	-1.0	0	0	-3.4e-2	-3.4e-2	5.0e-3	3.0e-4	2.8e-3
10	-5.1e-9	0	-1.0	0	0	0	-3.4e-2	0	2.5e-3	6.1e-3	0
11	-6.5e-9	0	0	-1.0	0	0	0	-3.4e-2	2.5e-3	0	6.0e-3

The matrix  $\{S_1\}$  is  $\{0, -3.7e-2, 3.5e-7, 4.2e-7, -5.2e-9, -5.8e-9, -2.8e-7, -3.7e-7, 0, 0, 0\}$ .

Now following the solution procedure from 8 to 11 the  $[\Delta X_i]$  can be obtained as

variables	1	2	3	4	5
$\Delta Q_i$	0	1.4e-2	2.4e-2	3.0e-2	3.2e-2
$\Delta Y_i$	-2.1e-3	-1.6e-3	-1.1e-3	-5.4e-4	0
$\Delta C_{1,i}$	0	-3.0e-7	-2.9e-7	-2.7e-7	-2.6e-7
$\Delta C_{2,i}$	0	-3.5e-7	-3.4e-7	-3.2e-7	-3.1e-7
$\Delta W_{1,i}$	-9.1e-9	4.4e-9	1.4e-9	4.9e-9	0
$\Delta W_{2,i}$	-1.0e-8	3.5e-9	1.2e-9	4.1e-9	0
$\Delta G_{1,i}$	0	6.4e-6	6.3e-6	6.2e-6	6.2e-6
$\Delta G_{2,i}$	0	8.1e-6	8.0e-6	7.8e-6	7.8e-6
$\Delta A z_i$	0	-3.3e-5	-3.1e-5	-2.3e-5	-2.0e-5
$\Delta \beta_{1,i}$	0	-5.2e-7	-4.2e-7	-2.2e-7	-1.4e-7
$\Delta \beta_{2,i}$	0	5.2e-7	4.2e-7	2.2e-7	1.4e-7

If the estimated criterion is not satisfied, the values at the upper time level are renewed using  $\{X_i^2\}^{m+1} = \{X_i^2\}^m + \{\Delta X_i\}$  and the process is continued from step 4 to 13 until the  $\epsilon$  corresponding to the required accuracy is satisfied. Then the simulation goes on to the next time increment.

#### 4.10 Stability and Accuracy

##### 4.10.1 Stability

The stability analysis of the Preissmann algorithm for the hydrodynamic equations has been undertaken by Abbott (1989). In his analysis the locally-constant coefficients in the non-linear equations were assumed so that the linear stability analysis was generalised to the quasi-linear case. He applied the von Neumann

condition for stability claiming that the spectral radius of the amplification matrix should be less than or equal to unity. It was found that for a specific value of the space weighting factor, such as 0.5, the stability firmly depends on the time weighting factor. The conclusions are summarised as follows; (i) When  $\theta = 0.5$  the Preissmann scheme is stable and non-dissipative. In this case for a perfectly centred situation the Preissmann scheme gives the exact solution and is equivalent to the method of characteristics. The details of the analysis, see Abbott (1989), show that there is no amplitude error for any combination of the Courant and Froude number. However, the phase error increases rapidly with the Courant number and the accuracy of results is influenced although the scheme still works without any limitation on the time increment; (ii) When  $0.5 < \theta < 1$ , the scheme is stable and dissipative. When more weight is put on the upper time level numerical dissipation is introduced to produce amplitude error. Taking  $\theta = 1$  provides the largest numerical dissipation and usually leads to inaccuracy in the results for unsteady flow simulations. However, this can provide a fast convergent rate for steady-state problems where the final solution is all that is required. Liggett and Cunge (1975) suggested using  $\theta \geq 0.67$  for steady flow problems; (iii) When  $\theta < 0.5$  this scheme is unstable.

The phase error varies with the Courant number  $Cr = C\Delta t/\Delta x$ , where the celerity is  $C = \sqrt{gA/B}$ ;  $A$  = the area of cross section;  $B$  = the top width of cross section;  $\Delta t$  = the time increment;  $\Delta x$  = the space step. When  $Cr < 1$ , then the phase error  $C_n/C > 1$  ( $C_n$  = the numerical celerity) and the computed numerical wave moves faster than its physical counterpart. When  $Cr = 1$ , then phase error  $C_n/C = 1$  and the numerical wave moves at correct speed. When  $Cr > 1$ , then phase error  $C_n/C < 1$  and numerical wave moves too slowly.

When a linearized friction is included, the von Neumann analysis of stability conducted by Fread (1974) demonstrates that the friction produces more damping,

some of it physically justified some of it arising numerically from the form of the resistance term.

Ponce and Simons (1977) considered the full nonlinear Saint Venant equations with bed slope and boundary shear. They concluded that the numerical amplitude error can occur depending on the Froude number, Courant number and wave number in a very complicated way.

It has been found that a weak instability can be caused by the friction term in the normal circumstances, especially if a small friction parameter is employed, see Abbott (1989). Samuels (1990) indicated that when the magnitude of the Vedernikov Number is less than unity, the linearized numerical equations are stable for the Preissmann scheme. The Vedernikov Number can be written as

$$V = \frac{mFrA}{nR} \frac{\partial R}{\partial A} \quad (4.50)$$

where  $Fr$  = the Froude number; parameters  $m$  and  $n$  are defined in following equation of friction slope  $S_f$ .

$$S_f = \frac{Cu|u|^{n-1}}{R^m} \quad (4.51)$$

where  $u$  = the mean velocity of cross section;  $C$  = the Chezy coefficient.

It should be emphasised that the analysis holds only for the quasi-linear hydrodynamic equations. The stability analysis for the whole system including equations from (4.1) to (4.7) is not yet available. The conclusion made so far can only serve to give guidelines for the numerical simulations conducted with the fully nonlinear equations in this model.

#### 4.10.2 Accuracy

Again accuracy analysis was also conducted based on the quasi-linear equations. A Taylor's series expansion is required to analyse the accuracy of the Preissmann scheme. It can be shown, see Abbott (1989), that

when $\psi = \theta = 0.5$ and $Cr = 1$	exact solution
when $\psi = \theta = 0.5$ and $Cr \neq 1$	$O(\Delta t^2, \Delta x^2)$
when $\psi = 0.5, 0.5 < \theta < 1$ and $Cr \neq 1$	$O(\Delta t^2, \Delta x)$

#### 4.11 Lateral Distribution of Deposition or Erosion

From equation (4.20) we can expect deposition or erosion at each cross section. As suggested by Chang (1988), the lateral distribution of this deposition or erosion is dependent on the lateral distribution of the bed shear stress. This can be written as

$$\Delta y_k = c' \tau_k = c' \rho g H_k S = c H_k \quad (4.52)$$

where  $c$  and  $c' =$  constants;  $H_k =$  the water depth at point  $k$  in the cross section;  $\Delta y_k =$  the thickness of deposition or erosion at the point  $k$ ;  $\tau_k =$  the shear stress at the point  $k$ ;  $S =$  the energy slope. The constant  $c$  can be determined using conservation of deposition or erosion mass as follows

$$\Delta A_z = \sum \Delta A_k \quad (4.53)$$

where  $\Delta A_k$  is shown in Figure 4.2 and written

$$\Delta A_k = \frac{1}{2} (\Delta y_k + \Delta y_{k+1}) \Delta z_k \quad (4.54)$$

Substitution of equation (4.54) into equation (4.53) results in

$$\Delta A_z = \sum \frac{1}{2} (\Delta y_k + \Delta y_{k+1}) \Delta z_k \quad (4.55)$$

Substitution of equation (4.52) into equation (4.55) yields

$$\Delta A_z = c \sum \frac{1}{2} (H_k + H_{k+1}) \Delta z_k \quad (4.56)$$

Therefore a constant  $c$  can be obtained as

$$c = \frac{\Delta A_z}{\sum \frac{1}{2} (H_k + H_{k+1}) \Delta z_k} \quad (4.57)$$

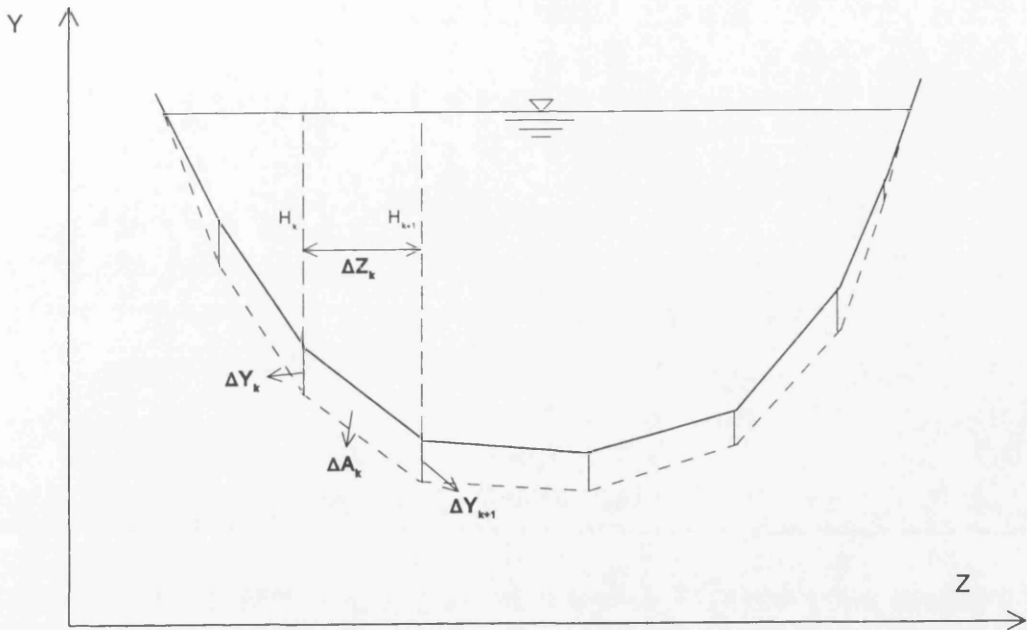


Figure 4.2 Lateral Distribution of Deposition or Erosion

The above approach is based on the linear assumption between the thickness of deposition or erosion and shear stress, see equation (4.52). If a non-linear relationship is considered such as in the HEC-6 model, the following expression is obtained.

$$\Delta y_k = cH_k^\alpha \tag{4.58}$$

Following same procedure above we have

$$c = \frac{\Delta A_k}{\sum \frac{1}{2} (H_k^\alpha + H_{k+1}^\alpha) \Delta Z_k} \tag{4.59}$$

where  $\alpha$  = a parameter to be calibrated. This model adopts a linear relationship (4.52) to avoid an additional parameter to be calibrated.

#### 4.12 Effective Depth and Effective Width

In an mobile bed river system, the irregular cross section causes the water depth to vary in the transverse direction. A question raised here is how to choose a water

depth appropriate for evaluating the sediment transport capacity. For example, if the maximum water depth is used, it will overestimate the transport capacity, if the mean water depth is calculated based on the top width and used this will underestimate the transport capacity. Therefore the concept of effective depth and effective width as used in the HEC-6 model is employed. The effective depth and effective width can be estimated through following formulae.

$$H_e = \frac{\sum A_k H_k^{5/3}}{\sum A_k H_k^{2/3}} \quad (4.60)$$

$$B_e = \frac{\sum A_k H_k^{2/3}}{H_e^{5/3}} \quad (4.61)$$

where  $H_e$  = the effective depth;  $B_e$  = the effective width;  $A_k$  = the area between each co-ordinate pair in the cross section;  $H_k$  = the average depth above each pair of co-ordinate. Hence the transport capacity for suspended-load and bedload is estimated based on the effective depth and width equations (4.60) and (4.61).

The effective depth is in general less than the maximum water depth and the effective width is less than the top width. This can be seen in Figure 4.3.

#### 4.13 Multi Functional Model

This numerical model was developed to operate on a multi functional basis to make it of more practical value. The first function is purely hydrodynamic simulation using the Saint Venant equations. The second function is for the simulation of uniform sediment transport. The final one is for graded sediment transport. The main advantage of multi functional model is that one can carry out different simulations within a model for different purposes. For example, for short term predictions such as flood wave simulation one would use the hydrodynamic function for estimating discharge and water level without considering the feedback effect of channel geometry

on the hydrodynamic parameters. For long term simulations especially in mobile bed river, the deposition or erosion is considerable so that the sediment transport function must be coupled with hydrodynamic function. Under this situation one could expect to use the uniform sediment transport function. If one is interested in the graded sediment transport where the material sorting is significant, the graded sediment transport function should be coupled with the hydrodynamic function.

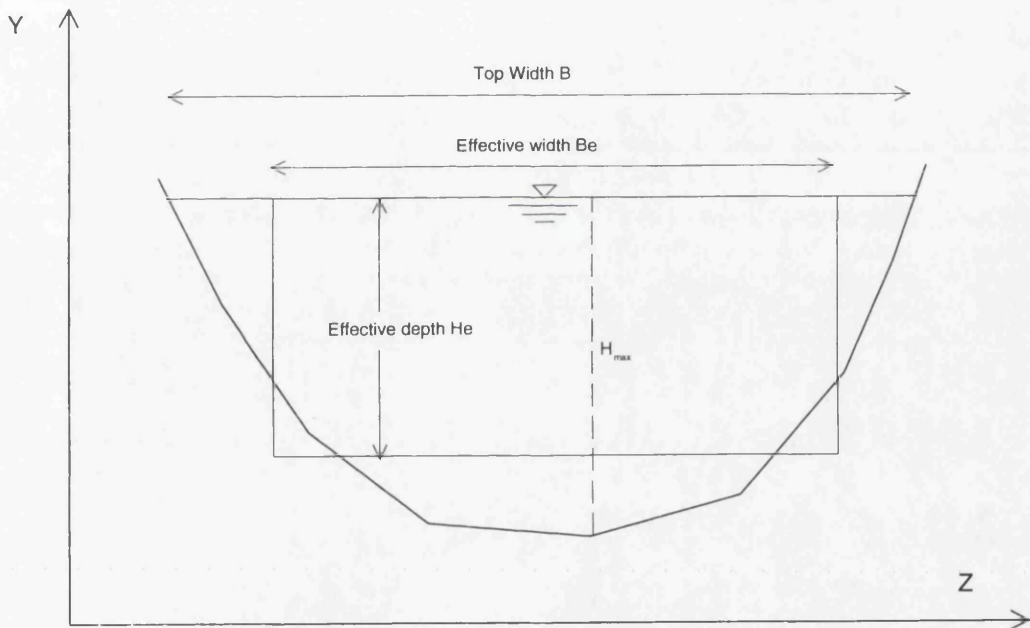


Figure 4.3 Effective Depth and Effective Width At A Cross Section

## **CHAPTER 5**

### **Test Applications of The Model**

#### **5.1 Introduction**

This chapter presents validation results from applying the model to hypothetical data. The important features of the model are demonstrated. The behaviour of the numerical techniques such as the fully coupled solution of the differential equations and the two point scheme used to solve the advection-dispersion equation are also demonstrated by analysing numerical results.

In the test applications described, the same empirical sediment relationships were used throughout. The main relationships are

- Van Rijn's bedload and suspended-load transport formulae to evaluate the transport capacity (1984);
- the reduced hiding function developed in chapter 3;
- the Engelund and Hanson's formula (1967) was used to predict the resistance factor for sand beds and Limerinos formula, see Limerinos (1970) was used for gravel;

#### **5.2 Performance of The Two Point Scheme**

Since the Preissmann scheme cannot be applied directly in the advection and dispersion equation which contains second derivatives with respect to space, the two point scheme is introduced to split the equation into two equations to which the Preissmann scheme can be applied.

The advection and dispersion process of suspended-load is treated by dividing an advection and dispersion equation into two equations each of which contains only one first derivative with respect to time and space. The advantage of this two point scheme is that it allows the Preissmann scheme to be used directly in the suspended-load transport calculation.

In the following the performance of the two point scheme is compared with other finite difference schemes such as the backward, central and QUICK finite difference scheme, see Abbott (1989) for details.

In order to demonstrate the different performance between the schemes the simple one dimension advection and dispersion equation, without a source term, was used. This can be written as

$$\frac{\partial C}{\partial t} + u \frac{\partial C}{\partial x} = D \frac{\partial^2 C}{\partial x^2} \quad (5.1)$$

where  $C$  = the concentration;  $u$  = the velocity;  $D$  = the dispersion coefficient.

For the two point scheme equation (5.1) can be split and re-written as

$$\frac{\partial C}{\partial t} + u \frac{\partial C}{\partial x} = D \frac{\partial W}{\partial x} \quad (5.2)$$

$$W = \frac{\partial C}{\partial x}$$

Applying the Preissmann scheme to equation (5.2) results in

$$(1-\psi) \frac{C_i^{n+1} - C_i^n}{\Delta t} + \psi \frac{C_{i+1}^{n+1} - C_{i+1}^n}{\Delta t} + u \left[ (1-\theta) \frac{C_{i+1}^n - C_i^n}{\Delta x} + \theta \frac{C_{i+1}^{n+1} - C_i^{n+1}}{\Delta x} \right] =$$

$$D \left[ (1-\theta) \frac{W_{i+1}^n - W_i^n}{\Delta x} + \theta \frac{W_{i+1}^{n+1} - W_i^{n+1}}{\Delta x} \right] \quad (5.3)$$

$$(1-\psi)(1-\theta)W_i^n + \psi(1-\theta)W_{i+1}^n + (1-\psi)\theta W_i^{n+1} + \psi\theta W_{i+1}^{n+1} =$$

$$(1-\theta) \frac{C_{i+1}^n - C_i^n}{\Delta x} + \theta \frac{C_{i+1}^{n+1} - C_i^{n+1}}{\Delta x} \quad (5.4)$$

Equations (5.3) and (5.4) can be rearranged into

$$A_{1i}C_i^{n+1} + B_{1i}W_i^{n+1} + E_{1i}C_{i+1}^{n+1} + F_{1i}W_{i+1}^{n+1} = G_{1i} \quad (5.5)$$

$$A_{2i}C_i^{n+1} + B_{2i}W_i^{n+1} + E_{2i}C_{i+1}^{n+1} + F_{2i}W_{i+1}^{n+1} = G_{2i}$$

Equation (5.5) can then be solved using standard double sweep solution procedure, see Abbott (1989).

Alternatively, equation (5.1) can be discretized using either backward, central or the QUICK finite difference schemes. To compare the performance of each of these schemes they were used to simulate advection and dispersion in an one-dimensional test reach. This test consisted of a steady unidirectional flow, with a pure plug source of conservative tracer being advected along the reach, i.e., both physical diffusion and dispersion were equated to zero. The reach is 20 km long with a grid spacing of 200 m. A constant velocity of 0.5 m/s is set in the reach. The plug lengths considered are  $5\Delta x$  (1 km),  $10\Delta x$  (2 km),  $30\Delta x$  (6 km). Three time increment are used based on a Courant Number less than 1, equal to 1 and greater than 1.

For  $Cr = 1$  the numerical predictions at 20,000 seconds from the start of the test when the advected plug is midway down the test reach can be seen in Figures 5.1 to 5.4. Figure 5.1 shows the numerical results from the backward finite difference scheme. Here the peak concentration is 31% of the true peak value. The results from the central finite difference scheme, Figure 5.2, show an improvement in the prediction of the peak concentration, to 82% of the true peak. However, a wide range of negative concentrations are predicted upstream. This is clearly a physical impossibility. This results can be improved further by using the QUICK scheme as shown in Figure 5.3. Here the peak concentration is the true value, and the negative concentrations are noticeably less. Figure 5.4 shows the numerical results from two point scheme which gives the exact solution. These results and comparisons are also

consistent with the results from the other tests with wide plug sources. From this results it can be seen that the two point scheme possesses significant improvements when compared with the backward, central and QUICK finite difference scheme.

The numerical performance of the two point scheme also depends on the choice of time and space weighting factors and on the Courant number. In general, the space weighting factor is set to 0.5. The time weighting factor should be between 0.5 and 1.0. Figure 5.5 shows the different numerical results for same test when the time weighting factor is 0.5, 0.55 and 0.75. Clearly, the numerical dissipation increases with the time weighting factor  $\theta$ . When  $\theta = 0.55$ , the prediction of the peak concentration is about 80% of true peak value.

Figure 5.6 shows the numerical behaviour under the different values of the Courant number  $Cr$ . When  $Cr$  is less than 1, the numerical celerity is larger than the physical one which produces the negative concentrations downstream of the slug. When  $Cr$  is greater than 1, the numerical celerity is less than the physical one and the negative concentrations are produced upstream of the slug. When  $Cr = 1$ , we can simulate the true concentration without any numerical dissipation.

### 5.3 Numerical Test For Stability

Numerical stability tests were carried out to examine the numerical stability of the model under different combinations of numerical parameters in the Preissmann scheme and the Courant number. The test channel used is the one described in section 4.11. Initially, the water flow in the channel is steady and the graded sediment transport is in equilibrium. The cross section is therefore uniform and the resistance factor constant. To test the model stability characteristics the time increment was increased until the solution began to diverge, during this test all other numerical parameters were held constant.

Numerical results demonstrate that the numerical simulation is stable until the Courant number reaches 3000 under different combination of the time weighting

parameters. However, the numerical instability may be increased by the resistance factor and using an irregular cross sectional shape. Therefore a safety margin for time weighting parameters in the Preissmann scheme is needed to prevent the numerical simulation from going unstable for irregular cross sectional shape and/or a small resistance factor.

#### 5.4 Hydrodynamic Model

To test the hydrodynamic model its performance in simulating a standard test case was compared with a method of characteristics solution. The test case used was for a 10 km long by 50 m wide rectangular channel with a flat bed. There are no inflows and outflows and friction in channel is assumed to be so small that it can be neglected. At time zero the water level was set to a slope of 1/5000 and released to oscillate back and forth. An accurate solution of the water levels after two cycles can be obtained using the method of characteristics.

For the numerical simulation, the whole length of the channel is divided into 11 cross sections with a space step of 1000 m. At the upstream boundary there is no inflow and at downstream boundary no outflow. The time increment was selected so that the average Courant number is equal to a particular value such as one or two.

The numerical predictions of the water levels varying with time at both the upstream and the downstream boundaries are shown in Figure 5.7 here the time weighting factor is 0.5 and the average Courant number, based on the average water depth, is one. Figure 5.7 shows that after two cycles of simulation the peak values of water levels for both boundaries are close to the initial values, implying that there is little error in the predictions of amplitude. However, the time to reach the peak values after two cycles is different between the upstream and downstream boundaries indicating that a phase error has been introduced. Theoretically, when the Courant number is one, phase errors should be zero, however the during the simulation the

Courant number is not equal to one at all points and the phase errors are generated. In this case the phase errors cannot be avoided.

The numerical results of water levels along channel after two cycles of simulation together with solution by characteristics are shown in Figure 5.8 for three time weighting factors 0.5, 0.55 and 0.75. The time for two cycle of simulation was chosen to be the averaged time for water levels at both boundaries to reach the peak. Figure 5.8 shows that when time weighting factor is equal to 0.5 and  $Cr = 1$ , the numerical results are very close to characteristics solution. But when the time weighting factor increases, the numerical results depart from the characteristics solution due to the numerical dissipation. This demonstrates that the numerical dissipation is proportional to value of time weighting factor and this is consistent with the theoretical analysis for the Preissmann scheme, see Abbott (1989). Figure 5.9 shows that the numerical dissipation is also controlled by the Courant number where the numerical dissipation for  $Cr = 2$  is clearly larger than one for  $Cr = 1$ . When the Courant number is equal to one, one would expect to receive the minimum numerical dissipation under the constant time weighting factor in the Preissmann scheme.

This numerical test demonstrates that the numerical results by using the Preissmann scheme are sensitive to the choice of time weighting factor and Courant number. In the following work the space weighting factor is taken as 0.5. The time weighting factor 0.55 and the Courant number is chosen to be as close to one as possible in order to minimise the numerical dissipation for hydrodynamic model. It is also possible to use other values for the time weighting factor and the Courant number where the numerical dissipation is needed such as the simulation of steady-state flow.

### **5.5 Trench Infilling Test**

In the following the infilling of a trench in the channel bed is simulated using both a graded bed material and a uniform material. The test is in a 5 km long channel with rectangular cross section. The whole channel is divided into 21 cross sections

with space step of 250 m. The trench is located 1500 m from inlet and the depth of the trench is 30 cm. The initial shape of this trench is shown in Figure 5.10. The initial bed slope is 1/5,000 and the constant unit inflow was 5 m<sup>3</sup>/s,m. The initial conditions were set up from steady flow theory. A constant water level of 2.69 m and the zero flux for suspended-load transport were imposed as the downstream boundary conditions. The sediment inflow at upstream is assumed to be in the equilibrium in which the transport rate is equal to transport capacity. The graded material is 0.2 mm (30%), 0.4 mm (40%) and 0.8 mm (30%). In order to compare the infilling process of graded sediment transport with uniform sediment transport under the equivalent single size assumption, the uniform material was taken to have an equivalent diameter of 0.455 mm (100%) based on the same sediment inflow as used in graded sediment transport situation. The time increment is chosen to be 1 hour. The parameters used in the Preissmann scheme for hydrodynamic equations, suspended-load transport, bedload transport and bed material conservation are listed in Table 5.1

**Table 5.1 Space and Time Weighting Factors Used In Simulation of Erosion Process**

	Hydrodynamic equations	Suspended-load Transport	Bedload transport	Bed material conservation
Time weighting, $\theta$	1.0	1.0	1.0	1.0
Space weighting, $\psi$	0.5	0.5	0.5	1.0

Figures 5.10 shows the infilling of the trench in the channel for the graded material, the bed profiles are drawn after 0.5, 1, 2 and 5 days of simulation. Figure 5.11 shows the predictions of bed profiles after 0.5, 1, 2 and 5 days of simulation for uniform bed material.

Figures 5.12 and 5.13 show the distribution of total transport rate and transport capacity along channel for suspended-load and bedload respectively. It can be seen

from Figures 5.12 and 5.13 that the distribution of transport rate is different from transport capacity.

Figure 5.14 shows the distribution of mean size in the bed material at a time of 12 hours and 1 day after start of simulation. Intuitively, one would expect deposition to cause the bed material to become finer and erosion to cause coarsening. It can be seen from Figure 5.14 that the model reproduces this trend. After a long duration, the bed material composition becomes constant when final equilibrium situation is reached where all hydrodynamic and sediment parameters are constant.

### 5.6 Test Application of The Armouring

In an mobile bed river, a coarse surface layer can be developed on the bed, with the material under this coarse layer being protected from erosion. This coarse layer is called an armour layer. Armour layers may be static, corresponding to vanishing or near-vanishing sediment supply, or mobile in the presence of an upstream sediment supply, see Parker & Sutherland (1990). This test is designed to examine the capability of the model to simulate the static armouring process due to selective erosion. As mobile armour layers have been demonstrated to be closely related to the static armour layer, see Parker & Sutherland (1990), the conclusions from this test are also suitable for the mobile armouring process.

The test reach is 2,000 m long with rectangular cross sectional shape. The initial bed slope is 1/2,000 with inflow constant at 5 m<sup>3</sup>/s,m. The initial bed material is divided into the 6 size fractions shown in Table 5.2. The range of this bed material is from 0.25 to 8 mm.

**Table 5.2 Initial Grain Size Distribution**

Intermediate size (mm)	0.25	0.50	1.00	2.00	4.00	8.00
Percentage %	4	8	18	35	25	10

The whole length of reach is divided into 21 cross sections with a constant space step 100 m. The time increment is 1 hour for a total simulation time of 50 days. The incoming suspended-load and bedload are zero and erosion will take place so that bed material will become coarser during the period of simulation. The details of boundary conditions are listed in Table 5.3.

**Table 5.3 Boundary Conditions For Armouring Process**

	Discharge (m <sup>3</sup> /s,m)	Water Level (m)	Suspended- load	Concentration flux	Bedload
Upstream	5	—	0	—	0
Downstream	—	2.47	—	0	—

The initial conditions were calculated using steady flow theory. The parameters in the Preissmann scheme are the as same as given in Table 5.1.

The numerical results are shown in Figure 5.15 to 5.19. Figure 5.15 shows that the unit width transport rate at a distance of 300 m from inlet decreases with time during the development of the armour layer. Figure 5.16 and 5.17 show that the distribution of the unit width transport rate and unit width transport capacity for suspended-load and bedload along channel respectively at time of 1 day. Figure 5.18 shows variations in  $D_{16}$ ,  $D_{50}$  and  $D_{84}$  at 300 m from inlet with time, from which it can be seen that the bed material is becoming coarser during the armouring process. Figure 5.19 shows the grain size distribution of the bed material and the transported material at 300 m from inlet at 50 days.

From above numerical results, it can be seen that the transport rate decreases as the armour layer is developed. When the armour layer is formed the transport rate is only about 1% of the initial value in this test application. This demonstrates that the model is able to capture this physical behaviour of graded sediment transport.

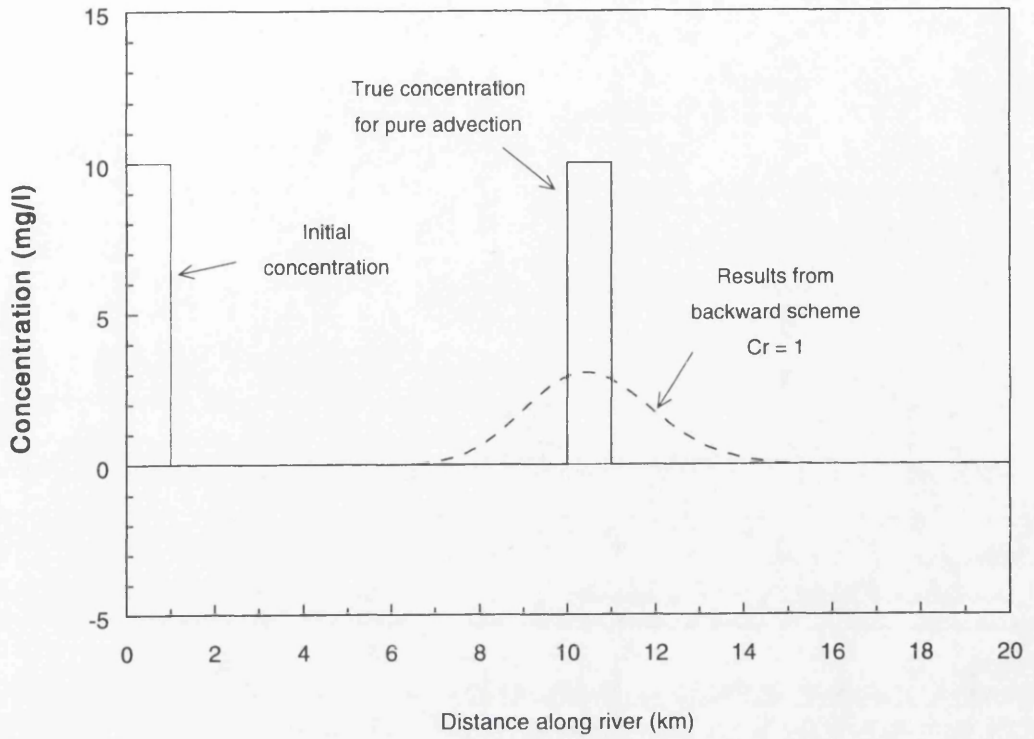


Figure 5.1 Numerical Prediction For Plug Source Concentration Distribution From Backward Scheme

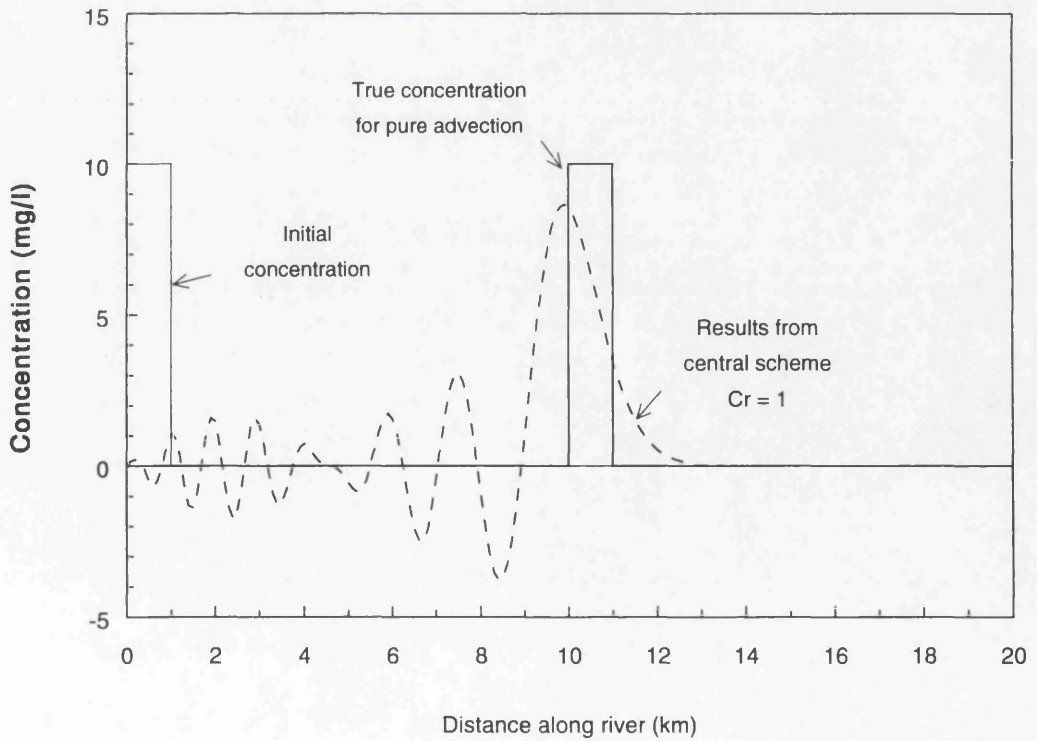


Figure 5.2 Numerical Prediction For Plug Source Concentration Distribution From Central Scheme

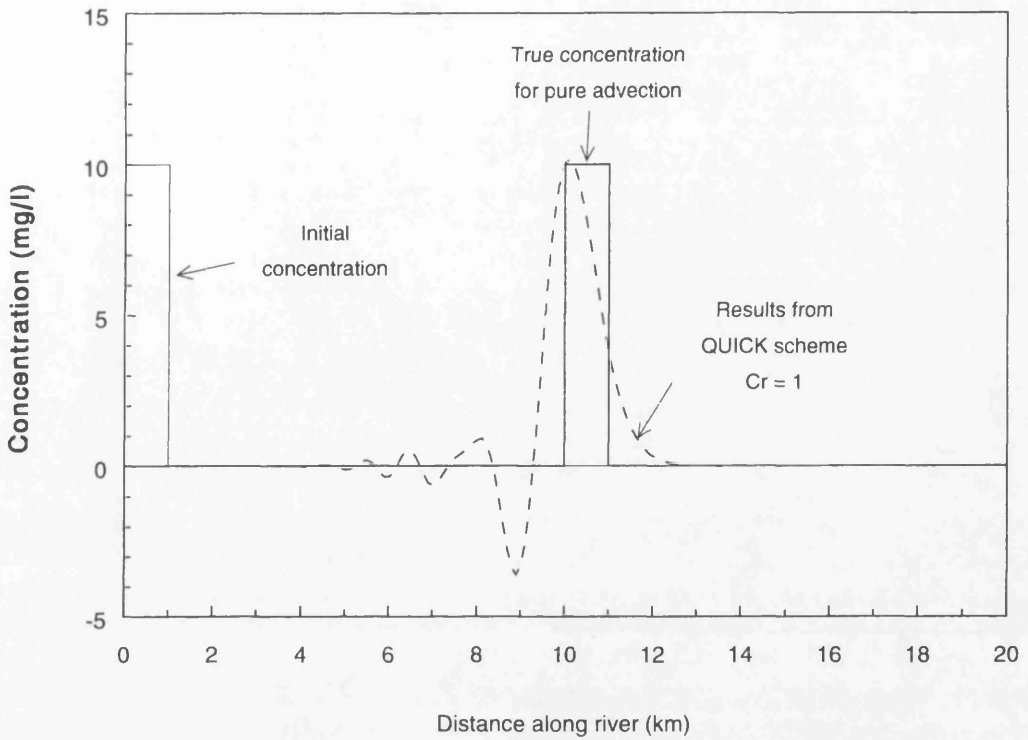


Figure 5.3 Numerical Prediction For Plug Source Concentration Distribution From QUICK Scheme

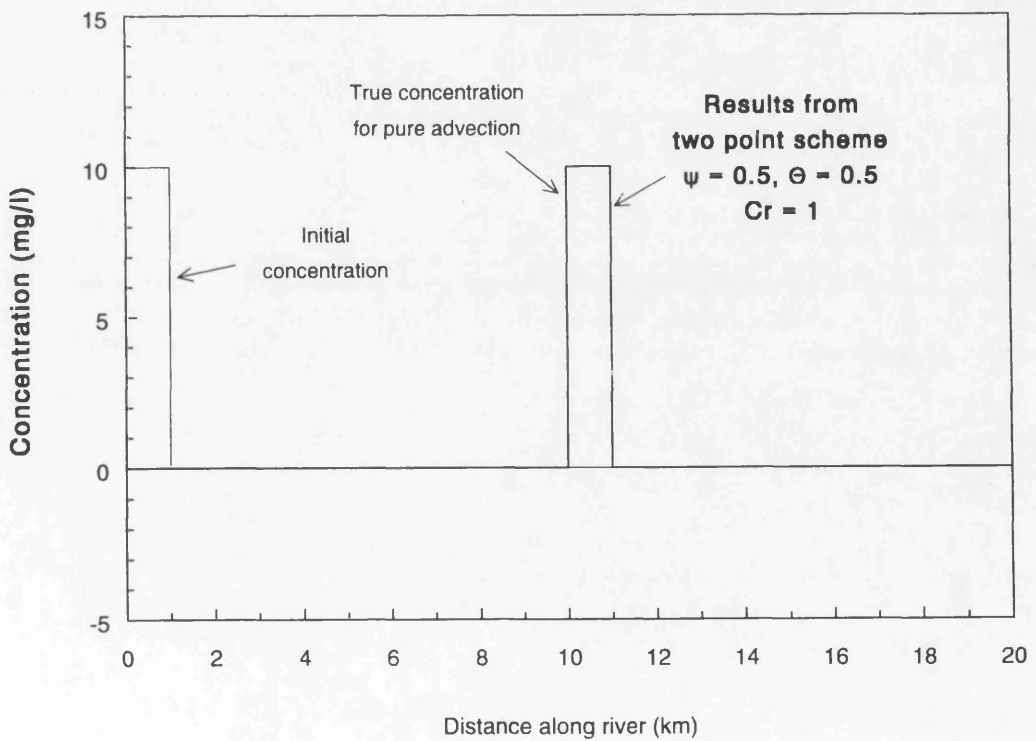


Figure 5.4 Numerical Prediction For Plug Source Concentration Distribution From Two Point Scheme

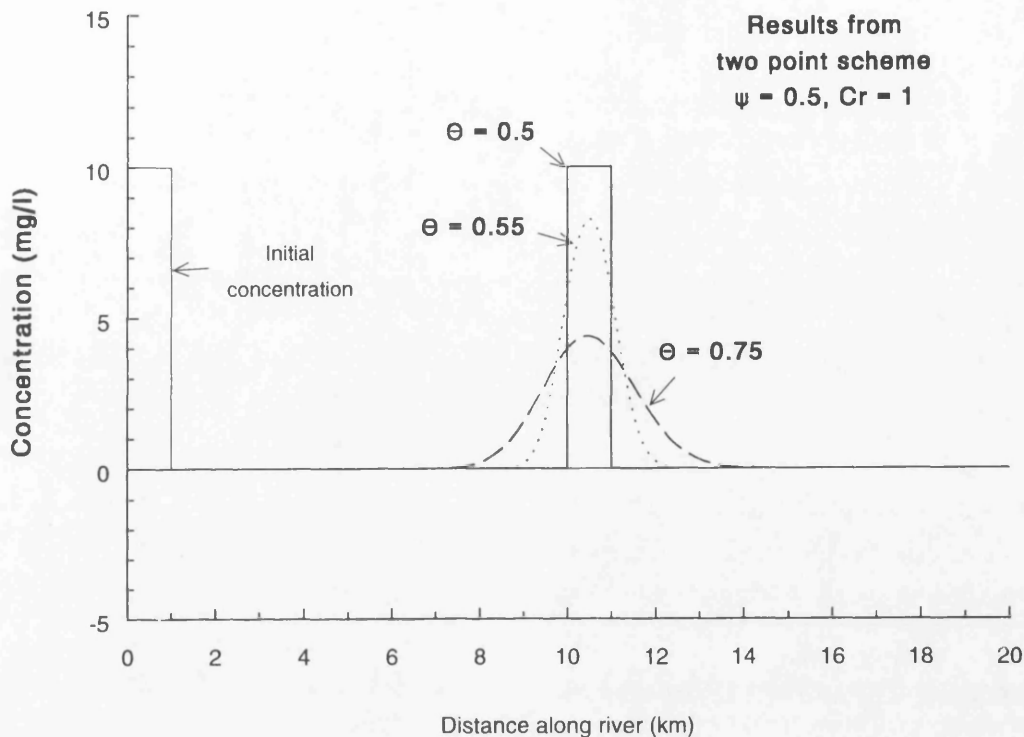


Figure 5.5 Prediction of Plug Concentration From Two Point Scheme For Different Time Weighting Factor

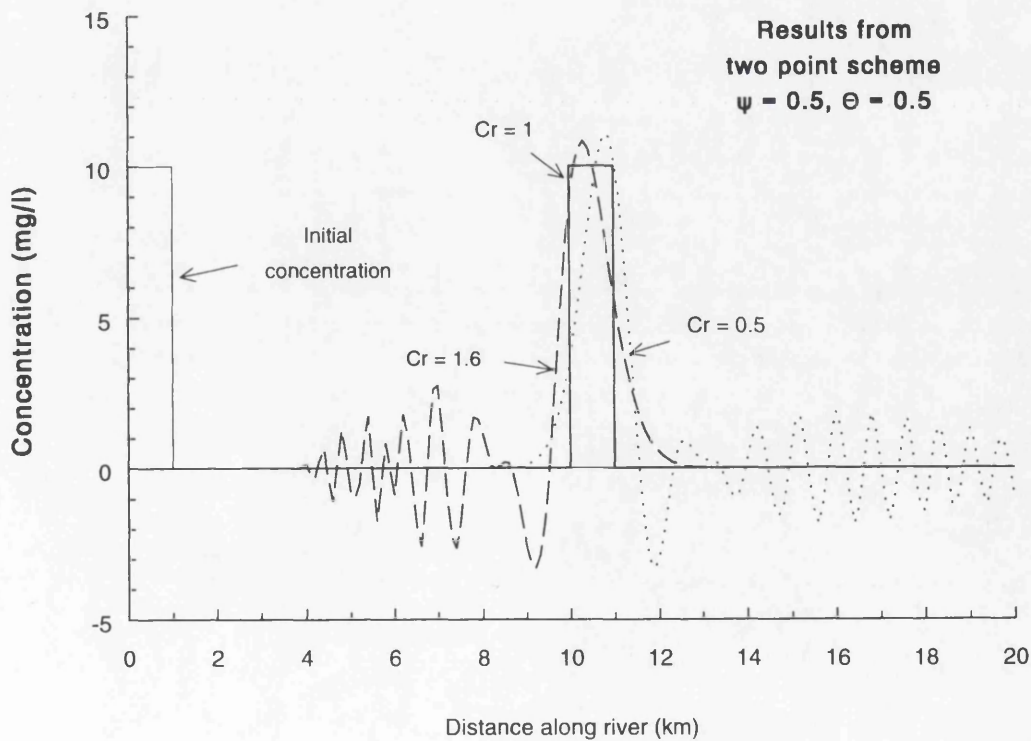


Figure 5.6 Prediction of Plug Concentration From Two Point Scheme For Different Courant Number

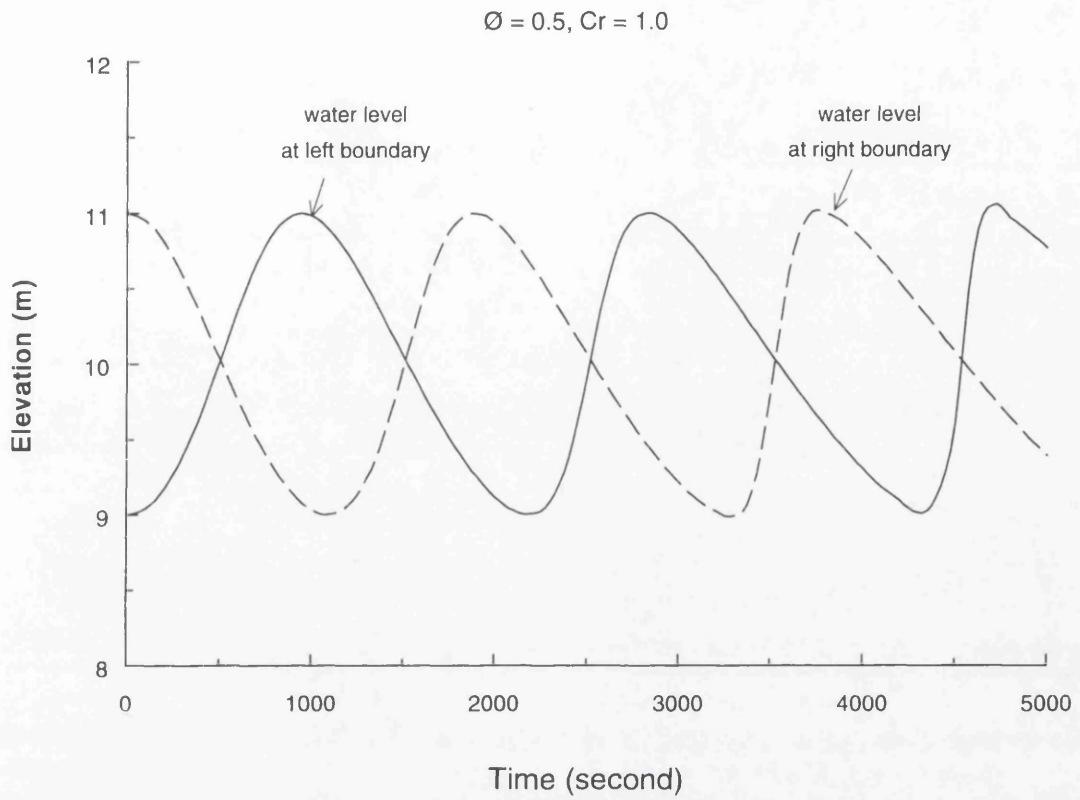


Figure 5.7 Numerical Results of Water Level at Upstream and Downstream Boundary

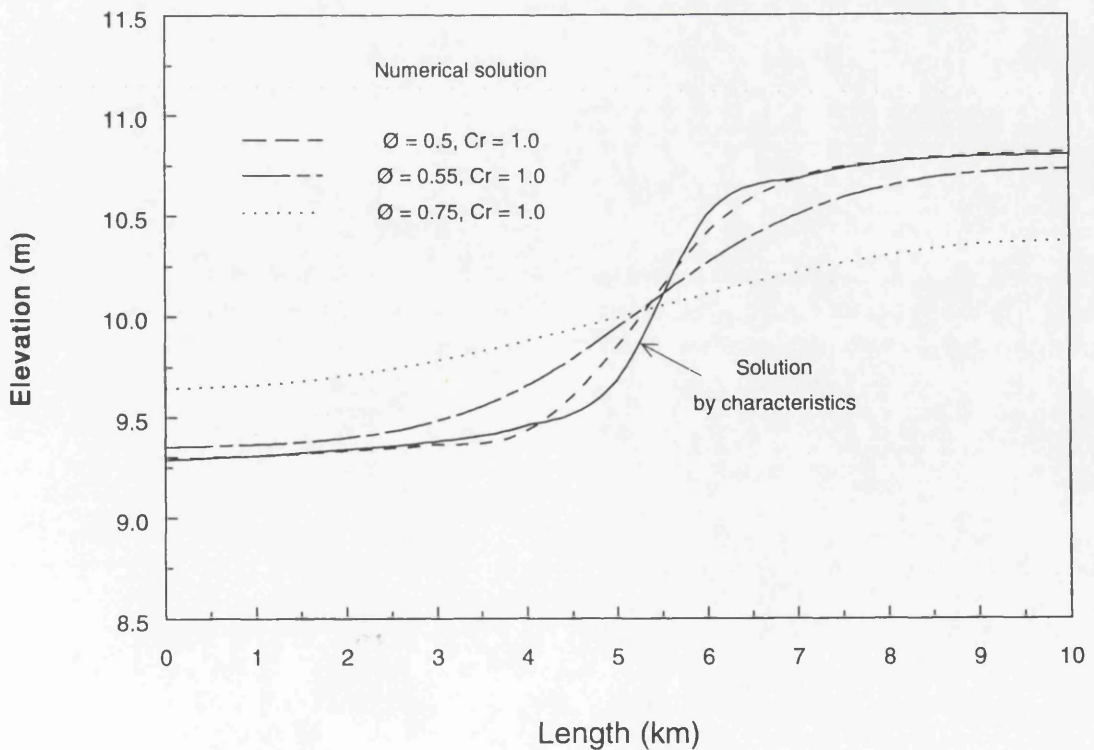


Figure 5.8 Comparison of Water Level Results Under Different  $\theta$

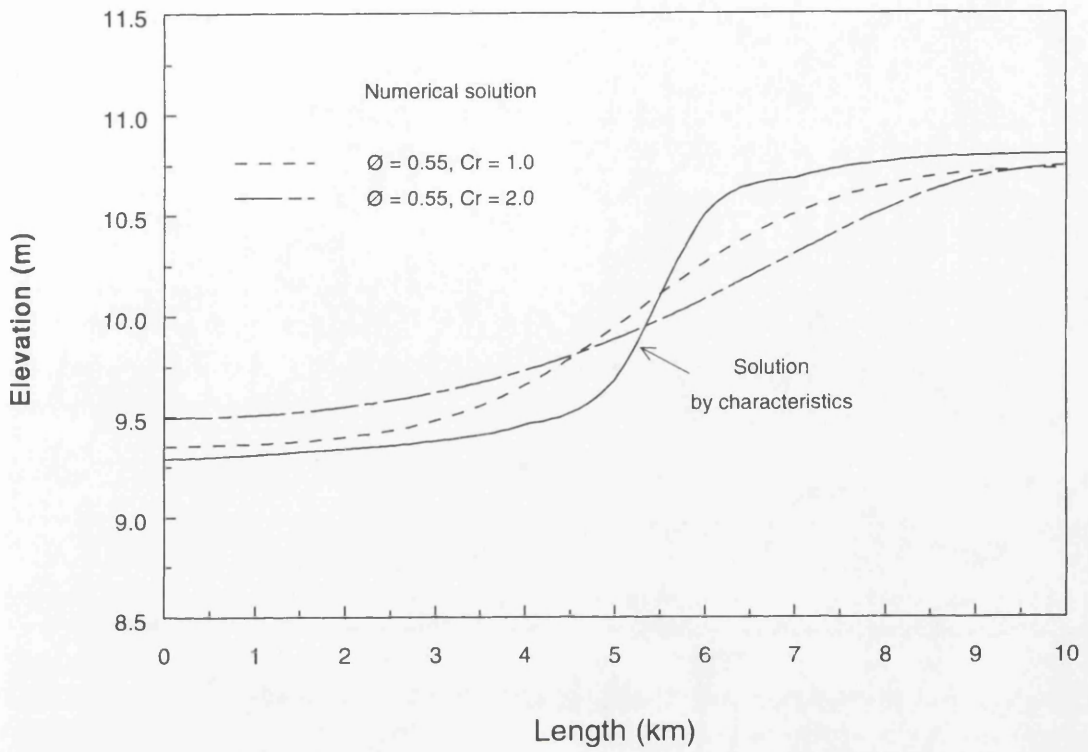


Figure 5.9 Comparison of Water Level Results Under Different Cr

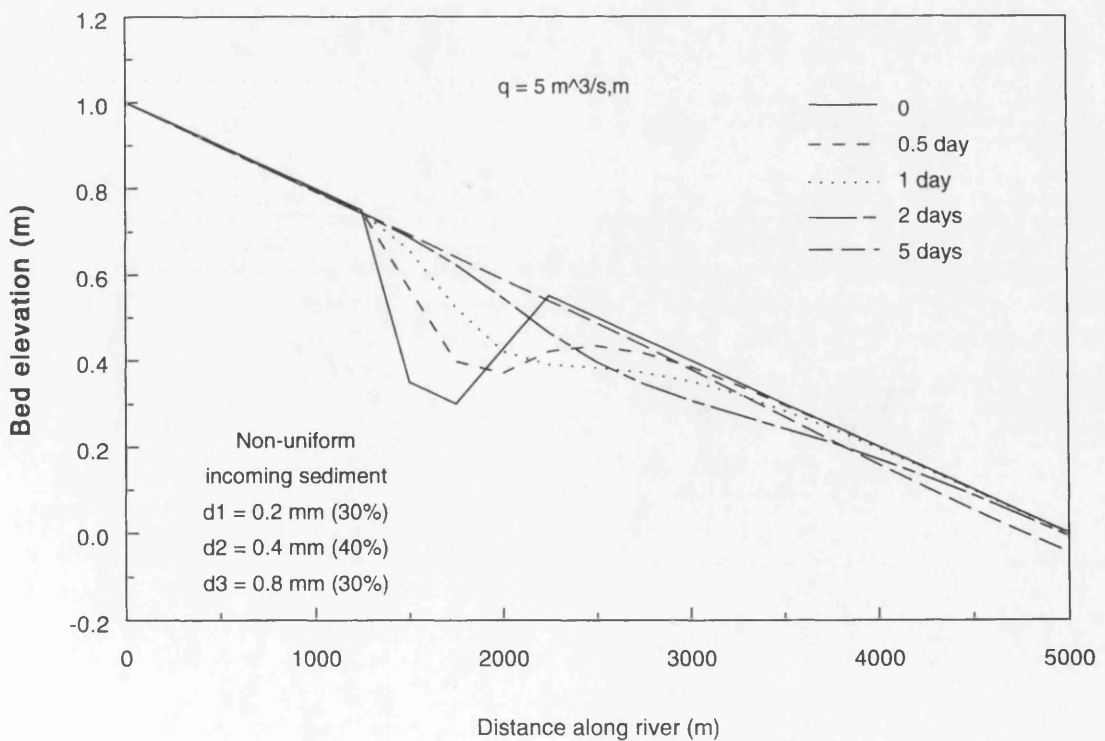


Figure 5.10 Infilling Process of Trench For Uniform Material

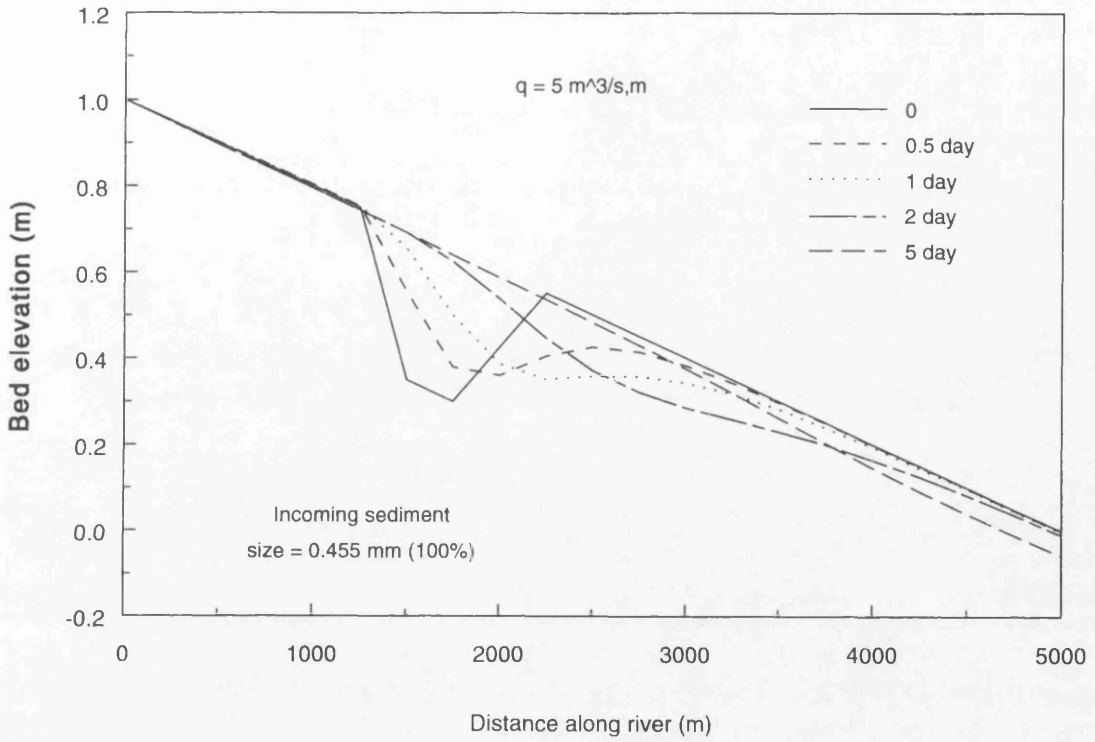


Figure 5.11 Infilling Process of Trench For Uniform Material

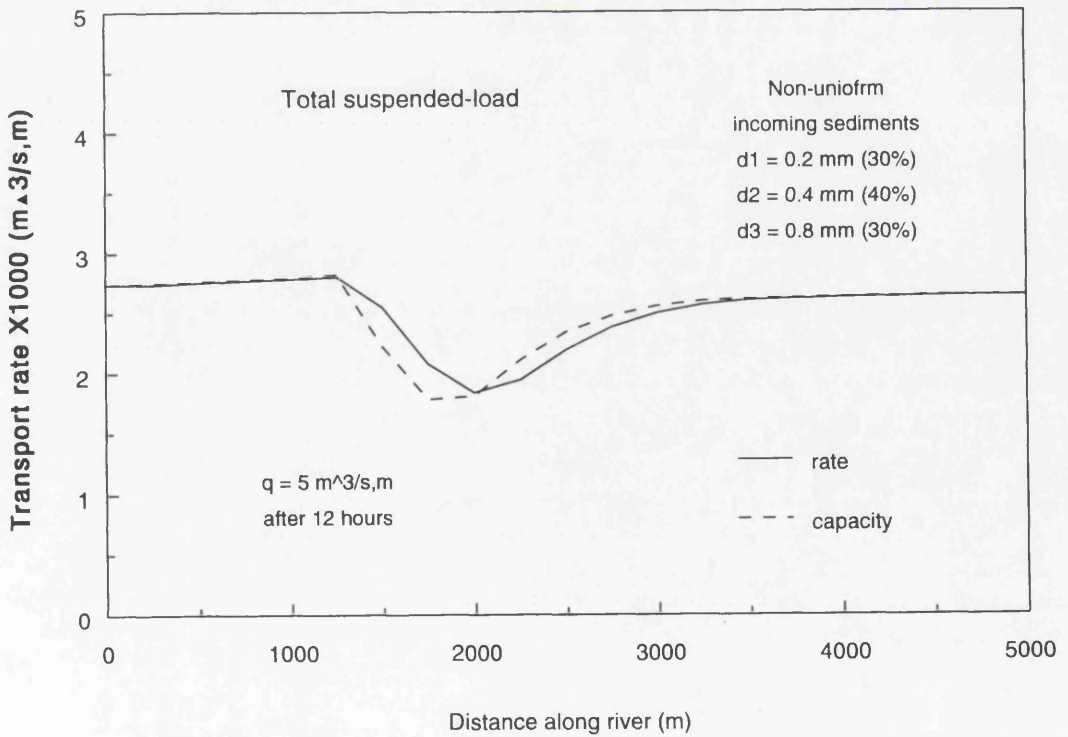


Figure 5.12 Distribution of Transport Rate and Capacity of Suspended-load Along Channel After 12 hours

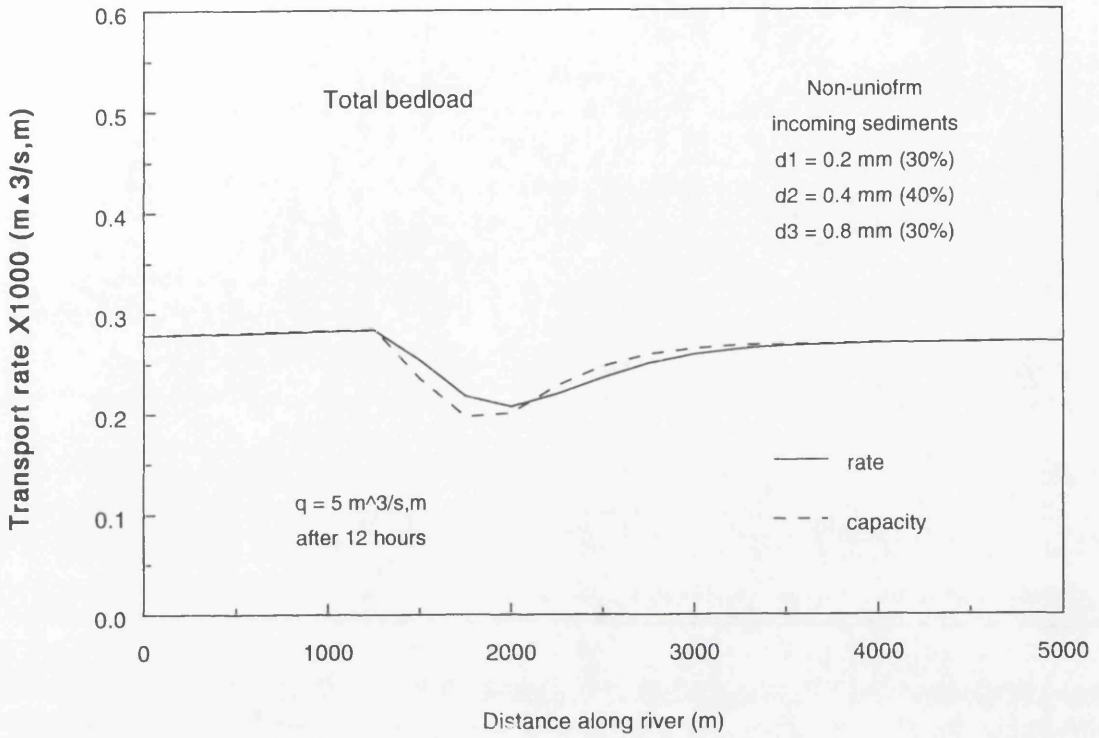


Figure 5.13 Distribution of Transport Rate and Capacity of Bedload Along Channel After 12 hours

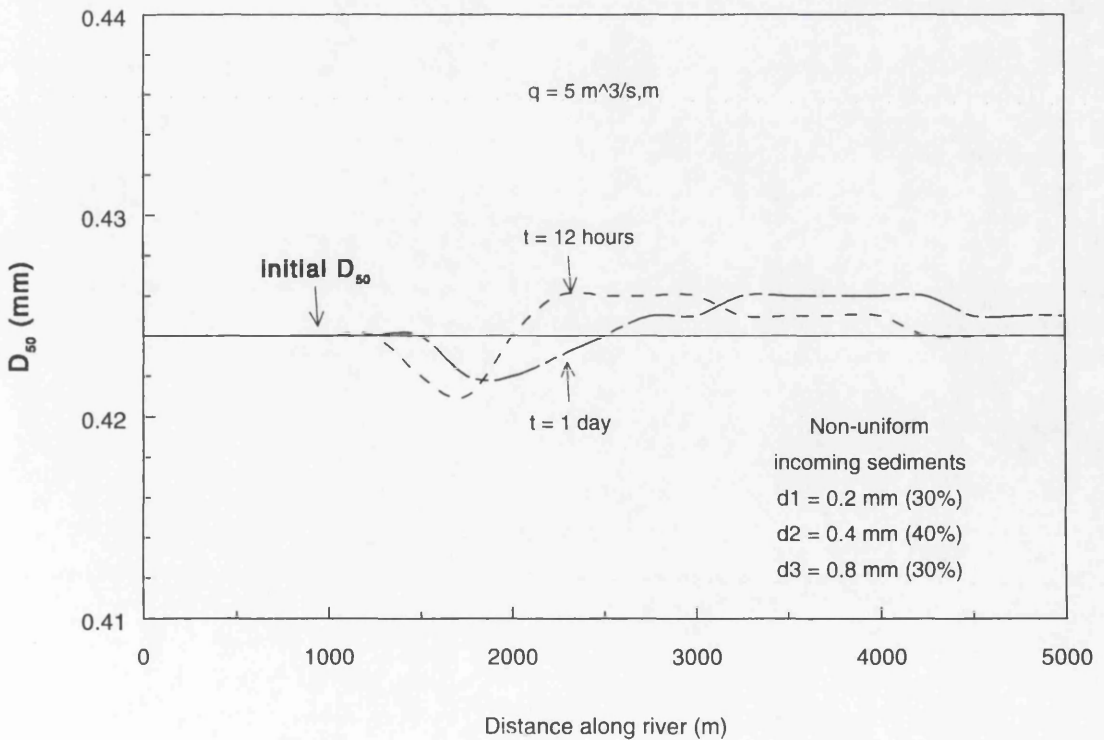


Figure 5.14 Distribution of Mean Size In Bed Material Along Channel

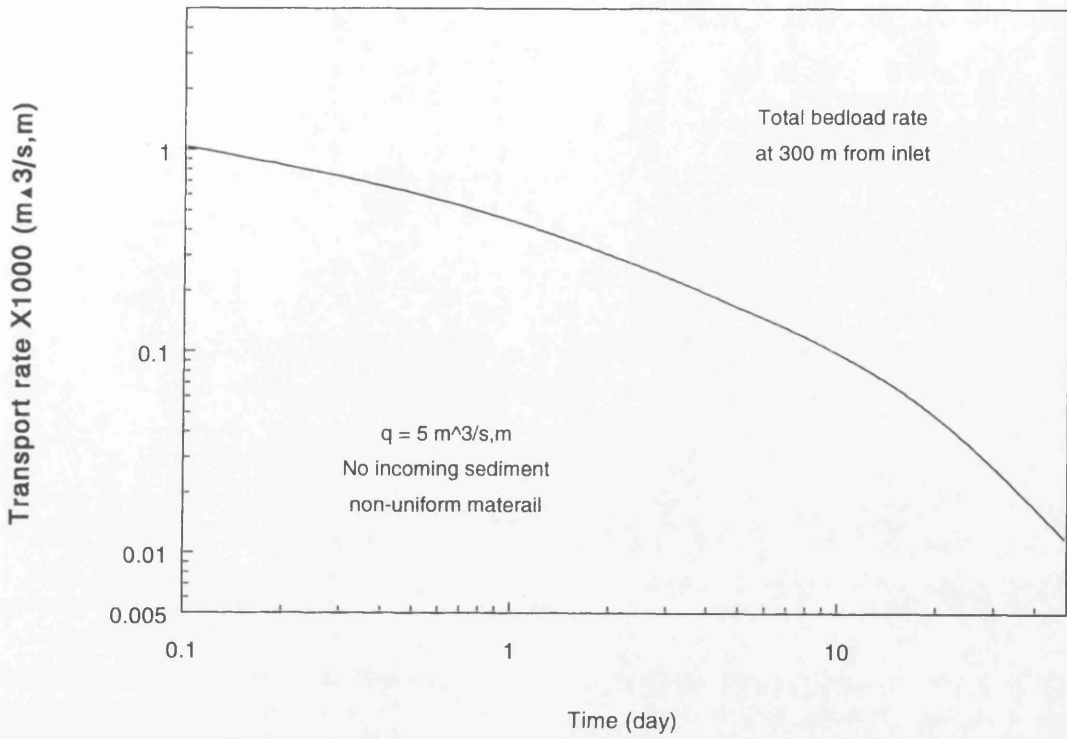


Figure 5.15 Transport Rate Varying With Time During Armouring Development

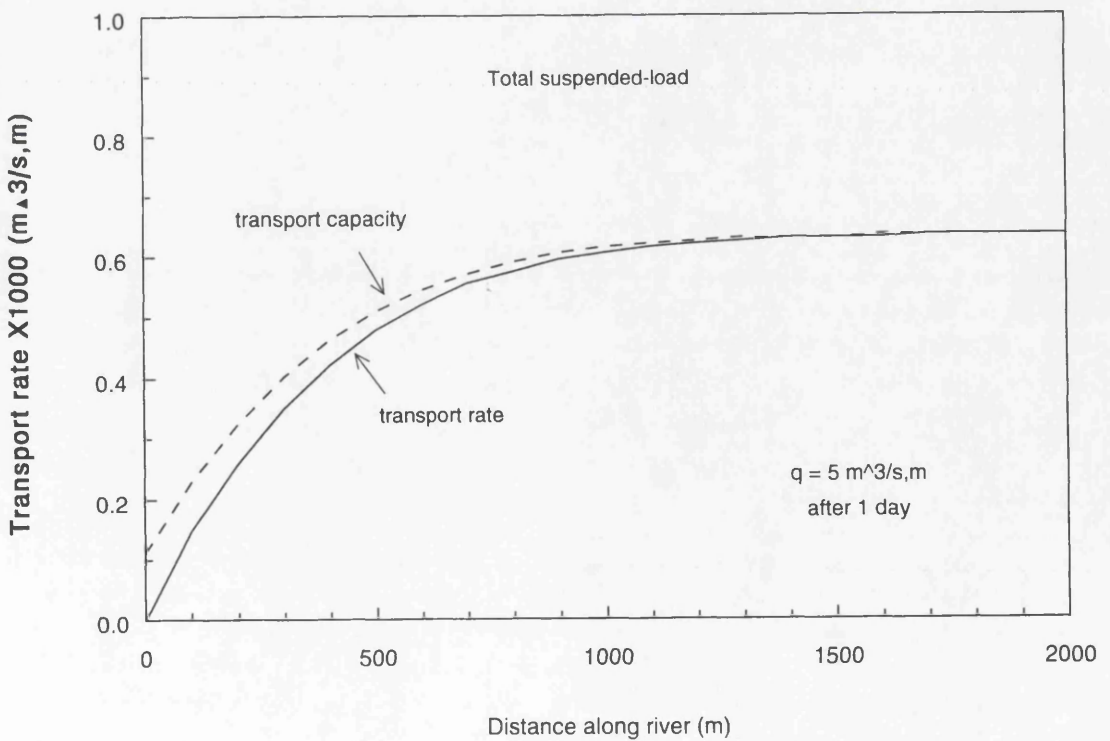


Figure 5.16 Suspended-load Transport Rate Distribution Along Channel After 1 Day

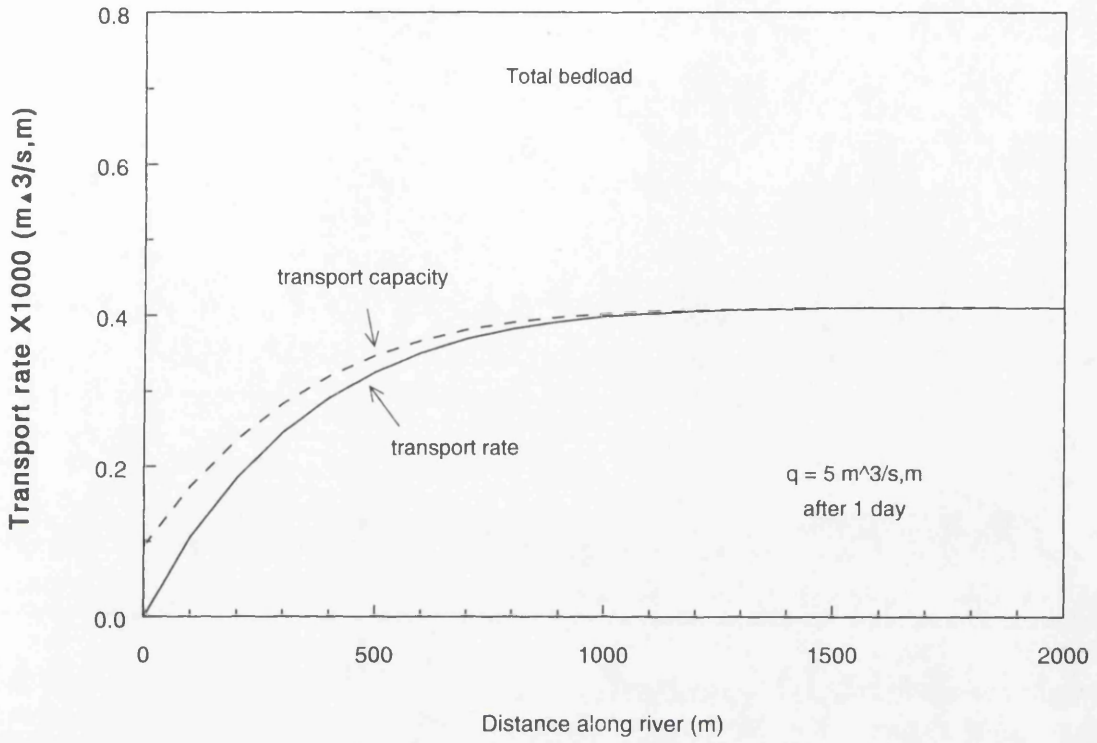


Figure 5.17 Bedload Transport Rate Distribution Along Channel After 1 Day

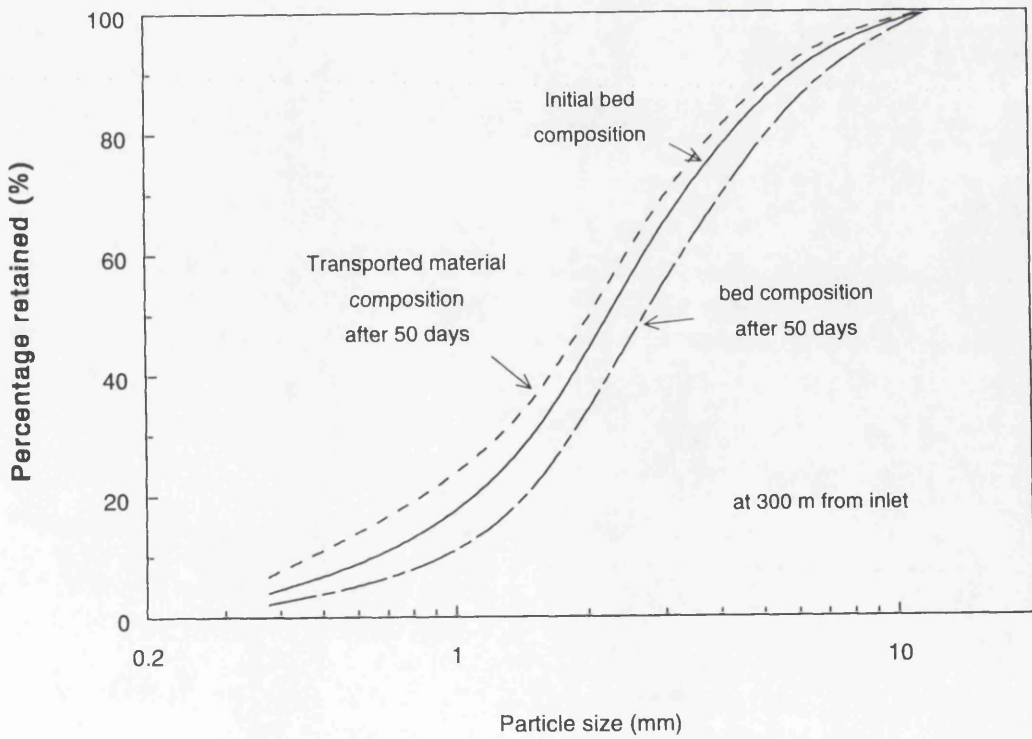


Figure 5.18  $D_{16}$ ,  $D_{50}$  and  $D_{84}$  Varying With Time At 300 m From Inlet

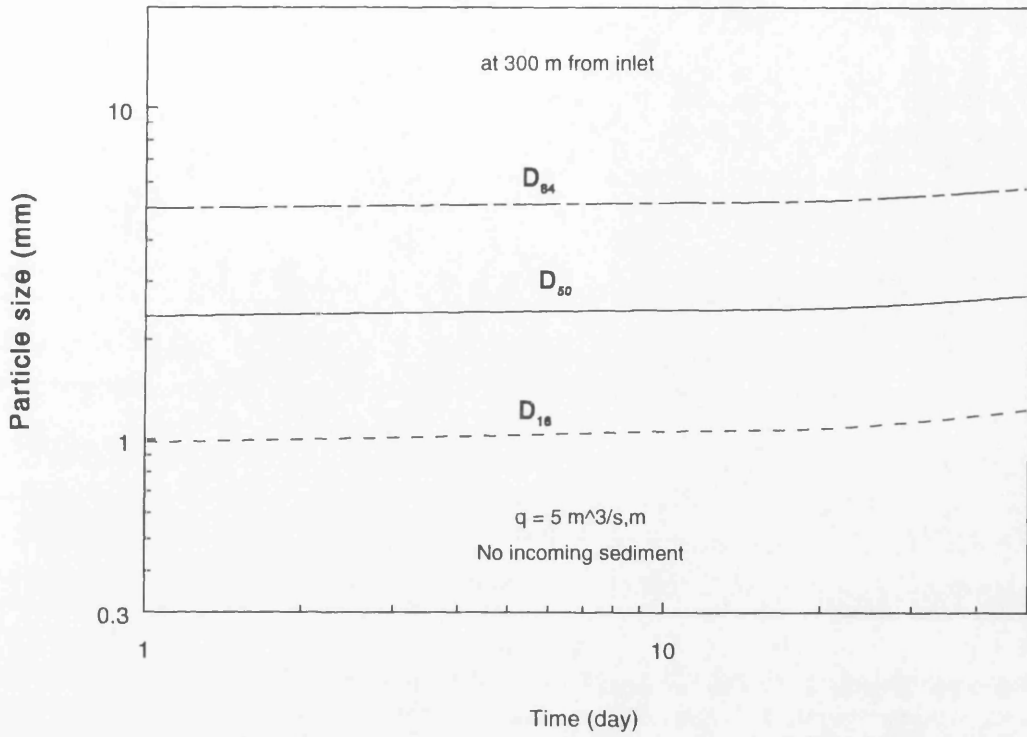


Figure 5.19 Composition of Bed Material and Transported Material After 50 Days At 300 m From Inlet

## **CHAPTER 6**

### **Application of The Model To Experiments of Static Armour Development**

#### **6.1 Introduction**

In a river reach with a gravel bed a layer of material that is coarser than the underlying substrate can develop. This layer is termed an armour layer and can be either static or mobile depending on sediment flow with no sediment entering the upstream end the bed of the river will form a static armour. In this case the sub-threshold material is gradually removed from the bed and the sediment transport rate reduces to zero. If a higher flow occurs the armour layer is broken up and the process begins again. Clearly, grain hiding plays an important role in the development of an armour layer. This chapter presents results from applying the hiding functions developed in chapter 3 together with the model and other sediment relationships to experimental measurements of the static armouring process. The experiments were conducted at the University of Aberdeen, see Tait, Willetts & Maizels (1992).

#### **6.2 Experimental Tests In Aberdeen University**

Four experiments were conducted at the University of Aberdeen to investigate graded sediment transport processes during the development of the armour layer. During the experiments, periodic observations were made of both the bedload composition, bedload transport rate and the grain size distribution of the surface bed material.

### 6.2.1 Experimental Apparatus

Four experiments were conducted in a recirculating, tilting glass-sided flume 12.5 m long by 0.3 m wide, see Figure 6.1. The slope of the flume was set at 0.001 for the first three experiments and 0.004 for the fourth experiment. Subcritical flow was employed throughout the tests. All water and bed level measurements were made relative to a datum plane defined by two parallel rails running along either side of the flume. The water and bed levels were measured using a point depth gauge with an accuracy of 0.1 mm. The water depth was controlled by an adjustable and sharp-edged tail weir at the downstream end of the flume. This was adjusted so as to minimise the drawdown effects and give as large a length of uniform flow as possible.

The total bedload rate and fractional bedload rate for each size fraction were measured using a bedload sediment trap which consisted of a 200 mm by 9 mm opening in the base of the flume, a valve and several interchangeable sediment collection boxes, see Figure 6.2. This dimension allowed the trap to collect the bedload across the whole width of the flume, and restricted the maximum grain size which could be trapped to 6 mm. This limited the maximum size fraction in any of the bed mixtures used. The trap was installed 10.5 m downstream from the flume inlet.

The bedload collection boxes were split into three sections laterally. The sediment was thus collected from three separate 100 mm wide zones across the width of the flume.

During the first three experiments the flow was measured by integrating a velocity profile obtained at a particular cross-section using a laser doppler anemometer system. The flow was held constant throughout each of these experiments by controlling the height of water above the downstream weir. In the final experiment the flow was monitored and thus kept constant using a pre calibrated orifice plate.

### 6.2.2 Experimental Procedure

Four experiments were carried out to obtain the stable armoured layer on the bed surface. The hydraulic influences in each experiment were kept as constant as possible so that any reductions in the sediment transport rates could be attributed to bed sediment composition changes rather than changes of the flow strength. The bed slope and water depths were monitored to discover if the average bed shear stress remained effectively constant throughout the experiment.

The base of the laboratory flume was covered with a layer of thoroughly mixed sediment for each experiment. The sediment was slowly flooded for its whole depth and then drained to aid settlement. It was then scraped level using a template running on the datum rails with the excess material being discarded. This produced a flat sediment bed with a constant slope equal to 0.001 in experiments 1, 2 and 3, and 0.004 in the experiment 4. The surface contained all of the grain sizes of the parent material.

The bed was first exposed to a low flow, below the estimated threshold of motion in order to remove any unnaturally exposed grains left by the bed-laying operations. The bed was then ready for the experiment to begin. The photographs and bed samples were taken to record the initial state of the sediment bed.

A steady flow was introduced and the tail weir adjusted to extend the uniform depth of flow to as large a length as possible. The discharge in each of the experiments was selected so that it could move only a certain proportion of the sediment grains present on the bed surface. Selective transport therefore occurred, and the bed began to armour progressively. The first experiment lasted only 50 hours, but the other three had a duration of 100 hours. The experiments were stopped when either the sediment transport rate had declined to 10% of its original value, or 100 hours has elapsed.

### 6.2.3 Sampling Techniques

The water and bed levels were recorded every 30 mm across the width of the flume and at 1 m intervals along the working length, from 3 m to 9 m measured from the flume inlet. The recorded level for each cross-section was obtained by averaging measurements. The values of the bed sediment depth, the water depth and the bed shear stress were calculated from these readings. The shear stress calculation employed a suitable sidewall correction.

The measurements of sediment transport rate were made every 30 min for approximately the first 6 hours. The time interval and the sampling period were then increased gradually to hourly, then every 2 hours, every 4 hours and eventually before and after overnight runs. The elapsed time of the transport rate measurements was taken as the time to the middle of the sample period. In experiment 4 the bed sampling interval was kept constant at 1 hour after the initial 6 hour period.

The sediment transport rate and the composition of the bedload were determined at intervals throughout the experiments from the bedload samples. The bedload samples were dried, weighed and then sieved. All the sediment samples were analysed using a series of sieves at  $1/2\Phi$  intervals.

#### **6.2.4 Initial Experimental Conditions**

The grain size distribution for all four bed materials are given in Table 6.1 and also shown in Figure 6.3.

The summary of the initial hydraulic conditions and bed material characteristics for all four experiments are given in Table 6.2

**Table 6.1 Grain Size Distribution By Weight For All Four Mixtures In Aberdeen University**

intermediate size (mm) <sup>a</sup>	percentage by weight			
	No.1	No.2	No.3	No.4
0.063	—	—	—	0.64
0.105	5.56	2.76	2.64	0.49
0.150	9.31	4.55	4.49	0.57
0.212	11.85	6.30	6.41	0.71
0.300	10.50	7.65	7.64	0.77
0.425	11.15	9.38	9.65	1.26
0.600	11.04	10.26	10.42	2.53
0.850	10.40	10.69	10.94	6.34
1.180	8.93	11.51	11.38	18.77
1.700	8.03	11.98	11.82	22.69
2.360	6.85	12.48	12.65	21.35
3.350	5.06	10.15	9.83	17.49
5.000	1.11	1.91	1.85	5.79
6.300	0.21	0.38	0.28	0.60

<sup>a</sup> Intermediate particle size determined as size half way between bracketing sieve sizes

**Table 6.2 Summary of Experimental Conditions In Aberdeen University**

Experimental No.	1	2	3	4
Discharge (l/s)	7.5	6.0	9.0	9.0
Initial bed slope	0.001	0.001	0.001	0.004
Initial water depth (mm)	65.70	57.80	72.80	62.53
Shear velocity (m/s)	0.0254	0.0238	0.0267	0.0495
Equivalent diameter from Shields (mm)	1.15	1.11	1.22	3.21
Range of $D_j$ (mm)	0.105—6.300	0.105—6.300	0.105—6.300	0.063—6.300
$D_{50}$ (mm)	0.447	0.808	0.793	1.578
$\sqrt{D_{84}/D_{16}}$	3.072	2.966	2.941	1.710
$D_g$ (mm)	0.559	0.871	0.864	1.745
$\sigma_g$	2.739	2.698	2.679	2.003

### 6.3 Numerical Model

In the numerical model the total flume length was divided into 26 cross sections with a constant distance increment of 0.5 m. A time increment of 1 hour was used and each simulation run for 100 hours of experimental time. The initial bed material composition matched those given in Table 6.1 with the hydraulic conditions matching those in Table 6.2. Upstream boundary conditions employed were constant water inflow and zero sediment inflow. At the downstream boundary a constant water level was maintained and the suspended-load transport flux was assumed to be zero. The porosity of the sediment was taken as 0.4 in each case. The numerical model computed sediment transport rate per unit width which was compared with the measurements from the central part of the bed load trap.

In this application the space parameter in the Preissmann scheme was centred and time parameter was unity for hydraulic and graded sediment components.

### 6.4 Comparison Between Two Hiding Functions

In the chapter 3 two hiding functions were developed, a hiding function and a reduced hiding function. In the following the performance of the two hiding functions has been examined through the application of the model to the armouring experiments described above.

#### 6.4.1 Hiding Function

The results of the numerical simulation from using the hiding function for experiment No.1 are shown in Figures 6.4 to 6.6. The total load predictions, Figure 6.4, are seen to be reasonable, and as expected the volume transported decreases with time as armouring progresses. Comparison of the measured and computed size fraction transport rates at time 361, 614 and 2331 minutes, Figure 6.5, are seen to be poor however. Indicating that the total transport rate predicted by the numerical model contains too great a proportion of the coarse grains. This is also reflected in Figure 6.6, which shows predicted changes to the composition of the active layer with time.

It can be seen that the predicted bed composition shows an increase in the percentage of fine material in the active layer. Intuitively, this is incorrect as one would expect a reduction in the proportion of fine material during armour formation. This is supported by the results from Aberdeen's experiments where a clear decrease in the proportion fine material is observed.

#### **6.4.2 Reduced Hiding Function**

Comparisons between the computed and experimental results from using a reduced hiding function for experiment No.1 are shown in Figures 6.7 to 6.10. It can be seen in Figure 6.7 that an improvement in the prediction of the total transport rate has been obtained. Comparing the computed results with the measured data in Figure 6.8 it can be seen that the predicted and measured rates of each size fraction are now in much better agreement. This is supported by Figures 6.9 and 6.10 where a coarsening of the bed material is predicted.

#### **6.4.3 Difference Between Two Hiding Functions**

It is clear that from the foregoing that a reduced hiding function provides significantly better results for the case considered. The reason for this can be seen in Figure 6.11, which shows the critical shear stress calculated using both hiding functions for each size fraction at time zero in the experiment No.1. It is clear from this that the hiding function over estimates the stability of grains with diameters less than 0.4 mm approximately. In fact, Figure 6.11 indicates that hiding function fails to meet the basic criteria for hiding, that the coarse fractions should be more mobile and the fine fractions less mobile, here the reverse is predicted. As the base data and optimisation techniques are identical for each hiding function it is believed that the reason for the difference is related to the physical nature of graded sediment.

### **6.5 Numerical Simulations**

After testing the hiding functions it was concluded that the reduced hiding function should be employed for further simulations of armouring experiments. The numerical simulations were undertaken for each of the four experiments. The results of these are presented in the following.

### 6.5.1 Experiment 1

The main results from the numerical simulations are presented in Figures 6.7 to 6.10 where appropriate experimental results are also shown. Figure 6.7 compares the simulated and measured sediment transport values. As commented previously, an encouraging level of agreement is obtained between the simulated and observed transport rates. As one would expect a general coarsening of the bed is observed. Indeed the model predicts an increase in  $D_{16}$  from 0.187 to 0.282 mm, in  $D_{50}$  from 0.544 to 0.833 mm and in  $D_{84}$  from 1.788 to 2.284 mm. Figure 6.8 compares the measured and computed bedload composition at 361, 614 and 2331 minutes after the start of the experiment. Good comparisons are achieved, but it should be noted that at the latter times the model is underpredicting the movement of fine material (size fractions 0.105 and 0.150 mm) and overpredicting the movement of coarse material (size fractions 1.7 mm, 2.36 mm and 3.35 mm). Figure 6.9 shows the composition of bed material at time 1500 and 6000 minutes. It can be seen in Figure 6.9 that the proportion of the grains finer than 0.4 mm is reduced and conversely the proportion of the grains greater than 0.4 mm is increased. The composition of the final armour layer from the numerical model and the experiment is shown in Figure 6.10 again the level of agreement is encouraging.

### 6.5.2 Experiment 2

The main results from the numerical simulations are shown in Figures 6.12 and 6.13. Figure 6.12 shows a comparisons of total bed load rates between the computed and observed values. The level of agreement is again good. In the experiment No.2 the applied shear stress of  $0.0238 \text{ N/m}^2$  is relatively low. Applying Shields threshold

condition to a uniform bed this shear stress would result grains of diameter 1.11 mm being at threshold. This is around  $D_{65}$  for the bed material in experiment 2, implying that 35% of the grains in the bed are above threshold. Consequently, a very low initial transport rate of 1.22 g/min/m is observed and as can be seen from Figure 6.3 there is little evidence of bed armouring after 100 hours. This is consistent with field investigations of Parker et al (1982) and Kuhnle (1989) where they argue that an armour layer cannot be developed and that equal mobility of size fractions is a valid assumption under these circumstances.

### 6.5.3 Experiment 3

Figures 6.14 to 6.18 show the results from the numerical simulations of experiment 3. Figure 6.14 compares the computed and measured results for the total bedload rate. The level of agreement is very good. Figure 6.15 shows the comparison of the composition in the transported material, here it can be seen that the agreement is encouraging, however at 2911 minutes the bedload rates were overestimated for fine material (size fractions 0.105, 0.15 and 0.212 mm) and underestimated for size fractions coarser than 0.425 mm. Figure 6.16 shows the composition of the bed material at 1500 and 6000 minutes. It is clear in Figure 6.16 that the bed material became coarser where the percentage of material finer than 0.7 mm was reduced and the percentage greater than 0.7 mm increased. Figure 6.17 compares the computed and measured results for three typical bed material diameters  $D_{16}$ ,  $D_{50}$  and  $D_{84}$ . It indicates that  $D_{16}$ ,  $D_{50}$  and  $D_{84}$  increase with time during the development of the armour layer. The level of agreement is satisfactory. Figure 6.18 shows the final composition of bed material between the computed and observed values. It is in good agreement.

### 6.5.4 Experiment 4

In the experiment No.4 where the bed shear stress was relative large, see Table 6.2, the total bedload rates observed decreased during the development of the armour

layer. The main results from the simulation are shown in Figures 6.19 to 6.23. In Figure 6.19 the computed total bedload rates are compared with the measured values and are in good agreement. In Figure 6.19 it can be seen that the total bedload rate increased slightly from the time zero to 100 minutes before decreasing, according to Tait et al (1992), this is a result of the initial bed composition. Figure 6.20 compares the compositions of transported material between computed and measured values. The level of agreement is satisfactory. Figure 6.21 shows the composition of bed material at 1500 and 6000 minutes and indicates that the coarsening process of the bed material was achieved. It is seen in Figure 6.21 that the percentage of material finer than 1.5 mm was decreased and increased for the fractions greater than this. The coarsening process is again shown in Figure 6.22 showing that  $D_{16}$ ,  $D_{50}$  and  $D_{84}$  increase with time during the development of the armour layer. Figure 6.23 shows the final composition of bed material between the computed and measured results, again the level of agreement is encouraging.

## 6.6 Analysis and Discussion

The bedload rate has been observed to decrease with time, see Figures 6.7, 6.12, 6.14 and 6.19. The main reason for this can be attributed to the development of an armour layer. The selective transport also caused a coarse layer to be developed on the bed surface preventing the material underneath this layer from being eroded. Consequently, the transport rates were reduced.

There are two distinct stages for bedload transport during the development of an armour layer, Figures 6.7, 6.12, 6.14 and 6.19. In first stage, the total bedload rate is likely to keep constant for a certain time which differs in each experiment. In experiment No.1 it took about 300 minutes, in No.2 2000 minutes, in No.3 100 minutes and in No.4 150 minutes. The duration for the first stage depends on the flow conditions and initial bed material. For example, the flow velocity in the experiment No.2 is less than in No.3. The initial bed materials in both No.2 and 3 are almost

same. The duration of the first stage in No.2 is much more longer than in No.3. In the experiment No.4, the bed material is coarser than in No.1. As a result, the duration of the first stage in No.4 is shorter than in No.1. Under the same flow conditions, the larger proportion of finer grains in the bed material will be supplied to the stream so that the time for the first stage will be longer. The second stage may be defined as when the bedload rate is decreasing with time due to the development of the armour layer. The duration for second stage also differs in different experiments and is dependent on the flow conditions and the composition of bed material. When the final armour layer is formed, the sediment transport rates is effectively ceased.

This two stage behaviour demonstrates that not only the flow strength but also size fraction interactions play a major role in the graded sediment transport and accordingly the bed levels. Under certain flow conditions the armour layer can be formed and the sediment transport rates are effectively ceased. It should be emphasised that if the flow strength is larger enough to move the coarsest grains in a graded sediment it is unlikely to develop the armour layer. Other parameters such as the fluctuation of turbulence pressure and grain rearrangement are also important to affect the development of armour layer.

During the development of the armour layer, the bed material in the active layer becomes coarser. The composition of bed material at time zero, 1500 minutes and 6000 minutes are shown in Figures 6.8, 6.16 and 6.21 for the experiments No.1, No.3 and No.4 respectively. Naturally, the  $D_{16}$ ,  $D_{50}$  and  $D_{84}$  also increase with time during the development of the armour layer.

The comparisons of bedload rate for individual size fractions in the mixture for experiments No.1, 3 and 4 at different times, shown in Figures 6.9, 6.15 and 6.20, are reasonable. These figures demonstrate that the hiding effects were reflected in the model. The threshold condition for each individual size fraction can be evaluated using a reduced hiding function and Shield's value of sediment geometric mean. This hiding function, taking into account the effect of composition of bed material and flow

condition, may provide a reasonably accuracy of predicted transport rate for each size fraction in a mixture. As discussed by Sutherland (1991), the bed geometry and the pressure fluctuation of turbulence near the bed surface are also important factors to affect the threshold condition for each size fraction. The effects of these two factors on the hiding function could be evaluated if the observed data in graded sediment transport experiments can be provided.

Figures 6.10, 6.18 and 6.23 show the composition of armour layer and transported material of the bedload at 6000 minutes for the experiments No.1, 3 and 4 respectively. Clearly, the bed material becomes coarser and the transported material is finer compared with the composition of the initial bed material.

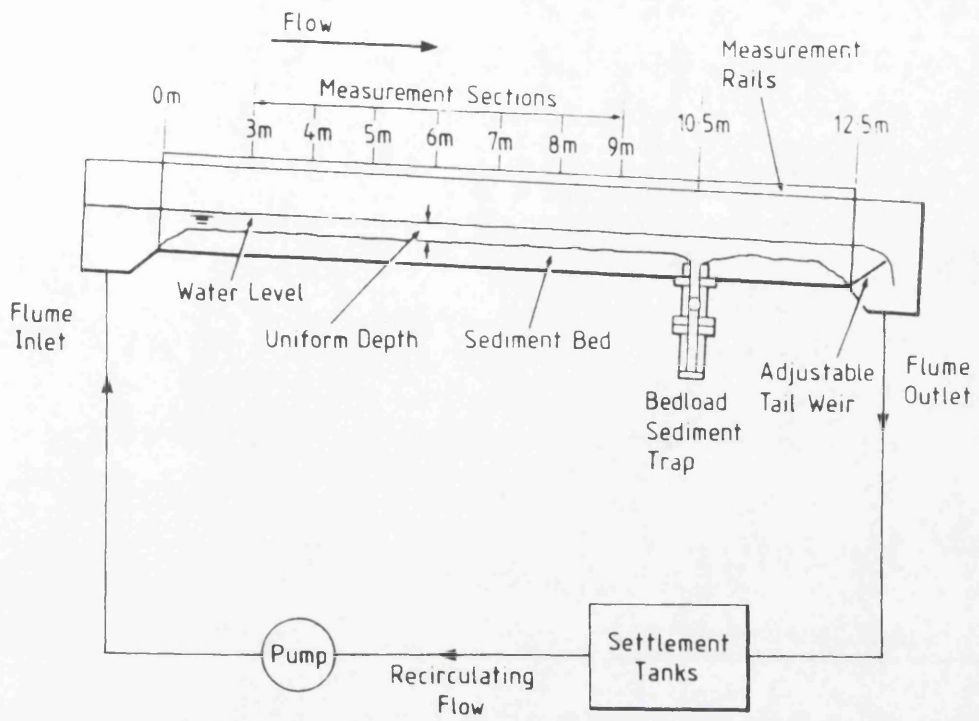


Figure 6.1 Sketch of Experimental Flume (Tait, Willetts and Maizels, 1992)

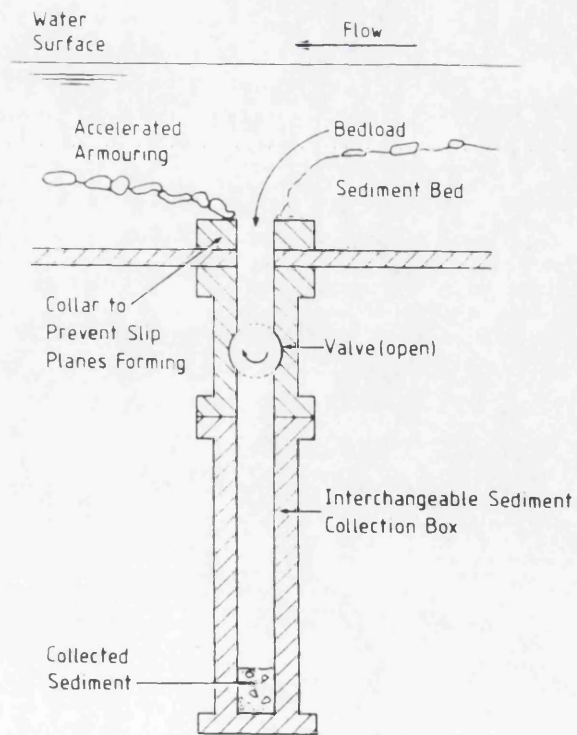


Figure 6.2 Cross Section of Bedload Trap (Tait, Willetts and Maizels, 1992)

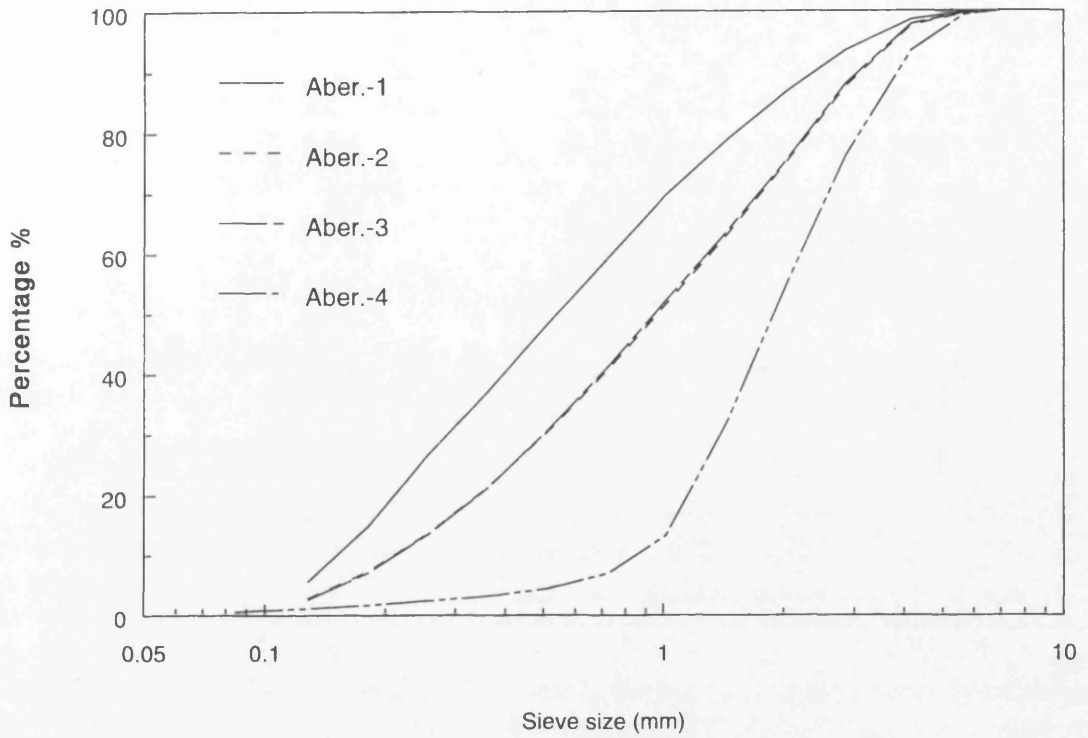


Figure 6.3 Grain-Size Distributions of Bed Mixtures In Experiments 1, 2, 3 and 4

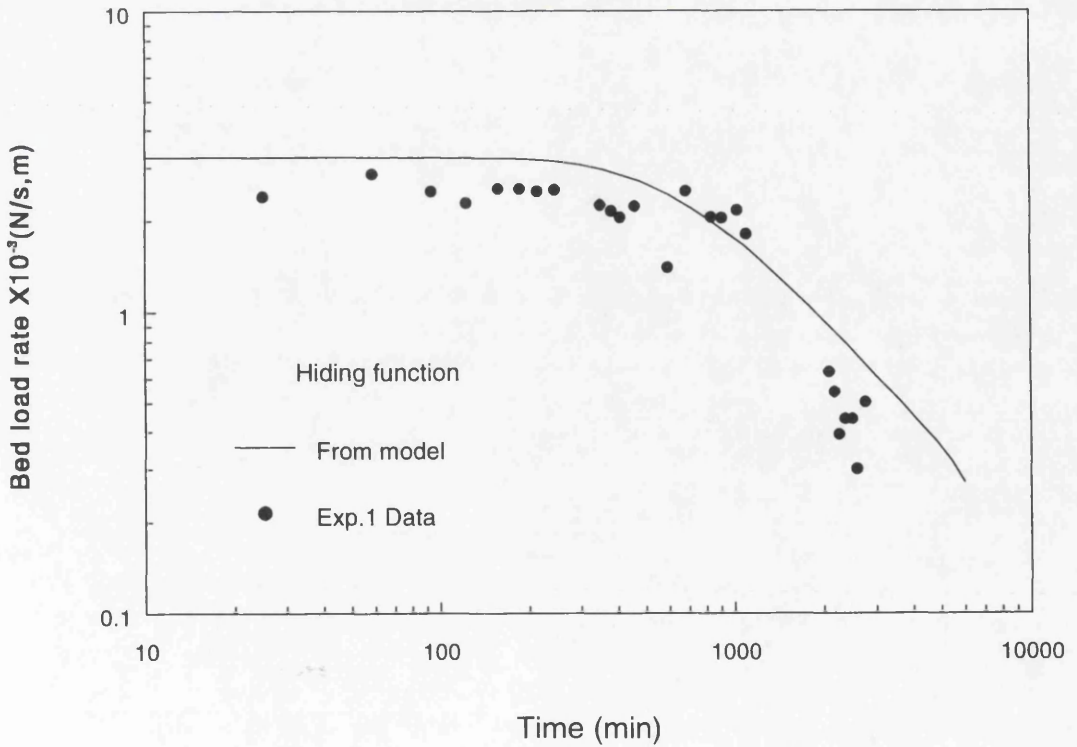


Figure 6.4 Simulation of Bedload Rate Experiment No.1 Using The Hiding Function

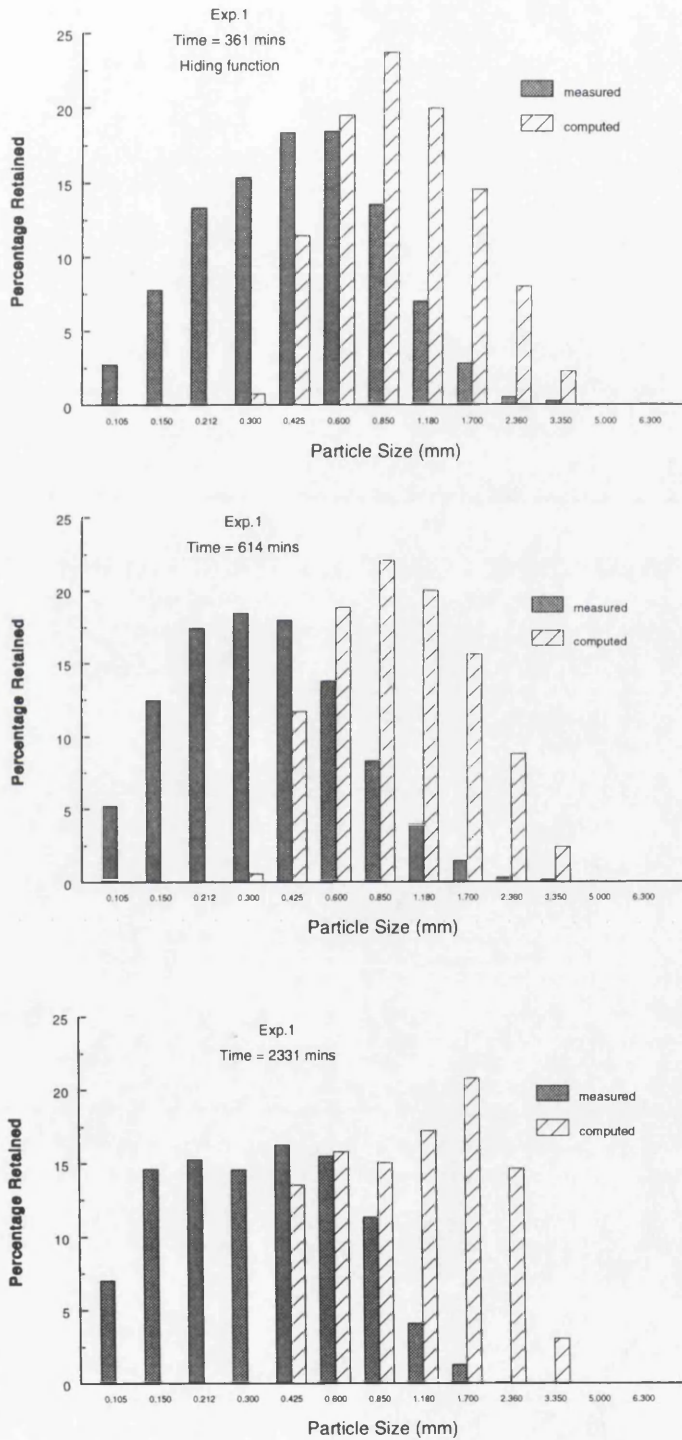


Figure 6.5 Comparison of Measured and Computed Size Fraction Transport Rates At Time 361, 614 and 2331 minutes Experiment No.1 Using Hiding Function

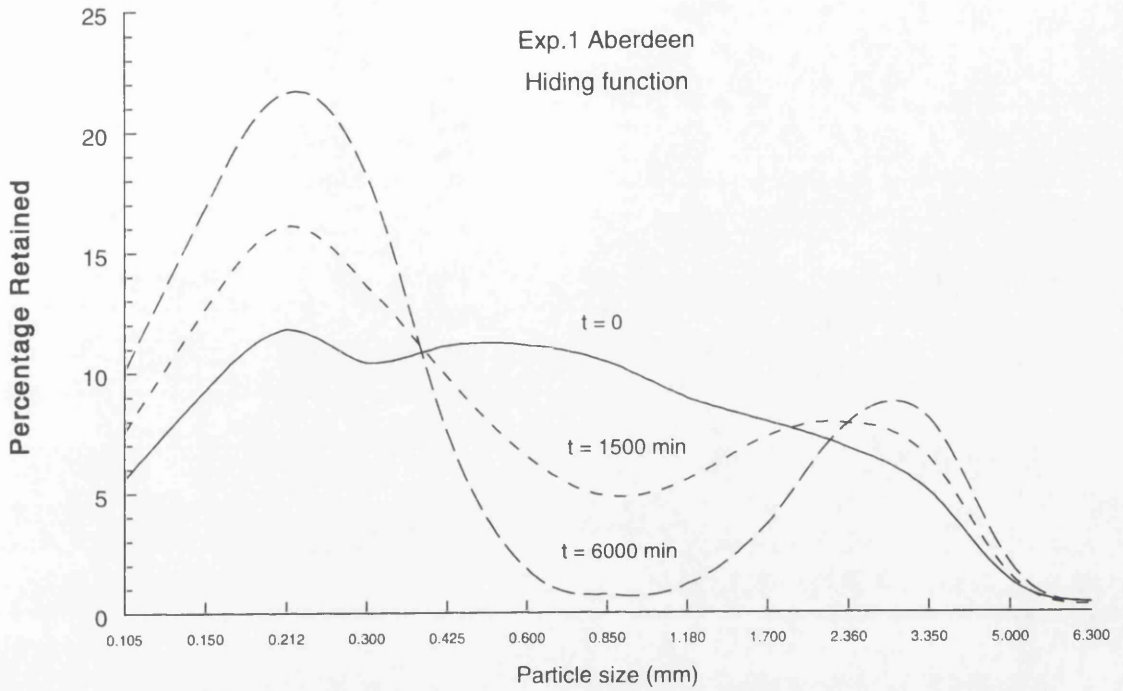


Figure 6.6 Computed Variation of Particle Size Distribution In Active Layer Experiment No.1 Using Hiding Function

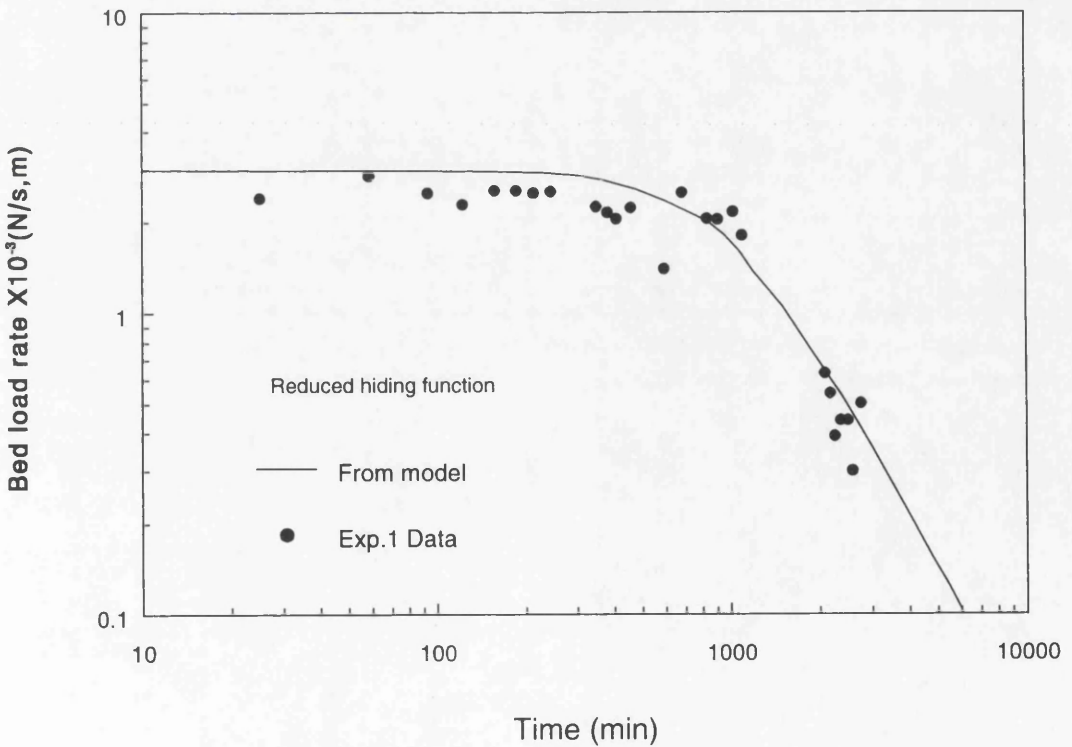


Figure 6.7 Comparison of Total Bedload Rate Varying With Time For Experiment No.1 From The Reduced Hiding Function

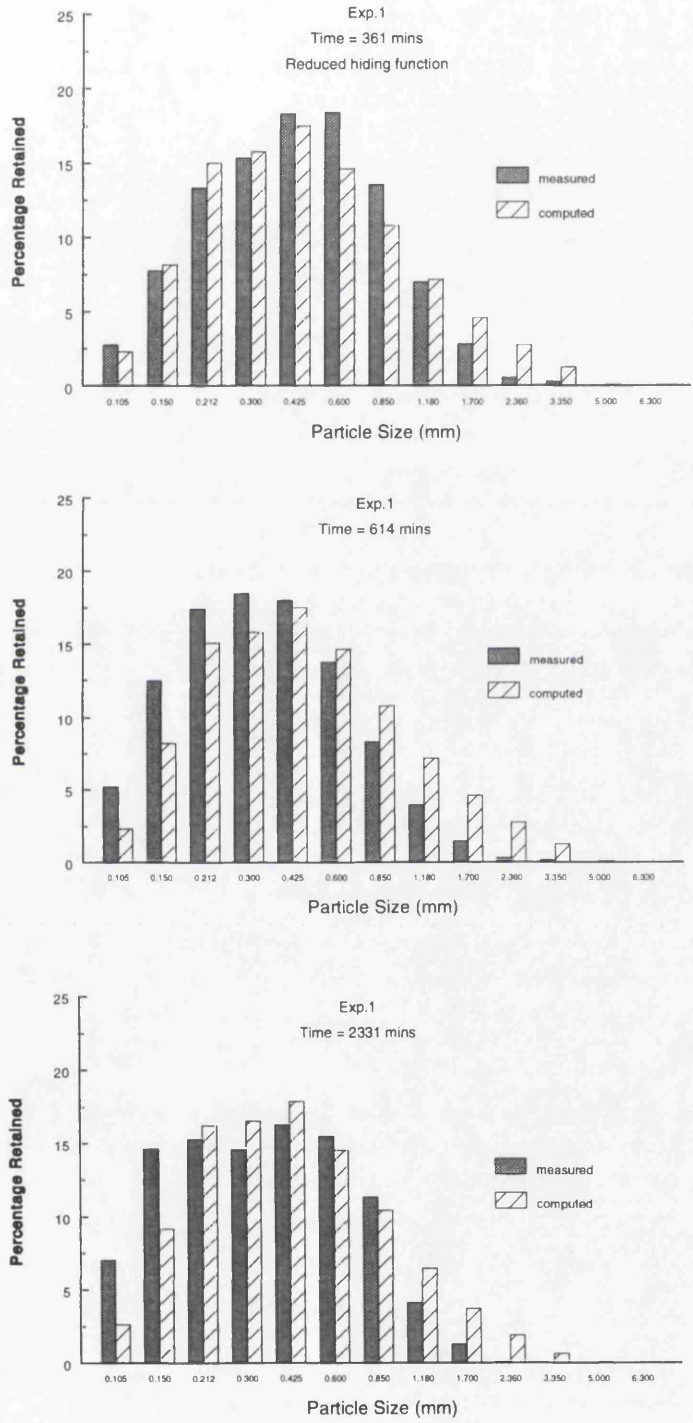


Figure 6.8 Comparison of Measured and Computed Size Fraction Transport Value For Experiment No.1 At Time 361, 614 and 2331 Minutes

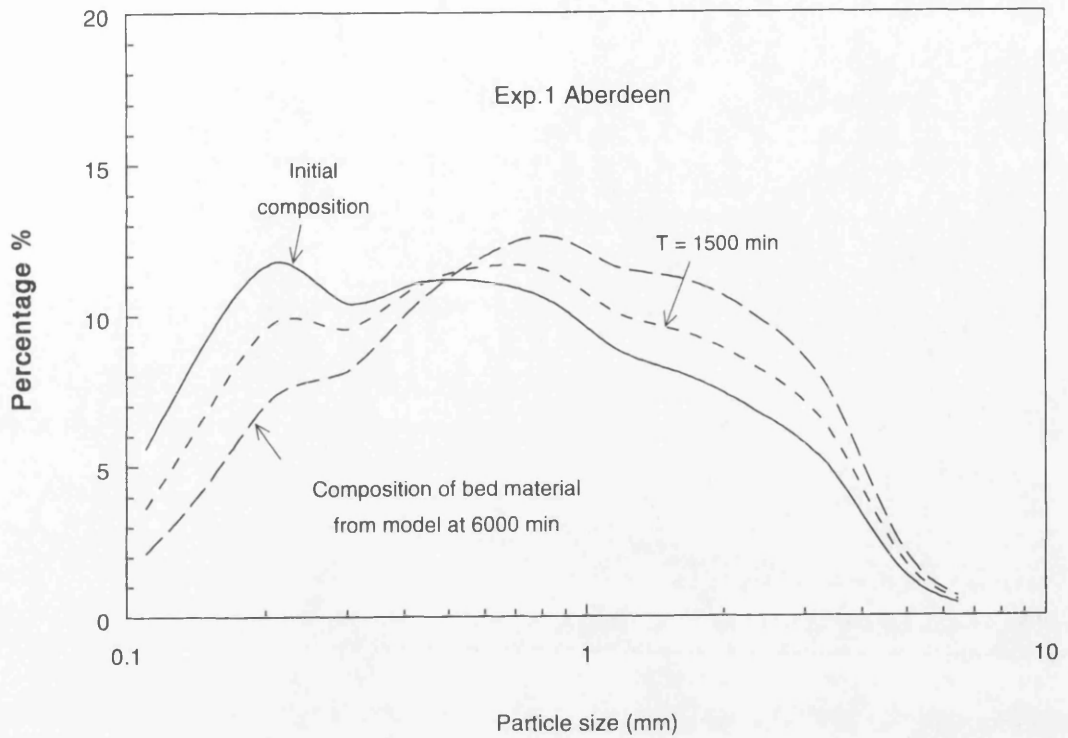


Figure 6.9 Numerical Results of Bed Material Composition In Active Layer For Experiment No.1

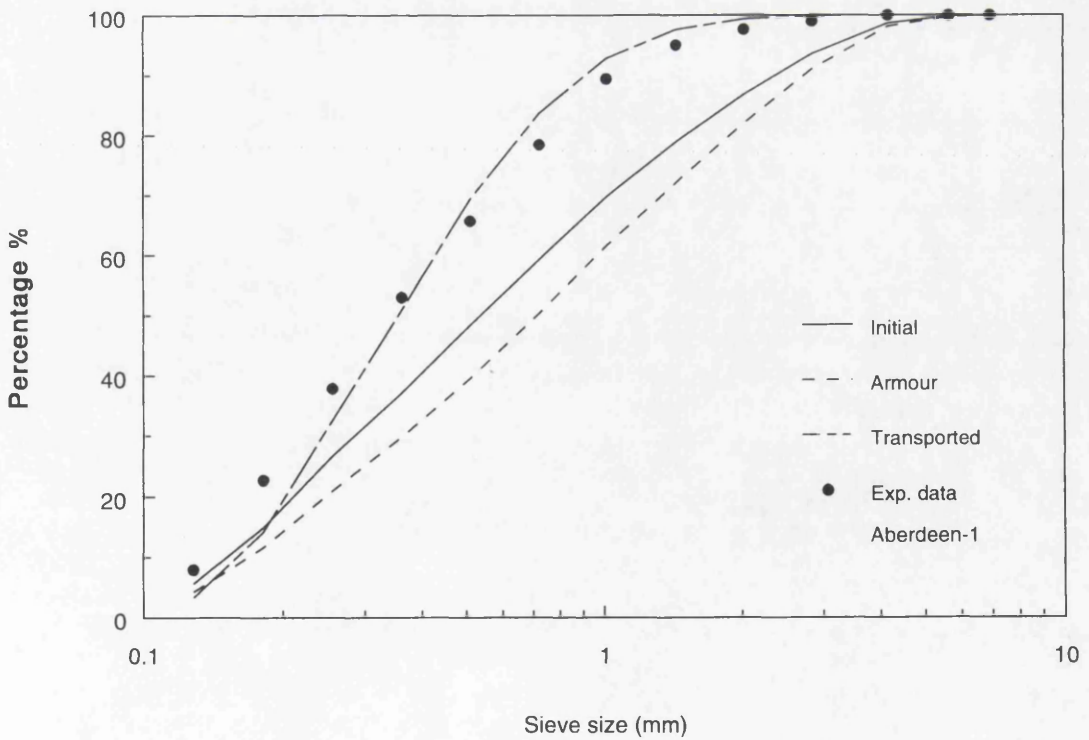


Figure 6.10 Comparisons of Composition of Armour layer and Transported Material Between Numerical and Observed Values For Experiment No.1

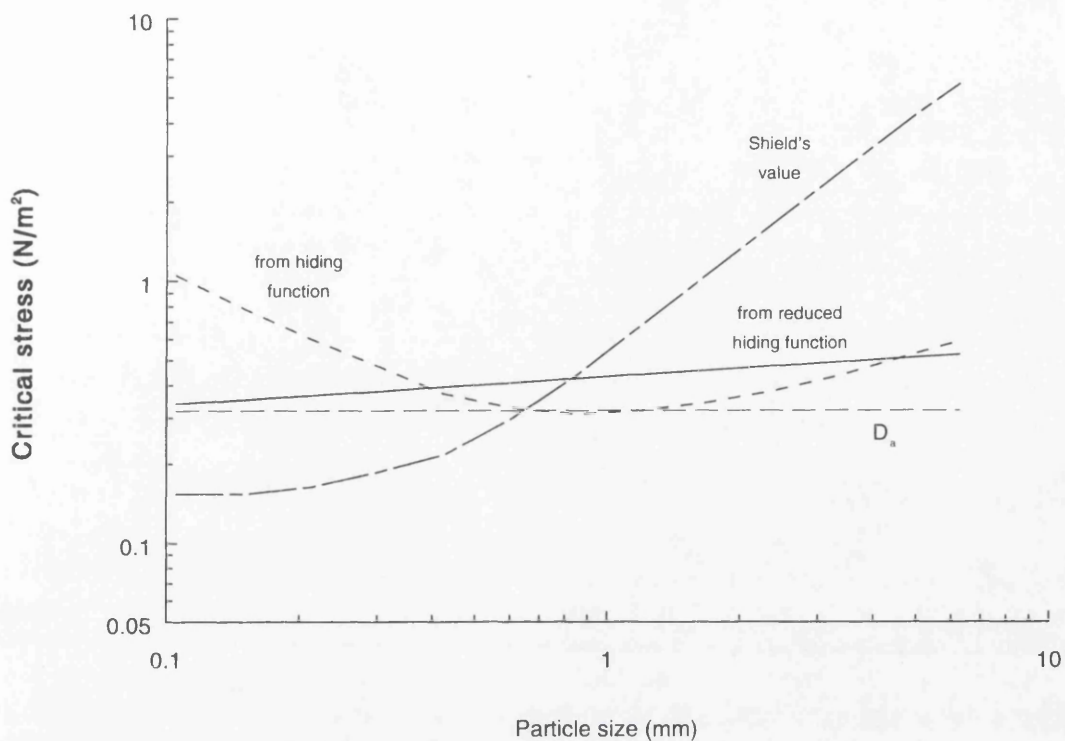


Figure 6.11 Critical Shear Stress For Each Size Fraction For Experiment No.1

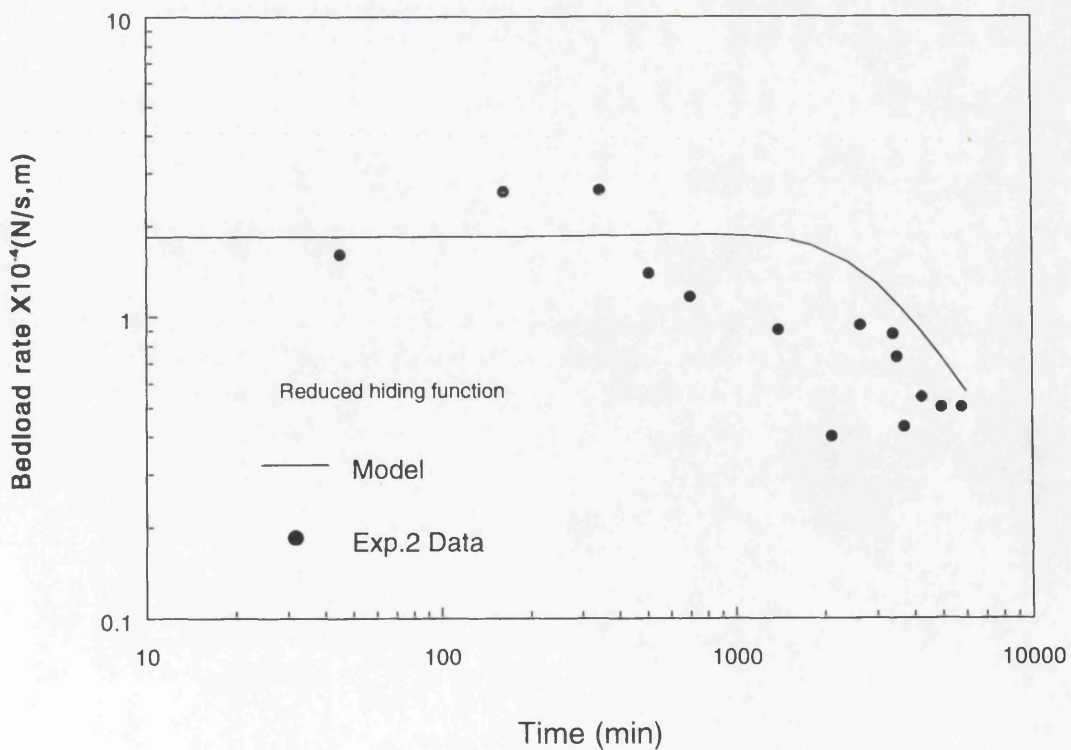


Figure 6.12 Simulation of Bedload Rate For Experiment No.2 Using The Reduced Hiding Function

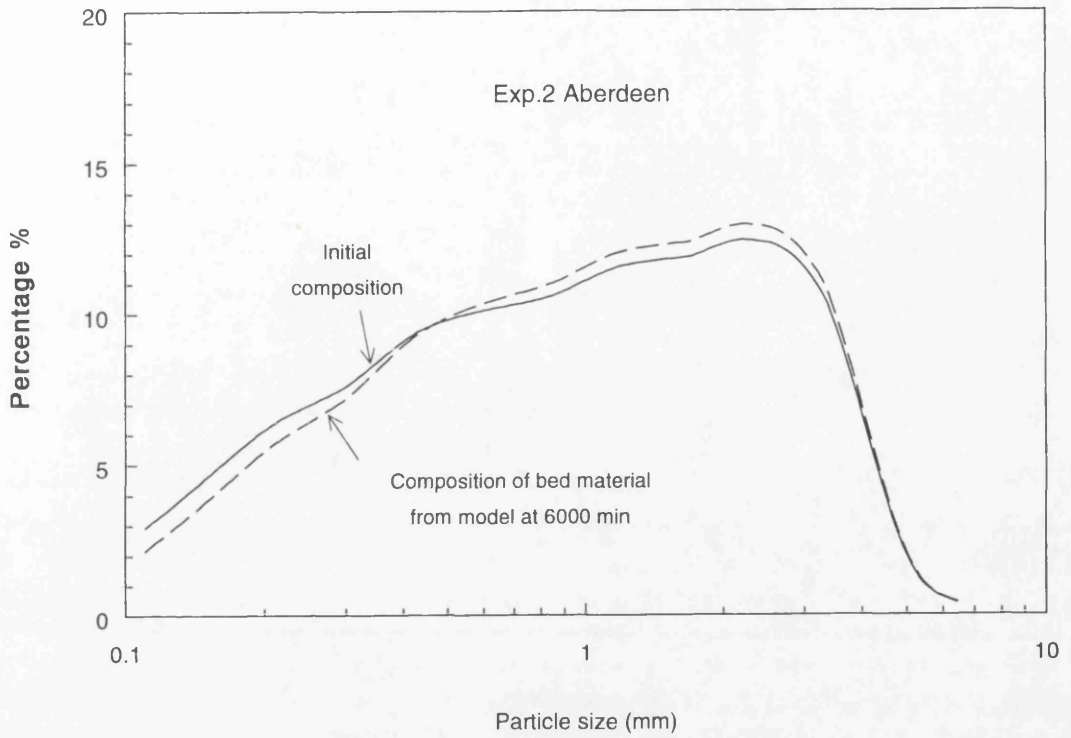


Figure 6.13 Numerical Results of Bed Material Composition In Active Layer For Experiment No.2

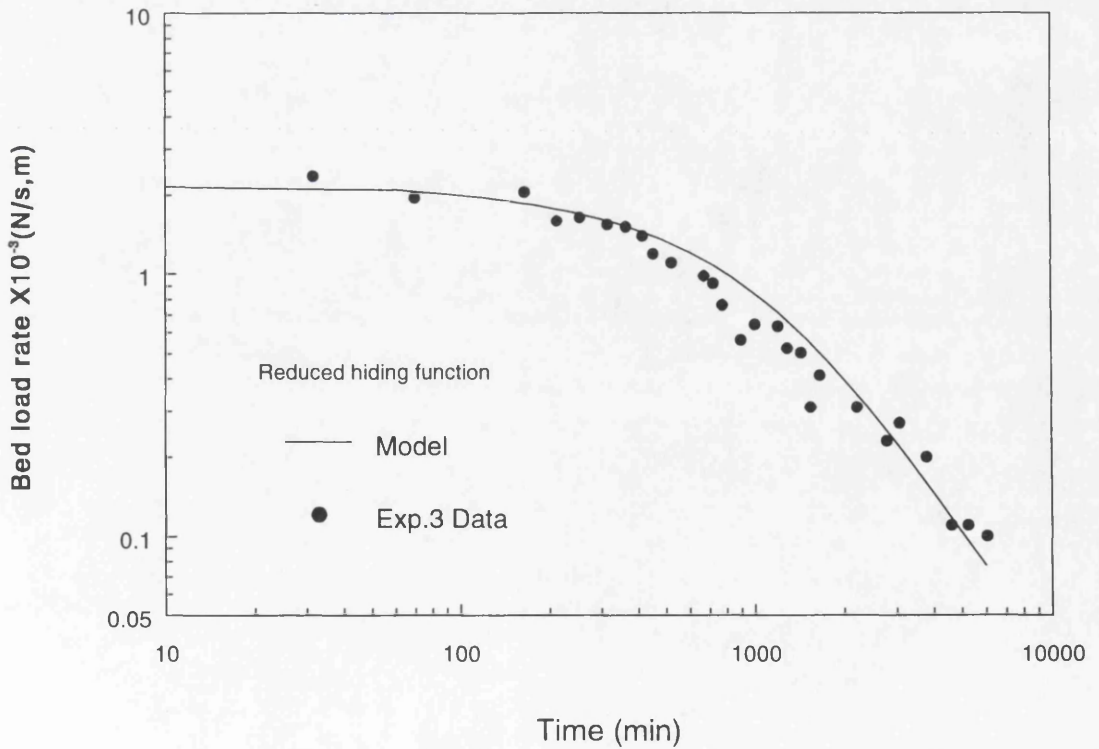


Figure 6.14 Simulation of Bedload Rate For Experiment No.3 Using The Reduced Hiding Function

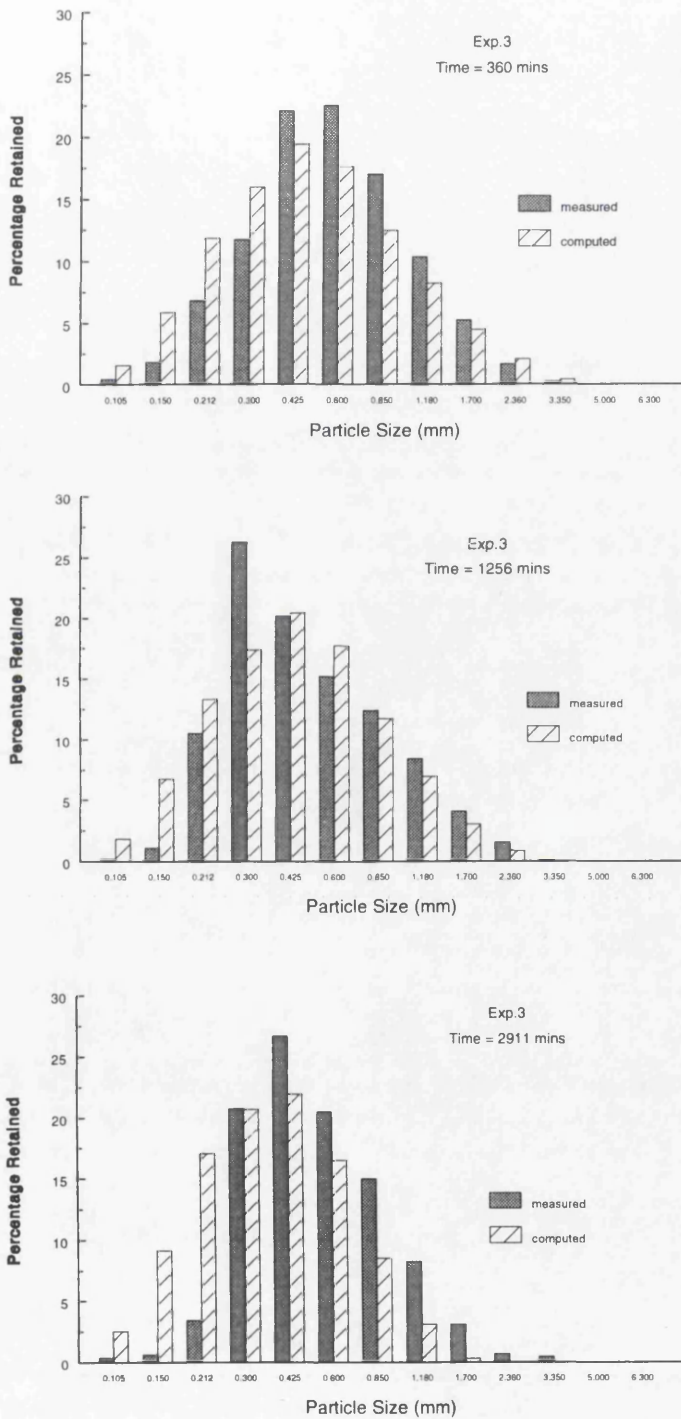


Figure 6.15 Comparison of Measured and Computed Size Fraction Transport Value For Experiment No.3 At Time 360, 1256 and 2911 Minutes

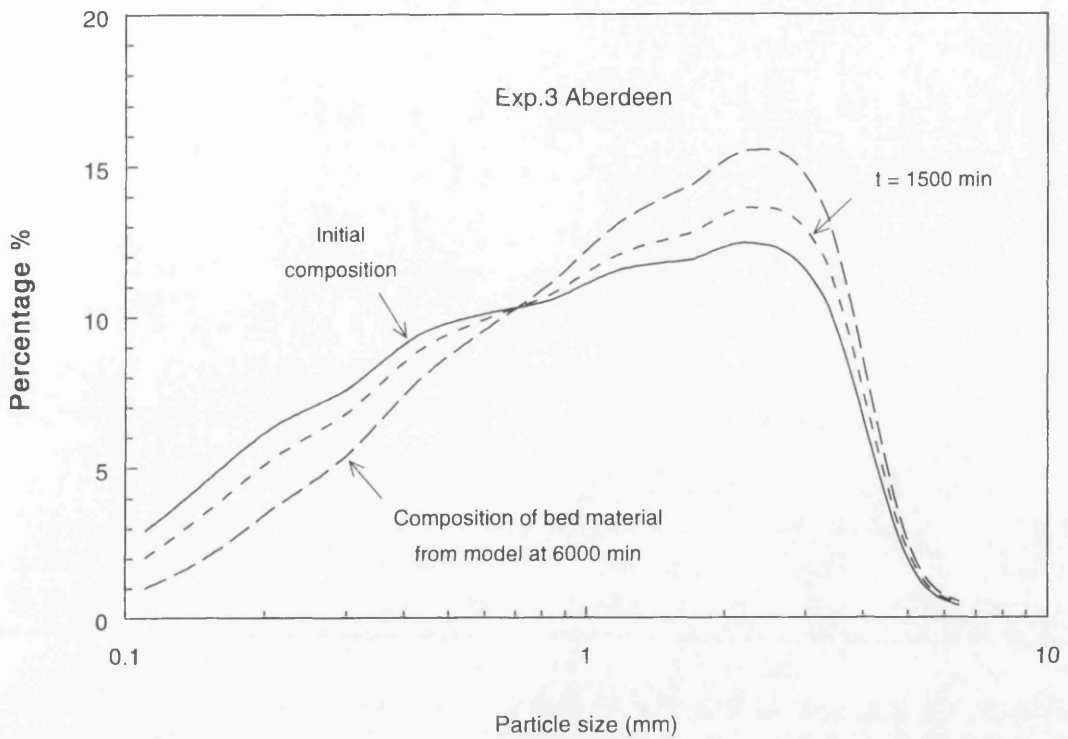


Figure 6.16 Numerical Results of Bed Material Composition In Active Layer For Experiment No.3

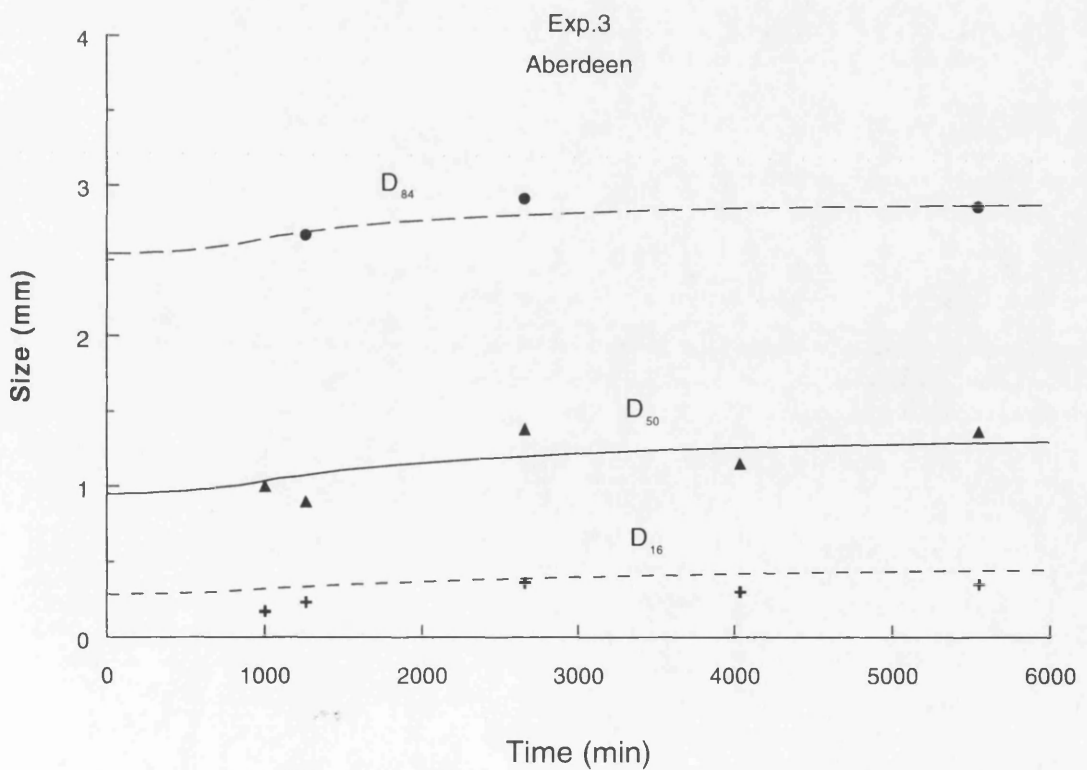


Figure 6.17 D<sub>16</sub>, D<sub>50</sub> and D<sub>84</sub> Varying With Time For Experiment No.3

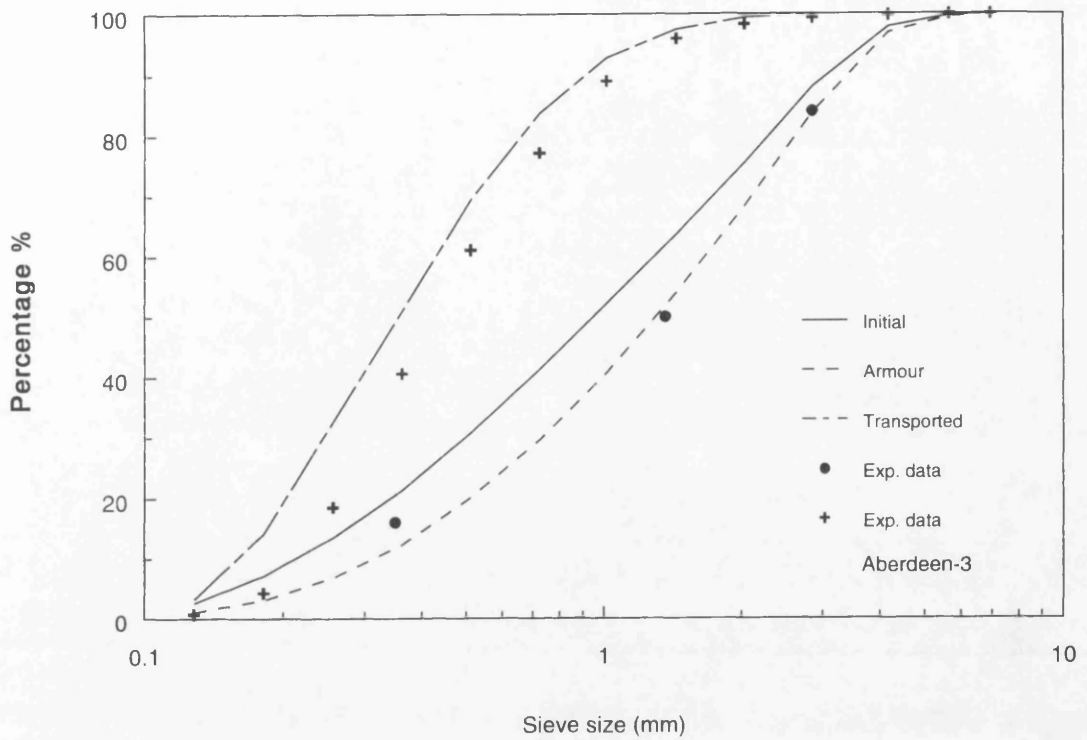


Figure 6.18 Comparisons of Composition of Armour layer and Transported Material Between Computed and Observed Values For Experiment No.3

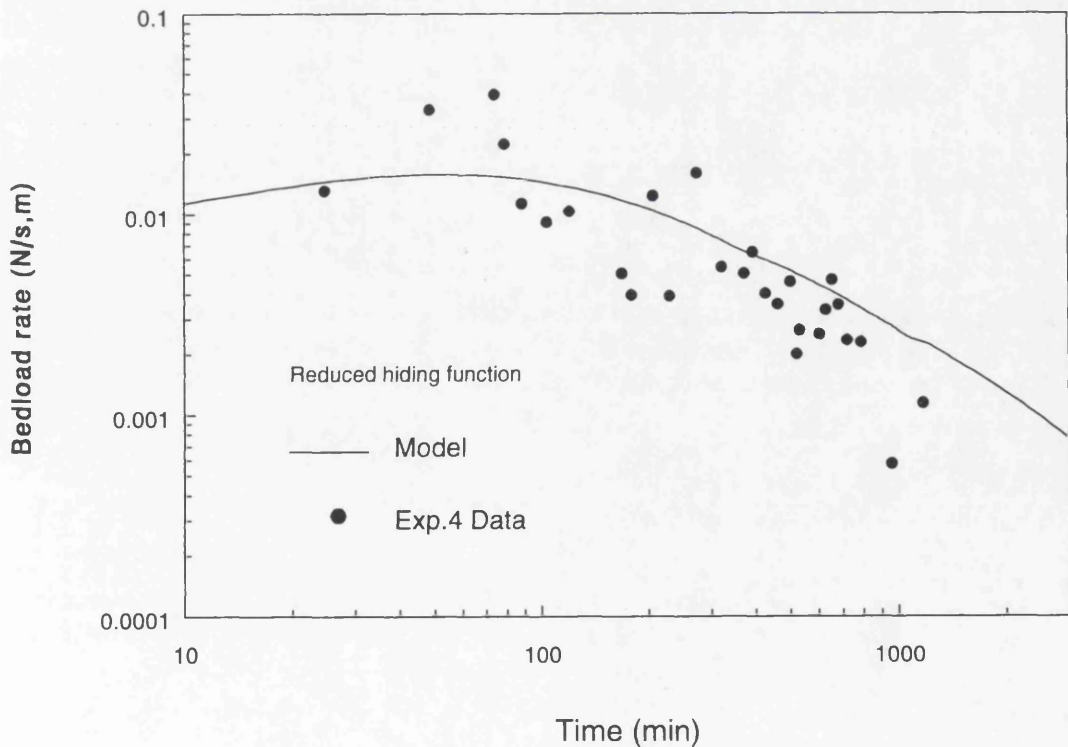


Figure 6.19 Simulation of Bedload Rate For Experiment No.4 Using The Reduced Hiding Function

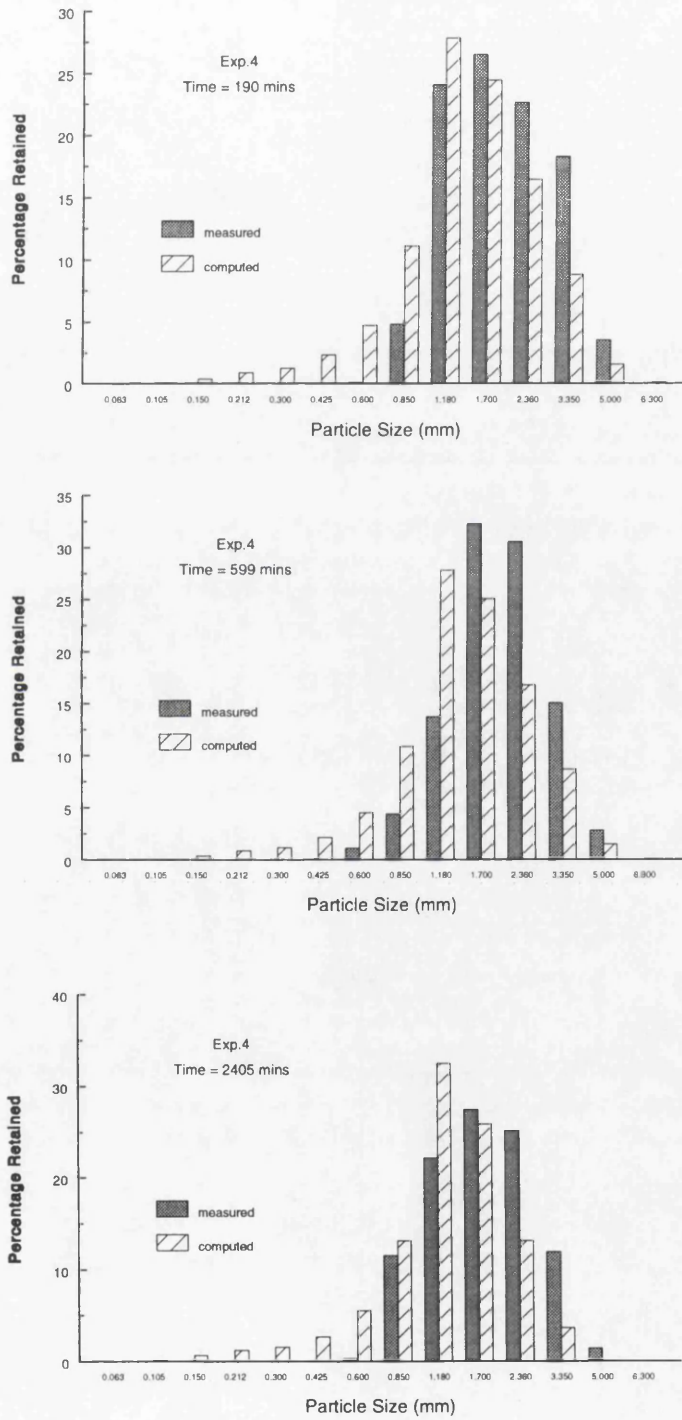


Figure 6.20 Comparison of Measured and Computed Size Fraction Transport Value For Experiment No.4 At Time 190, 599 and 2405 Minutes

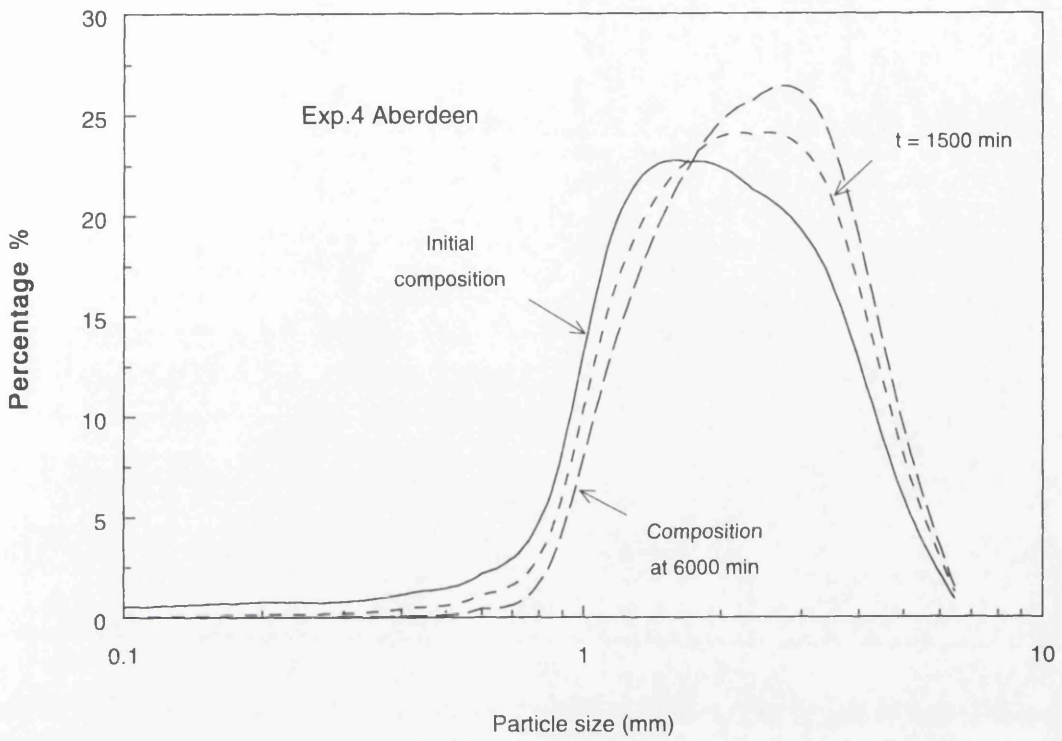


Figure 6.21 Numerical Results of Bed Material Composition In Active Layer For Experiment No.4

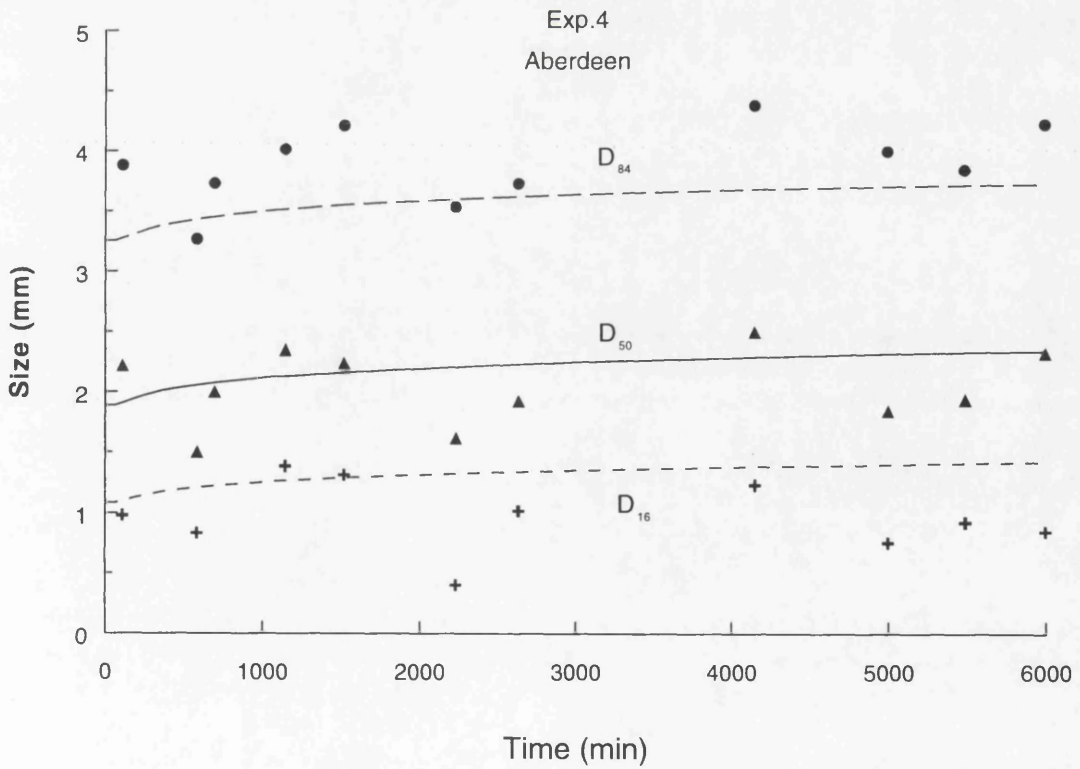
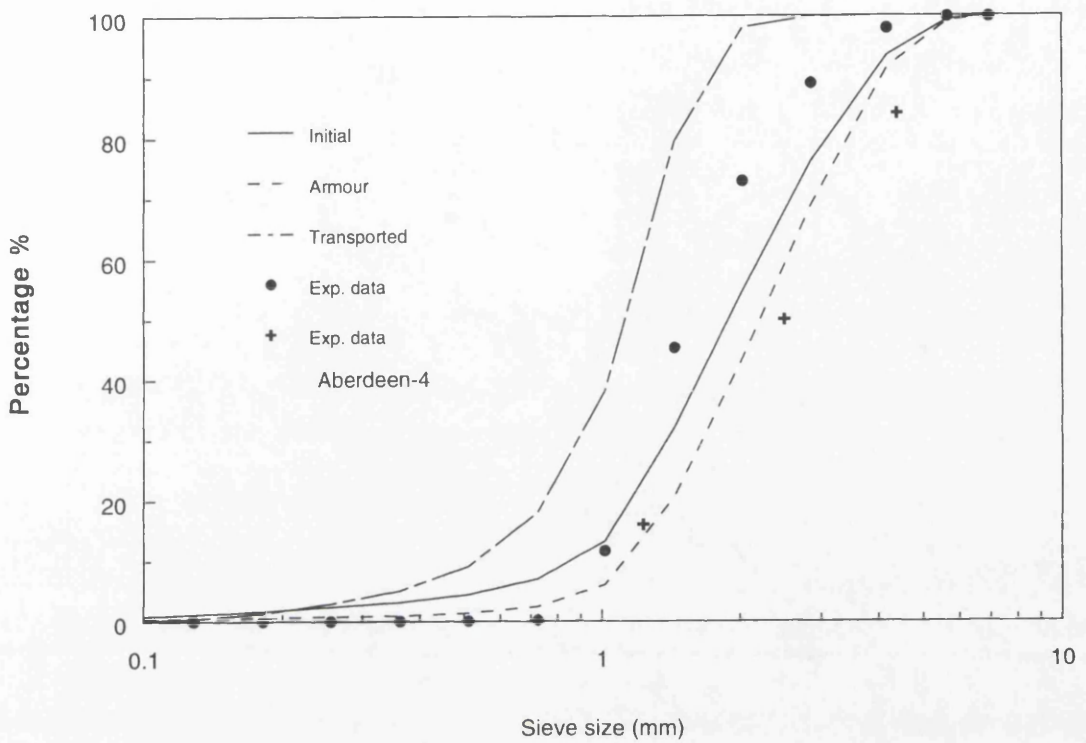


Figure 6.22  $D_{16}$ ,  $D_{50}$  and  $D_{84}$  Varying With Time For Experiment No.4



**Figure 6.23 Comparisons of Composition of Armour layer and Transported Material Between Computed and Observed Values For Experiment No.4**

## CHAPTER 7

### Graded Sediment Transport In Goodwin Creek

#### 7.1 Introduction

Since 1984, field investigations have been undertaken in Goodwin Creek to study graded sediment transport and channel stability, see Kuhnle (1992). These studies have resulted in an extensive data set of graded sediment transport rates during unsteady flows.

It was considered desirable to take advantage of the existence of these and further test the numerical model by attempting to simulate this data. This was for three reasons:

- i. The data set provides genuine unsteady flow data with significant variations in flows and water levels during the passage of the flood wave.
- ii. The hiding function implemented in model was derived from experiments where the bed material was well sorted. At Goodwin Creek the bed material is bimodal. This provided an opportunity to apply the hiding function to bimodal sediment.
- iii. For most published data of graded bed streams the peak bedload transport rates have been below 0.3 kg/s/m, Parker et al (1982), Andrews (1983) and Wilcock & Southard (1988). In Goodwin Creek, however, the bed shear stress reached in excess of seven times the critical value and maximum measured cross-sectional averaged bedload transport rates were up to 3.0 kg/s/m, see Kuhnle (1992). This therefore is data set from a very active gravel channel.

## 7.2 Goodwin Creek

The Goodwin Creek Research Watershed is operated by the United States National Sedimentary Laboratory and located in the Bluff-hills region of north-central Mississippi. It possesses relatively steep slopes and provides a wide variety of hydraulic and graded sediment transport conditions. The gauging stations were designed in the form of concrete V-shaped supercritical flumes serving to measure flow discharge and sediment transport rates.

The drainage area upstream of this flume is 17.9 km<sup>2</sup>. Low base flow occurs most of time in the channel and larger flows which are sufficient to move the coarsest grains in the bed occur during most runoff events.

The discharge is measured from the water depth and discharge relationships for the supercritical flow flume. Bedload was sampled using a modified Helley-Smith (MHS) sampler at the upstream end of the flume, see Kuhnle (1992).

The entrance nozzles of the MHS sampler is a square 7.62 cm orifice to a trapezoidal shape which rests firmly on the sloping floor surface of the supercritical flume. When the sample is in place no void exists beneath the orifice and the flume base. The area of the inlet orifice is 58.06 cm<sup>2</sup>. The ratio between the outlet and inlet orifice of the MHS samplers is 3.54. The MHS sampler is attached to a rigid strut suspended on a footbridge over the upstream end of the concrete flume. This sampling arrangement eliminates the problems of sampler location and of sampling on an uneven bed surface. A quick-release clasp on the 0.25 mm mesh sampler bag allows samples to be collected with a maximum frequency of about one every two minutes. Sampling with the MHS samplers consisted of lowering the sampler to the flume bottom for a measured time interval such that the sampler became approximately one-third full.

The mean point velocity was estimated from the average of 60 samples of the voltage output of the pressure transducer. Discharges through the inlet orifice and

through an equal volume in the free stream were calculated for the area around each velocity measurement.

### 7.3 Description of Observed Data

The field investigations were conducted from November of 1984 to September of 1988 for 21 separate transport events. Data from four of these events was available for testing the numerical model. These four events were took place on 18 November 1984 (18/11/84), 6 June 1986 (06/06/86), 8 November 1986 (08/11/86) and 16 November 1987 (16/11/87). For each event bedload transport rates, discharge and water surface levels were measured. A summary of the observed data is given in Table 7.1.

**Table 7.1 Summary of Hydraulic Information In Goodwin Creek (from Kuhnle)**

Event	Duration (hours)	Number of samples	Discharge (m <sup>3</sup> /s)	Mean velocity (m/s)	Bedload rate (kg/s)	Fr
18/11/84	10.1	33	3.8064~26.0545	0.531~1.230	0.0105~7.0355	0.219~0.342
06/06/86	4.6	45	6.4333~20.9610	0.681~1.119	0.0001~0.5618	0.250~0.325
08/11/86	8.7	126	1.3740~23.7760	0.231~1.138	0.0001~27.8367	0.103~0.317
16/11/87	4.1	19	1.5651~12.9808	0.225~0.911	0.0019~0.0688	0.094~0.287

From Table 7.1 it is seen that under similar flow strengths the maximum observed bedload rates vary considerably from one event to another. For example, for the event 18/11/84 the maximum velocity was 1.230 m/s and the corresponding bedload rate was 7.0355 kg/s. For the event 06/06/86 the maximum velocity was 1.119 m/s, but the corresponding bedload rate was only 0.5618 kg/s. A factor of variation in bedload rates is 12.5 between events 18/11/84 and 06/06/86. A similar situation is observed when comparing the event 08/11/86 with the event 06/06/86.

Here the difference in bedload rates is around 49.5 times. The large fluctuations in observed bedload rates indicate that bed material mobility must vary considerably with time.

Kuhnle (1989) has suggested that the bed forms are an important factor in influencing graded sediment transport in Goodwin Creek. This effect can be divided into two parts. Firstly, there is the effect of the bed form on the hydraulic conditions. Secondly, there is the effect of the bed form on the interaction between the size fractions. The manner in which bed form affects interaction of size fractions have not been studied.

Nine cross-sections were surveyed in 1986 upstream of the measuring section. The details of these are listed in Table 7.2. The bedload rates and other hydraulic parameters were measured at section No.9. The cross sections were not re-measured at the beginning of each flood event, it is, therefore, assumed that the changes of cross sections due to deposition or erosion have not been significant and do not unduly affect hydraulic and sediment transport parameters. The cross sectional shape at No.9 is shown in Figure 7.1.

**Table 7.2 Cross Sectional Information In Goodwin Creek (from Kuhnle)**

cross section number	chainage (m)	minimum bed level (m)
1	0	74.19
2	15.2	74.30
3	30.5	74.30
4	45.7	74.22
5	61	74.08
6	76.2	73.79
7	91.4	74.09
8	106.7	73.91
9	150.3	74.13

Data on the grain size distribution of the bed material in Goodwin Creek was measured for the surface layer and the subsurface layer near cross section No.7 in 1986. The surface layer was taken to have a thickness equal to the coarsest grain diameter, approximately 64 mm. This was only information available on the bed material composition. Table 7.3 shows the percentage of each size fraction in the surface and subsurface layers. The figures given are the average values over ten samples. It is clear from Table 7.3 that the bed material is bimodal in nature with a predominance of profile at diameter around 0.5 and 25 mm.

**Table 7.3 Details of Bed Material Composition In Goodwin Creek**

$\Phi$	Sieve size $D_i$ (mm)	Percentage in surface layer	Percentage in subsurface layer
3	0.125	0.00	0.00
2.5	0.177	0.07	0.14
2	0.250	1.14	1.78
1.5	0.354	3.71	6.20
1	0.500	6.18	9.64
0.5	0.707	5.31	7.18
0	1.000	3.20	3.72
-0.5	1.414	3.67	3.76
-1	2.000	2.86	2.77
-1.5	2.830	2.99	2.82
-2	4.000	3.36	3.43
-2.5	5.660	5.49	4.81
-3	8.000	7.39	6.90
-3.5	11.310	8.65	8.09
-4	16.000	11.29	11.42
-4.5	22.630	14.91	13.68
-5	32.000	14.74	11.23
-5.5	45.250	4.46	2.41
-6	64.000	0.55	0.00

The characteristics of surface and subsurface bed material are given in Table 7.4. From these it is clear that the bed material in the surface layer is coarser than the subsurface layer. For example, the mean size diameter of bed material in the surface layer is 11.452 mm compared with 8.122 mm in the subsurface layer. The standard geometric deviations show that the grain size distribution in the surface layer is more skewed than in the subsurface layer. The grading curve for each of these distributions is shown in Figure 7.2.

**Table 7.4 Characteristics of Bed Material In Goodwin Creek**

Layer	$D_{50}$ (mm)	$\sqrt{D_{84}/D_{16}}$	$D_g$ (mm)	$\sigma_g$
surface	11.452	5.892	6.920	4.558
subsurface	8.122	6.642	4.824	5.056

#### 7.4 Empirical Sediment Relationships Used In Goodwin Creek

As before the graded sediment transport capacity was evaluated using van Rijn's formulae with the reduced hiding function described in section 3.5. The channel resistance factor was calculated using Limerinos equation. The thickness of the active layer is assumed to be equal to roughness height with a minimum value of 5% of the water depth. The characteristic length of suspended-load was evaluated using the expression suggested by Armanini and Silvio (1988). The travel length of bedload is assumed to be equal to the characteristic length for same size fraction. The mean bedload velocity was obtained from Bagnold's equation (1973).

#### 7.5 Numerical Model

The nine surveyed cross-sections were used in the model. As discussed previously this survey data was obtained in 1986. As no other survey data was available this was assumed to be representative of the cross-sectional geometry for

each of the four flood events covering the period 18 November 1984 until 16 November 1987.

Recorded flow hydrographs provided the upstream boundary conditions and at the downstream boundary water level hydrographs were constructed from measured water depths and minimum bed levels. Sediment inflows (both bed and suspended load) were assumed to be equal to the equilibrium values where the sediment transport rate for each size fraction is equal to the transport capacity computed from van Rijn's sediment transport formulae. This implies no net deposition or erosion at cross-section 1. At the downstream boundary zero suspended load flux is imposed. This implies that at this point the suspended load is advected but not dispersed.

The bed material was represented by 19, half  $\Phi$ , size fractions ranging from 0.125 mm to 64 mm. The details of this distribution were previously provided in Table 7.3. As with the cross-sectional data the bed composition data collected at cross-section 7 in 1986 was assumed to be representative of the initial bed material at all cross-sections throughout the period from 18 November 1984 until 16 November 1987.

The time increment employed for each of the four simulations was 5 minutes (300 seconds) giving a maximum Courant number of 80. The five minute time increment ensured adequate resolution of the inflow hydrographs, while a Courant number of 80 should ensure that numerical dissipation in the resolution should remain within reasonable bounds.

The values of the numerical parameters employed in the Preissmann scheme are selected as, the space weighting factor in the St Venant, suspended load and bedload equations is 0.5, centring the spatial gradients in the finite difference terms; all time weighting factors are set to 0.55, ensuring stable results with limited numerical dissipation.

The numerical model performance was assessed by comparing model results for cross-section 9 with field observations.

## 7.6 Strategy In Simulations

In order to achieve successful simulations, the following strategy has been used in the application of the model in Goodwin Creek.

To demonstrate the benefit of using the reduced hiding function in Goodwin Creek, the results obtained from using the equal mobility hypothesis were compared with those obtained from applying the hiding function. For the equal mobility simulations the geometric mean diameter was used as the basis to evaluate the threshold condition for all size fractions in the mixtures.

Fractional sediment transport is sensitive to empirical sediment relationships. To demonstrate the difference in accuracy of predictions between different relationships, Parker's formula with a reduced hiding function, see Parker (1990), was implemented in the model instead of van Rijn's bedload formulae. As Parker's formula applies to bedload only, it was coupled with van Rijn's suspended-load formula to simulate suspended-load transport.

According to this strategy, there are six sets of simulations to be conducted in the application of the model to Goodwin Creek.

1. Use of van Rijn's formulae with a reduced hiding function based on the bed material composition in the surface layer (model 1);
2. Use of Parker's formula and his reduced hiding function based on the bed material composition in the surface layer (model 2);
3. Use of equal mobility hypothesis instead of using a reduced hiding function for van Rijn's formulae (model 3);
4. Use of van Rijn's formulae with a reduced hiding function based on the bed material composition in the subsurface layer (model 4);
5. Evaluate the effect sediment inflows (model 5).
6. Evaluate the effect of the inflow hydrograph (model 6);

## 7.7 Numerical Results For Model 1

In model 1 van Rijn's suspended and bed load formulae with the reduced hiding function was employed. The bed material composition in the surface layer is used as the initial bed material condition for all four events. The sediment inflow is assumed to be equal to the transport capacity. Other parameters have been described in previous sections.

The total bedload rates and corresponding hydraulic information for all four events are shown in Figures 7.3 to 7.6. The overall comparisons between computed and observed data can be said to be satisfactory. For events 18/11/84 and 08/11/86 the numerical results underestimated the total bedload rates, and for events 06/06/86 and 16/11/87 overestimated. The reason for this may be related to the boundary conditions and the empirical sediment relationships. Because some assumptions were made on boundary conditions in model 1 it is difficult to assess the quality of the numerical results and indicate if the empirical sediment relationships are adequate in Goodwin Creek. Therefore following models are designed to investigate which factors are more sensitive to numerical results.

### 7.8 Numerical Results From Model 2

In model 2 Parker's bedload formula with his reduced hiding function was used instead of van Rijn's bedload formula. Parker (1990) revised his bedload formula which was derived empirically in 1982. This new formula is based on the bed material composition in the surface layer and recognises the hiding effect.

Parker introduced two parameters to represent dimensionless transport and mobility parameters. The dimensionless transport parameter  $W_{b,j}^*$  is written as

$$W_{b,j}^* = \frac{\Delta g G_{b,j}}{u_*^3 \beta_j} \quad (7.1)$$

where  $G_{b,j}$  = the unit bedload capacity ( $m^3/s,m$ );  $u_*$  = the shear velocity ( $m/s$ );  $g$  = the gravitational acceleration;  $\Delta$  = the specific submerged density;  $\beta_j$  = the fractional

representation for size fraction  $j$  in the surface layer. The mobility parameter  $\phi_{sg0}$  is given from

$$\phi_{sg0} = \frac{\tau_{sg}^*}{\tau_{rsg0}^*}, \quad \tau_{sg}^* = \frac{\tau}{\rho \Delta g D_{sg}}, \quad \tau_{rsg0}^* = 0.0386 \quad (7.2)$$

where  $\tau$  = the shear stress;  $D_{sg}$  = the geometric mean particle size in a mixture;  $\rho$  = the density of water. The relationship between these two parameters was given as

$$W_{b,j}^* = 0.00218F(\omega \phi_{sg0} g_0) \quad (7.3)$$

where  $g_0$  = the reduced hiding function which was given by Parker (1990) as

$$g_0 = \left( \frac{D_j}{D_{sg}} \right)^{-0.0951} \quad (7.4)$$

where  $D_j$  = the mean particle diameter for size fraction  $j$ . The function  $F(x)$  in Equation (7.3) is written as

$$F(x) = \begin{cases} 5474(1 - 0.853/x)^{4.5} & x > 1.59 \\ \exp(14.2(x-1) - 9.28(x-1)^2) & 1 \leq x \leq 1.59 \\ x^{14.2} & x < 1 \end{cases} \quad (7.5)$$

A generalised straining function,  $\omega$ , in equation (7.3) is evaluated from a formulae, see Parker (1990).

$$\omega = 1 + \frac{\sigma_\phi}{\sigma_{\phi_0}} (\omega_0 - 1) \quad (7.6)$$

where  $\sigma_\phi$  = the arithmetic standard deviation of the surface size distribution,  $\sigma_{\phi_0}$  and  $\omega_0$  are the function of  $\phi_{sg0}$  shown in Figure 7.7.

It can be seen from Equation (7.2) that Parker's formula is quite sensitive to the resistance factor. Therefore the correct prediction for resistance factor is a preliminary condition in using Parker's formula. In this run initially the resistance has been

calibrated by comparing with a measured value. This gives that the predictions from Limerinos's formula need to be multiplied by 0.652 for event 06/06/86. The numerical results are shown in Figures 7.8 to 7.11. From overall results it is seen that Parker's formula with his reduced hiding function over estimated the bedload rates for all four events in Goodwin Creek. For events 06/06/86 and 16/11/87 in comparison with the results from the model 1 van Rijn's formulae give better predictions for the cases considered. For events 18/11/84 and 08/11/86 unlike van Rijn's formulae Parker's formulae over estimates the bedload rates, indicating how important it is to select a suitable sediment formula in the real river applications.

It should be emphasised that the numerical results in model 2 were obtained after the resistance factor was calibrated at the beginning of each event. Because Parker's formula is interlinked with resistance factor, the correct estimation of resistance factor becomes crucial to the numerical results. In addition, Parker's formula is a bedload predictor. Therefore it is only appropriate in the situation where suspended-load is small.

### **7.9 Numerical Results From Model 3**

In model 3 the equal mobility hypothesis is used instead of the reduced hiding function for van Rijn's formulae. Therefore the results from model 3 can be used to judge the difference between using hiding function and equal mobility hypothesis in Goodwin Creek. Here it is assumed that the equal entrainment mobility is calculated from the geometric mean particle size of bed material in the surface layer and that equal transport mobility will hold for any bed material composition and flow strength.

The numerical results from using equal mobility are shown in Figures 7.12 to 7.15. It is clear that in general for all four events the predicted bedload rates are less than those obtained using model 1. For events 18/11/84, 06/06/86 and 16/11/87 the numerical results are much worse.

### **7.10 Numerical Results From Model 4**

To test the sensitivity of predictions to the initial bed material composition, the model 4 uses the bed material composition in the subsurface layer instead of the surface layer as used in model 1. The runs were carried out for events 18/11/84 and 06/06/86 only since the predicted total bedload rates for these two events were underestimated by model 1. The results could therefore be improved by using a finer bed material for the surface layer.

The numerical results are shown in Figures 7.16 and 7.17, where it can be seen that the improvement has been achieved. Therefore these runs demonstrate that the numerical results are sensitive to the initial bed material. Without the correct information for bed material composition, the model is unable to predict sediment transport, especially for short term predictions.

### **7.11 Numerical Results From Model 5**

Another factor influencing numerical results is the sediment inflow to Goodwin Creek. Sediment inflow information is not available the assumption was made that this was equal to the equilibrium sediment transport rate. To illustrate the effect of sediment inflow on the numerical results this run uses non-equilibrium conditions at the upstream boundary. For event 08/11/86 twice equilibrium sediment transport rates are employed as upstream boundary condition. The results are shown in Figure 7.18. The results shows that this gives a minor improvement to the predicted values. In other words the sediment inflows are also important for reliable simulations.

Using non-equilibrium sediment inflow condition can cause a net deposition or erosion so that the cross sectional shape will be changed accordingly. The feedback effect of cross sectional changes can be embedded into the hydraulic and transport components for future events.

### **7.12 Numerical Results From Model 6**

For event 08/11/86 the measurements started from close to the peak flow. It was suspected that it may be possible to improve the results if the whole hydrograph was

used. Therefore in this model 6 the original hydrograph is extended back in time to give same estimate of previous conditions. New hydrograph started from 2 am and is almost symmetrical. Other parameters are kept as same as in model 1. The numerical results obtained from this run indicate that they are very close to those obtained from model 1. This indicates that the extension of hydrograph does not significantly improve the numerical results for this case.

### 7.13 Comparison of $D_{50}$ in Bedload

Comparison of  $D_{50}$  in the bedload from observed and computed values from model 1 and model 4 are shown in Figures 7.19 to 7.22. It is seen that for all four events the numerical results from using Parker's formula are better than van Rijn for the cases considered. However, it is hard here to make a solid judgement. There are two reasons for this. Firstly, the measured data fluctuate considerably. This has been explained by Kuhnle (1989) that bed form plays a major role in graded sediment transport of Goodwin Creek. However, there are not quantitative information for the bed forms available. Secondly, in graded sediment transport formula the effect of the bed forms is not accounted for. Therefore the comparison does not provide final conclusion, but serves to indicate that bed form may need to be included in the development of hiding functions to improve predictions in Goodwin Creek.

### 7.14 Discussion and Conclusions

The reasons for the application of this model on Goodwin Creek are explained below. Firstly, the study in Goodwin Creek has been undertaken for a number of years to collect bedload rates using a Helley-Smith bedload sampler and other hydraulic parameters. Secondly, bed material is well graded ranging from 0.1 to 64 mm and has a bimodal feature. This can provide a good opportunity to verify the performance of model and empirical sediment relationships. Thirdly, the measurements were focused on flood events, giving an example of graded sediment transport under unsteady and non-equilibrium circumstances. Therefore the ability of model to simulate graded

sediment transport under unsteady flow and non-equilibrium sediment transport conditions can be examined.

The numerical results of simulations for the four events in Goodwin Creek provide some useful insights. Numerically it is seen that the numerical results are sensitive to the sediment transport relationships used and the initial bed material compositions. In order to predict true life of graded sediment transport these relationships and boundary conditions need to be defined correctly, and before being applied they should be judged if they are adequate to that particular situation. Of these relationships the fractional graded sediment transport capacity and its corresponding hiding function are important. Without a good evaluation of transport capacity it is impossible to predict graded sediment transport correctly even although you have a good mathematical model and numerical solution technique. Most of the transport formulae such as Parker, Engelund and Hanson, and Ackers and White are strongly linked with resistance factor, the prediction of resistance factor is crucial in using transport formula. In this respect van Rijn's formula is not affected directly by resistance factor since it uses critical velocity as tractive force instead of using shear stress.

The true life simulations require true life initial and boundary conditions especially for short term simulations. In Goodwin Creek, there are three factors to affect the numerical results significantly. Firstly, the cross section information was not surveyed before every event. It is likely that the cross sections were changed from different events because of deposition or erosion. The extent of this problem can be seen in Table 7.5 where observed and computed velocities are significantly different. This demonstrates that the cross sections changed with time, and this influences the accuracy of predictions. Secondly, the bed material composition used as initial bed conditions for the four events was not available. In fact the bed material composition changes from one event to another due to selective transport. As a result the accuracy of numerical results could be affected, especially for a strong sorting process. Thirdly,

sediment inflows were not available for these events. Therefore the equilibrium fractional sediment transport was assumed for sediment inflow. This may be not correct since sediment inflow may vary with time depending on the catchment properties.

**Table 7.5 Comparison of Velocity Between Observed and Computed Values For Four Events**

Events	Observed Velocity (m/s)	Computed Velocity (m/s)
18/11/84	1.00	1.06
06/06/86	0.69	0.78
08/11/86	1.08	1.08
18/01/87	0.236	0.25
16/11/87	0.78	0.82

From this application it is found that the short predictions for unsteady and non-equilibrium graded sediment transport needs true life initial and boundary conditions including cross sectional information, bed material composition, and water and sediment inflows. Without these it is difficult to obtain the satisfactory numerical results. Because in selection of model parameters the numerical dissipation was minimised as small as possible therefore all comparison between observed and computed values are believed to be attributed to the effect of either initial and boundary conditions or empirical sediment relationships. Currently it is difficult to judge which factors are more important. However, in the empirical sediment relationships the effect of bed form on hiding function was obviously not taken into account. If this is the case that the bed form is vital for graded sediment transport as mentioned by Kuhnle (1989) the bed form effect should be reflected quantitatively in the empirical sediment relationships in Goodwin Creek.

The thickness of the active layer is also a important factor in graded sediment transport. Change of bed material composition is directly related to this and it affects material sorting process.

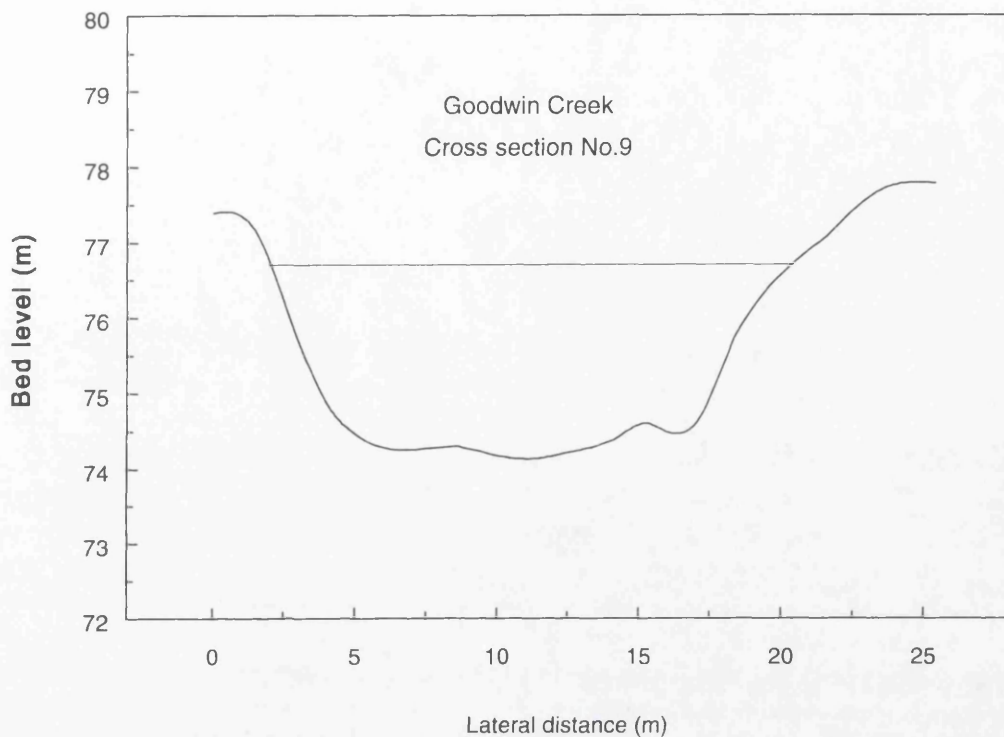


Figure 7.1 Cross Section No.9 In Goodwin Creek

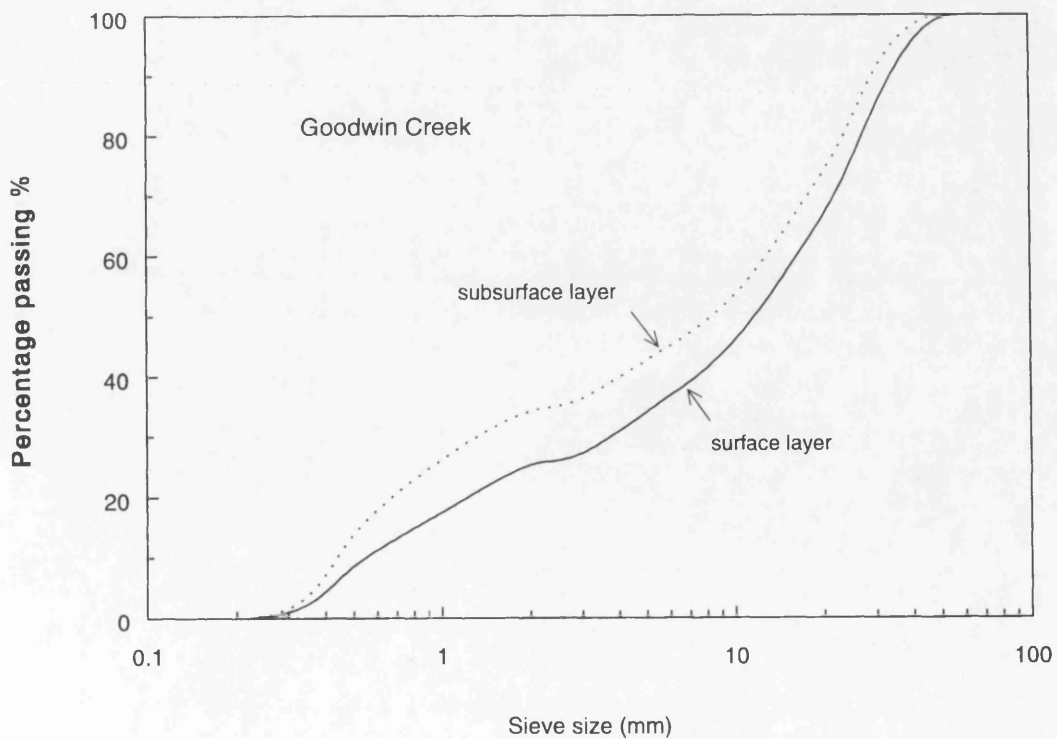


Figure 7.2 Grading Curves of Bed Material In Surface and Subsurface Layer In Goodwin Creek

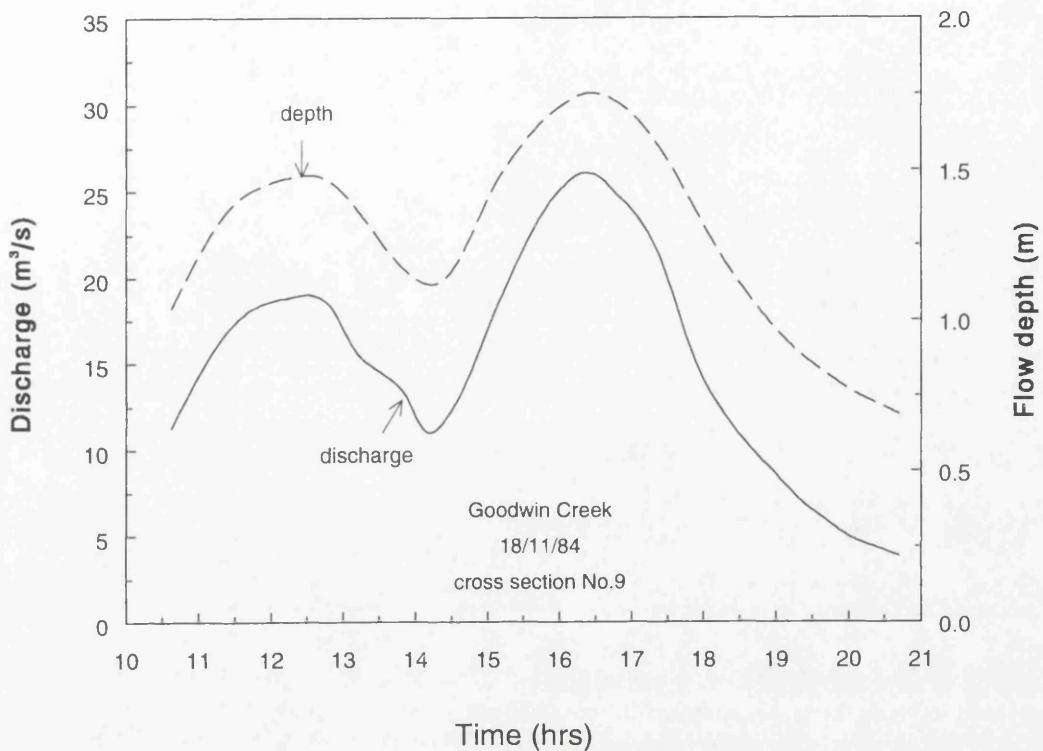


Figure 7.3a Discharge and Water Depth Varying With Time For Event 18/11/84 In Goodwin Creek

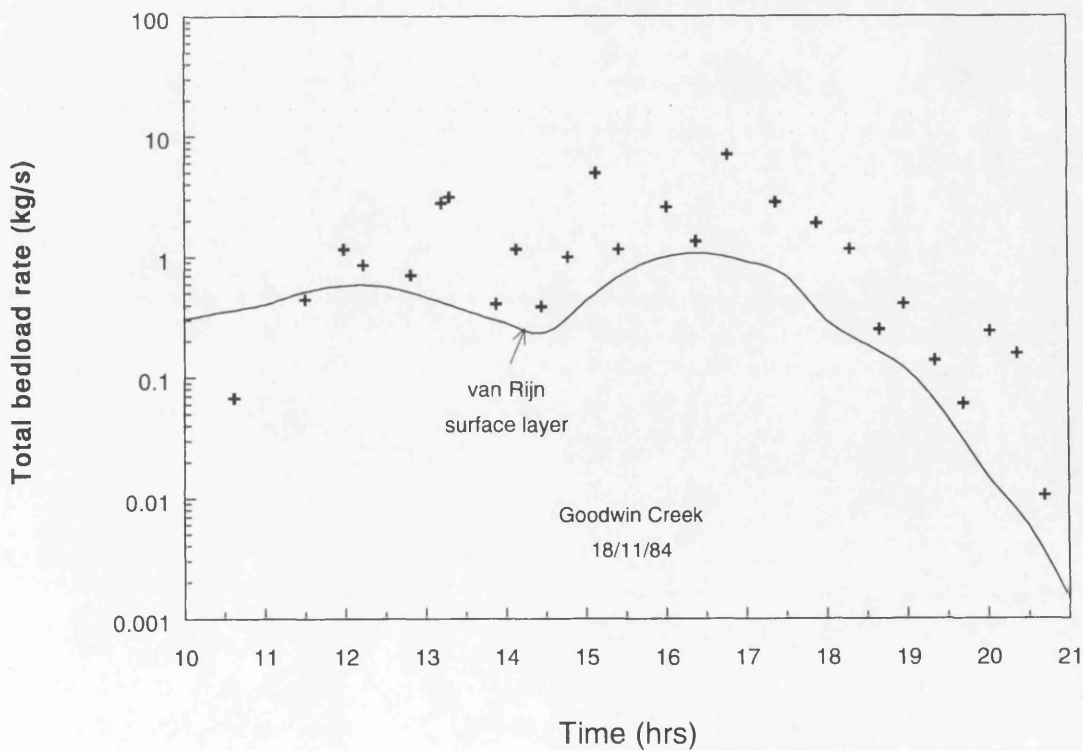


Figure 7.3b Comparison of Total Bedload Rates Between Observed and Calculated Values For Event 18/11/84

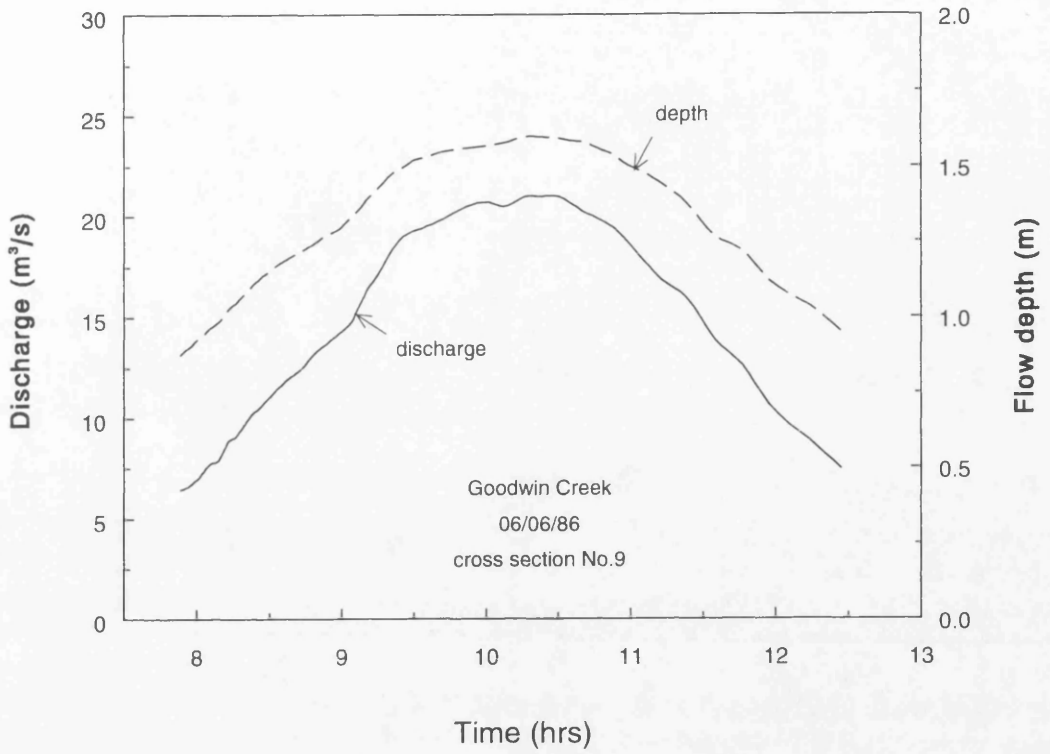


Figure 7.4a Discharge and Water Depth Varying With Time For Event 06/06/86 In Goodwin Creek

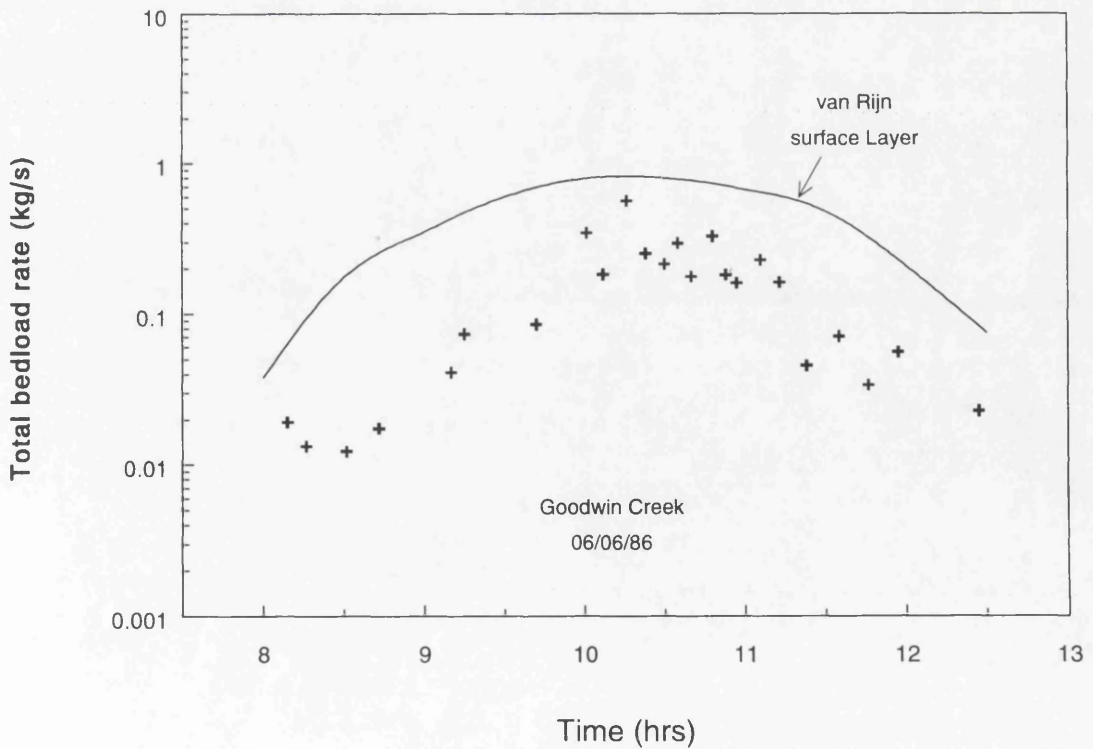


Figure 7.4b Comparison of Total Bedload Rates Between Observed and Calculated Values For Event 06/06/86

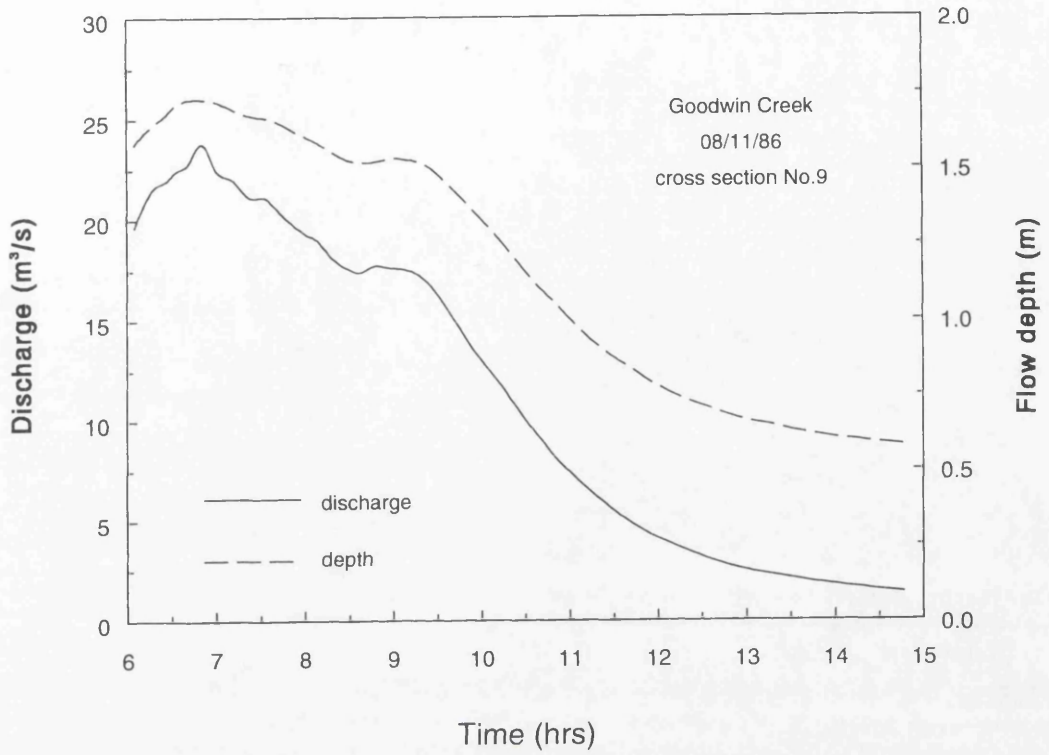


Figure 7.5a Discharge and Water Depth Varying With Time For Event 08/11/86 In Goodwin Creek

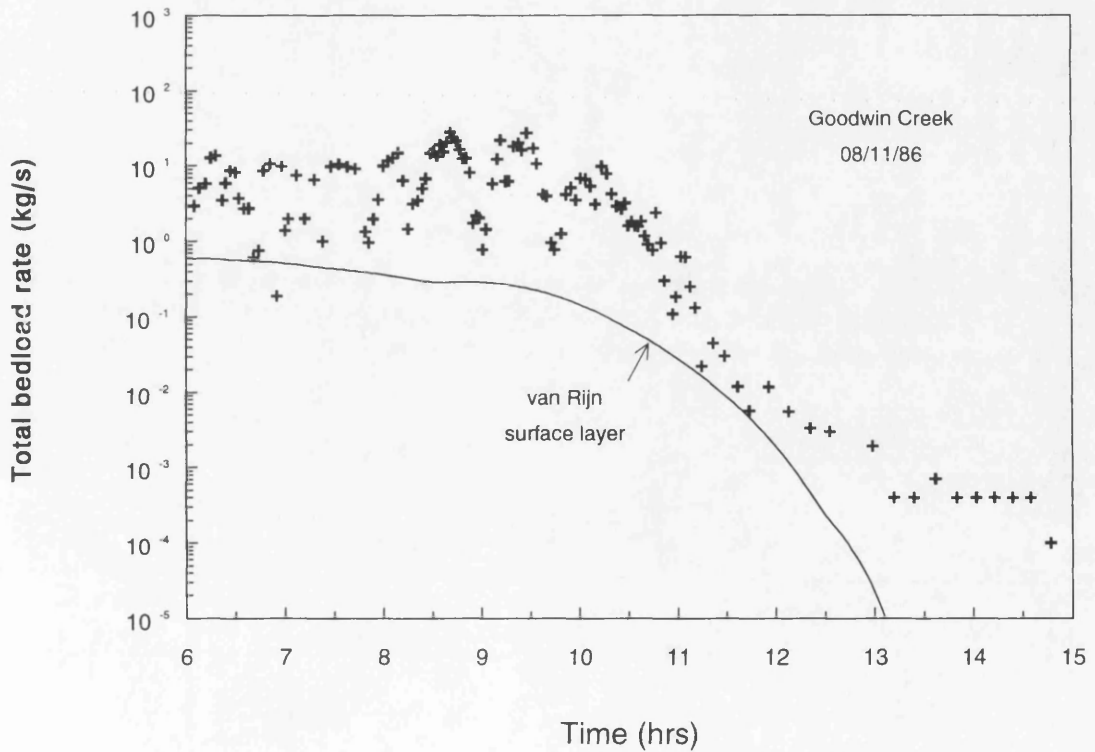


Figure 7.5b Comparison of Total Bedload Rates Between Observed and Calculated Values For Event 08/11/86

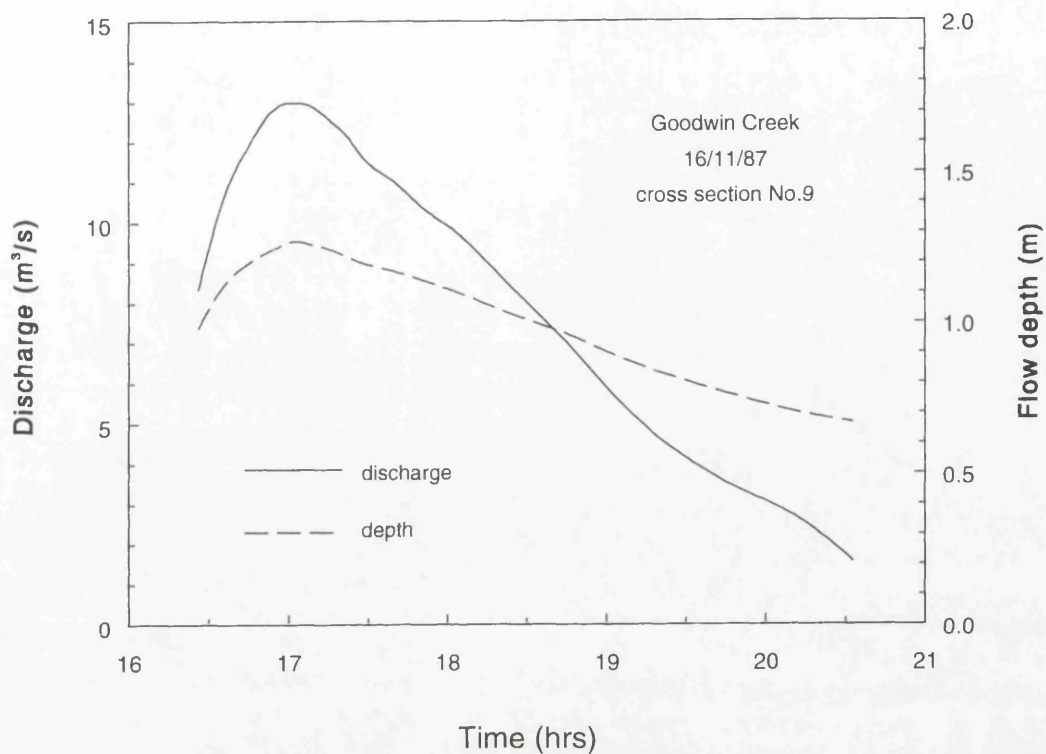


Figure 7.6a Discharge and Water Depth Varying With Time For Event 16/11/87 In Goodwin Creek

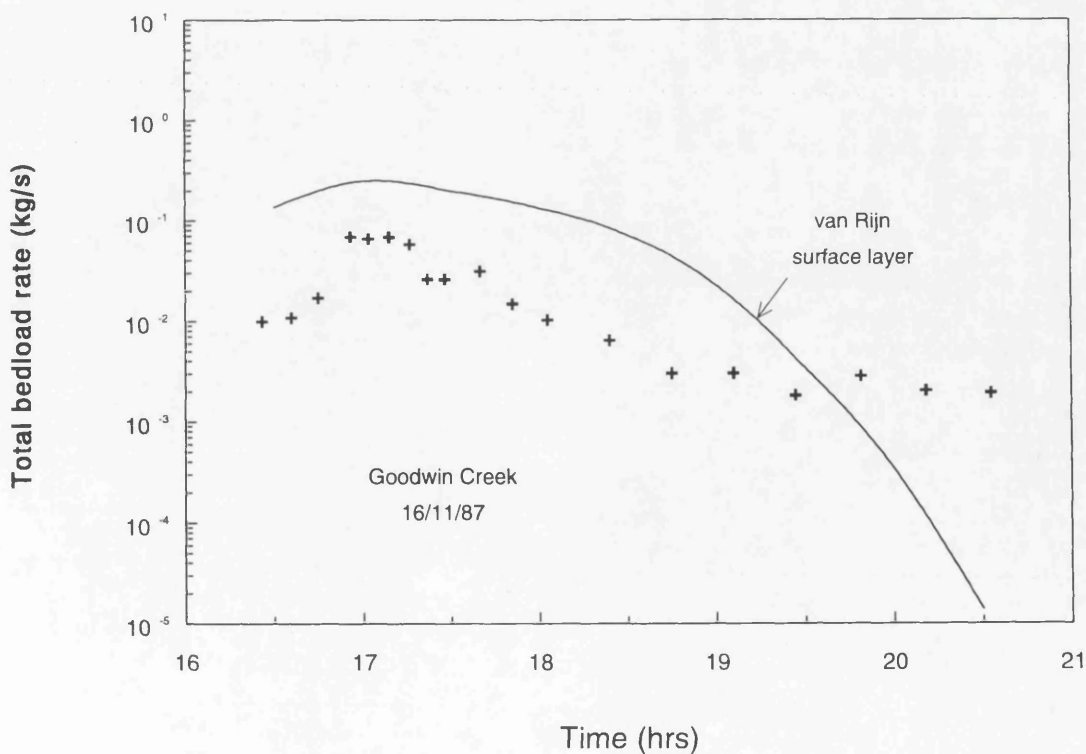


Figure 7.6b Comparison of Total Bedload Rates Between Observed and Calculated Values For Event 11/18/87

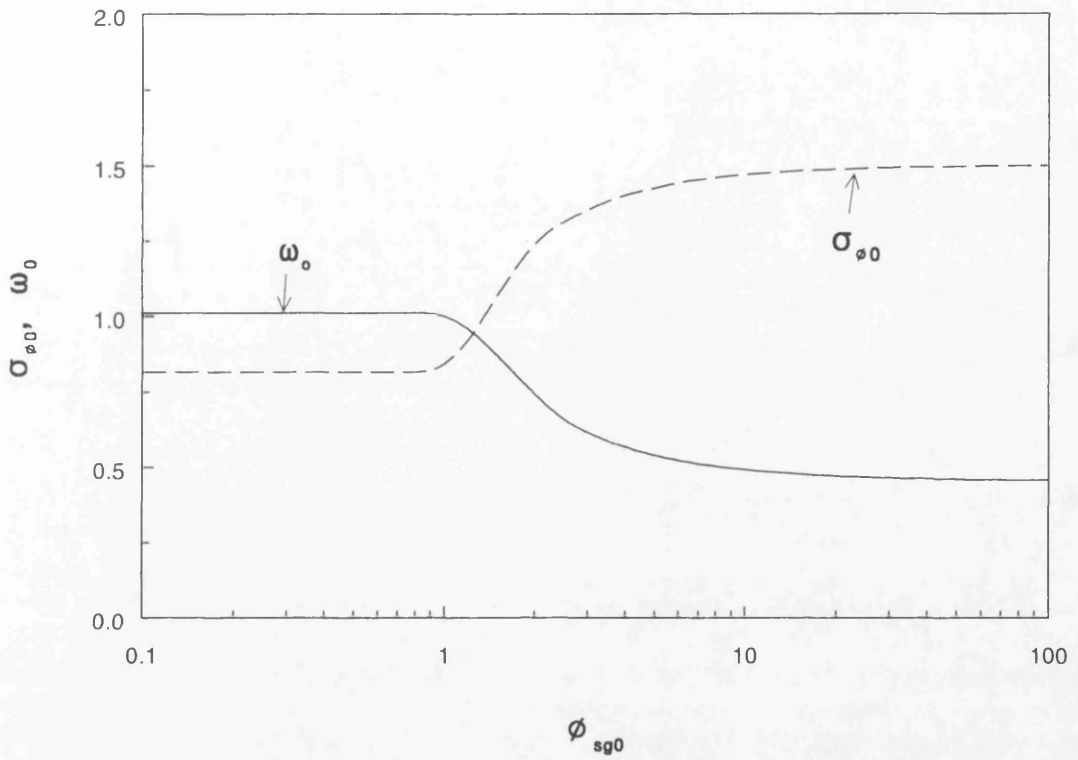


Figure 7.7 Plots of  $\omega_0$  and  $\sigma_{\phi_0}$  versus  $\Phi_{sg0}$  (From Parker, 1990)

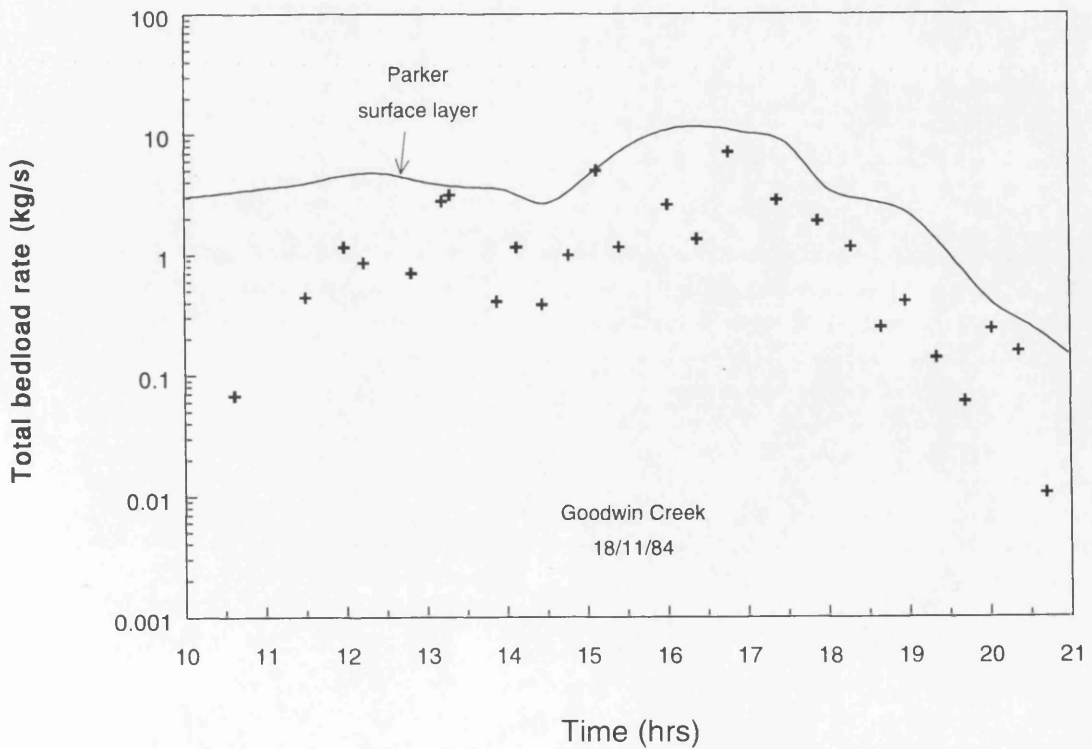


Figure 7.8 Predictions of Bedload Rates Using Parker's Formula For Event 18/11/84

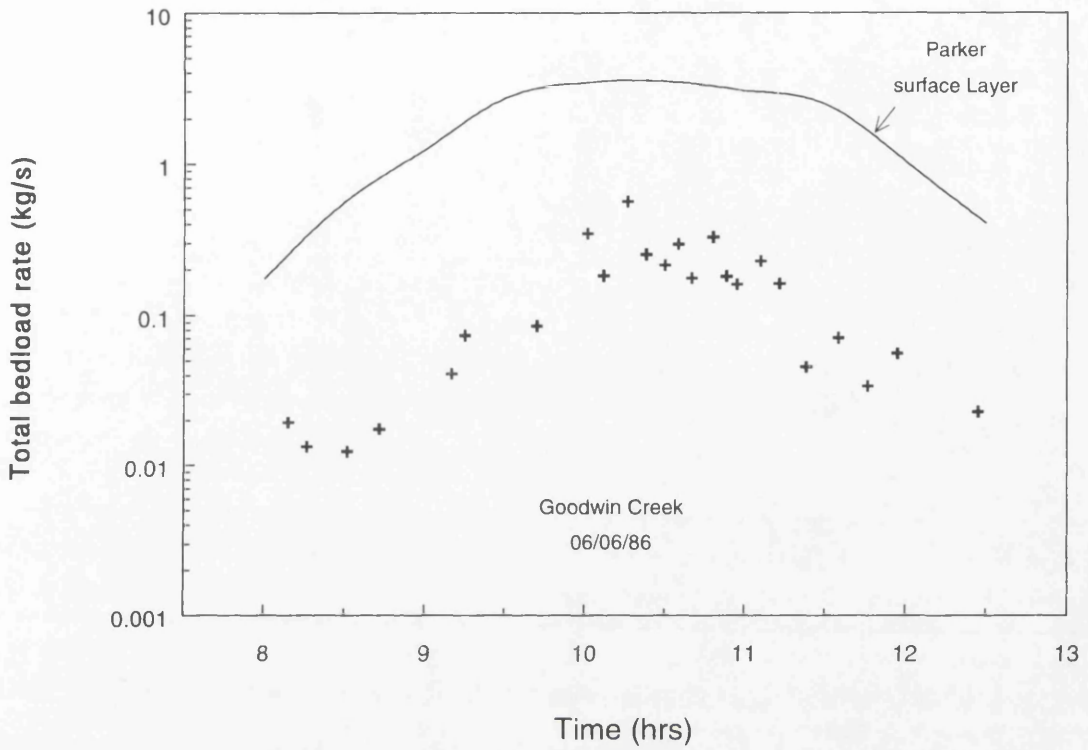


Figure 7.9 Predictions of Bedload Rates Using Parker's Formula For Event 06/06/86

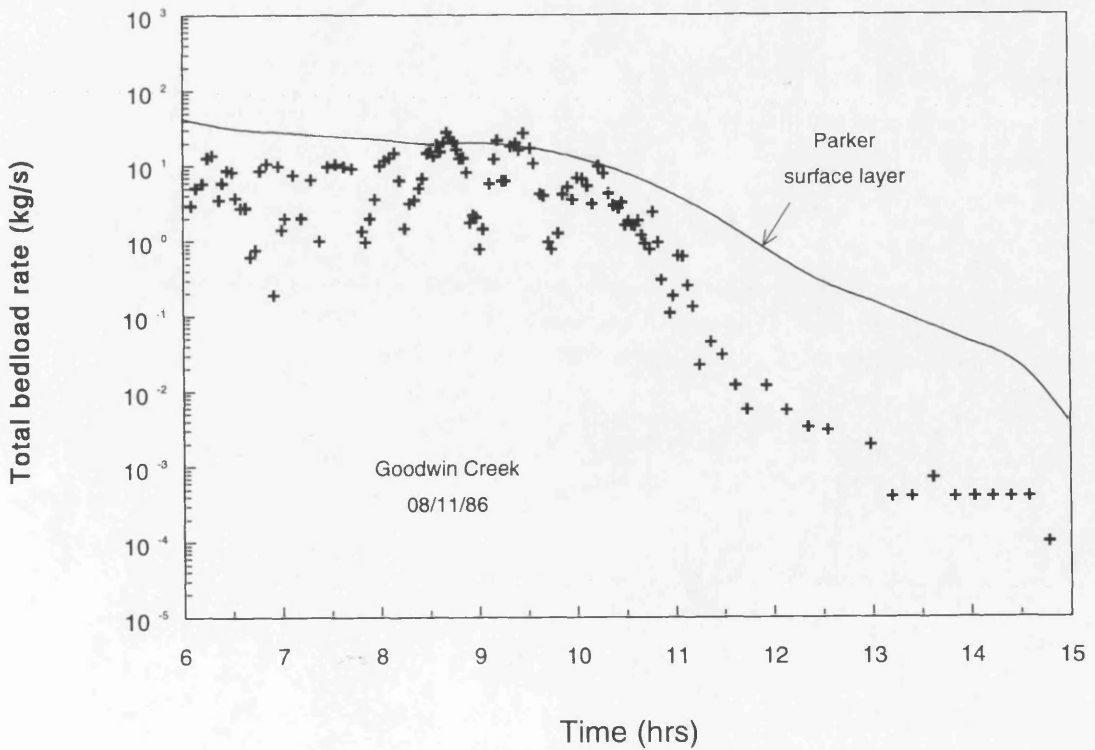


Figure 7.10 Predictions of Bedload Rates Using Parker's Formula For Event 08/11/86

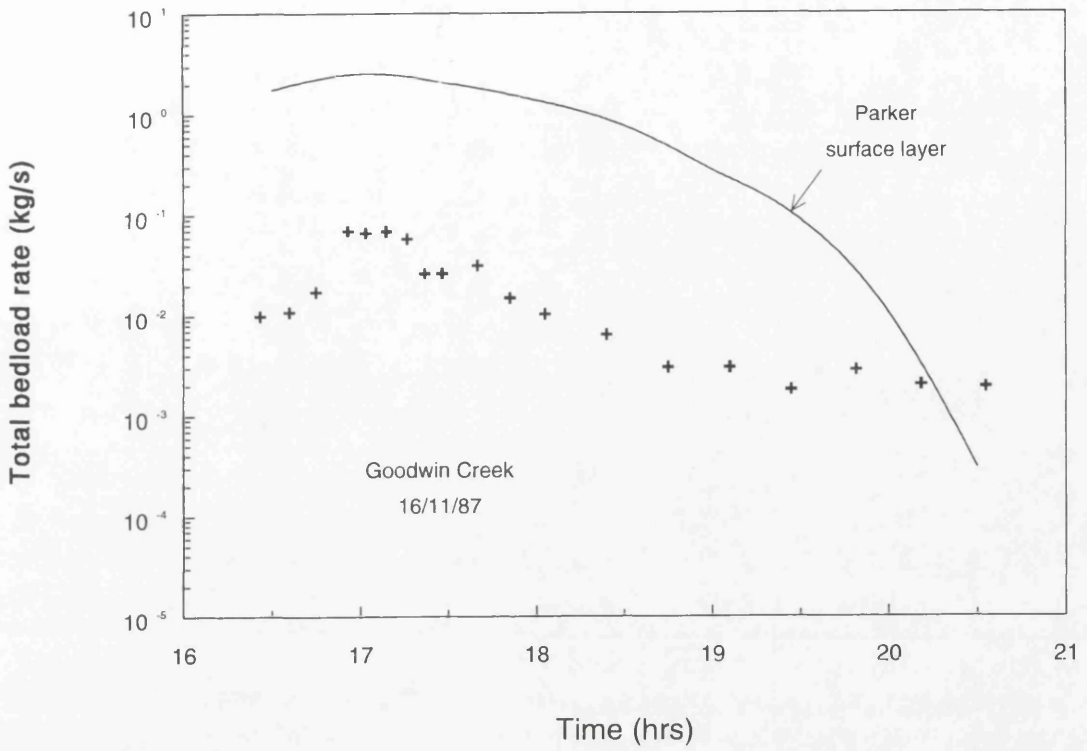


Figure 7.11 Predictions of Bedload Rates Using Parker's Formula For Event 16/11/87

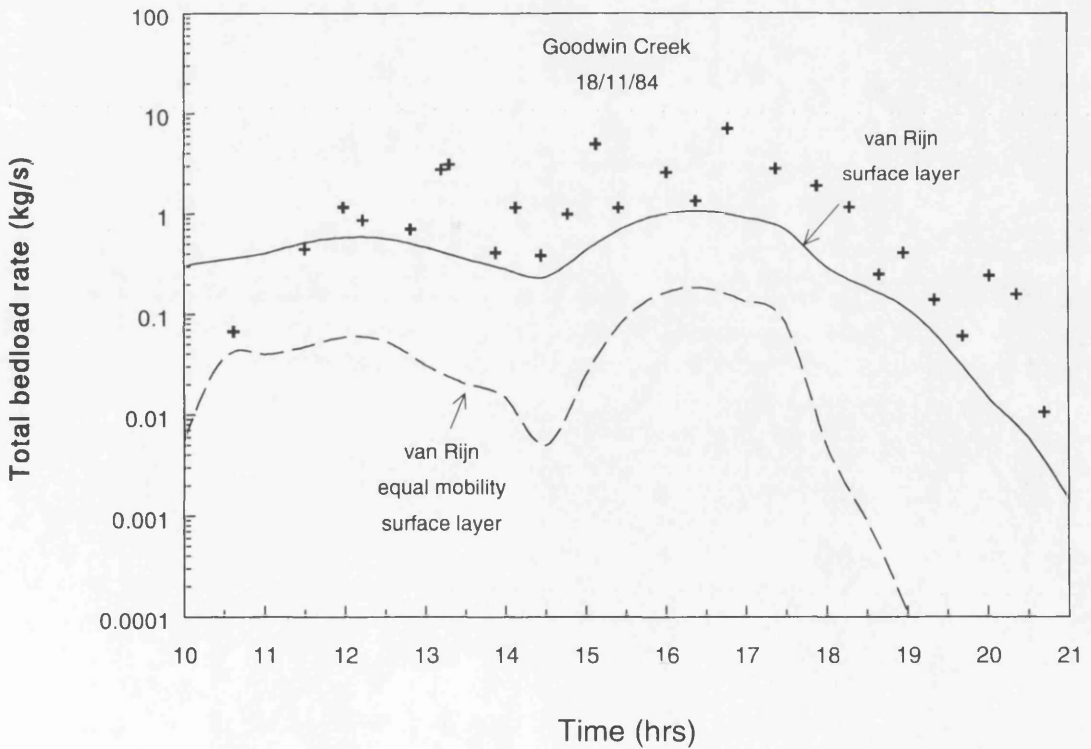


Figure 7.12 Predictions of Bedload Rates Using Equal Mobility For Event 18/11/84

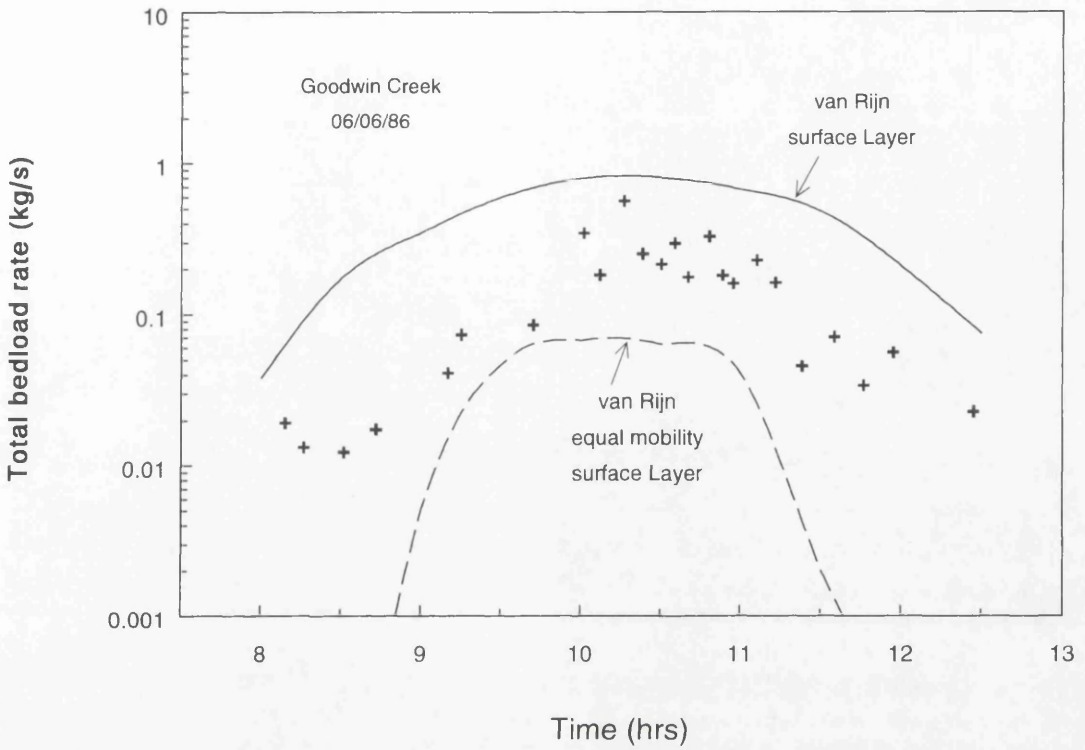


Figure 7.13 Predictions of Bedload Rates Using Equal Mobility For Event 06/06/86

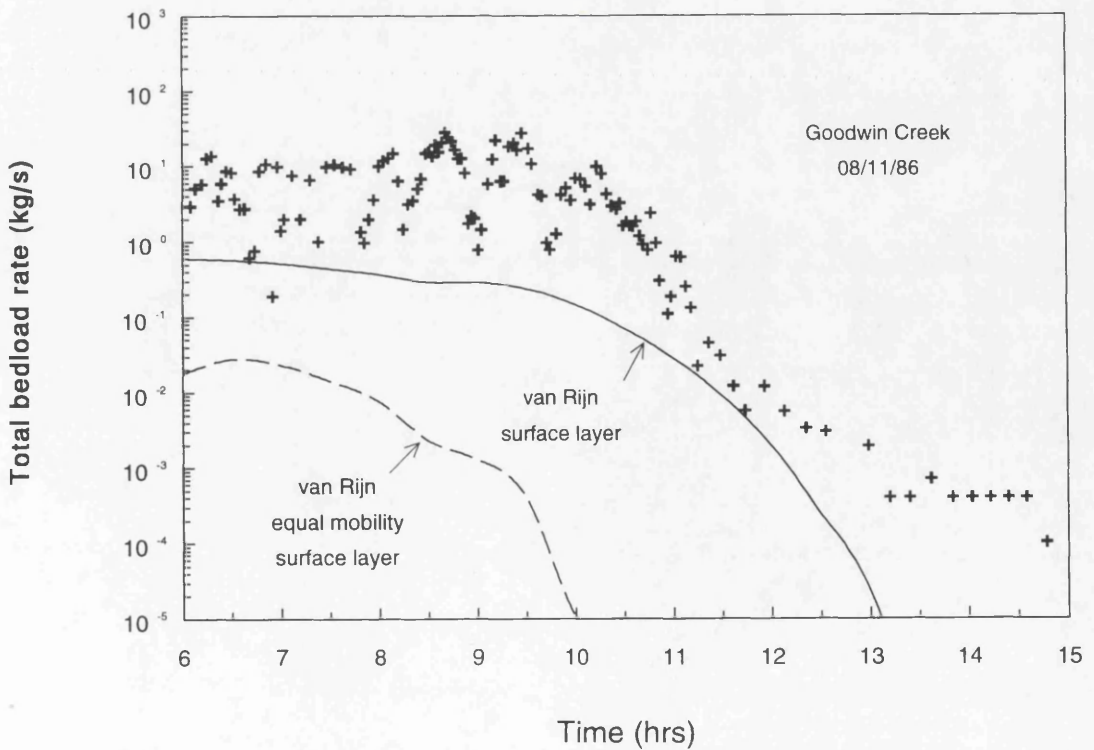


Figure 7.14 Predictions of Bedload Rates Using Equal Mobility For Event 08/11/86

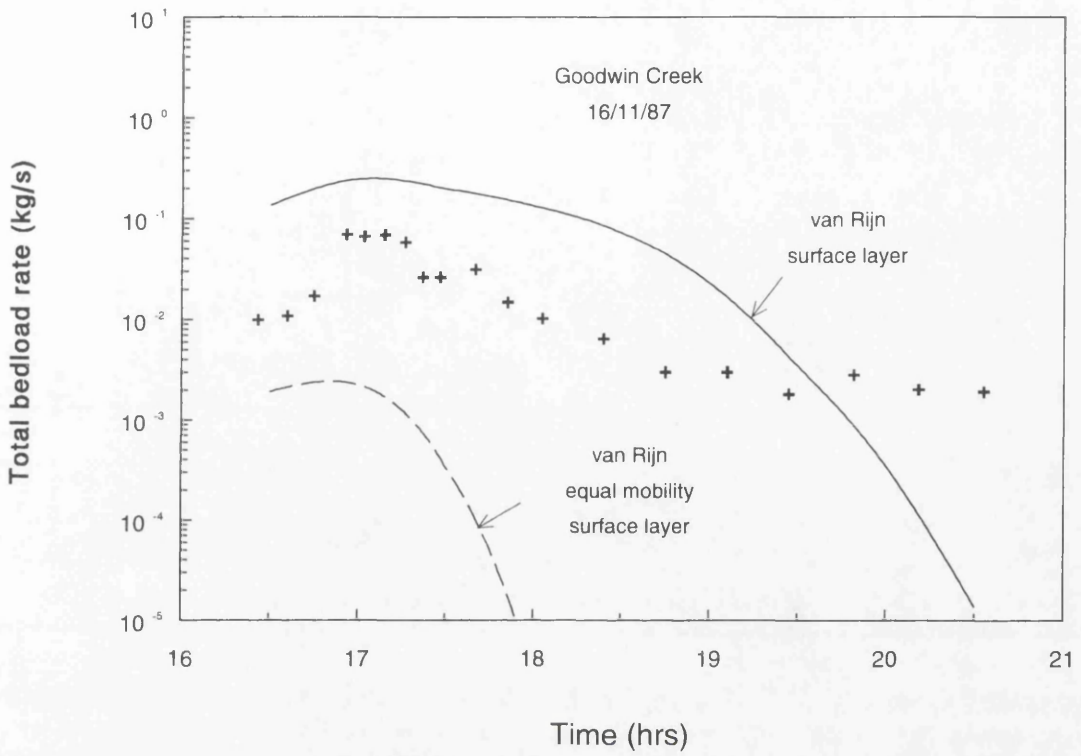


Figure 7.15 Predictions of Bedload Rates Using Equal Mobility For Event 16/11/87

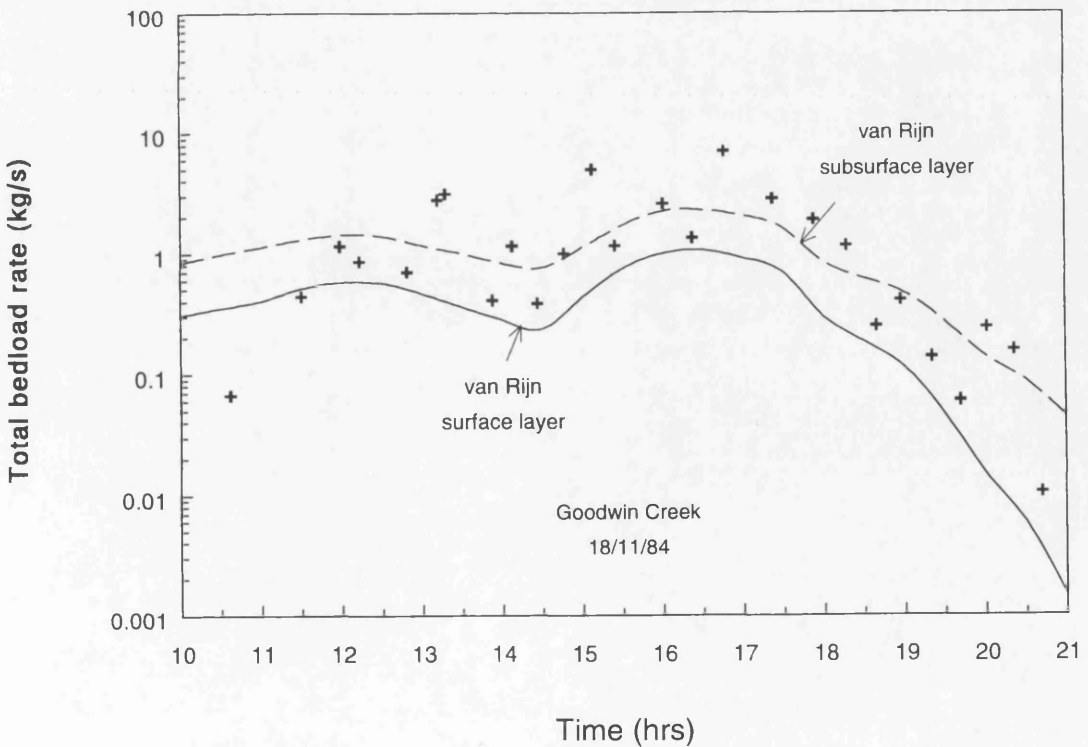


Figure 7.16 Predictions of Bedload Rates Using van Rijn's Formulae and Subsurface Layer For Event 18/11/84

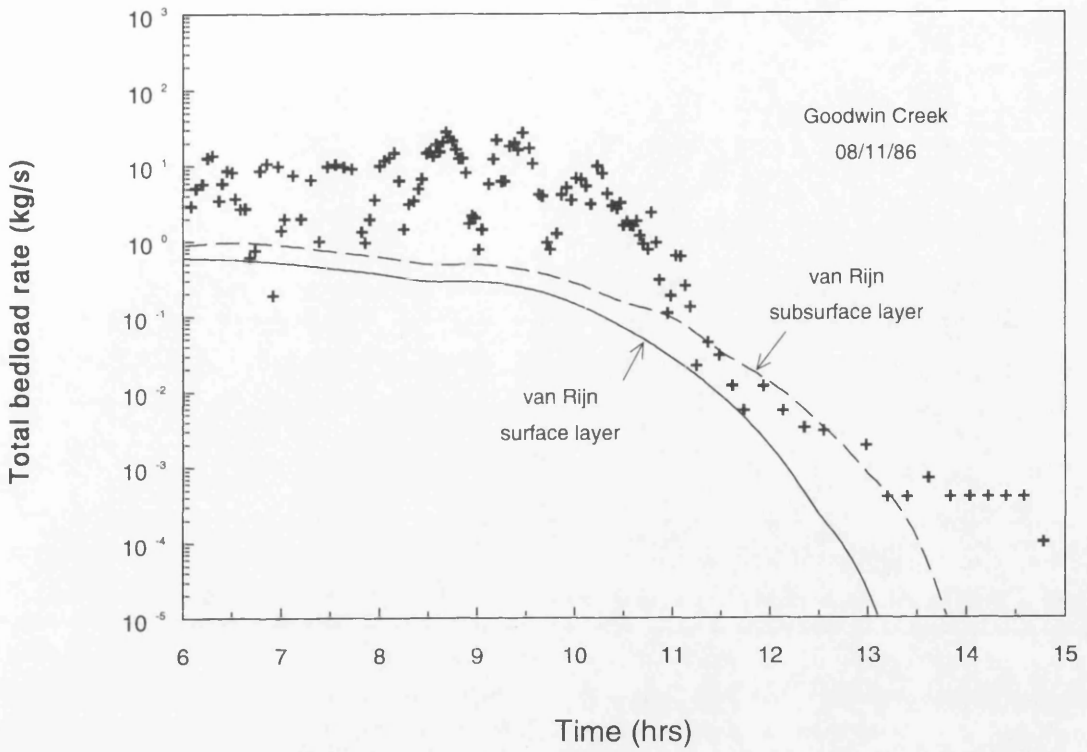


Figure 7.17 Predictions of Bedload Rates Using van Rijn's Formulae and Subsurface Layer For Event 0/11/86

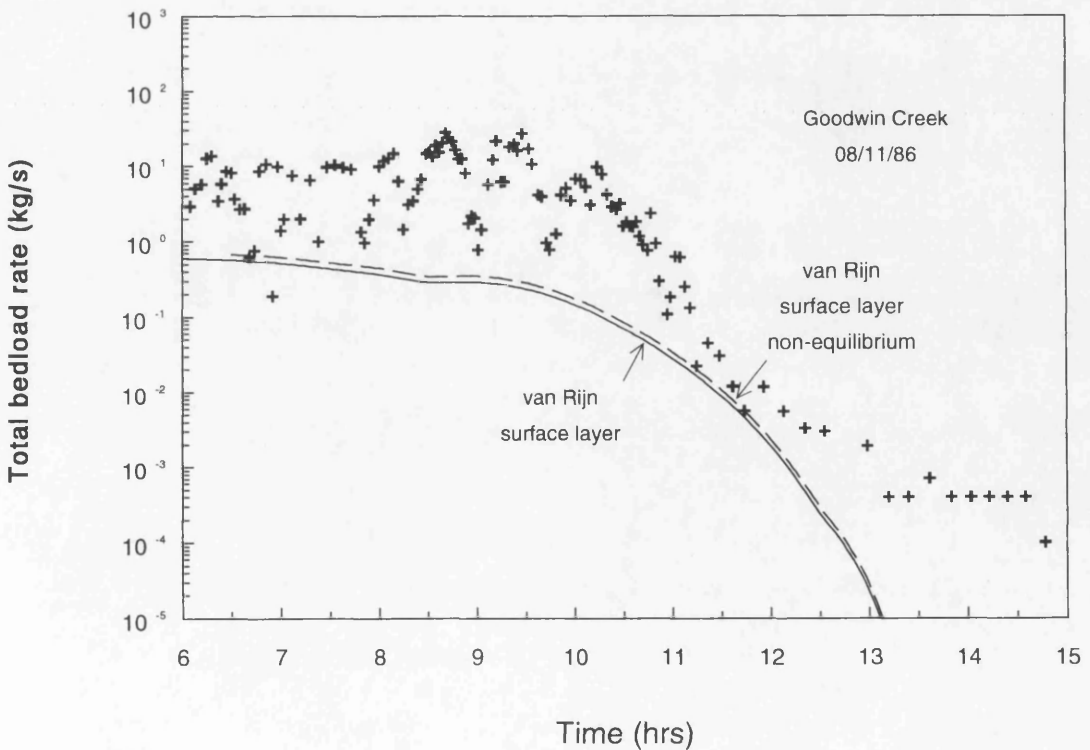


Figure 7.18 Comparison of Bedload Between Equilibrium and Non-equilibrium Upstream Boundary Conditions For Event 08/11/86

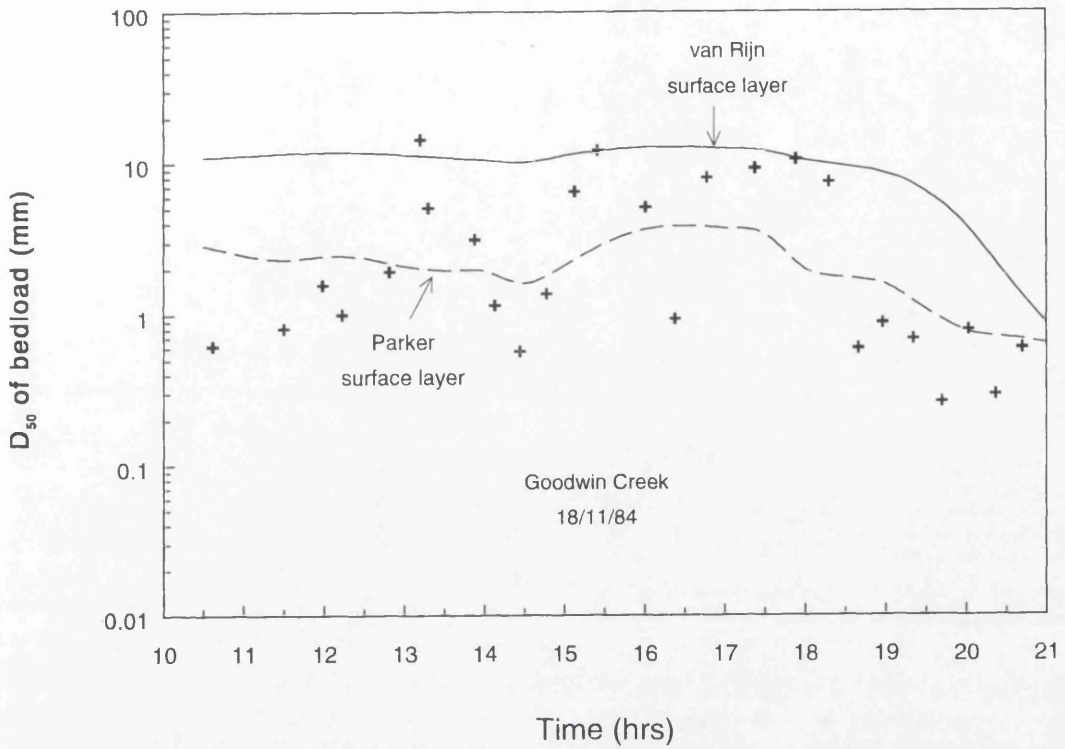


Figure 7.19 Comparison of  $D_{50}$  in Bedload For Event 18/11/84

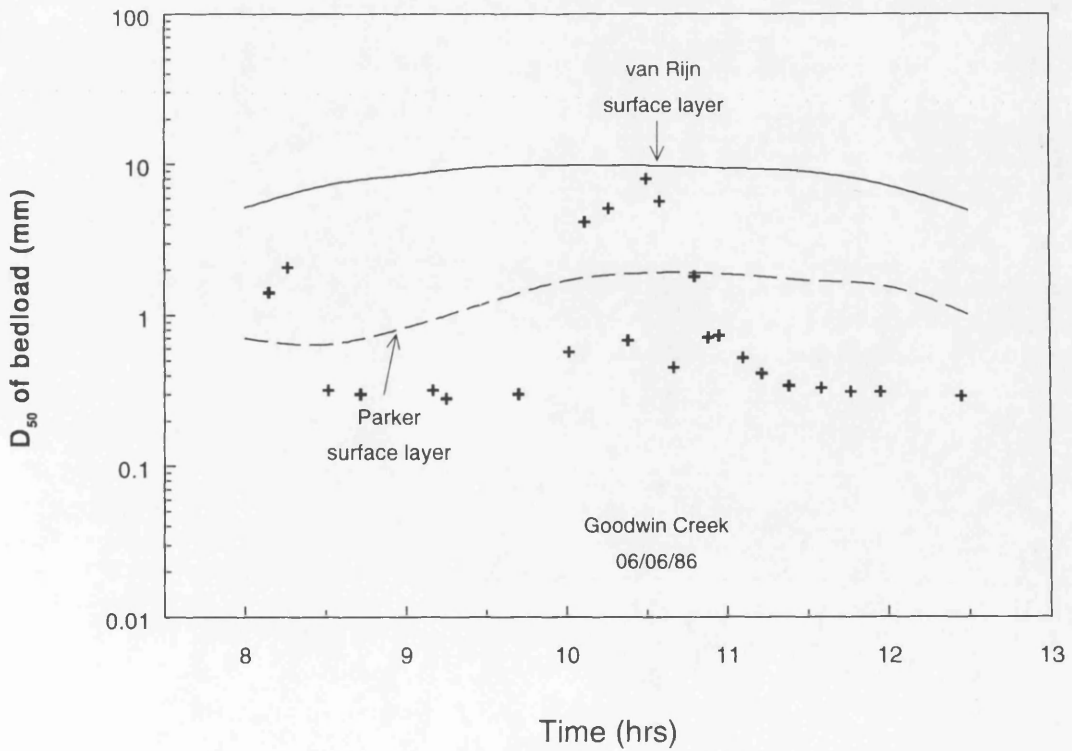


Figure 7.20 Comparison of  $D_{50}$  in Bedload For Event 06/06/86

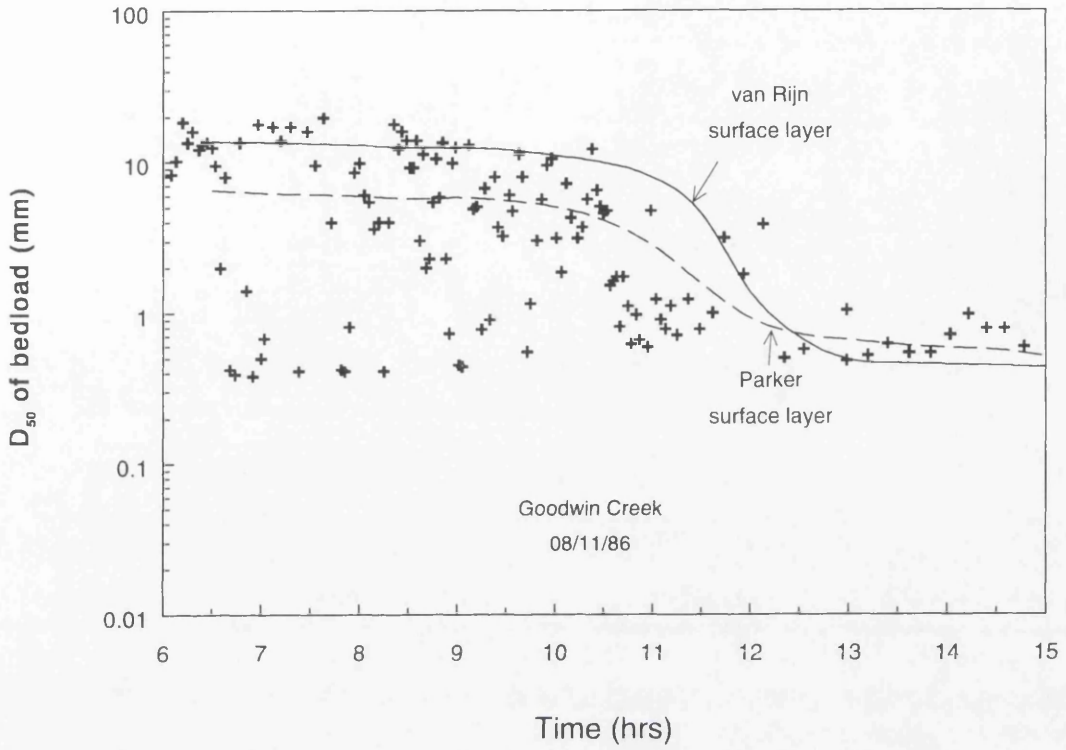


Figure 7.21 Comparison of  $D_{50}$  in Bedload For Event 08/11/86

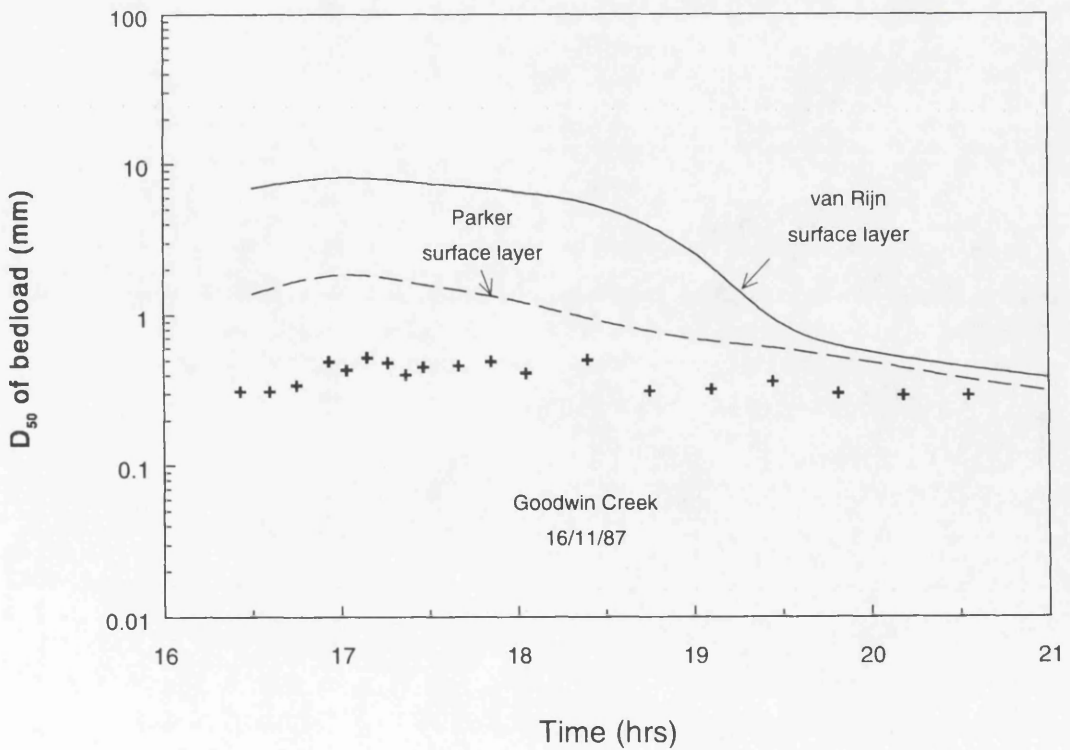


Figure 7.22 Comparison of  $D_{50}$  in Bedload For Event 16/11/87

## CHAPTER 8

### Model Verification Using The River Clyde Data

#### 8.1 Introduction

General plan and key locations in the River Clyde are shown in Figure 8.1. It flows from the south of Scotland and passes through the city of Glasgow entering the Firth of Clyde at Greenock. From Greenock to Erskine the River Clyde is a typical tidal river with the sand and mud banks exposed at low tide and the water depth shallower than that in the Firth of Clyde. Upstream of Erskine to the city of Glasgow, the channel becomes more confined.

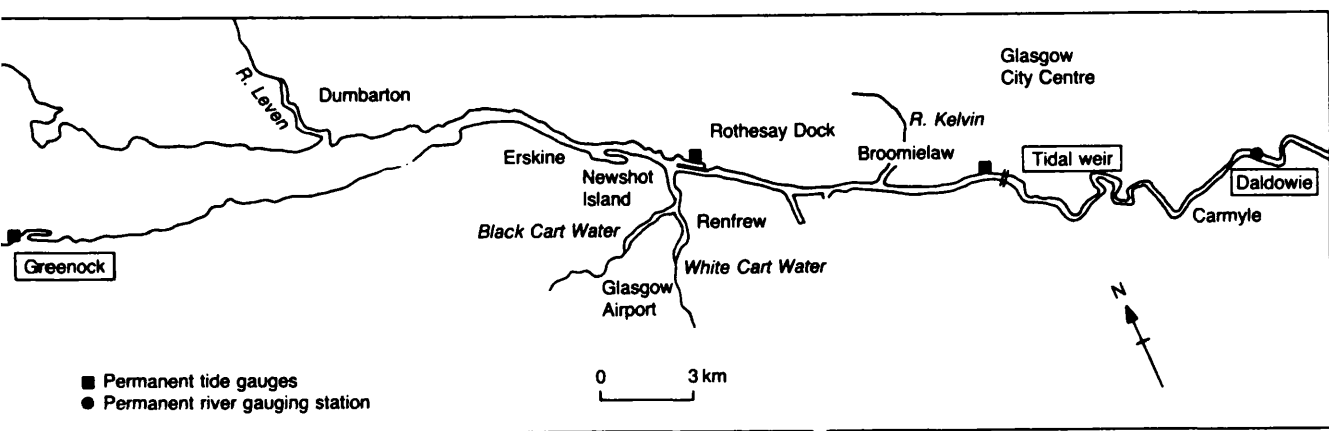


Figure 8.1 General Plan and Key Locations In The River Clyde (from Falconer et al, 1992)

The River Clyde has played a significant role in the development of Glasgow both as a waterway to enable commercial vessels to reach the centre of the city, and as a home for City's ship building industry. At the end of the 17th century, the river was in its natural state and sufficiently shallow in many places as to be easily forded at low tide. As commerce developed and pressure grew to improve shipping access to Glasgow, the 36 km channel between Greenock and the city was extensively widened, straightened and deepened. This work was undertaken first by training walls and later by dredging, see Falconer et al (1992). As a result of these engineering activities an artificial channel was formed that had a very much greater cross-sectional area than its natural state.

It has been found that the channel upstream of Glasgow is in regime since the long term average sediment load is transported without significant net deposition or erosion, see Falconer et al (1992). However, on reaching the deepened cross-section downstream of Glasgow, the reduction in flow velocity results in the deposition of both suspended-load and bedload. This deposition occurs along the full length of the dredged channel from the tidal weir at Glasgow Green to Greenock, and is increased by the sediment inflows from the main tributaries of the Rivers White Cart, Kelvin and Leven. In the past the Clyde Port Ltd has removed 280,000 m<sup>3</sup> per annum of the deposited sediment from the dredged channel.

With the construction of new deep water port facilities at Greenock in 1969 and Hunterston in 1979 and the decline of the shipbuilding industrial, the number of commercial vessels wishing to use the facilities at Glasgow has been reduced considerably. Therefore on commercial grounds the commitment to dredging was considered as uneconomical. The financial benefits that would result from a reduction in dredging commitment are obvious.

Before the cessation of dredging could be considered as a viable option its impact on the many and varied industrial and commercial activities which still rely on the maintained channel required to be assessed. These will include any change in

flood risk, tidal range, drainage or river environments. Two studies have been commissioned by the Clyde Port Ltd and Strathclyde Regional Council Drainage Development to investigate these potential problems. Both of these studies were undertaken by Babbie Group Ltd in conjunction with the University of Strathclyde. These studies used a mathematical model of hydrodynamics to predict bed shear stress. Regime cross-sections were then estimated using hand calculations. Therefore the purpose of analysis undertaken here is not to duplicate this previous work but to:

- i. use the data available from the previous studies to provide a test application of the present model to a large UK river;
- ii. use the results of the previous studies to verify the model;
- iii. investigate the impact of the proposed tidal weir on regime conditions in the Clyde;
- iv. provide more detail information for the shape of cross-sections in the final regime conditions.

## 8.2 Previous Work

The first dredging study of the River Clyde was carried out to estimate the regime conditions of the river channel from Glasgow to Greenock and to assess its impact, see Dredging in the River Clyde, phase I report (1988) and phase II report (1989). To assist with the predictions of water levels and velocities, a numerical hydrodynamic model, called *FLOODTIDE*, was constructed to estimate the water levels and flow rates between Greenock and the tidal weir at Glasgow. The main flow inputs comprise the tidal hydrograph at Greenock together with the fresh water inflow from the Clyde, the Cart, the Kelvin and the Leven.

For the calibration of the model, the data available from the permanent tide and river flow gauging stations were supplemented by continuous observation of water surface levels at two additional locations, Broomielaw and Rothesay Dock. For the events considered, the model parameters were adjusted until a good correlation was

achieved at all locations generally well within 100 mm during the entire period of observation. Bed roughness values expressed in terms of Manning's  $n$  averaged 0.019 downstream of the tidal weir.

The model verification was based on the flow events covering a range of flow and tidal conditions, including the high surge tide observed on 9 February 1988 which was very close to the previous highest recorded tide level at Greenock. A satisfactory correlation was achieved with all these verification events such that the model could be used with confidence for the predictions of water level changes associated with changing bed profiles.

It is reported by Falconer et al (1992) that the river upstream of Kingston Bridge was abandoned to navigation some years before the study and subsequently infilled to a regime state. From the Clyde Port hydrographic surveys there is a considerable amount of bathmetric data available. This data was used to develop the empirical regime equations linking the water depth, the width, the discharge, the sediment transport and the bed material characteristics. Using this in parallel with the numerical model enables final regime conditions from Greenock to the tidal weir to be predicted, see Figure 8.2.

Table 8.1 shows the resulting values of average bed level at regime in the main Clyde channel, the levels being compared with the present maintained depth.

**Table 8.1 Bed Level at Regime Condition in River Clyde (from Falconer et al, 1992)**

Chainage (m)	Location	Regime bed level average cross-section (m) OD	Channel maintained level (m) OD
1000	Broomielaw	-3.2	-7.8
4000	Yorkhill	-3.8	-9.3
6500	Shieldhall	-4.2	-9.7
11000	Rothesay Dock	-4.7	-9.7
16000	Erskine	-5.1	-9.7
23000	Dumbarton	-5.5	-9.7
36000	Greenock	-6.2	-9.7 and -13.3

Time to regime was established from the infill volumes required and the rate of sediment input. The latter took account of the contributions from the different tributaries. The calculations showed that the Clyde would be in regime as far downstream as the River Cart (chainage 11 km), the limit of the most existing port and shipyard facilities, about 44 years after the cessation of dredging; and that regime would extend to Dumbarton (chainage 23 km) after about 100 years; and the whole channel downstream to Greenock (chainage 36 km) would be in regime after 215 years. Table 8.2 shows the rising rate of the bed level at different locations.

**Table 8.2 Typical Bed Level Rising Rate (from Falconer et al, 1992)**

Location by Chainage (m)	Type of Area	Rising Rate (mm/yr)
1000 — 3500	upstream channel	270
3500 — 4100	wide channel	420
4600 — 5700	wide channel	340
7500 — 36000	off-channel basin	250

The predicted longitudinal profile at regime is shown in Figure 8.2. The assumption in this prediction is that the sediment inflow will remain of similar magnitude and nature to those found today. Since the sediment inflow is likely to vary considerably from year to year, the short term predictions could be overestimated or underestimated.

The numerical model data was modified to reflect the predicted regime conditions, the critical storm tides and the flood conditions. These runs demonstrated that the increase in maximum water levels at Glasgow for an extreme 100 year tide was generally less than 100 mm shown in Figure 8.3. Maximum water levels were found to be a function of extreme tide levels. The water inflows had only a small effect on these levels, from Falconer et al (1992).

The regime method is regarded as an approach of long term prediction which uses the average long term discharge and sediment transport rate. However, the water

and sediment inflows vary with time especially during the flood period. The regime method is unlikely to give the predictions of channel geometry changes in such case.

Implicit in the regime method is the assumption of the similarity for bed material characteristics and river pattern. The characteristics of bed material and river pattern in the regime channel where the regime equations are derived should be similar to that in the applied channel. Falconer et al (1992) have demonstrated that the use of the regime method to predict the bed profile in the regime conditions was appropriate in the Clyde because of its relatively simple sediment inflow pattern and the canalised artificial cross-sections created by capital dredging. The use of such an approach might not be suitable for general applications subject to complex river pattern and sediment inflow. The numerical modelling based on the extensive field studies would provide more precise predictions. Therefore by using the comprehensive numerical model to simulate water flow, sediment transport and channel geometry change in the Clyde, it is intended to demonstrate that the numerical model can be used for long term predictions in a real river with same degree of confidence.

### **8.3 Descriptions of The River Clyde**

#### **8.3.1 Study Area**

The study area of the Rive Clyde is from the tidal weir in Glasgow to Greenock with 36 km long, shown in Figure 8.1. Along this reach there are three rivers, the River Kelvin, the River Cart and the River Leven, which join the Clyde at chainages of 4,300 m, 11,100 m and 23,000 m respectively. The catchment data is shown in Table 8.3.

The Clyde channel can be divided into two sections, see Falconer et al (1992). The first section comprised the 13 km reach from Glasgow to Newshot Isle. Over this length the present waterway is confined by either quay walls or protected riverbank. The breadth is virtually equal at high and low waters and varies from about 120 m in

Glasgow to about 150 m at Newshot. Within this reach, it was assumed that the existing fixed banks would remain in place. It was also anticipated that this reach would infill and reach regime first.

**Table 8.3 Catchment Area and Long Term Average Discharge**

Catchment	Approximate catchment area (km <sup>2</sup> )	Approximate long term average discharge (m <sup>3</sup> /s)
Clyde	1930	45
Cart system	450	15
Kelvin	335	8
Leven	785	41

The second section comprising the lower 23 km reach, extended from Newshot Isle to the natural deep water off Greenock. In this area, the estuary widened rapidly at high water to form the normal trumpet-shaped plan profile. Most of the banks were unconfined and in a natural state. The deepened shipping channel was constrained in part by a longitudinal training wall. The area between the channel and the high water mark dries at low tide.

### 8.3.2 Cross-Section Information

The cross-section information was obtained from the hydrographic survey drawings produced by the Clyde Port Ltd and Admiralty Chart (1994, 2007) of the River Clyde. The hydrographic survey drawings cover the cross-sectional information of the main channel from the tidal weir in Glasgow to Greenock. It was decided to use the hydrographic survey drawings as the initial cross-sectional information before the cessation of dredging. The cross-sectional information in the tidal mud flats was obtained from the Admiralty Chart with the scale of 1:15,000. All data on the mud flat are considered to relate to circumstances before the cessation of dredging. Therefore both sources of data are compatible.

When constructing the cross-sectional data it was considered that the data in hydrographic survey drawings were accurate and as many as possible were used; the data from the Admiralty Chart were only used in areas where suitable data from the hydrographic survey drawings was not available. The combination of the two data sources gave enough information to construct the model. A summary of the drawings used is given in Table 8.4.

In the model the Clyde has been divided into 86 cross sections with space increments from 100 m to 650 m, subject to the variation of the shape between the cross sections. It is believed that these 86 cross sections are accurate enough to represent the Clyde channel and assumed that there will be no engineering activity in the future to disturb the cross sections. The key locations and chainage are shown in Figure 8.4. The typical cross-sections are shown in Figures 8.5 to 8.8. It can be seen from Figures 8.5 and 8.6 that the cross sections at Broomielaw and Rothesay Dock are quite regular and confined by the training wall on both sides of the bank. The cross sections at Dumbarton and Greenock, see Figures 8.7 and 8.8, demonstrate that here the river is typical of many tidal rivers containing two main water ways and a mud flat.

### **8.3.3 Properties of Bed Material**

A typical sample of the bed material in the Clyde, provided by the Clyde Port Ltd, shows that the diameter of the bed material ranges from 0.63 to 2.00 mm. This sample is summarised in Table 8.5.

This sample was taken from the low tide flat. However it has been found, see Babbie Group Ltd (1988), that the bed material in the main channel has the similar size distribution. Therefore the properties of the bed material is assumed not to change significantly at different locations.

Table 8.4 Summary of Hydrographic Survey Drawings In The River Clyde

Drawing No. HM	Location	Scale	Time of Surveying	Meters Below O.D.
1000-1-1	Glasgow - Upper Harbour	1:1000	20/06/85	2.50
1001-1-5	Glasgow - Lower Harbour	1:1000	01/03/83	2.50
1002-1-7	Glasgow - Lower Harbour	1:1000	28/02/83	2.47
1003-1-9	Glasgow - Lower Harbour	1:1000	79	2.43
1004-1-14	Glasgow - Lower Harbour	1:1000	05/91	2.42
1005-1-2	Meadowside	1:1000	05/82	2.39
1006-1-1	Merklands	1:1000	14/09/82	2.36
1007-1-2	Shieldhall Reach	1:1000	82	2.32
1008-1-4	King George Dock & Approaches	1:1000	01/82	2.32
1009-1-1	Braehead Reach	1:1000	03/83	2.32
1010-1-2	Elderslie	1:1000	07/04/82	2.25
1011-1-2	Renfrew Reach	1:1000	81	2.25
1012-1-2	Renfrew Reach	1:1000	04/83	2.25
1013-1-3	Rothsay Dock & Approaches	1:1000	26/02/81	2.20
1014-1-2	Clydebank - Newshot Bend	1:1000	04/82	2.20
1021-1-1	Erskine - Bowling Bend	1:1000	04/81	2.00
1023-1-2	Longhaugh Reach & Long Dyke	1:2500	08/83	1.94
1024-1-2	Dumbuck Reach & Long Dyke	1:2500	30/04/84	1.94
1025-1-6	Dumbarton - River Channel	1:2500	08/05/84	1.79
1026-1-9	Dumbarton - Puddledeep- River Channel	1:2500	19/08/85	1.79
1028-1-8	Cardross Reach - River Channel	1:2500	17/06/87	1.64
1030-1-2	Port Glasgow - River Channel	1:2500	11/80	1.62
1031-1-4	Greenock - River Channel & Cockle Bank	1:2500	27/08/87	1.62
1034-1-2	Greenock - River Channel	1:2500	05/87	1.62

**Table 8.5 Sieve Analysis For Bed Material of The River Clyde (from Clyde Port Ltd)**

Sieve Size $D_j$ (mm)	$\Phi = -\text{Ln}_2(D_j)$	Percentage Weight	Cumulative Percentage Weight
2.000	-1	0.54	0.54
1.400	-0.5	0.65	1.19
1.000	0	1.75	2.94
0.710	0.5	3.00	5.94
0.500	1	6.48	12.42
0.355	1.5	16.68	29.10
0.250	2	31.42	60.52
0.180	2.5	26.89	87.41
0.125	3	8.35	95.96
0.090	3.5	1.80	97.56
0.063	4	0.92	98.48
< 0.063	< 4	1.52	100

\* Low tide surface sample

\* Sample weight 50 g

The grain size distribution of this typical sample is shown in Figure 8.9. The mean diameter is around 0.3 mm and the standard geometric deviation  $\sigma_g$  is 1.746. The bed material with the diameter from 0.18 to 0.5 mm is about 75% in total. This implies that the bed material is in the very narrowed range and the bed material sorting is not significant and unlikely to affect the sediment transport. Uniform sediment transport was therefore assumed to be appropriate for this model. The mean diameter and deviation of the sample are shown in Table 8.6.

**Table 8.6 Properties of Bed Material In The River Clyde**

$D_{50}$ (mm)	$\sqrt{D_{84}/D_{16}}$	$D_g$ (mm)	$\sigma_g$
0.290	1.547	0.295	1.746

The bed material in the Clyde can be treated as a cohesiveless sediment and the particle shape effect is considered to be insignificant. It is also assumed that all material has same density and porosity. The representative diameter of the bed material was taken to be 0.3 mm.

## 8.4 Boundary Conditions

The numerical simulation of water flow and uniform sediment transport requires the use of three boundary conditions which are

- i. incoming water flow at the upstream boundary;
- ii. incoming sediment at the upstream boundary;
- iii. water surface level at the down stream boundary;

### 8.4.1 Water Inflow

The water inflows from the catchment of the River Clyde and each of the major tributaries were recorded by the Clyde River Purification Board. The peak flows for specific flood return periods were estimated based on these data, see Falconer et al (1992). They are shown in Table 8.7.

**Table 8.7 River Flow Data (from Falconer et al, 1992)**

River	Long term average flow (m <sup>3</sup> /s)	Mean annual flood (m <sup>3</sup> /s)	10 year flood (m <sup>3</sup> /s)	50 year flood (m <sup>3</sup> /s)	100 year flood (m <sup>3</sup> /s)
Clyde	45.3	434	623	810	884
Kelvin	8.3	73	87	101	107
White Cart	7.0	124	159	194	209
Black Cart	4.4	39	56	72	80
Gryffe	3.6	67	81	96	102
Leven	41.5	116	141	165	175

The regime simulations require the careful selection for the dominant water inflow. It has been found that most of sediments were entering the Clyde channel

during flood periods. During low flow periods the sediment inflow is less important. Therefore it was decided to use the mean annual flood of 434 m<sup>3</sup>/s as the dominant water inflow at the upstream boundary for long term prediction of regime conditions in the Clyde. The lateral inflows from the three main confluences into the Clyde were also the mean annual floods for the same simulation.

For calibration of the model, the water inflow was selected on the basis of a typical tidal events because the tide plays an major role in controlling the water levels in the Clyde. For all simulations the density current from the seaward end was neglected and it was assumed that the density of the water is constant.

#### **8.4.2 Sediment Inflow**

The assessment of sediment inflow for the major rivers within the River Clyde catchment was carried out using two methods by Babbie Group Ltd as follows.

- i. An extensive period of flow data, 1963 to 1987 was processed using a sediment rating curve method based on suspended-load measurements taken within the river network over a period of time and range of flows.
- ii. The Strathclyde River Basin Model was used to derive a fully calibrated rainfall/runoff model for the period 1963 to 1973 and 1981/82 and subsequently used to investigate land erosion within the Clyde River Basin.

The results from these two methods have been compared with each other. The sediment inflow to the Clyde channel is approximately 110,000 t of dry solids per annum. The majority of this material enters from the main Clyde catchment, but a proportion comes from three tributaries - the Cart, the Kelvin and the Leven.

The grain size distribution of the sediment inflow is taken to identical to bed material. In other words, the sediment inflow can be assumed to be uniform with the mean diameter of 0.3 mm.

#### **8.4.3 Tide Levels**

Tidal data at Greenock, Rothesay Dock and Broomielaw are recorded by Clyde Port Ltd and summarised in Table 8.8. The data at Greenock provides the downstream boundary conditions, whereas the data at Rothesay Dock and Broomielaw can be used for calibration.

**Table 8.8 Tidal Data for Greenock, Rothesay Dock and Broomielaw (from Falconer et al, 1992)**

	Greenock: OD (m)	Rothesay Dock: OD (m)	Broomielaw: OD (m)
Highest recorded water level	+3.33 (1936) +3.71 (1991)	+4.35 (1926)	+4.64 (1882)
Highest astronomical tide (HAT)	+2.48 2.38 (1991)	+2.88	+3.04
Mean high water springs (MHWS)	+1.78	+2.04	+2.20
Mean high water neaps (MHWN)	+1.28	+1.44	+1.60
Mean low water neaps (MLWN)	-0.62	-0.74	-0.90
Mean low water springs (MLWS)	-1.22	-1.63	-1.70
Lowest astronomical tide (LAT)	-1.72 -1.92 (1991)	-2.30	-2.60
Lowest recorded water level	-2.53 (1980)	-3.03 (1980)	-3.16 (1980)

## 8.5 Application of Hydrodynamic Model

### 8.5.1 Calibration of The River Clyde Model

For the calibration of the hydrodynamic model, the tidal record in 16 August, 1989 was chosen. There are two reasons for this; firstly, this tidal event is similar with the mean spring tide and is likely to be dominant in controlling the water levels, secondly, the tidal records observed in Rothesay Dock and Broomielaw for same tidal event can be used to compare with the numerical results. The recorded tide event is shown in Figure 8.10.

As the effect of inflow at the tidal weir in Glasgow on water levels is not significant compared with the tidal effect, the long term average inflow was chosen as the upstream boundary inflow. The use of constant water inflow instead of using the observed inflow hydrograph will not affect the accuracy of predictions for water levels considerably. The observed water levels at Rothesay Dock and Broomielaw were used to calibrate the parameters in the model. These parameters are summarised as;

- i. the resistance factor Manning's coefficient;
- ii. the time weighting factor in the Preissmann scheme;

The calibration run was started from one day before 16 August 1989 to eliminate the effect of the initial conditions on the numerical results. The initial water flows were constant and equal to the water inflow, and the initial water levels were set up from the steady flow calculations. After around 6 hours, the distortion of water flows and levels caused by the estimated initial conditions were negligible. Therefore the total period of simulation was 48 hours though the results from first 24 hours were disregarded.

Initially a time increment of 300 seconds was employed with a time weighting factor of 0.55 in the Preissmann scheme. The Manning's coefficient was adjusted until a good agreement was achieved at all locations during period of observation. After the Manning's coefficient was determined, the influence of different time increments and time weighting parameters in the Preissmann scheme was examined.

Figures 8.11 and 8.12 show the comparison between the predicted and observed water levels at Rothesay Dock and Broomielaw for different Manning's coefficients of 0.015, 0.02 and 0.025. The calibration shows that the good agreement was achieved when the Manning's coefficient equals 0.02. This value is very close to the value of 0.019 reported by Falconer et al (1992).

The predicted water levels at Rothesay Dock and Broomielaw have been compared with the observed values which are shown in Figures 8.13 and 8.14 for the

Manning's coefficient of 0.02. These figures show that at peak the waver levels are underestimated. The reason for this may be a result of the location of the tide gauge at Greenock which is positioned on south bank. It is thought that as the tide enters the upper Clyde from the Firth, the super elevation effect will result in higher levels on the north bank than the south bank. If this is the case the numerical model should use a boundary condition on the channel centre line, not on the south bank as at present.

The numerical dissipation in the Preissmann scheme is directly proportional to time weighting parameter and time increment. In general the time weighting parameter is chosen to be 0.55 for flood wave simulation because it will provide stable results with the minimum dissipation. Since the space increment between each section is fixed, the numerical dissipation increases only with increases in time increment. Therefore we need to check what the range of suitable time increments are appropriate without producing the significant numerical dissipation. Initially 300 seconds was used to calibrate the model. In order to demonstrate the numerical dissipation, the time increment is reduced to 60 seconds. The numerical results are shown in Figures 8.15 and 8.16. From these two figures, it is seen that the results from using 60 seconds are very close to that of using 300 seconds. So using the time weighting parameter of 0.55 and the time increment of 300 seconds, the numerical dissipation is not significant in this case.

After calibration the parameters used in model are summarised in Table 8.9 and used for verifications of the model.

**Table 8.9 Parameters Used in Model After Calibration**

	Value used in Model
Manning's coefficient	0.02
Time weighting parameter in Preissmann scheme	0.55
Time increment (s)	300

### 8.5.2 Verification of Model

The verification of the model was carried out for three tidal events. The first one was selected to be similar with the tidal event used for calibration. This took place on the 15 August, 1989. The second one was selected for an extremely high tidal event which happened on the 5 January, 1991. The third one was chosen for a low tidal event on the 13 August, 1989. The results of verification runs are shown in Figures 8.17 to 8.22 for Rothesay Dock and Broomielaw. The comparison of the numerical results with the observed values is considered to be satisfactory. However, the peak value for water level is again underestimated with maximum difference of 20 cm. The reason for this was previously explained in section 8.5.1.

A good correlation achieved in all verification runs demonstrates that the model can be applied for predictions with confidence. All parameters listed in Table 8.9 are assumed to be fixed for predictions of water levels under any tidal event. For regime simulation, it is assumed that the Manning's coefficient will remain the same magnitude as what is found in existing channel.

### **8.5.3 Water Levels Caused By A 100 Year Tide And A 100 Year Flood**

It has been suggested, see Falconer et al (1992), that a combination of an extreme 100 year tide in conjunction with a 100 year flood is a practical upper limit for consideration of flood risk assessment. Therefore the prediction of water level under this event was performed. A 100 year tide at Greenock is shown in Figure 8.23. A 100 year flood inflow is listed in Table 8.7. The numerical results of water levels at Rothesay Dock and Broomielaw are shown in Figure 8.24.

## **8.6 Prediction of Final Regime Condition**

After calibration and verification the model was used to predict final regime conditions following the cessation of dredging.

### **8.6.1 Boundary Conditions**

Boundary conditions employed were

- i. fresh water inflow;
- ii. sediment inflow;
- iii. controlling water level at upstream;

### 8.6.1.1 Freshwater Inflow

When estimating a channel regime state it is necessary to select the dominant hydraulic conditions which control the sediment transport over a long duration. For the River Clyde that is the mean annual flood, see section 8.4.1. The inflows detailed in Table 8.10 were therefore adopted in this study.

**Table 8.10 Mean Annual Flood In The River Clyde and Its Tributaries**

River	Mean annual flood (m <sup>3</sup> /s)
Clyde	434
Leven	116
Cart	230
Kelvin	73

Total mean annual flood inflows including all tributaries in the Clyde is 853 m<sup>3</sup>/s which equals to the mean annual flood outflow at Greenock.

The use of mean annual flood inflow can be considered appropriate for regime simulation in the Clyde. However this may be not suitable for the short term predictions. The detail tidal and inflow hydrographs should be used in this case.

### 8.6.1.2 Sediment Inflow

The sediment inflow was evaluated based on the record of dredging from 1982 to 1986, see Falconer et al (1992). The dredged quantities have been recorded in terms of barge meters, which is equivalent typically to 0.8 in situ m<sup>3</sup> of sediment. The 1982-1986 period indicated an annual average maintenance dredging of 280,000 barge m for the channel upstream of Erskine which is 224,000 m<sup>3</sup> annually.

The majority of this material enters from a tidal weir in Glasgow, but a proportion comes from the three tributaries. Therefore for regime simulation, the sediment inflow from the tidal weir was taken to be 224,000 m<sup>3</sup> annually and the sediment inflow from other tributaries was assumed to be zero. It is believed that this can provide reasonable and relevant results without producing significant errors.

The total sediment inflow was divided into 10% bedload and 90% suspended-load, see Babbie Group Ltd (1988). Averaged over the year this equates to  $6.51 \times 10^{-3}$  m<sup>3</sup>/s of suspended-load and  $5.90 \times 10^{-4}$  m<sup>3</sup>/s of bedload.

From the grain size distribution in Figure 8.9 and Table 8.6, it can be seen that the bed material is not well graded. This indicates that an assumption of uniform grain size based on representative size of the bed material is appropriate in the River Clyde. Therefore a particle size of 0.3 mm was taken as a representative of the bed material. The sediment inflow is also assumed to be uniform with the diameter of 0.3 mm. This implies that the material sorting is not significant.

### 8.6.1.3 Controlling Water Level At Upstream

It has been reported, see Babbie Group Ltd (1987), that upstream of a tidal weir in Glasgow is in the equilibrium and that the sediment is transported without net deposition or erosion over a long period. For regime simulation, this phenomenon must be reflected and can be realised in the following way. Firstly, the mean annual outflow of 853 m<sup>3</sup>/s is imposed at the downstream boundary. This is equivalent to using the mean annual inflow at the upstream boundary. Secondly, the controlling water level at the end upstream is calculated for the equilibrium sediment transport and used as an upstream boundary condition. This results in the water level of 3.20 m OD. The whole boundary conditions for regime simulation are listed in Table 8.11.

**Table 8.11 Boundary Conditions For Regime Simulation of The River Clyde**

	Water flow (m <sup>3</sup> /s)	Water level (m) O.D.	Suspended-load inflow (m <sup>3</sup> /s)	Bedload inflow (m <sup>3</sup> /s)
Upstream	—	3.20	$6.51 \times 10^{-3}$	$4.90 \times 10^{-4}$
Downstream	853	—	zero flux	—

The use of a water level at the upstream boundary is considered to be suitable for the Clyde because it reflects the true equilibrium sediment transport conditions at the tidal weir and there is guaranteed not to cause any deposition or erosion at the cross-section. Accordingly the water level at the downstream boundary will be free in the regime simulation.

The boundary conditions in Table 8.11 imply that the sediment inflow from the seaward, larger-scale density current and tide generated internal sediment deposition, erosion and transport are not taken into account for regime simulation. It has been found, see Falconer et al (1992) that these assumptions are appropriate for the Clyde but may not be in the case of other estuaries.

### 8.6.2 Time To Reach Final Regime Condition

The Manning's coefficient for the regime simulation is constant with the value of 0.02. This implies that the resistance to flow in the existing channel is similar to that in the final regime conditions. In other words not only is the grain roughness similar but also the skin roughness.

The time weighting factor in the Preissmann scheme was 1.0 instead of 0.55. The time increment was 25 days. The total simulation time was 400 years.

The numerical results from the model indicated that the time to reach final regime condition at various locations is as follows down to Rothesay Dock in about 40 years after the cessation of dredging; extending to Dumbarton after about 110 years; and the whole river down to Greenock would be in regime after about 250 years. The results from the model simulation is shown in Figure 8.25. The comparison of the

longitudinal profile in the regime conditions between the model and the regime method used in Babbie Group Ltd (1988) is shown in Figure 8.26. In the Figure 8.26 the predicted bed level from the model is higher than one from the regime method. As a result the time to reach the final regime conditions from the model is longer than one from the regime method. There are two reasons for this difference. Firstly, the channel from Greenock to Erskine is a typical tidal channel where the width is much greater than that from Erskine to a tidal weir in Glasgow. For example, at Dumbarton the width is about 1,400 m and at Rothesay Dock the width is only around 200 m. The much wider channel down to the Greenock results in the big reduction of velocity. This will cause the material to deposit not only on the main channel but also on the mud flat. Secondly, applying the regime formulae derived from the regime channel upstream of a tidal weir in Glasgow would underestimate the bed level from Greenock to Erskine where the shape of cross sections is totally different from one in the regime channel.

The use of such average values for long term infilling assumes that sediment loads will remain of similar magnitude and nature to those found today. With regard to the short term predictions, the use of average values could significantly underestimate or overestimate conditions, as it is quite possible for sediment inflow to vary very considerably from year to year.

### **8.6.3 Cross-Sectional Shape In Final Regime Condition**

From an one dimensional model, it is impossible to calculate the distribution of deposition or erosion in the transverse direction at each cross section directly. However, in real engineering problems such as in the River Clyde, not only the bed profile but also the cross-sectional shape are important to assess problems such as the flood risk. This problem can be solved by applying a two dimensional depth averaged model where the sediment transport in the transverse direction needs to be evaluated. Since in the alluvium the secondary currents are less important than the longitudinal

velocity and may be less than the critical velocity, it is not easy to calculate the transverse sediment transport rates accurately. As an alternative way, the distribution of deposition or erosion in the transverse direction can be calculated using the transverse shear stress distribution as suggested by Chang (1988). In other words from an one dimensional model, the total volume of deposition or erosion in each cross section can be given and the thickness of deposition or erosion in the transverse direction is assumed to be proportional to the transverse shear stress distribution. The details of the procedure can be found in Chapter 3.

The cross-sectional shape in the Clyde changes considerably during the progression to the regime conditions. The results from the model are shown in Figures 8.27 to 8.36. A comparison of cross-sectional predictions between the model and the regime method applied in Babbie Group Ltd (1988) is shown in Figures 8.29 to 8.33. At the chainages 6 km, 10 km and 15 km the comparisons of the cross-sectional predictions between two methods are comparable. But at Scotstoun of chainage 9 km and Rothesay Dock of chainage 11 km, there exists the difference of the cross-sectional predictions between two methods, especially in the centre part of the cross sections. Obviously, the prediction of bed level from the model is higher than one from the regime method, for example at Scotstoun the maximum difference of bed level is about 2 m and at Rothesay Dock about 4 m. It is difficult to provide an exact reason for these differences. It is believed that the hydraulic parameters are dominant factors to control the final cross-sectional shape in order for the equilibrium sediment transport condition at each cross section to be satisfied. The numerical model is able to give more detail information for cross-sectional shape but this needs to be justified.

Since the cross-sectional shapes predicted by the regime method are not available from Erskine to Greenock, we cannot compare the results there between the model and the regime method.

#### **8.6.4 Comparison With Previous Regime Calculations**

After 10 years cessation of dredging the calculations from the model suggests that the regime section will reach 3 km downstream of tidal weir. The deposition can approach up to a chainage of 11 km. The comparison of the bed profiles after 10 years between the model and the regime method are shown in Figure 8.37.

After 20 years cessation of dredging the regime section from the model will go further to 6 km and the cross section up to 16 km of chainage will be influenced. The comparison of the bed profiles after 20 years between the model and the regime method are shown in Figure 8.38.

After 40 years cessation of dredging the regime section from the model will reach 11 km at Rothesay Dock. The cross-section up to Dumbarton with chainage 23 km will be affected. The comparison of the bed profiles after 40 years between the model and the regime method are shown in Figure 8.39.

After 250 years of cessation of dredging whole channel of the Clyde from the model will reach the final regime condition up to 36 km of chainage at Greenock. The comparison of the bed profiles at the final regime conditions between the model and the regime method are shown in Figure 8.26.

## **8.7 Effect of A New Tidal Weir On Final Regime Condition**

### **8.7.1 Introduction**

For a number of years consideration has been given to the construction of a new tidal weir on the upper River Clyde. The intention is to improve the city centre environment by maintaining the water level at 1.70 m O.D.. Construction of this tidal weir would change radically the hydraulic regime in the river and would have an effect on water levels. This requires further investigations to ensure that this project will not result in unexpected detrimental effects. Therefore the study here is to focus on the regime process after the cessation of dredging and the construction of a new weir.

The model was used to carry out this study. The location and type of the tidal weir was referred to the previous study conducted by Babbie Group Ltd (1987 and 1988).

The general requirements for the weir are summarised as: (i) dimensions of lock to allow pleasure craft passage 25 m by 7 m; (ii) design capacity for a river flood of 1,000 year return period.

### 8.7.2 Location and Type of The Tidal Weir

In this study the location of the tidal weir was assumed to be at the confluence of the Clyde and the Kelvin as suggested in Babbie Group Ltd (1987). This corresponds to chainage 4,170 m in the model.

The type of the tidal weir was suggested by Pender (1993) as twin under flow gates. The general features may be summarised as:

- (i) two under flow gates and each one with 35 m wide;
- (ii) bottom level of gate is -3.00 m O.D.;
- (iii) other facilities including mitre gates for pleasure craft lock, maintenance bridge and fish pass. A typical drawing of a gate is shown in Figure 8.40.

### 8.7.3 Numerical Treatment of The Tidal Weir

The discharge from the under flow gate can be determined by

$$Q = bac\sqrt{2g} \frac{Y - Z_b}{\sqrt{Y - Z_b + \phi a}} \quad (8.1)$$

where  $Q$  = the discharge;  $b$  = the width of the gate;  $a$  = the open height of the gate;  $c$  = the discharge coefficient which is related to the relative depth  $((Y - Z_b)/a)$ ;  $g$  = the acceleration due to gravity;  $Y$  = the water level in the front of the gate;  $Z_b$  = the bottom level of the gate;  $\phi$  = the converse coefficient which is also related to the relative depth  $((Y - Z_b)/a)$ .

The tidal weir was treated as the internal boundary condition in the model. As illustrated in Figure 8.40, a tidal weir is located between cross-sections  $i$  and  $i+1$  and from the mass conservation of water flow and sediment transport, we have

$$(i) \quad Q_{i+1} = Q_i$$

$$(ii) \quad C_{i+1} = C_i$$

$$(iii) \quad G_{i+1} = G_i$$

Equation (8.1) is employed at the cross section  $i$  to represent the discharge and stage relationship. All parameters used in Equation (8.1) for regime simulation are listed in Table 8.12.

**Table 8.12 Physical Parameters For The Tidal Weir**

Parameter	a (m)	b (m)	$Z_b$ (m O.D.)	c	$\phi$
Value	1.00	70	-3.00	0.603	0.624

The boundary conditions at the upstream and downstream boundary used in this simulation are listed in Table 8.13. The water level at the downstream boundary was taken from the results of the regime simulation without the internal tidal weir, see section 8.6.

**Table 8.13 Boundary Conditions For Regime Simulation of The River Clyde With A Internal Tidal Weir**

	Water flow ( $m^3/s$ )	Water level (m) O.D.	Suspended-load inflow ( $m^3/s$ )	Bedload inflow ( $m^3/s$ )
Upstream	434	—	$6.51 \times 10^{-3}$	$4.90 \times 10^{-4}$
Downstream	—	-0.43	zero flux	—

#### 8.7.4 Effect of A Tidal Weir On Final Bed Profile

The results of the bed profile on approaching the final regime condition is shown in Figure 8.41 when a tidal weir is to be built at the confluence of the River Kelvin. From the overall results a tidal weir does not have the significant effect on the

final bed profile in comparison with Figure 8.26. But the weir does have some local impact on the channel geometry. The main reason is the changes in water levels caused by the tidal weir.

The type of the tidal weir can also affect the bed profile on the regime conditions. If a over flow gate is used instead of using the under flow gate, the weir would create the stillwater pond which would encourage the deposition of sediment upstream of the weir.

The study was based on the assumption of mass conservation at the weir. This assumption reflects the true situation for water flow through the weir, but for sediment transport this should be justified using field investigations.

## 8.8 Conclusion

The study undertaken has used all existing data relating to incoming flow and sediment, and channel geometry. When the channel reaches the final regime condition all incoming sediments pass through the channel without net changes in channel cross section area with regard to the long term average. The following conclusions are obtained from this study.

1. Calibration using a typical tidal event on 16 August, 1989 similar to the mean spring tide gives the Manning's coefficient 0.02. Time and space weighting parameters in the Preissmann scheme are of 0.55 and 0.5 respectively. A time increment of 300 seconds is employed in the model;
2. It takes 40, 110 and 250 years for the Clyde to reach its regime condition down to Rothesay Dock, Dumbarton and Greenock;
3. The calculations suggest that the effect of a tidal weir located at the confluence of the River Kelvin will have little effect on the regime conditions;

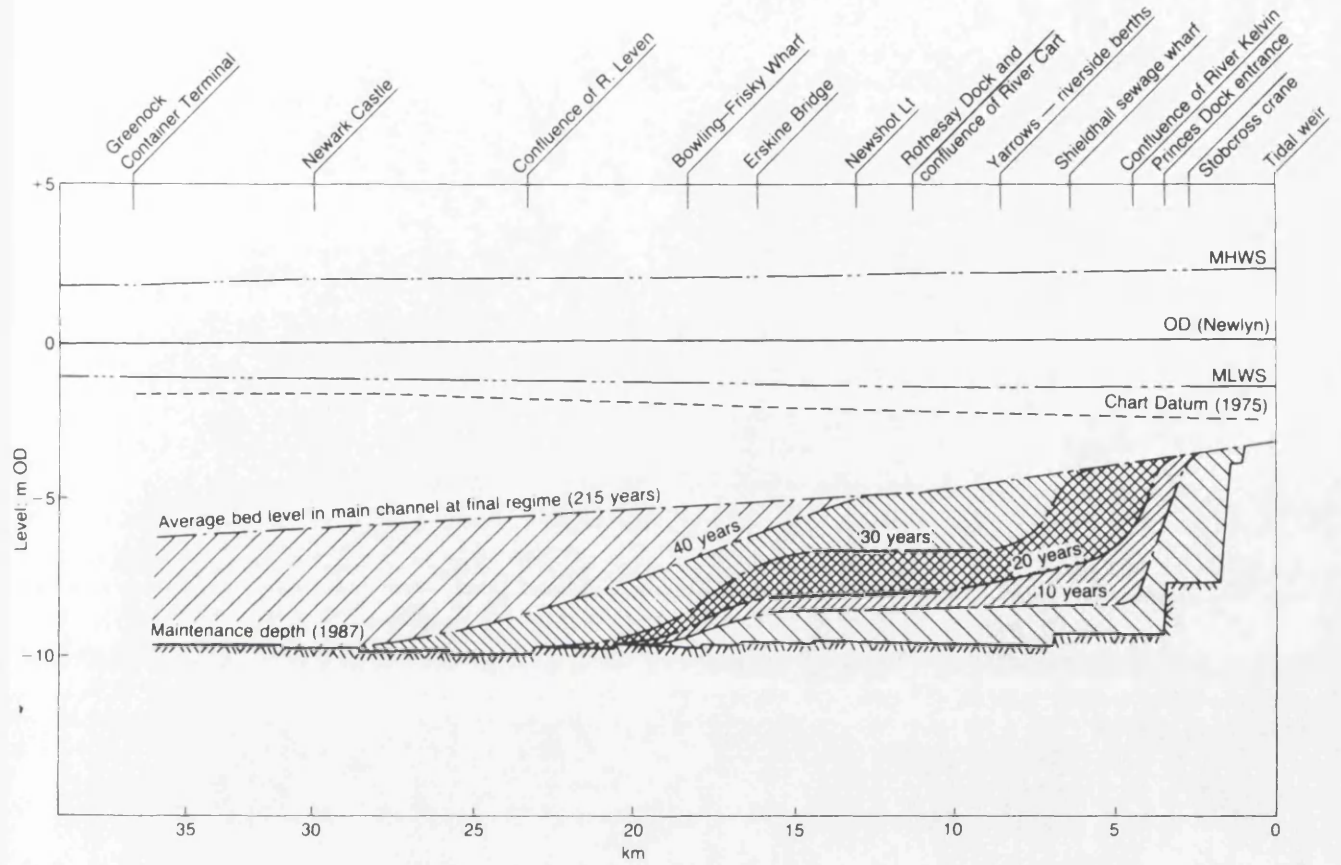


Figure 8.2 Estimated Ultimate and Intermediate Bed Profiles By Regime Method (from Falconer et al, 1992)

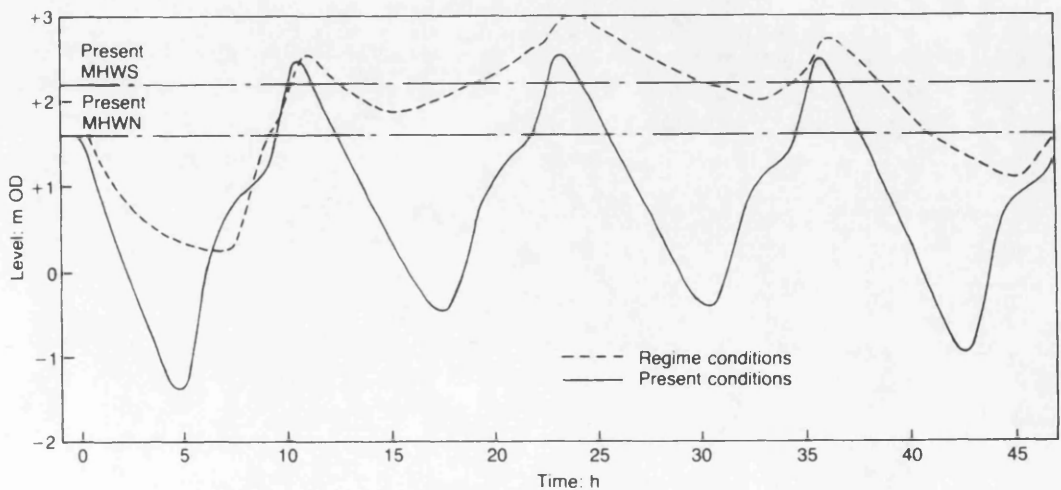


Figure 8.3 Tidal Variation at Broomielaw for Present and Regime Conditions (spring tide/100 year flood) (from Falconer et al, 1992)

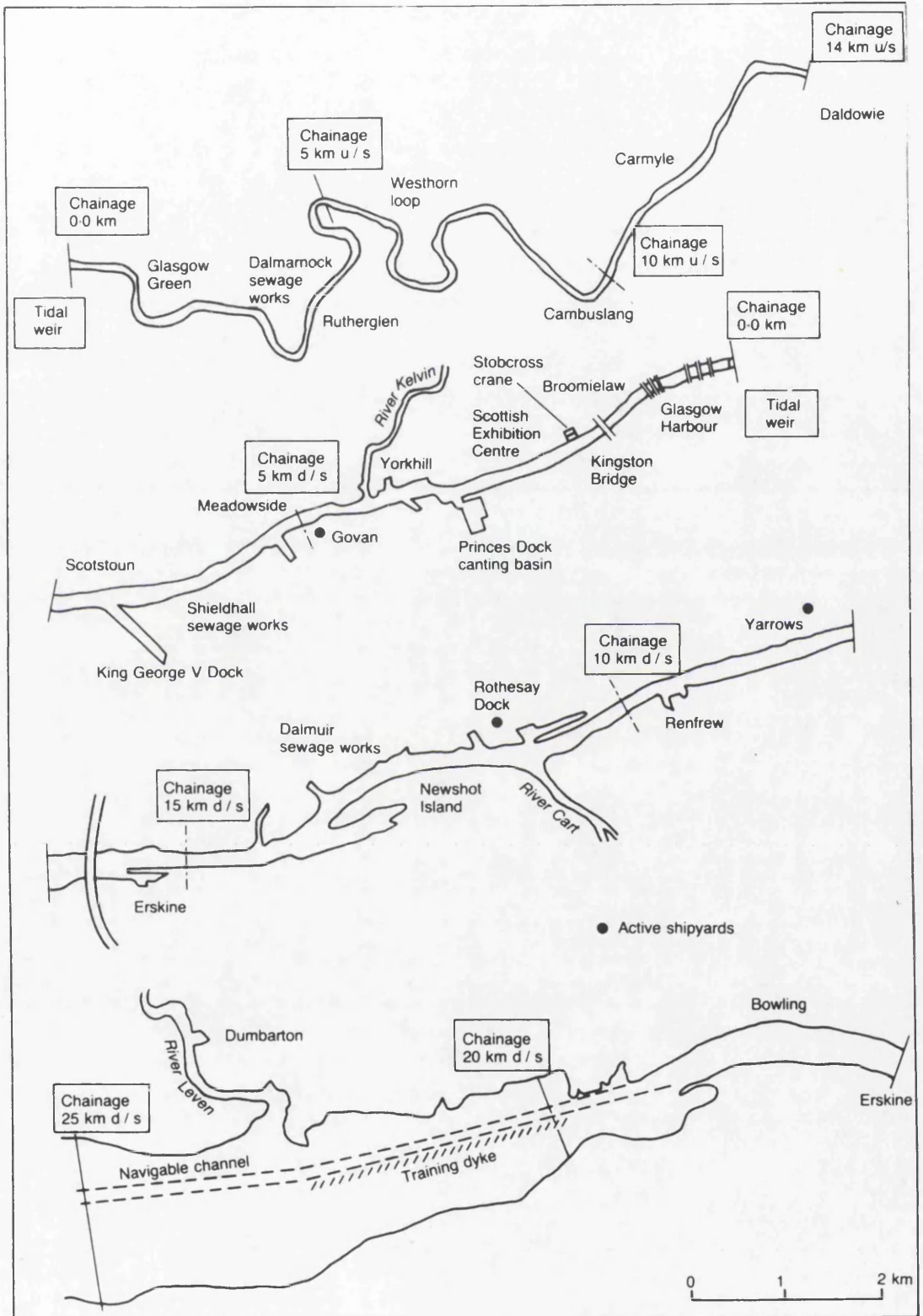


Figure 8.4 Key Locations and Chainage In The River Clyde (from Falconer et al, 1992)

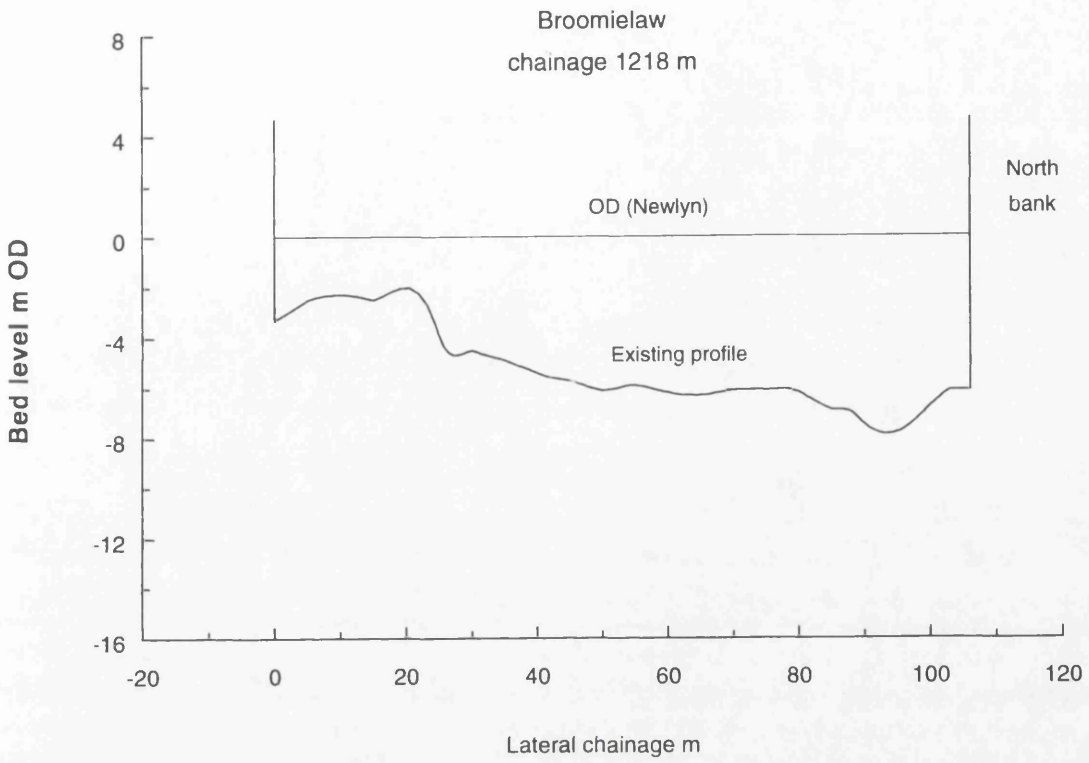


Figure 8.5 Cross-Section at Broomielaw

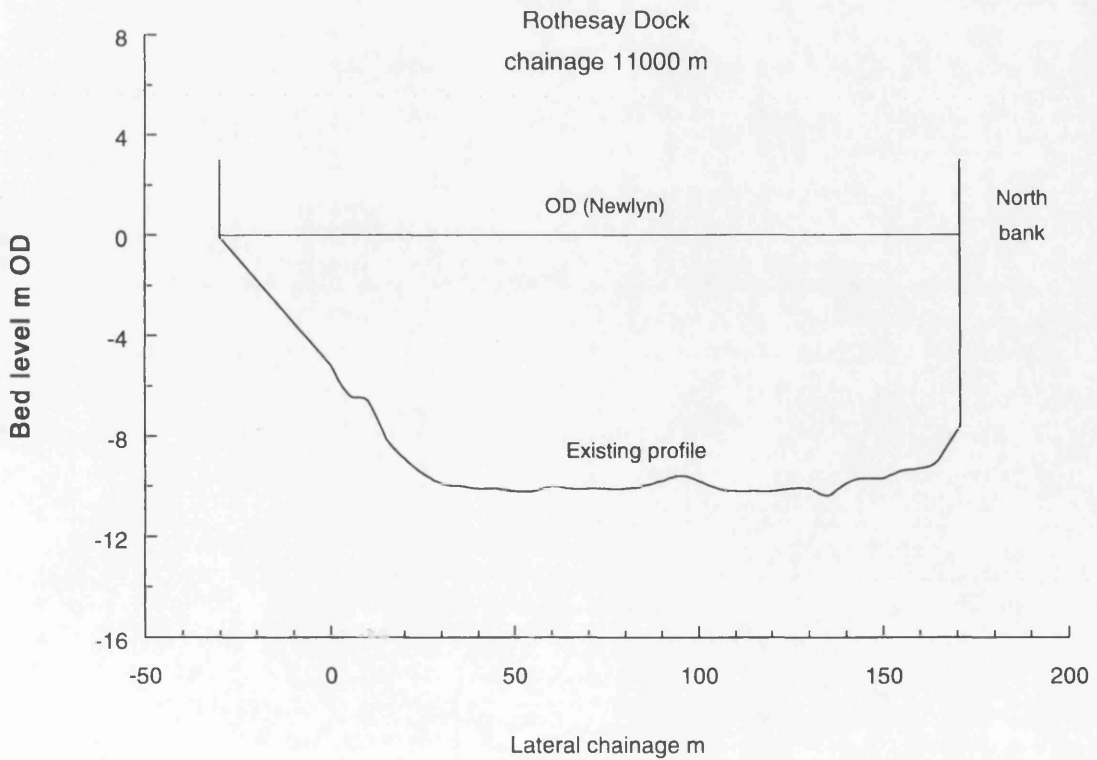


Figure 8.6 Cross-Section at Rothesay Dock

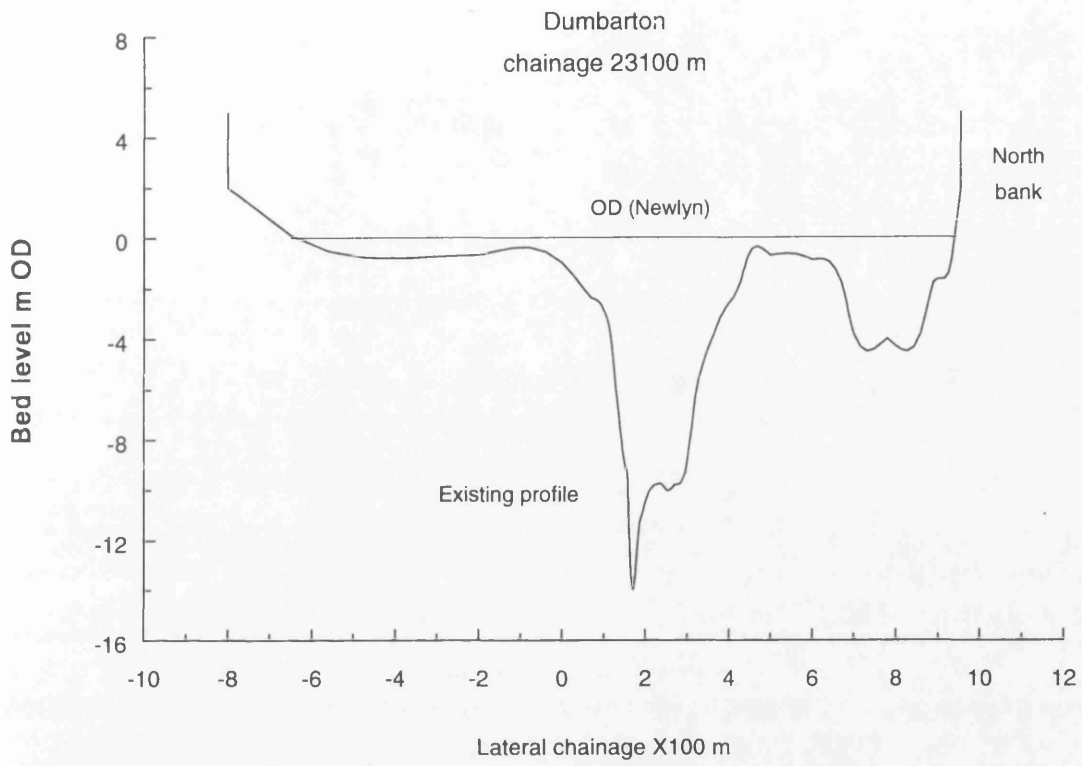


Figure 8.7 Cross-Section at Dumbarton

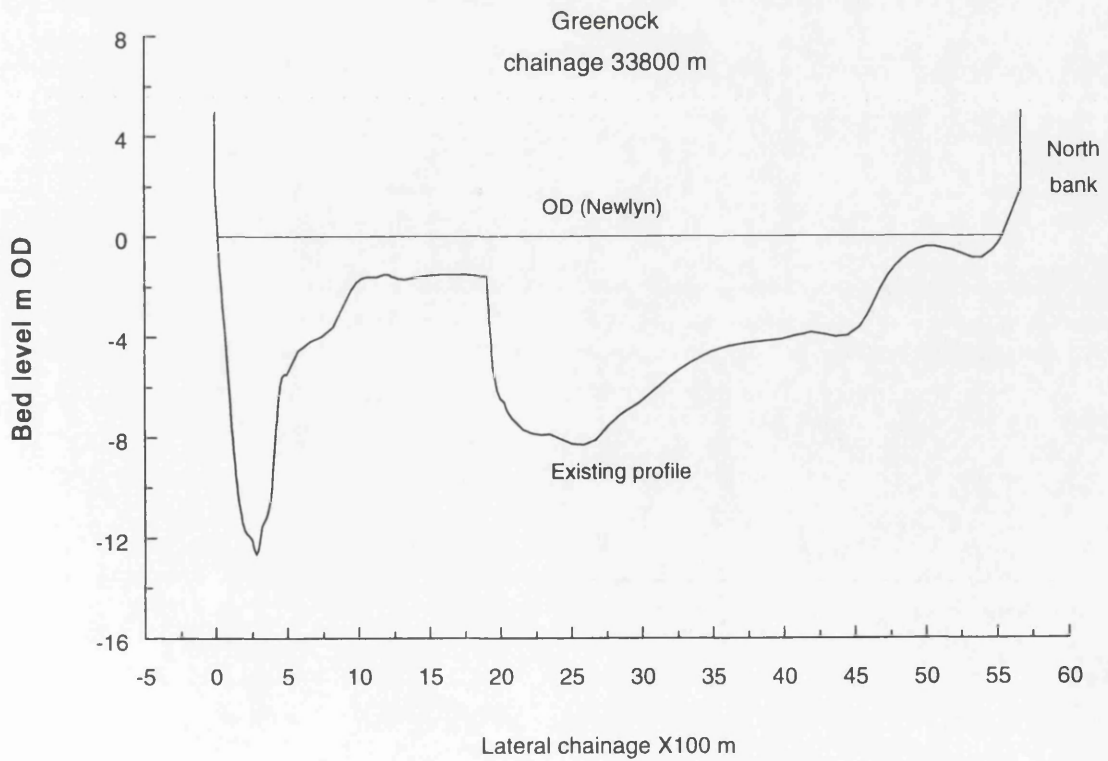


Figure 8.8 Cross-Section at Greenock

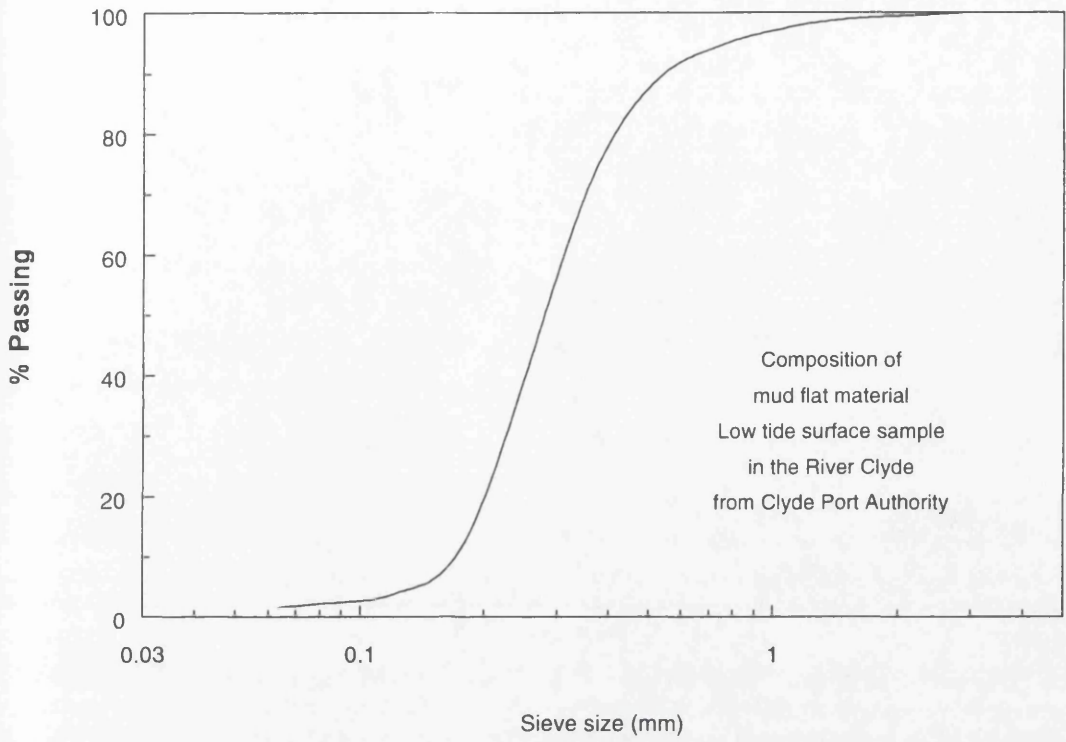


Figure 8.9 Grading Curve of Bed Material In The River Clyde

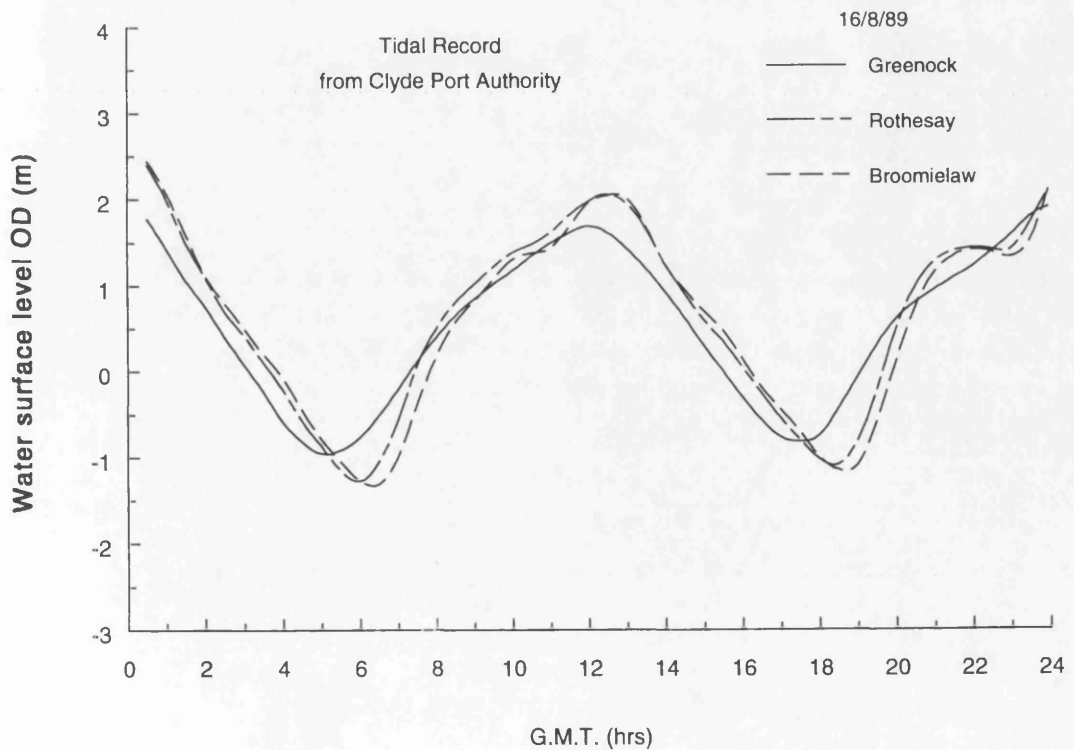


Figure 8.10 Tidal Record For Greenock, Rothesay Dock and Broomielaw in 16/8/89

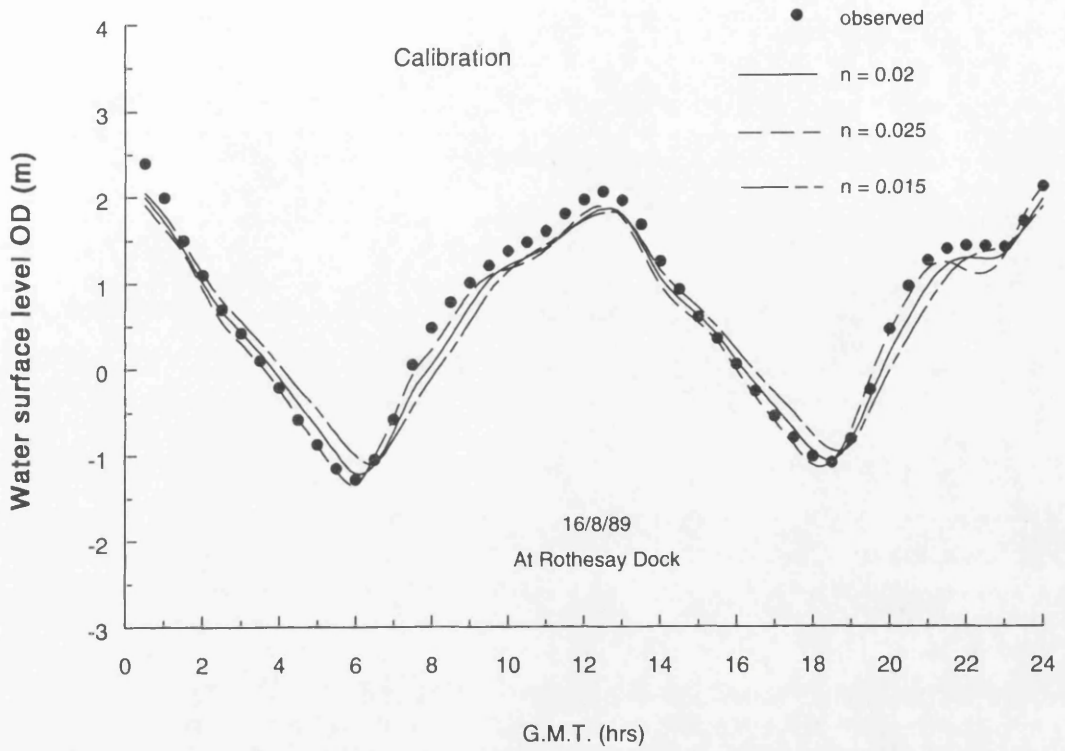


Figure 8.11 Predicted Water Level For Manning's Coefficient 0.015, 0.02 and 0.025 at Rothesay Dock

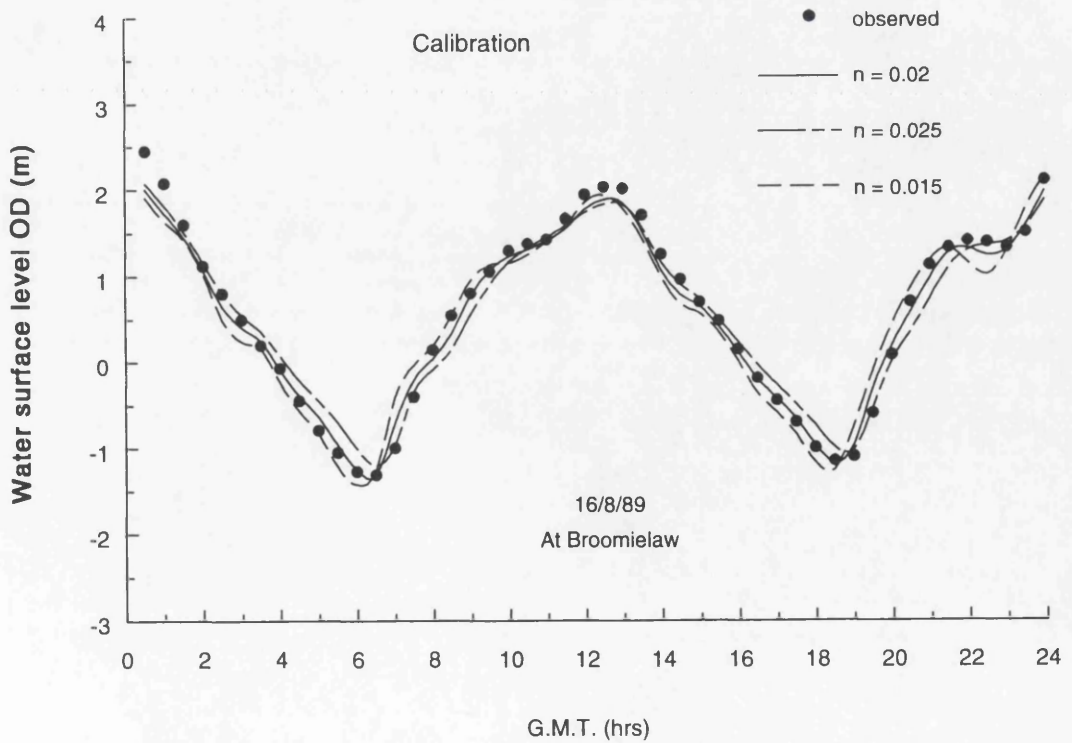


Figure 8.12 Predicted Water Level For Manning's Coefficient 0.015, 0.02 and 0.025 at Broomielaw

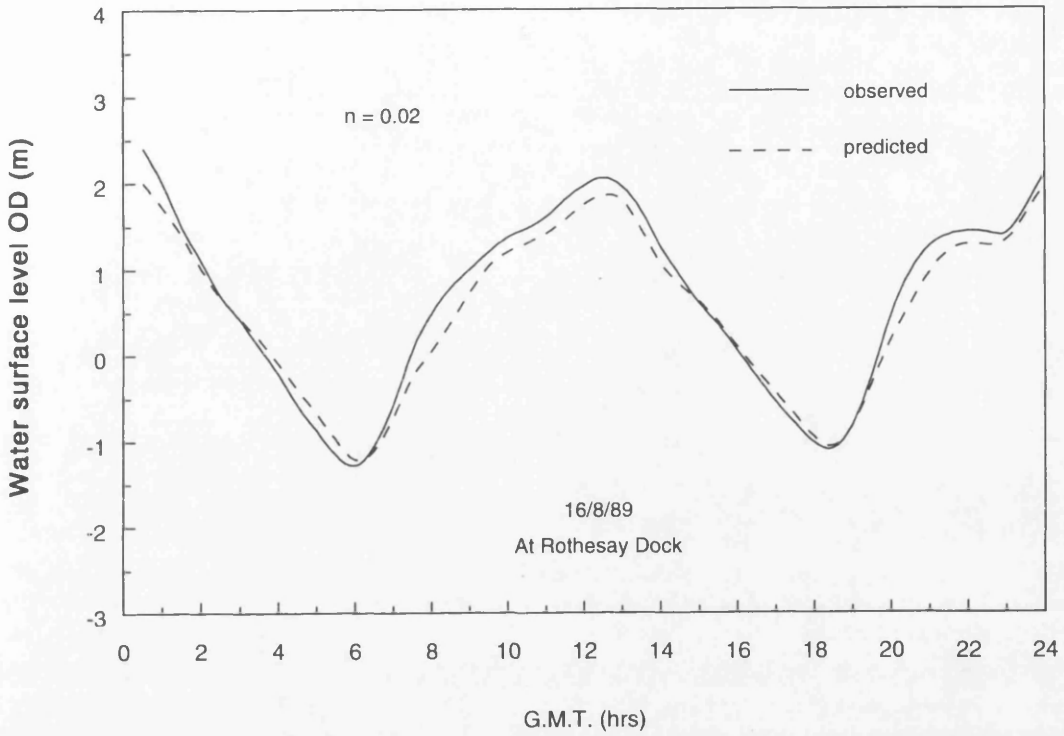


Figure 8.13 Predicted and Observed Water Level at Rothesay Dock

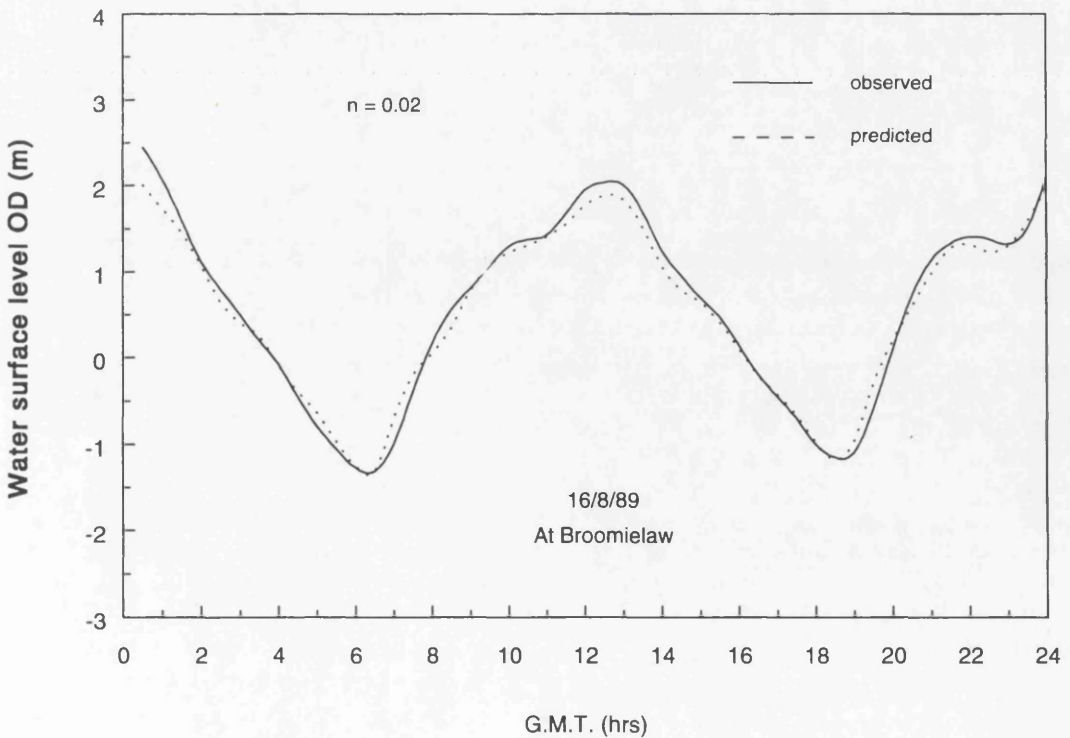


Figure 8.14 Predicted and Observed Water Level at Broomielaw

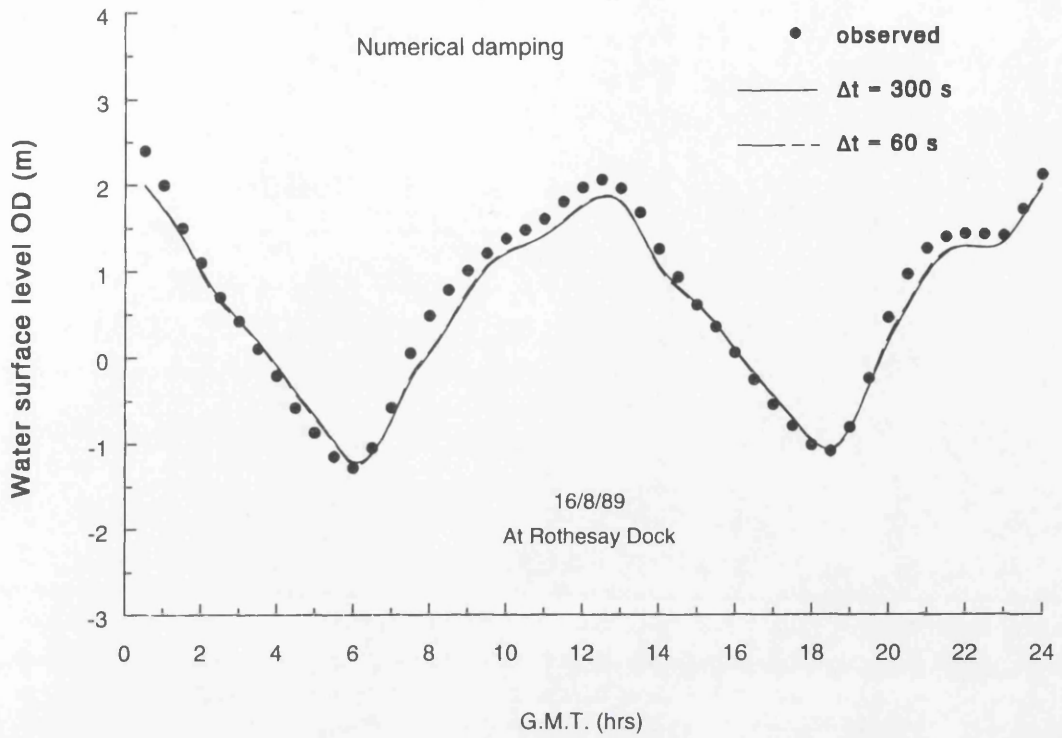


Figure 8.15 Predicted Water Level at Rothesay Dock Using Time Increment 300 s and 60 s

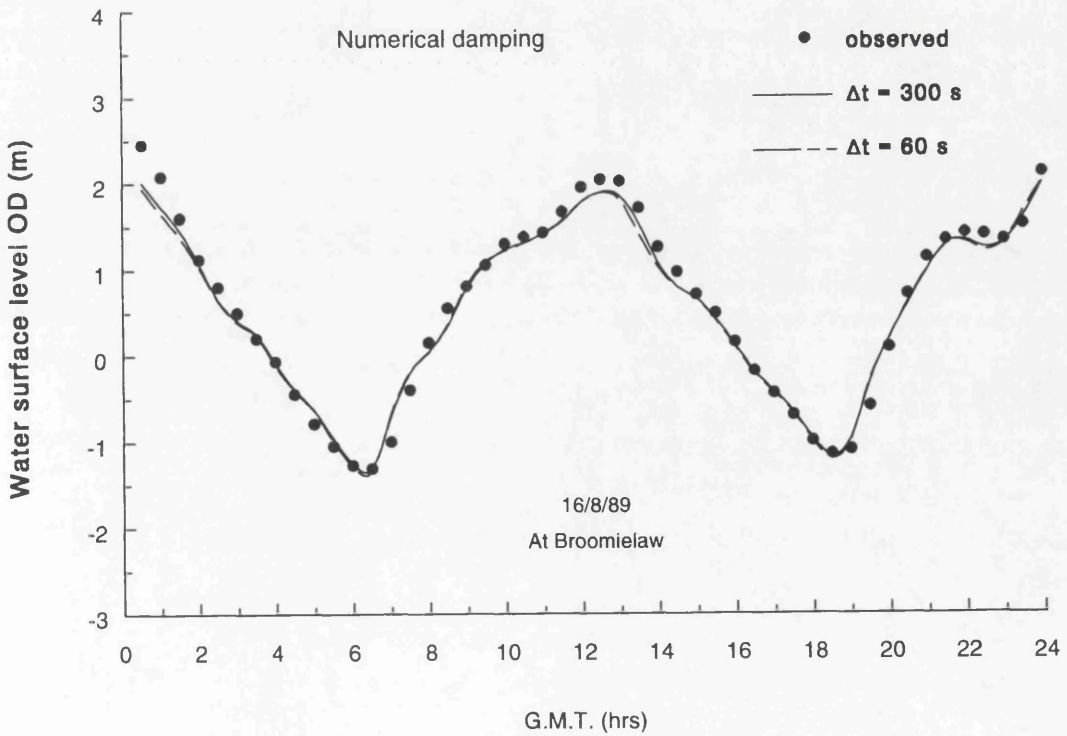


Figure 8.16 Predicted Water Level at Broomielaw Using Time Increment 300 s and 60 s

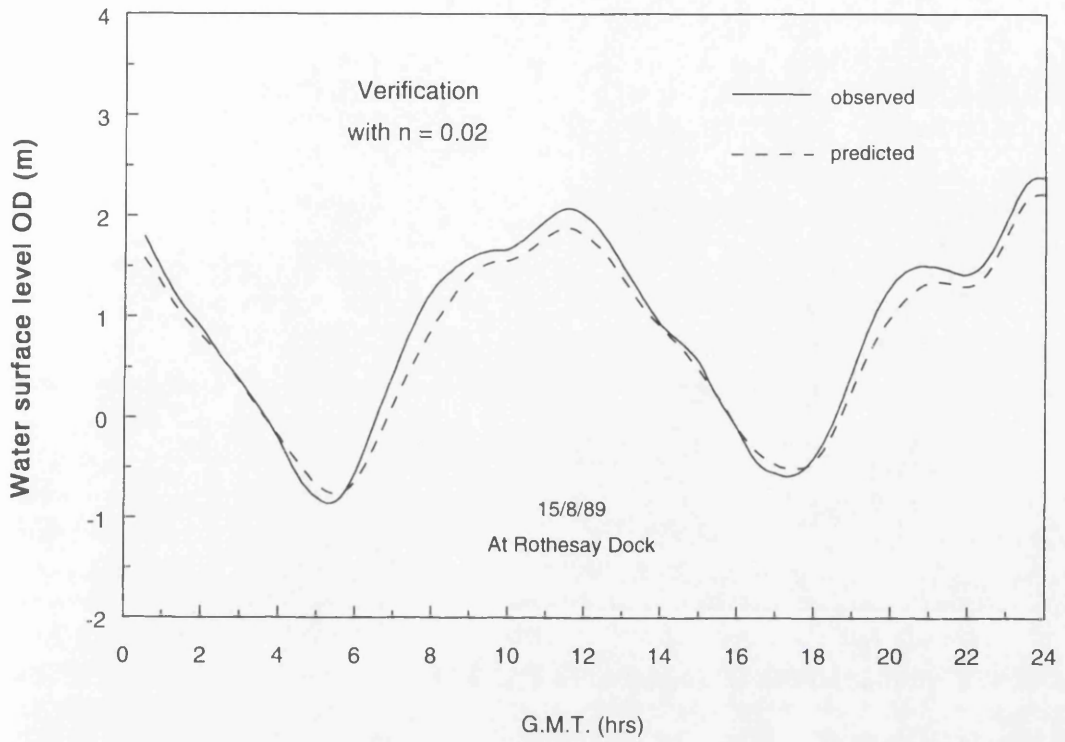


Figure 8.17 Verification of Model For Tidal Event of August 15, 1989 at Rothesay Dock

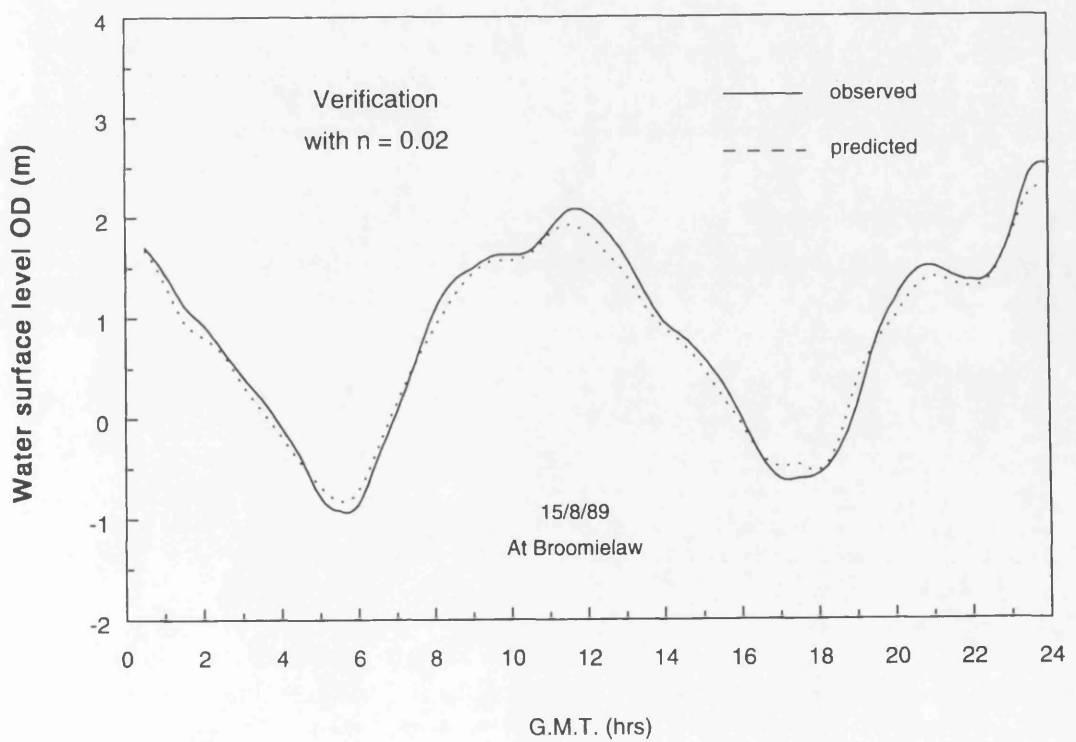


Figure 8.18 Verification of Model For Tidal Event of August 15, 1989 at Broomielaw

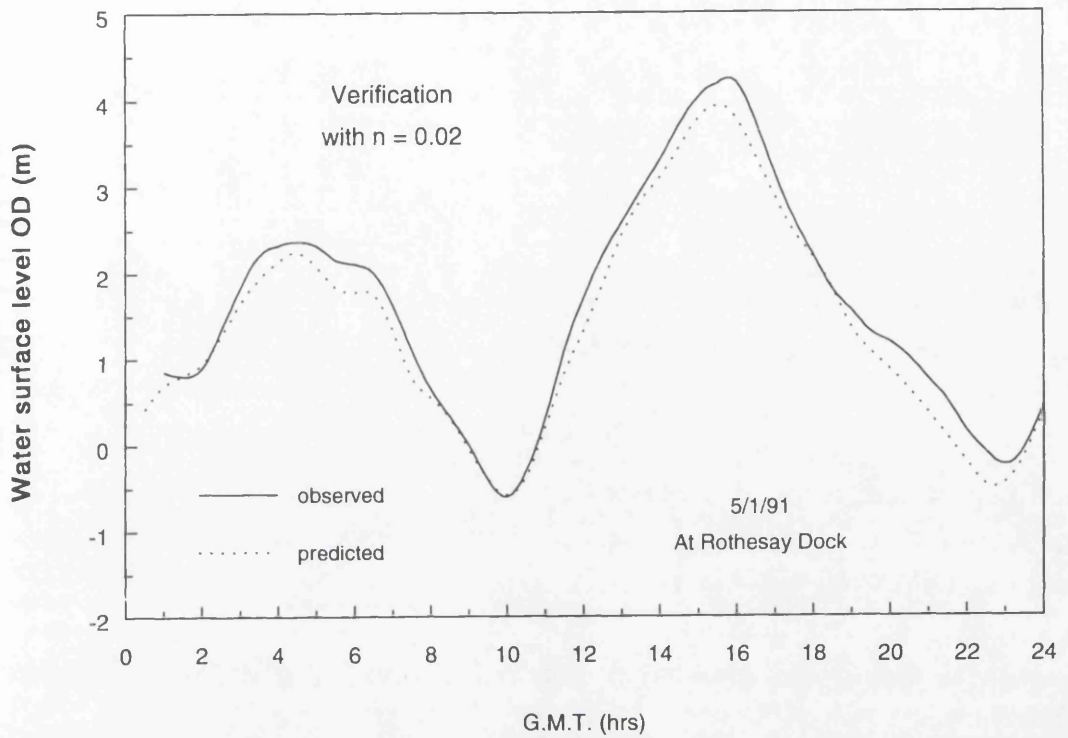


Figure 8.19 Verification of Model For Tidal Event of January 5, 1991 at Rothesay Dock

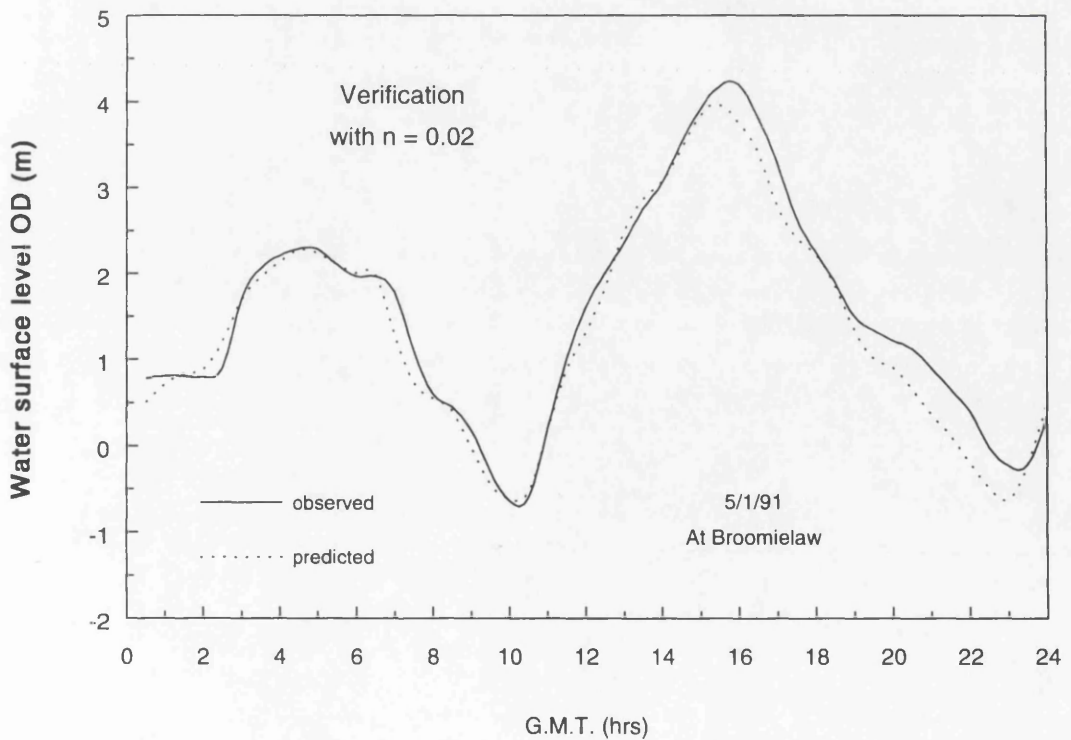


Figure 8.20 Verification of Model For Tidal Event of January 5, 1991 at Broomielaw

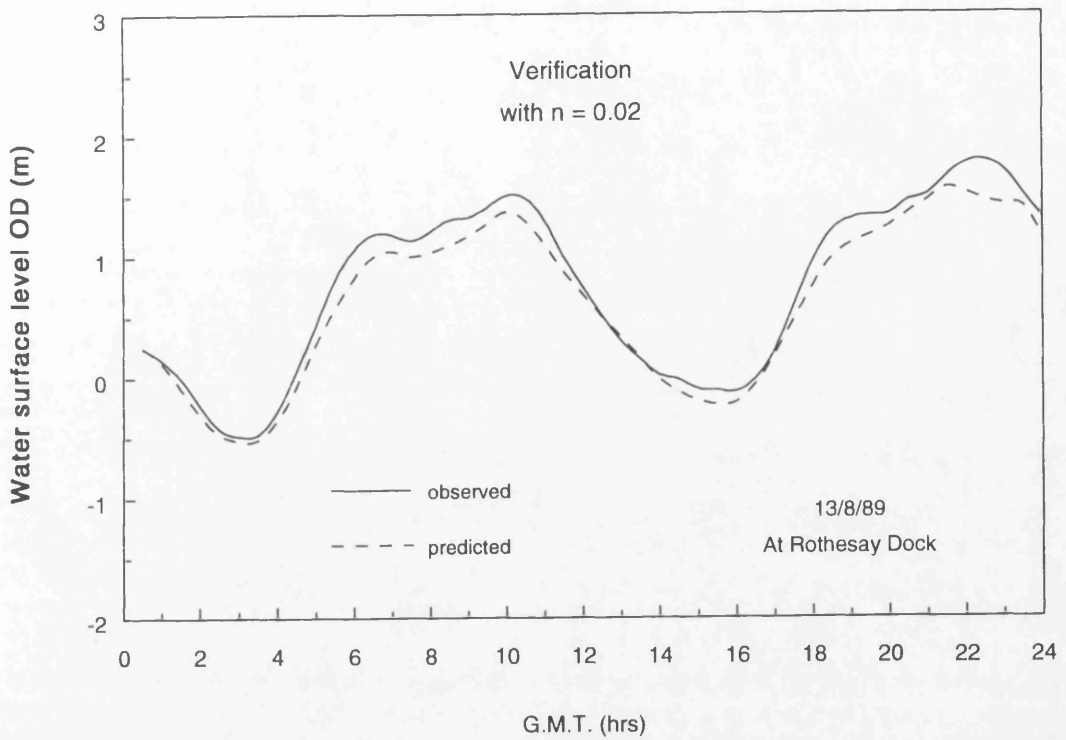


Figure 8.21 Verification of Model For Tidal Event of August 13, 1989 at Rothesay Dock

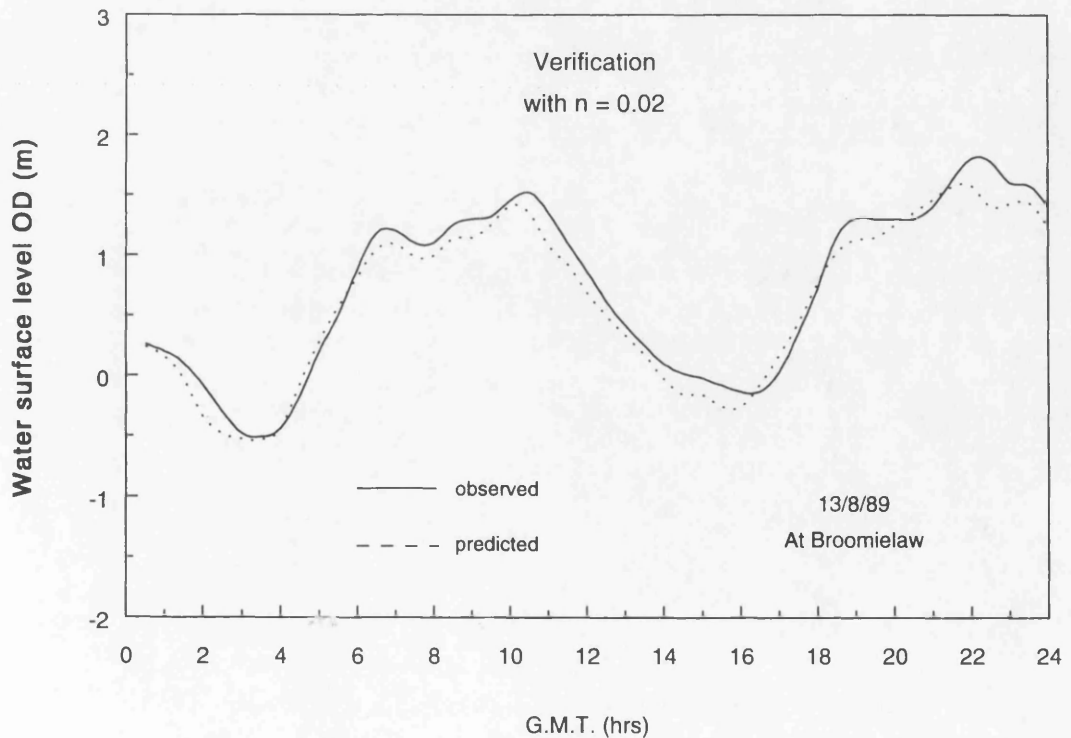


Figure 8.22 Verification of Model For Tidal Event of August 13, 1989 at Broomielaw

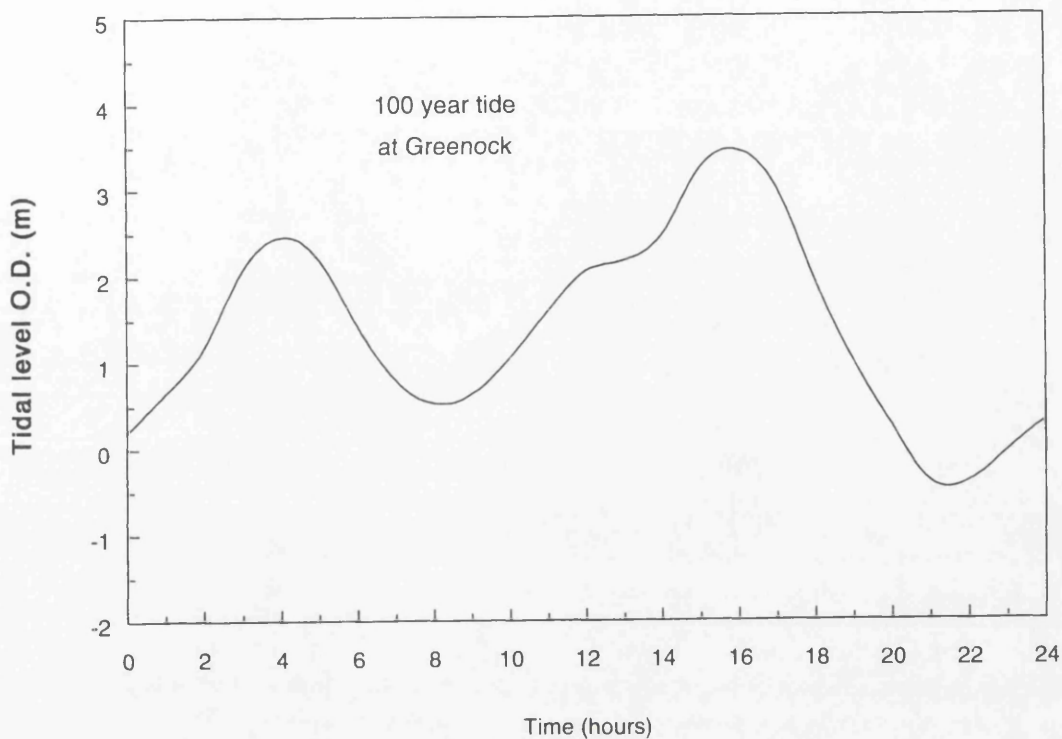


Figure 8.23 100 Year Tide at Greenock

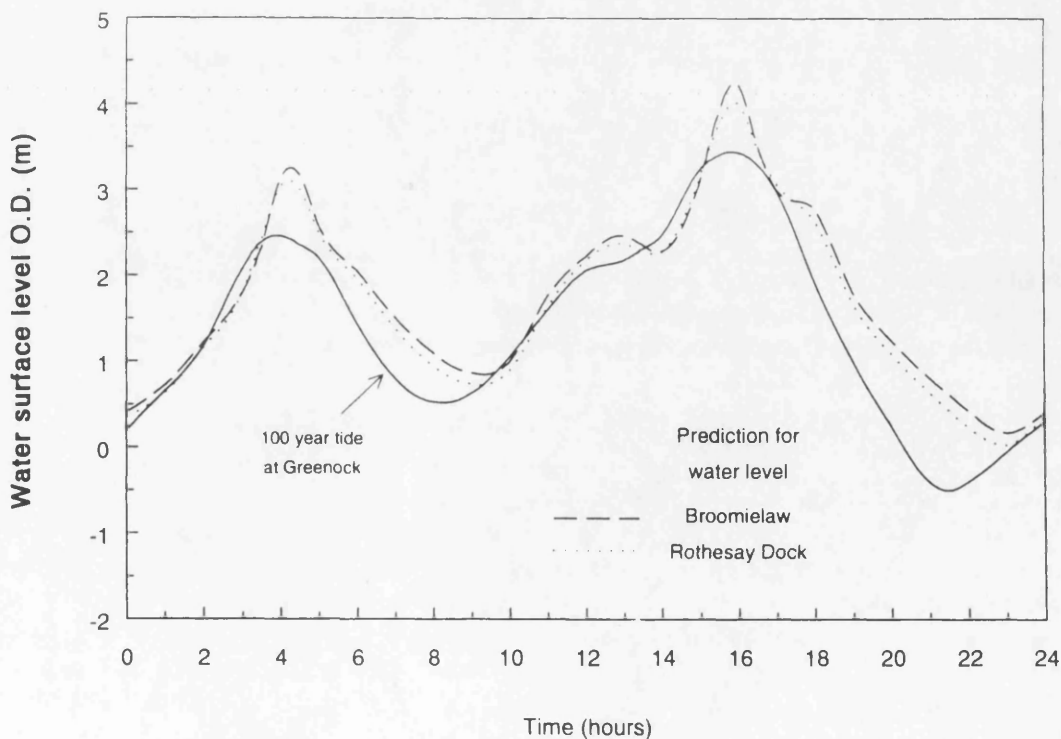


Figure 8.24 Prediction of Water Level For 100 Year Tide at Greenock and 100 Year Flood at Tidal Weir

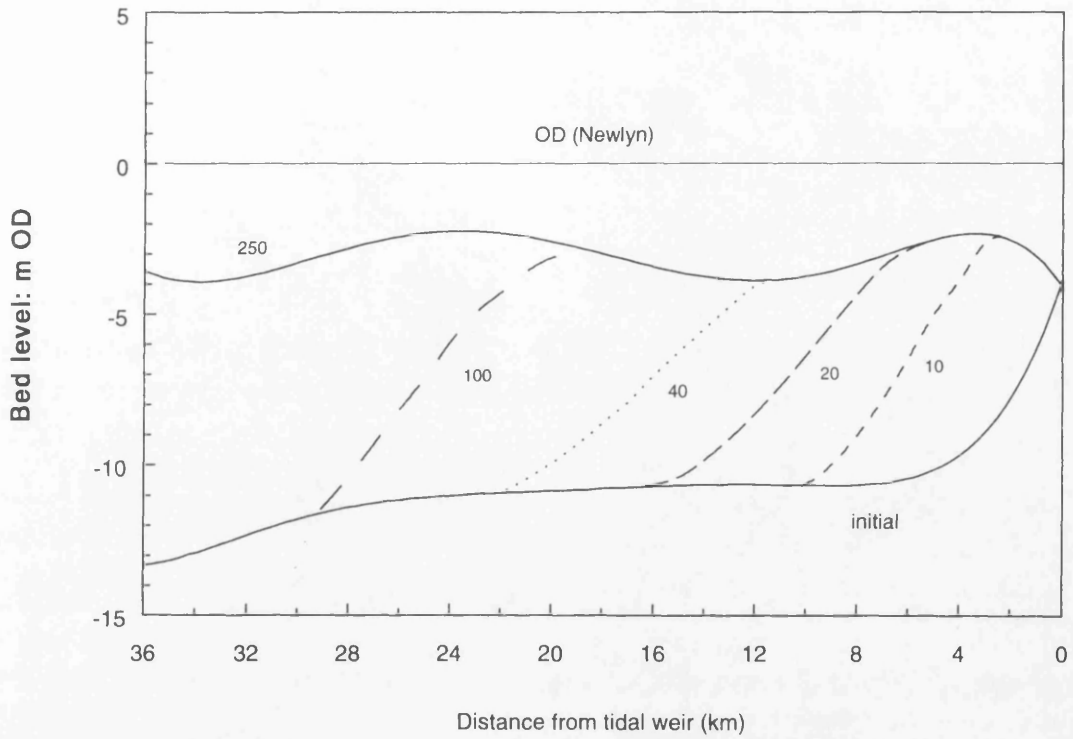


Figure 8.25 Estimated Ultimate and Intermediate Bed Profile After Cessation of Dredging In The River Clyde

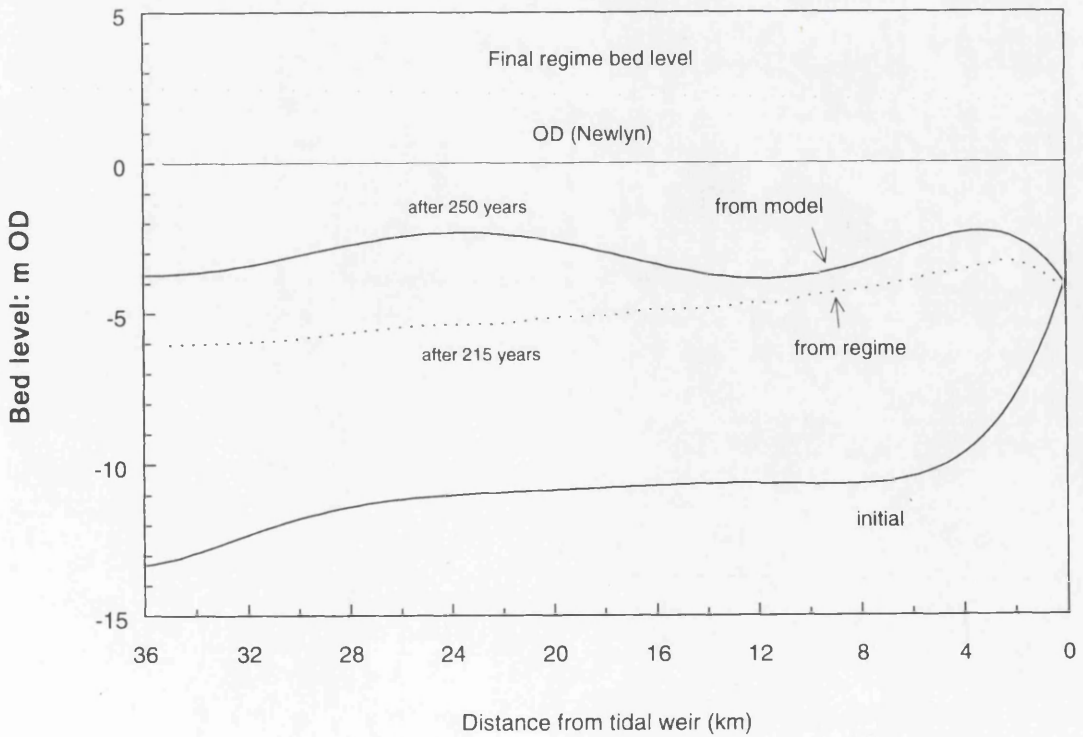


Figure 8.26 Comparison of Bed Profile At Regime Conditions Between Model and Regime Method

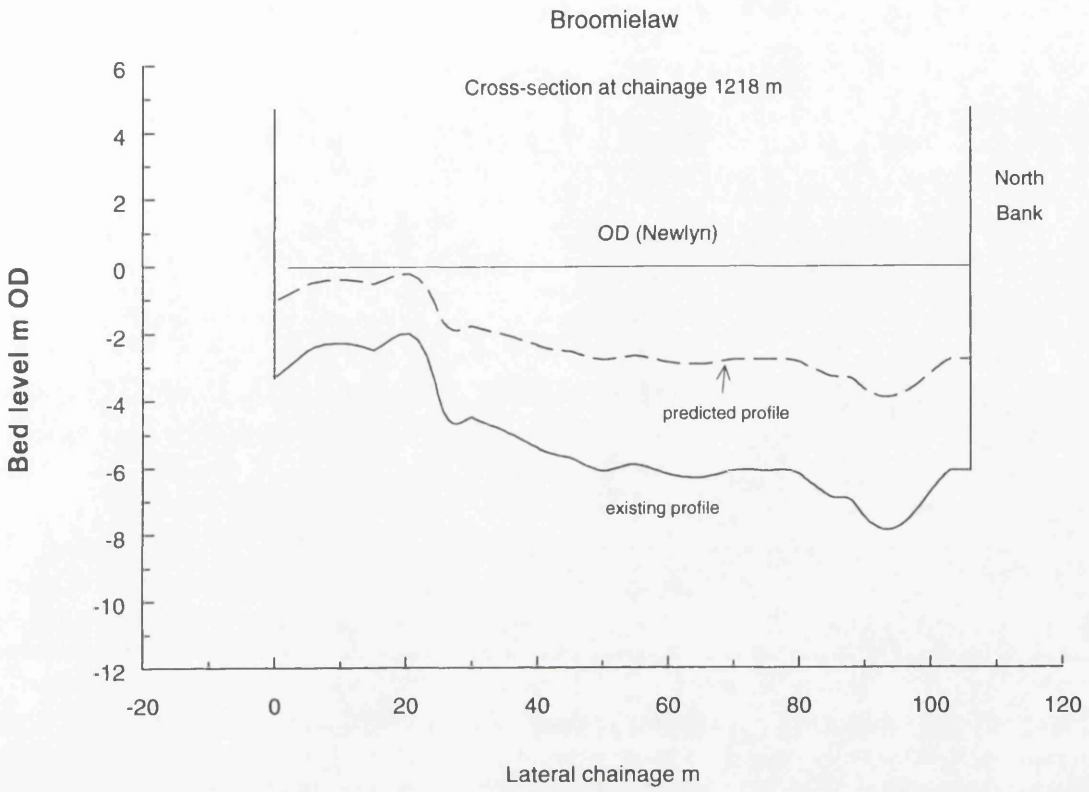


Figure 8.27 Estimated Cross-Section Shape In Final Regime Condition at Broomielaw

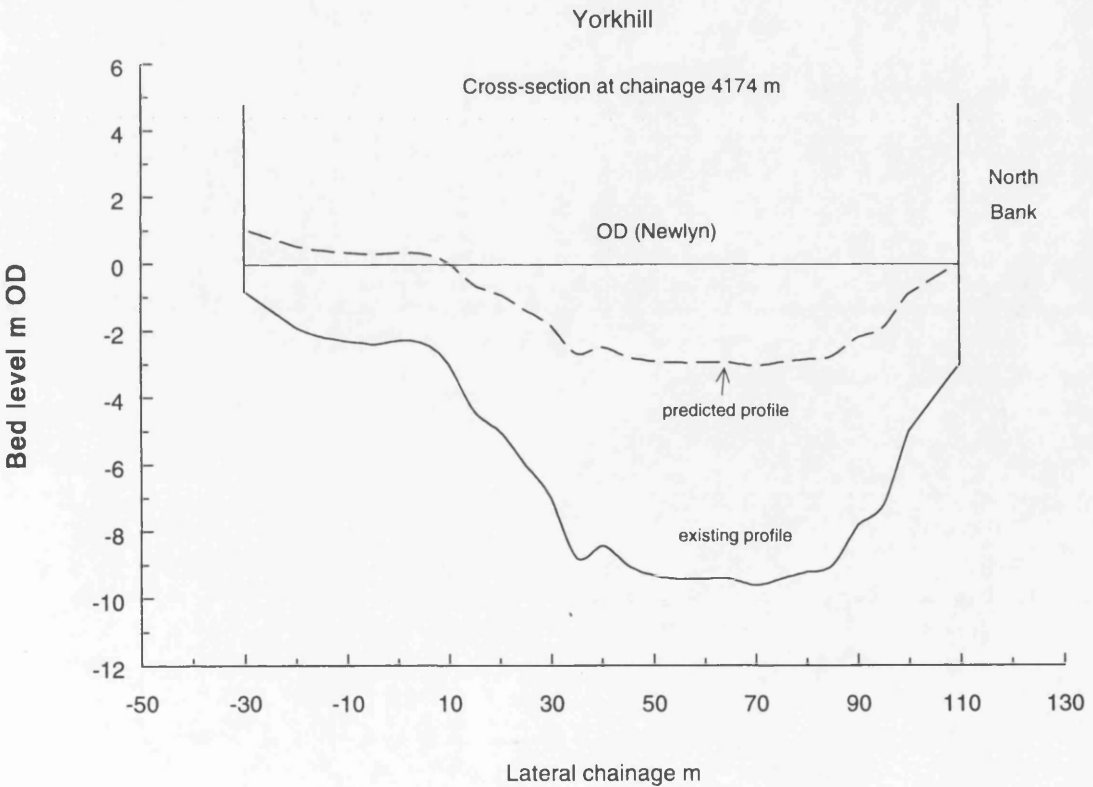


Figure 8.28 Estimated Cross-Section Shape In Final Regime Condition at Yorkhill

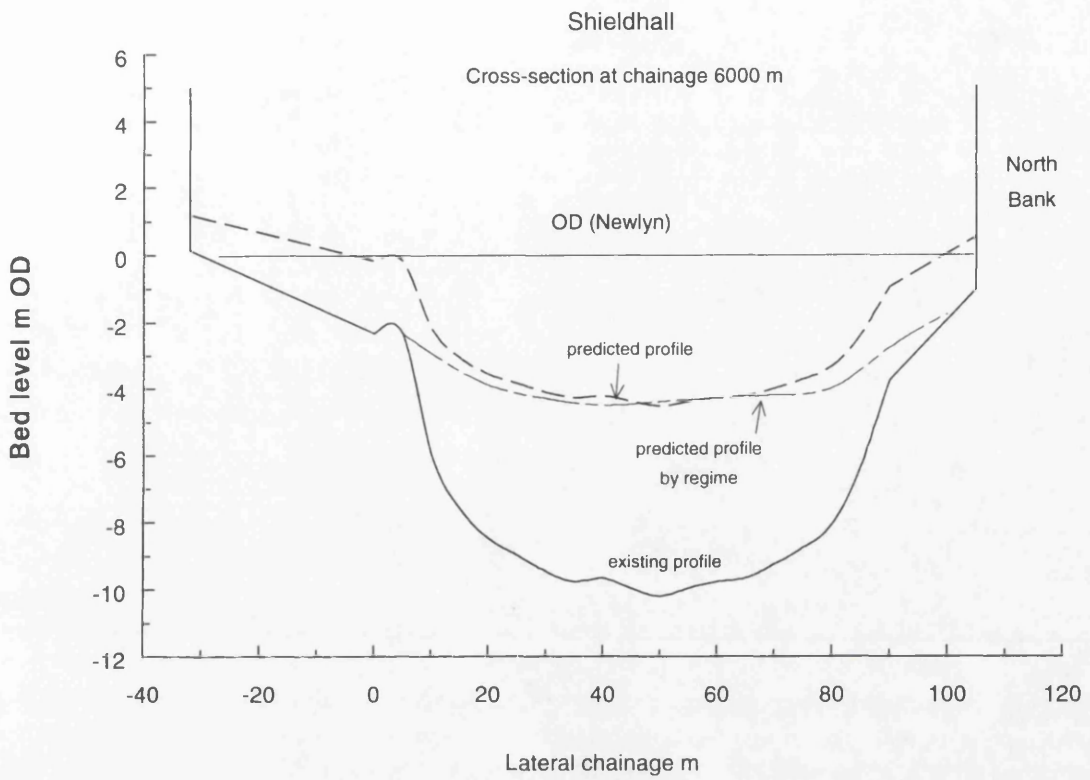


Figure 8.29 Estimated Cross-Section Shape In Final Regime Condition at Shieldhall

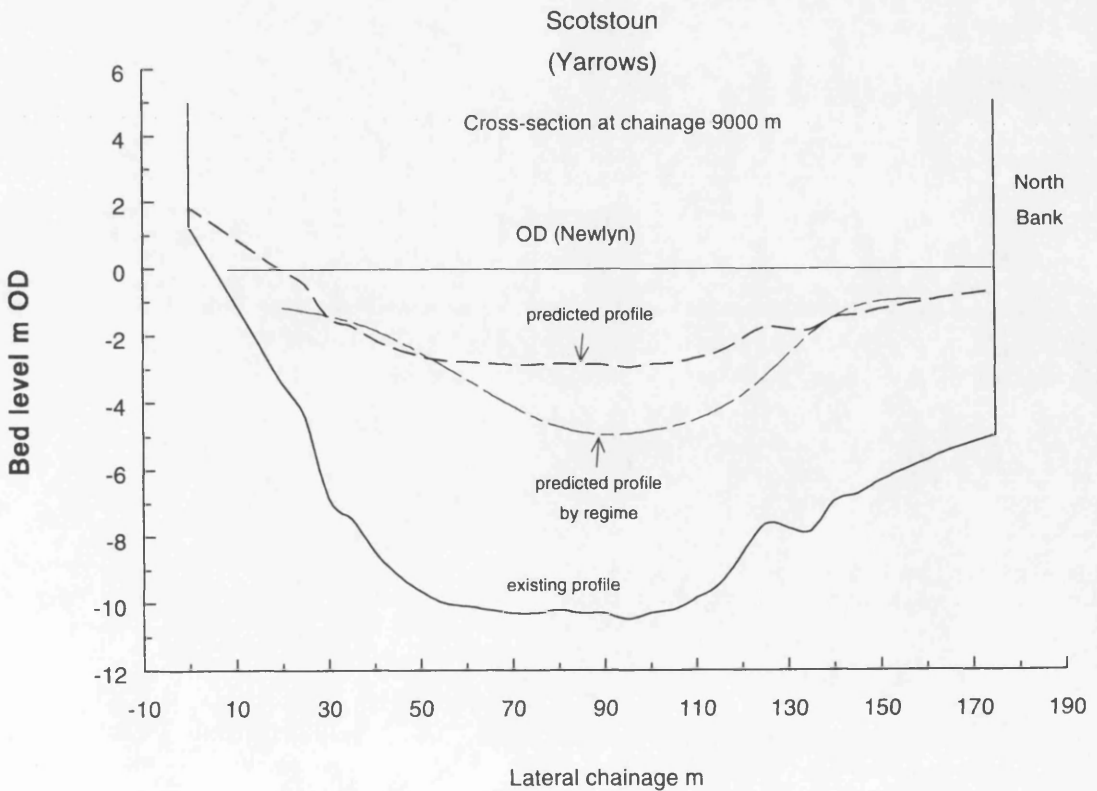


Figure 8.30 Estimated Cross-Section Shape In Final Regime Condition at Scotstoun

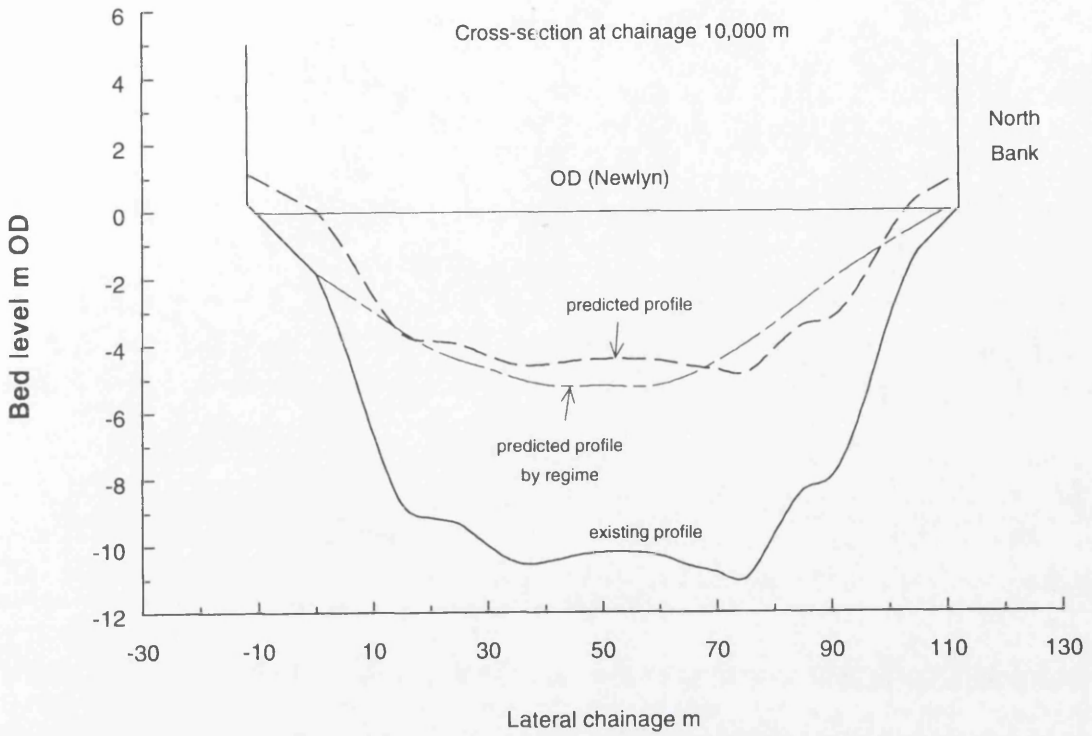


Figure 8.31 Estimated Cross-Section Shape In Final Regime Condition at Chainage 10 km

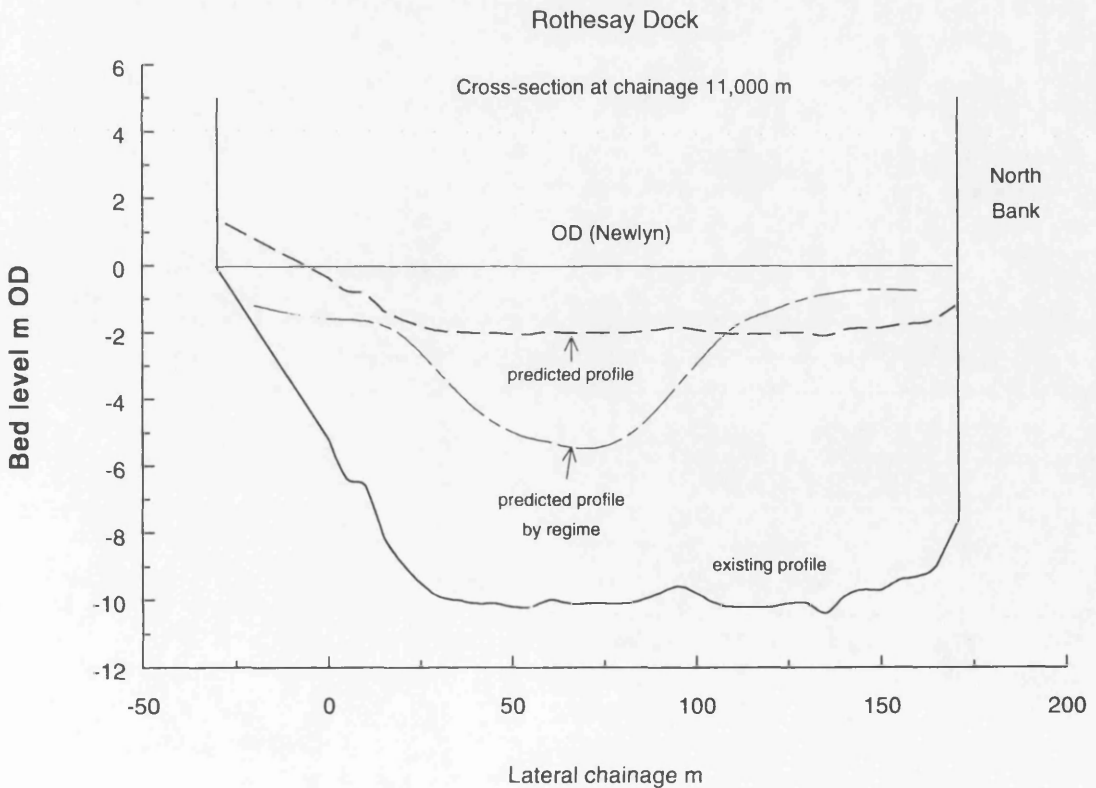


Figure 8.32 Estimated Cross-Section Shape In Final Regime Condition at Rothesay Dock

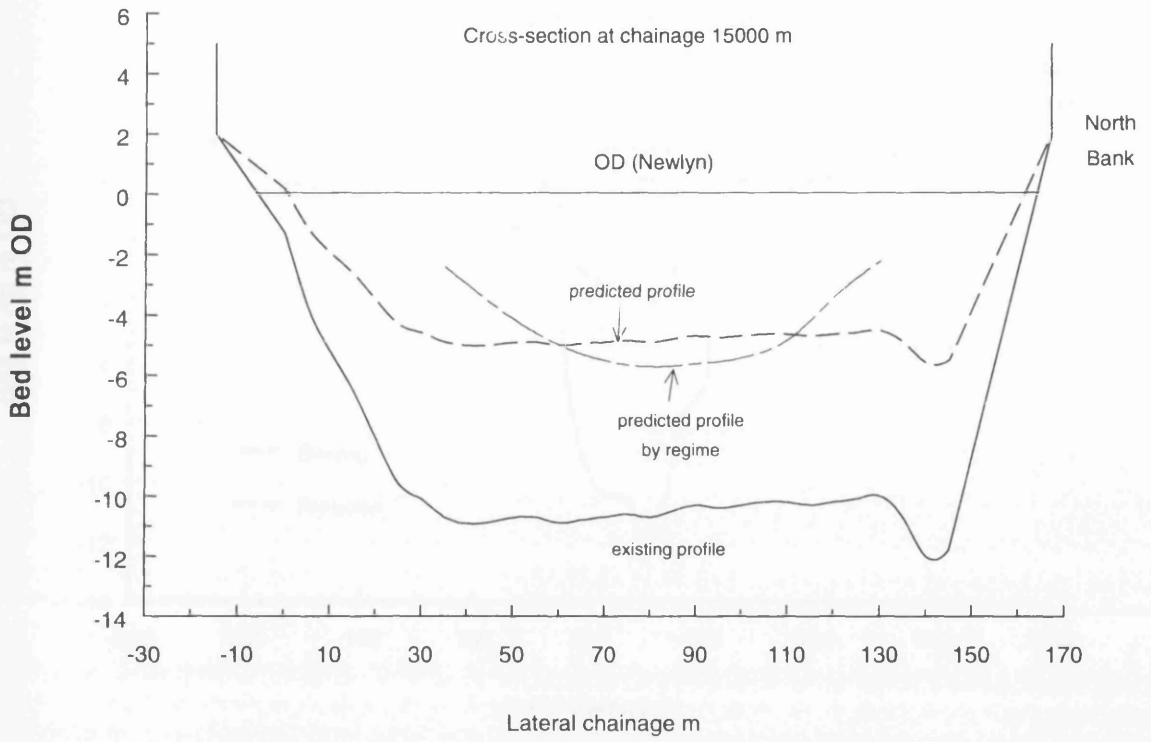


Figure 8.33 Estimated Cross-Section Shape In Final Regime Condition at Chainage 15 km

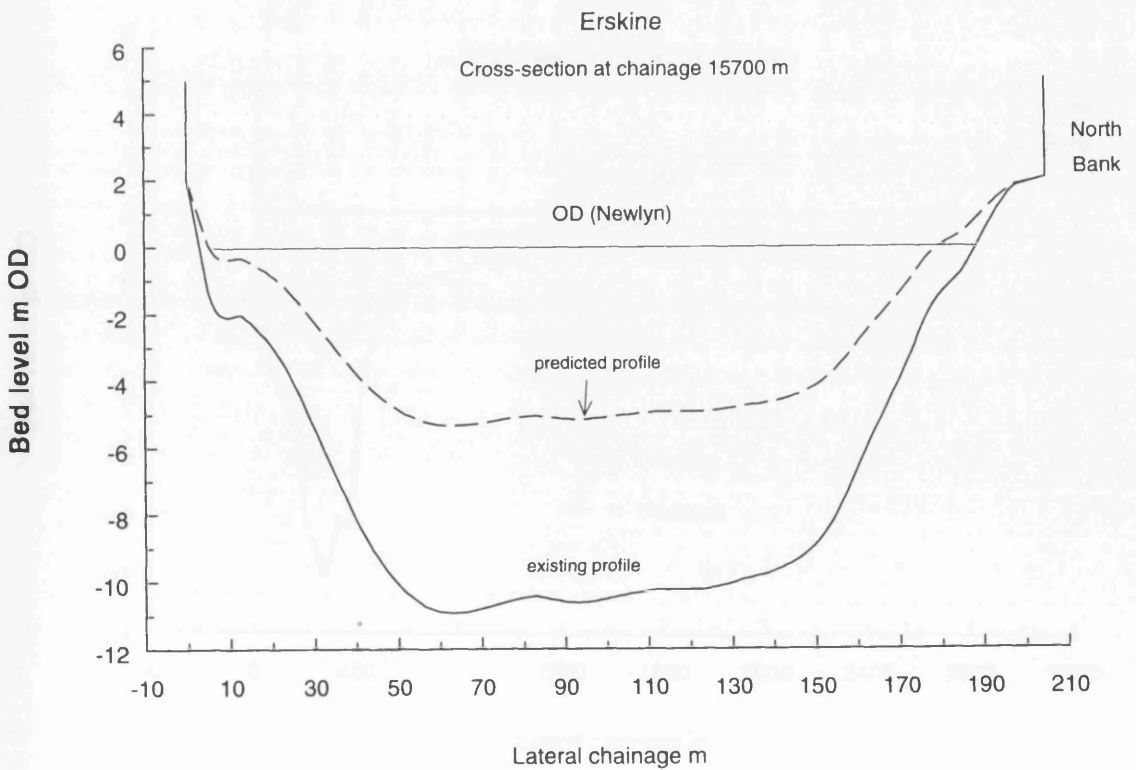


Figure 8.34 Estimated Cross-Section Shape In Final Regime Condition at Erskine

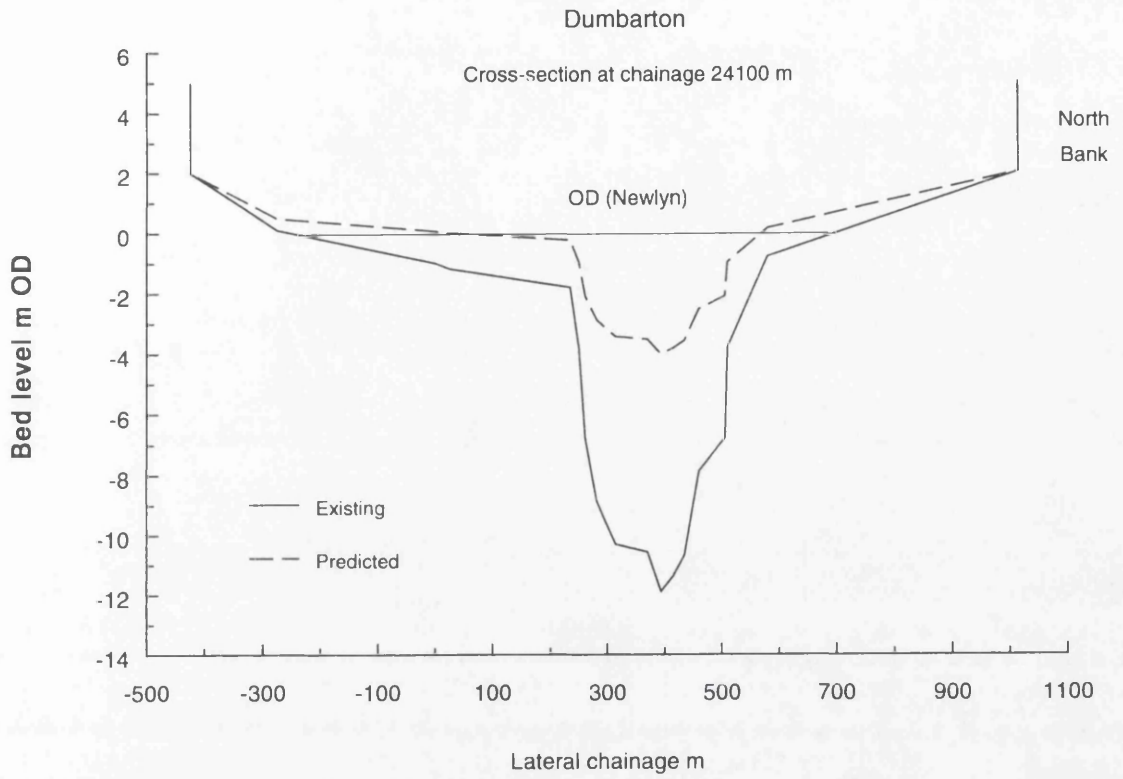


Figure 8.35 Estimated Cross-Section Shape In Final Regime Condition at Dumbarton

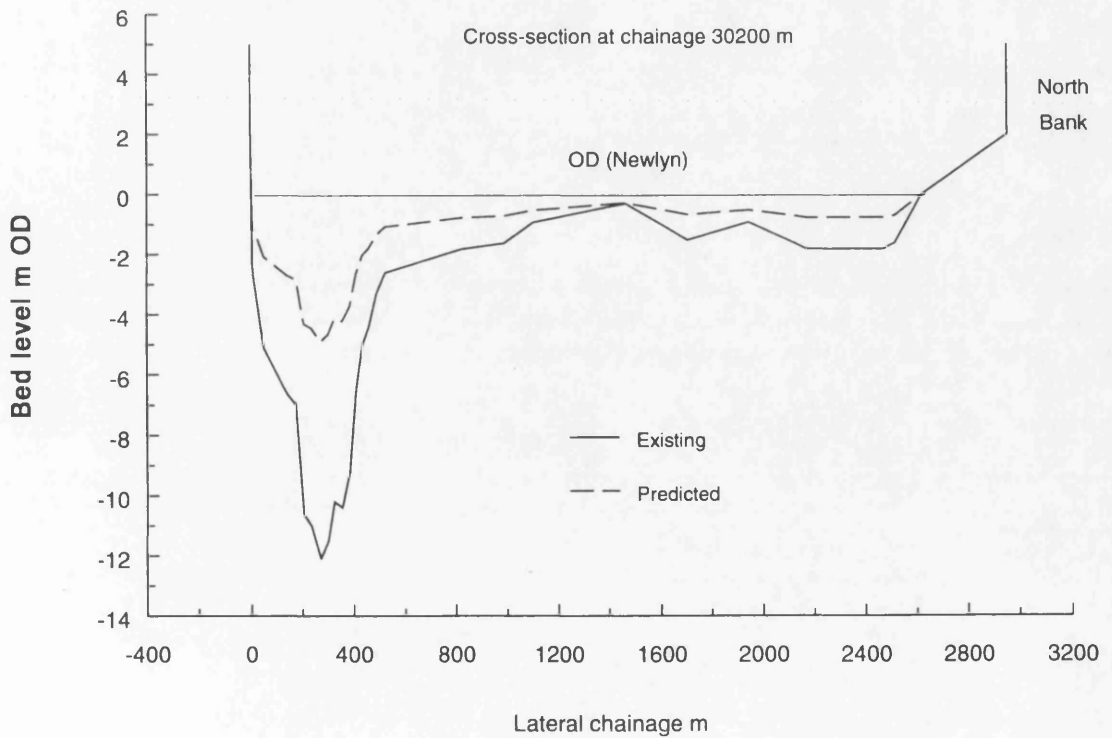


Figure 8.36 Estimated Cross-Section Shape In Final Regime Condition at Chainage 30.2 km

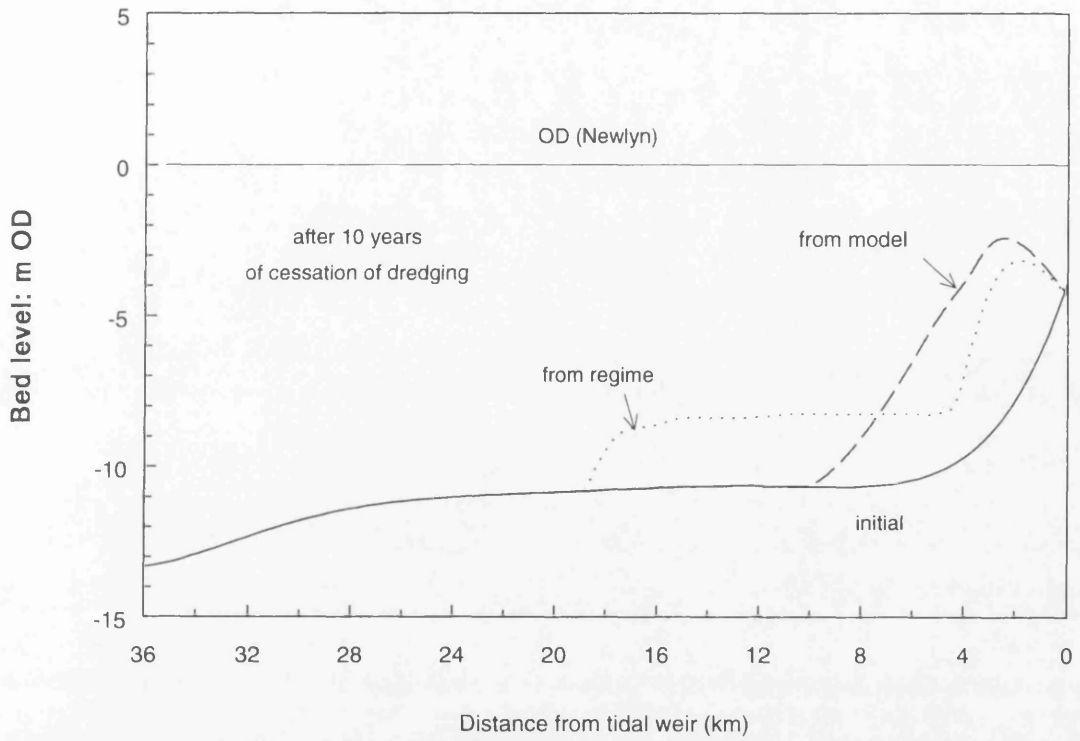


Figure 8.37 Comparison of Bed Profile After 10 Years of Cessation Between Model and Regime Method

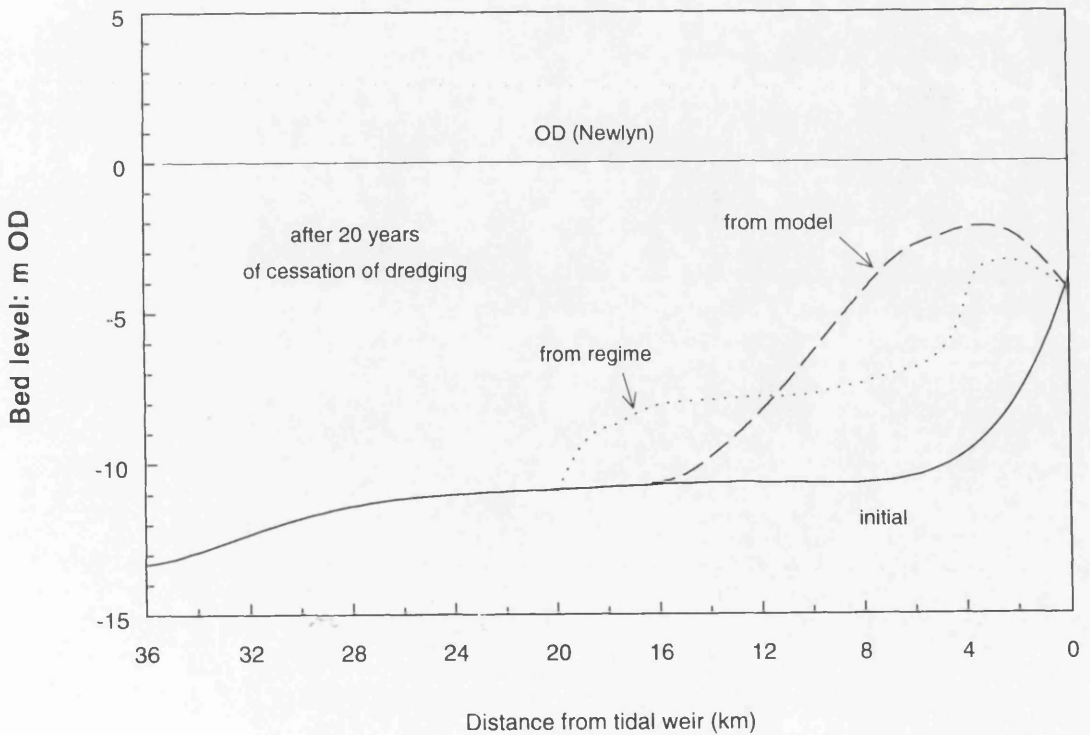


Figure 8.38 Comparison of Bed Profile After 20 Years of Cessation Between Model and Regime Method

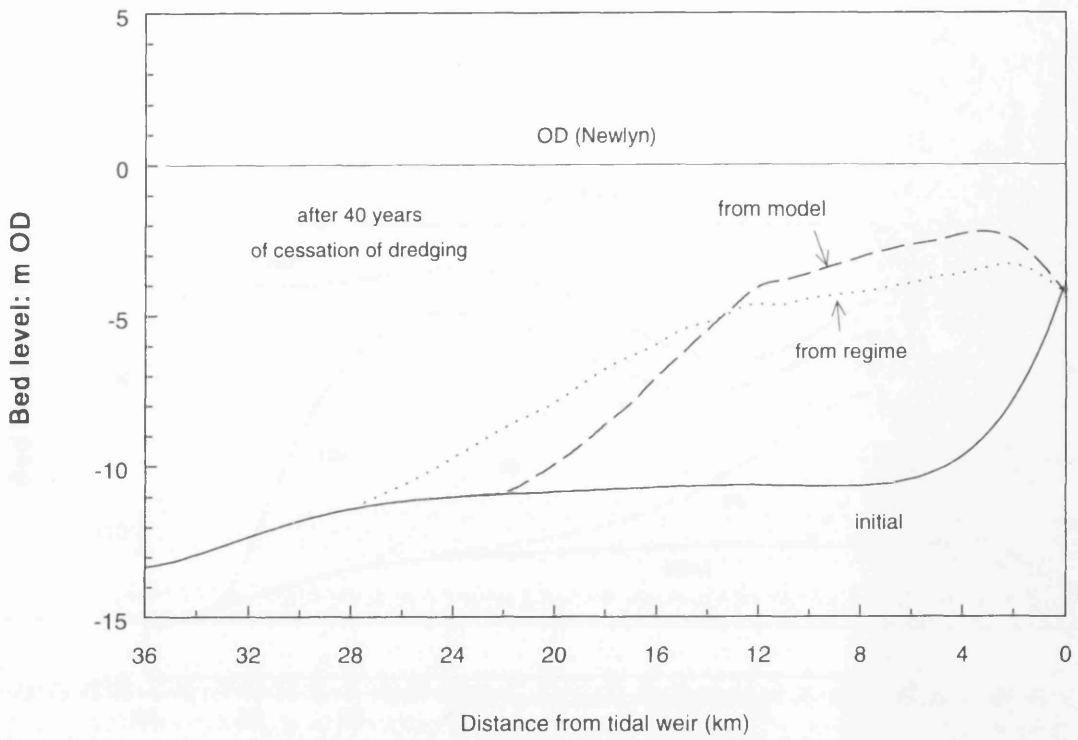


Figure 8.39 Comparison of Bed Profile After 40 Years of Cessation Between Model and Regime Method

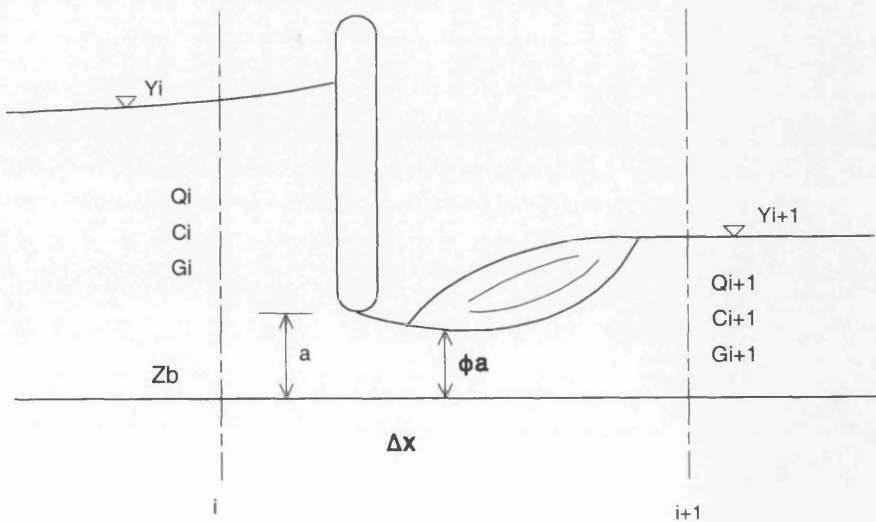
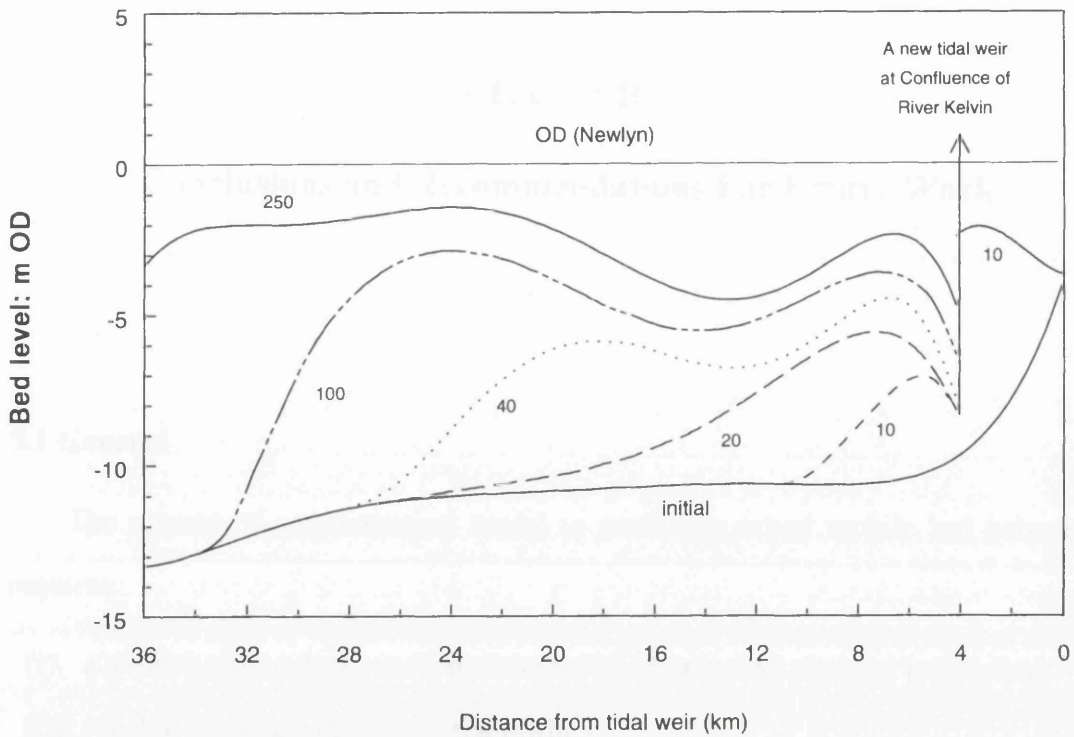


Figure 8.40 Daft Layout of A New Tidal Weir At Confluence of River Kelvin in River Clyde



**Figure 8.41 Estimated Ultimate and Intermediate Bed Profile After Cessation of Dredging In The River Clyde With A New Tidal Weir**

## **CHAPTER 9**

### **Conclusions and Recommendations For Future Work**

#### **9.1 General**

The success of any numerical model in predicting actual mobile bed behaviour requires:

- (i). a good mathematical conceptualisation based on sound physical principles;
- (ii). reliable empirical sediment relationships;
- (iii). a stable and robust numerical scheme.

#### **9.2 Conclusions For Framework of Non-equilibrium Graded Sediment Transport Modelling**

Following conclusions can be made for the framework of the non-equilibrium graded sediment transport modelling.

1. The current model includes the following:
  - (i). The four layer concept where in the stream layer the suspended-load is transported, in the bottom layer the bedload transport takes place, the bed material sorting takes place in the active layer and in the subsurface layer no bed material sorting occurs.
  - (ii). The full St. Venant equations are used to describe unsteady flow in which the feedback effect of channel geometry due to deposition or erosion is taken into account through the resistant factor and changes in the channel cross section.

- (iii). An mobile bed river system including hydrodynamic and graded sediment transport components is time and space dependent. There are three in-depth layers in this statement. Firstly, all independent variables in system vary with time and space. Secondly, the time and space dependency can be expressed mathematically. Thirdly, the system is governed by principles of continuity and momentum conservation.
  - (iv). The total sediment is divided into suspended and bed load. The suspended-load is transported at an order-of-magnitude-greater water velocity and described by an advection and dispersion equation. The bedload is transported at a relatively slow kinematic wave type propagation velocity and its movement is described by an advection equation only.
  - (v). Non-equilibrium sediment transport was adopted for suspended and bed load. This makes the model possible to reflect the spatial and temporal lags between transport rate and transport capacity.
  - (vi). The residual transport capacity was used to reflect the potential of system, that is the exchange rate between different layers is directly proportional to the residual transport capacity.
  - (vii). The interaction between size fractions is taken into account in evaluating fractional sediment transport capacity by using the concept of a hiding function or reduced hiding function.
  - (viii). The equal transport mobility holds for any flow situation.
  - (ix). The evaluation of fractional transport capacity takes account of the fact that some size fractions may not be transported as bedload, but as suspended-load.
2. The following empirical sediment relationships require to be described appropriately to achieve a reliable simulation;

- (i). The resistance factor is an important parameter in this model and includes grain and skin roughness depending on whatever the bed is sand or gravel. In real applications it is necessary to calibrate against observed data.
  - (ii). Suitable sediment transport formulae with an appropriate hiding function are required to evaluate fractional sediment transport capacity.
  - (iii). The active layer thickness is vital for simulating bed material sorting process. Therefore this parameter needs to be defined very carefully.
  - (iv). Other parameters include the characteristic length for suspended-load, travel length for bedload, mean velocity of bedload and fall velocity.
3. This model, developed using above concepts, is able to approach features of graded sediment transport such as armour development and formation under certain flow conditions, bed material sorting processes due to selective transport and downstream fining etc.

### 9.3 Conclusions For The Numerical Scheme and Solution Technique

The numerical scheme and solution technique should not distort the physical behaviour of graded sediment transport. In addition, they must be stable, reliable and robust.

1. The Preissmann scheme was selected in this model due to its stability, flexibility and robustness.
2. When space parameter is placed on central and time parameter is between 0.5 and 1.0, the Preissmann scheme is believed to be unconditionally stable. The numerical dissipation can be produced when the time weighting parameter is greater than 0.5. The numerical dissipation also increases with the Courant number.
3. The two point scheme is adopted for suspended-load equations so that the Preissmann scheme can be applied.

4. The Newton-Raphson iteration method can be used in connection with the Preissmann scheme to treat the highly non-linear behaviour of the system and to provide fast convergence within a time increment. A relaxation parameter is needed when the Courant number is larger.
5. A fully coupled solution technique, called the block double sweep method, is an efficient solution technique requiring minimum use of computer memory.
6. With the block double sweep method, the first sweep should be performed with care to keep values in the matrices of the current relations bounded, for second sweep the care is also required to ensure that successive rounding errors do not cause divergence of the solution.
7. The numerical tests demonstrate that simulation is stable for a Courant number of up to 3000. The two point scheme is adequate for suspended-load if the parameters in the Preissmann scheme are chosen properly. The numerical dissipation can be controlled according to model requirements.

#### **9.4 Conclusions For The Hiding Functions**

1. Two hiding functions have been developed for use with van Rijn's sediment transport formulae based on the experimental data from H.R. Wallingford (Day, 1980), USWES (1935) and Gibbs & Neill (1972 & 1973).
2. A hiding function was developed based on the definition given by Einstein (1950) and a reduced hiding function based on the definition given by Parker (1990).
3. The main difference between these two hiding functions is that the first one is evaluated based on Shields critical shear stress value for each size fraction, but the second is based on the Shields critical shear stress value for the sediment geometric mean size.
4. The two parameters are involved in the formulation of the hiding functions, geometric mean particle size and deviation characterising the grain size distribution and the flow Froude number characterising the flow conditions.

5. The form of hiding function was determined based on the fact that the hiding effect should vanish as the bed material approaches uniformity.
6. The strategy of developing hiding functions is that they were formulated using data from USWES and HR Wallingford, and verified against an independent data set from Gibbs & Neill. The verification results are in good agreement.
7. The constants in both hiding functions were evaluated using an optimisation technique to minimise the total relative error.
8. Other factors such as bed geometry and pressure fluctuations of turbulence were ignored quantitatively because of lack the observed data.
9. The limitations of the two hiding functions is that they can only be applied in subcritical flow with bed material possessing a standard geometric deviation less than 3.5. It should be noted that both hiding functions were developed using the experimental data only.

## **9.5 Conclusions For Applications**

### **9.5.1 From Applications in Experiments of Armouring Development**

1. The application of the model on experiments of armouring development conducted in Aberdeen University are successful. The comparison between predicted and observed values for total bedload rate and fractional bedload transport rates are satisfactory.
2. This application demonstrates that van Rijn's formulae with a reduced hiding function are adequate for simulating Aberdeen's experimental data. In other words, if the Froude number is ranging from 0.2 to 0.8, standard geometric deviation from 1 to 3.5 and particle size from 0.1 to 10 mm the reduced hiding function can simulate hiding effect correctly.
3. The verification of the hiding function in the experiments indicates that a hiding function overestimated the threshold condition for the finer grains and this results

in an incorrect evaluation of transport capacity for finer grains. A reduced hiding function overcomes this disadvantage.

4. The armouring development and formation under the experimental situation and single modal bed material can be simulated in this model in connection with van Rijn's formulae and a reduced hiding function.

### **9.5.2 From Application of Goodwin Creek**

1. This application demonstrate that real life simulation needs real life boundary and initial conditions. Without these the reliable numerical simulations cannot be achieved.
2. The sensitivity analysis for initial and boundary conditions indicates that from the numerical results it is very difficult to assess the performance of selected empirical sediment relationships such as van Rijn's formulae with a reduced hiding function and Parker's formula with his reduced hiding function. Because the real life sediment inflow and bed material composition were not available.
3. This application provides a real test for model's performance in a graded sediment transport events in an active mobile bed river. The numerical results address the difficulties that face the numerical modeller when trying to simulate such events.
4. Parker's formula with his reduced hiding function can be used in conjunction with the model. However, in order to use Parker's formula correctly the resistance factor should be estimated and calibrated because Parker's formula is very sensitive to this parameter.
5. For short term unsteady simulations it is suggested that the time weighting factors in the Preissmann scheme be set to be 0.55 to reduce numerical dissipation.

### **9.5.3 From Application of River Clyde**

1. This application provides a test for the model in the medium mobile bed river system in UK.

2. The numerical results for channel geometry have been compared with that from regime method. They are in good agreement.
3. Calibration using a typical event on 16 August, 1989 similar to the mean spring tide gives a Manning's coefficient 0.02.
4. It takes about 40 and 110 years for the Clyde to reach its regime condition down to Rothesay Dock and Dumbarton.
5. The final regime condition will be reached 250 years after the cessation of dredging which confirms the previous results from using regime method.
6. If a tidal weir is built in the confluence of the River Kelvin and Clyde with chainage of 4100 m from existed tidal in Glasgow, it has been found from simulations that it will have a little effect on the regime condition of the Clyde from overall results.

#### **9.6 Recommendations For Future Work**

1. The resistance factor should be evaluated correctly because it is not only important for the hydrodynamic simulation but also for the estimation of the transport capacity. The difficulty is that the skin roughness is not easy to estimate because it varies with flow strength.
2. The interaction of size fractions needs to be investigated further so that the better understanding can be used in estimating the threshold condition for each size fraction in graded sediment. This is crucial for graded sediment transport.
3. The selection of sediment transport formulae is another important task. The study should focus on a formula which can be used to calculate the fractional transport capacity with an adequate hiding function.
4. The thickness of the active layer should be estimated carefully because it is a vital factor influencing bed material sorting process. In addition, poor estimation of the active layer thickness can lead to unstable numerical results.

5. It has been suggested by Kunhle (1989) that the bed form in Goodwin Creek plays a very important role in the sediment transport, especially for explaining fluctuations in the observed bedload rates. But the effect of bed form on the hiding effect has not been included in the current hiding function. The future study should be undertaken to investigate the physical behaviour of bed forms.
6. The model with the selected empirical sediment relations should be verified further to test its performance especially for bimodal or multimodal feature of bed material.
7. The model can be developed further with a user-friendly interface and visualisation software so that the model can be used more easily and the results can be directly viewed on the screen.
8. The mathematical acceleration procedure for Newton-Raphson method could be included to reach the solution more efficiently

## REFERENCES

1. Abbott,M.B., 1979, Computational Hydraulics: Elements of The Theory of Free Surface Flow, Pitman, London
2. Abbott,M.B., McCowan,A. and Warren,I.R., 1981, Numerical modelling of Free Surface Flows That are Two-Dimensional In Plan, In Fisher H B, Transport Models For Inland and Coastal Waters, Ch.7, Academic Press, New York
3. Abbott,M.B., Larsen,J. and Tao,J.H., 1985, Modelling Circulation in Depth-integrated Flows, Part 1: The Accumulation of The Evidence, J. Hydr. Res, 23(4), 309-326
4. Abbott,M.B. and Basco,D.R., 1989, Computational Fluid Dynamics, An Introduction For Engineers, Longman Science & Technical, John Wiley & Sons, Inc., New York
5. Abbott,M.B., 1989, Review of Recent Developments in Coastal Modelling, Int. Conf. Paper, ed by Falconer,R.A., et al
6. Abbott,M.B., Havno,K. and Lindberg,S., 1991, The Fourth Generation of Numerical Modelling in Hydraulics, J. Hydr. Res. IAHR, 29(5), 581-600
7. Abdalla,E.M., Chollet,J.P. and Bouvard,M., 1986, Mathematical Modelling of Alluvial River Bed Phenomena, Pro. 2nd Int. Conf. Paper
8. Ackers,P. and White,W.R., 1973, Sediment Transport: New Approach and Analysis, J. Hydr. Div. ASCE, 99(11), 2041-2060
9. Ackers,P., 1983, Sediment Transport Problems in Irrigation System Design, Developments in Hydraulic Engineering - 1, ed by Novak,P., Applied Science Publishers
10. Adams,J., 1979, Gravel Size Analysis From Photographs, J. Hydr. Engrg. ASCE, 105(6), 1247-1255
11. Adams,E.W. and Rodi,W., 1990, Modelling Flow and Mixing In Sedimentation Tanks, J. Hydr. Engrg. ASCE, 116(7), 895-913
12. Akanbi,A.A. and Katopodes,N.D., 1988, Model For Flood Propagation On Initially Dry Land, J. Hydr. Engrg. ASCE, 114(7), 689-706
13. Alfrink,B.J. and Rijn,L.C.van, 1983, Two-Equation Turbulence Model For Flow in Trenches, J. Hydr. Engrg. ASCE, 109(3), 941-958

14. Andrews,E.D., 1983, Entrainment of Gravel From Naturally Sorted Riverbed Material, *Geol. Soc. Am. Bull.*, 94, 1225-1231
15. Andrews,E.D. and Parker,G., 1987, Formation of a Coarse Surface Layer as the Response To Gravel Mobility. *Sediment Transport In Gravel Bed Rivers*, ed by Thorn,C.R. et al, 269-325.
16. Antsyferov,S.M. and Kos'yan,R.D., 1980, Sediments Suspended in Stream Flow, *J. Hydr. Div., ASCE*, 106(2), 313-330
17. Armanini,A. and Silvio,G.D., 1987, On the Coexistence of Bedload and Suspended Transport For a Mixture Grainsize Material, *Sediment Transport Modelling*, ed by Sam S.Y. Wang, 581-587
18. Armanini,A. and Silvio,G.D., 1988, A One Dimensional Model For The Transport of A Sediment Mixture In Non Equilibrium Conditions, *J. Hydr. Res.*, 26(3), 275-292
19. Armanini,A., 1993, Variation of Bed and Sediment Load Mean Diameter Due To Erosion and Deposition Process, *Dynamics of Gravel Rivers*, ed. by Billi et al, John Wiley & Sons, 351-359
20. Asaeda,T., Nakai,M., Manandhar,S.K., and Tamai,N., 1989, Sediment Entrainment in Channel With Rippled Bed, *J. Hydr. Engrg., ASCE*, 115(3), 327-339
21. ASCE Task committee on turbulence models in hydraulic computations, 1988, *Turbulence Modelling of Surface Water Flow and Transport*, *J. Hydr. Engrg. ASCE*, 114(9), 970-1073
22. Ashworth,P.J. and Ferguson,R.I., 1989, Size Selective Entrainment of Bedload in Gravel Bed Stream, *W.R.R.*, 25(4), 627-634
23. Aziz,N.M. and Prasad,S.N., 1985, Sediment Transport In Shallow Flows, *J. Hydr. Engrg., ASCE*, 111(10), 1327-1343
24. Babtie Group Ltd, 1987, Consideration For The Impounding of Glasgow Harbour By A Tidal Barrage
25. Babtie Group Ltd, 1988, Clyde Weir - Preliminary Engineering Study
26. Babtie Group Ltd, 1988, Dredging Study in The River Clyde, Phase I Report
27. Babtie Group Ltd, 1989, Dredging Study in The River Clyde, Phase II Report
28. Bagnold,R.A., 1973, The nature of Saltation and of Bedload Transport in Water, *Proc. Royal Soc. London*, A332
29. Barton,J.R. and Lin,P.N., 1955, A Study of Sediment Transport Problem in Alluvial Streams, Report No.55 JRB2, Civil Engineering Department, Colorado College, Fort Collins, Colorado
30. Bayazit,M., 1978, Scour of Bed Mathematical In Very Rough Channels, *J. Hydr. Div. ASCE*, 104(9), 1345-1349
31. Beam,R.M. and Warming,R.F., 1976, An Implicit Finite Difference Algorithm For Hyperbolic Systems in Conservation Law Form, *J. Comp. Phy.* 22, 87-110

32. Begin,Z.B., Meyer,D.F. and Schumm,S.A., 1981, Development of Longitudinal Profile of Alluvial Channels in Response To Base-level Lowering, *Earth Surface Processes and Land Forms*, 6(1), 49-68
33. Bell,R.G. and Sutherland,A.J., 1983, Non-equilibrium Bedload Transport By Steady Flow, *J. Hydr. Engrg. ASCE*, 109(3), 351-367
34. Bettess,R. and White,W.R., 1981, Mathematical Simulation of Sediment Movement in Streams, *Proc. Instn. Civ. Engrs*, Part 2, 171, 879-892
35. Bhallamudi,S.M. and Chaudhry,M.H., 1991, Numerical Modelling of Aggravation and Degradation In Alluvial Channels, *J. Hydr. Engrg., ASCE*, 117(9), 1144-1164
36. Bhowmik,N.G. and Demissie,M., 1982, Carrying Capacity of Flood Plains, *J. Hydr. Div. ASCE*, 108(3), 443-452
37. Bochteler,W. and Schrimpf,W., 1984, Improved Numerical Model For Sedimentation, *J. Hydr. Engrg., ASCE*, 110(3), 234-246
38. Borah,D.K., Alonso,C.V. and Prasad,S.N., 1982, Routing Graded Sediments in Streams: Formulations, *J. Hydr. Div., ASCE*, 108(12), 1486-1504
39. Borah,D.K., Alonso,C.V. and Prasad,S.N., 1982, Routing Graded Sediment In Streams: Applications, *J. Hydr. Div., ASCE*, 108(12), 1504-1517
40. Bowles,D.S., Fread,D.L. and Grenney,W.J., 1977, Coupled Dynamics Stream Flow-temperature Models, *J. Hydr. Div. ASCE*, 515-530
41. Bray,D.I, 1982, Flow Resistance in Gravel-bed Rivers, *Gravel Bed Rivers*, ed by Hey,R.D. et al, John Wiley & Sons Ltd, 109-133
42. Burkham,D.E. and Dawdy,D.R., 1976, Resistance Equation For Alluvial-Channel Flow, *J. Hydr. Div., ASCE*, 102(10), 1479-1489
43. Ceballos,R.P., 1989, Transport of Sediments: Analytical Solution, *J. Hydr. Res.*, 27(4), 501-518
44. Celik,I. and Rodi,W., 1988, Modelling Suspended Sediment Transport in Non-equilibrium Situation, *J. Hydr. Engrg. ASCE*, 114(10), 1157-1191
45. Celik,I. and Rodi,W., 1991, Suspended Sediment Transport Capacity For Open Channel Flow, *J. Hydr. Engrg., ASCE*, 117(2), 191-204
46. Chadwick,A.J., 1991, An Unsteady Flow Bore Model For Sediment Transport In Broken Wave, Part 1: The Development of the Numerical Model, *Pro. Instn. Civ. Engrs. Mat.*, 91, 719-738
47. Chadwick,A.J., 1991, An Unsteady Flow Bore Model For Sediment Transport In Broken Wave, Part 2: The Properties, Calibration and Testing of the Numerical Model, *Pro. Instn. Civ. Engrs. Mat.*, 91, 739-753
48. Chang,H.H. and Hill,J.C., 1976, Computer Modelling of Erodible Flood Channels and Deltas, *J. Hydr. Div., ASCE*, 102(10), 1461-1477
49. Chang,H.H., 1982, Mathematical Model For Erodible Channels, *J. Hydr. Div., ASCE*, 108(5), 678-689

50. Chang,H.H., 1984, Analysis of River Meander, J. Hydr. Engrg., ASCE, 110(1), 37-50
51. Chang,H.H., 1984, Modelling of River Channel Changes, J. Hydr. Engrg., ASCE, 110(2), 157-172
52. Chang,H.H., 1988, Fluvial Processes in River Engineering, John Wiley & Sons, New York
53. Chin,C.O., Melrille,B.W. and Raudkivi,A.J., 1994, Streambed Armouring, J. Hydr. Engrg. ASCE, 120(8), 899-918
54. Chiu,C.L. and Hsiung,D.E., 1981, Secondary Flow, Shear Stress and Sediment Transport, J. Hydr. Div. ASCE, 107(7), 879-898
55. Chow,V.T., 1959, Open-Channel Hydraulics, McGraw-Hill Book Company, New York
56. Coleman,N.L., 1970, Flume Studies of the Sediment Transfer Coefficient, Water Resources, 6(3)
57. Colombini,M., Tubino,M. and Whiting,P., 1992, Topographic Expression of Bars in Meandering Channels, *Dynamics of Gravel Bed Rivers*. ed by Billi,P. et al, 457-474
58. Colosimo,C., Copertino,V.A. and Veltri,M., 1988, Friction Factor Evaluation in Gravel Bed Rivers, J. Hydr. Engrg. ASCE, 114(8), 861-876
59. Copeland,P.P. and Thomas,W.A., 1992, Numerical Modelling of Gravel Movement in Concrete Channels, *Dynamics of Gravel Bed Rivers*. ed by Billi,P. et al, 373-397
60. Corps of Engineers U.S. Army, 1956, Hydraulic Capacity of Meandering Channels in Straight Floodways, Technical Memorandum, Bo.2-429
61. Cunge,J.A. and Perdreau,N., 1973, Mobile Bed Fluvial Mathematical Models, La Houille Bdauche, No.7
62. Cunge,J.A., Holly,F.M. and Verwey,A., 1980, Practical Aspects of Computational River Hydraulics, Pitman Adv. Pub. Program
63. Cunge,J.A., 1989, Review of Recent Developments In River Modelling, Int. Conf. Paper, Int. Conf. Paper, cd by Falconer,R.A. et al
64. Davies,T.R.H. and Damad,M.F.A., 1978, Fluid Dynamic Lift On A Bed Particle, J. Hydr. Div., ASCE, 104(8), 1171-1182
65. Davies,T.R.H., 1980, Bedform Spacing and Flow Resistance, J. Hydr. Div., ASCE, 106(3), 423-433
66. Day,T.J., 1980, A Study of the Transport of Graded Sediments. Hydraulic Research Wallingford, UK, Report No.IT 190.
67. De Vries,M., 1973a, River Bed Variations - Aggravation and Degradation, Delft Hydraulic Lab., Publ., No.107
68. De Vries,M., 1973b, Application of Physical and Mathematical Models For River Problems, Delft Hydraulic Lab., Publ., No.112

69. Dennis,A.L., 1987, Unsteady Sediment Transport Modelling, J. Hydr. Engrg. ASCE, 113(1), 1-15
70. Design Manual For Straight Compound Channels, Summary and Design Method, 1991, Wallingford
71. DeVantier,B.A. and Larock,B.E., 1983, Sediment Transport In Stratified Turbulent Flow, J. Hydr. Engrg., ASCE, 109(12),1622-1635
72. Diplas,P. and Sutherland,A.J., 1988, Sampling Techniques For Gravel-sized Sediments, J. Hydr. Engrg. ASCE, 114(5), 484-501
73. Drazin,P.G. and Reid,W.H., 1981, Hydrodynamics Stability, Cambridge University Press
74. Drew,D.A., 1979, Dynamic Model For Channel Bed Erosion, J. Hydr. Div., ASCE, 105(6), 721-736
75. Egiazaroff,I.A., 1965, Calculation of Non-uniform Sediment Concentrations, J. Hydr. Div. ASCE, 91(4), 225-247
76. Einstein,H.A., 1941, Formula For the Transportation of Bedload, American Society of Civil Engineering
77. Einstein,H.A., 1950, The Bed-Load Function For Sediment Transport In Open Channels. *Tech. Bull.* 1026, US, Dept. of Agriculture
78. Einstein,H.A. and Barbarossa,N.L., 1952, River Channel Roughness, Trans. ASCE, 117, 1121-1132
79. Einstein,H.A. and Chien,N., 1953, Transport of Sediment Mixtures With Larger Ranges of Grain Sizes, MRD Sediment Series No.2, US Army Eng. Div. Corps of Engineering, Omaha, Nebraska
80. Einstein,H.A. and Abdel-Aal,F.M., 1972, Einstein Bedload Function at High Sediment Rate, J. Hydr. Div., ASCE, 98(HY1)
81. Elder,J.W., 1959, The Dispersion of Marked Fluid in Turbulent Shear Flow, J. Fluid Mech., Vol.5(4), 1959, 544-560
82. EL-gamal,F.S., 1993, Critical Shear Stress of Sediment Mixtures, Advances in Hydro-Sciences and Engineering, ed. by Sam S.Y. Wang, 1, 678-683
83. Ellis,J., 1991, Preliminary Study of The River Leven To Establish The Feasibility of a General Lowering of the Channel, Report in Couch, Hogg Waterman Consult.
84. Ellis,J., 1994, Study of The River Leven To Determine The Optimum Lowering of The Channel Cross Section, Report in Couch, Hogg Waterman Consult.
85. Engelund,F. and Hanson,E., 1967, A Monograph on Sediment Transport in Alluvial Stream, Teknisk Forlag Copenhagen
86. Ervine,D.A. and Ellis,J., 1987, Experimental and Computational Aspects of Overbank Flood Plain Flow, Earth Sciences, 78, 315-325

87. Elliott,S.C.A. and Sellin,R.H.J., 1990, SERC Flood Channels Facility: Skewed Flow Experiments, *J. Hydr. Res.*, 28(2), 197-214
88. Falconer,R.H., Banks,D.J., Riddell,J.F. and Thomson,D.S, 1992, The Clyde Dredging Study, *Proc. Instn Civ. Engrs Wat. Marit & Energy*, 96, 81-94
89. Fenton,J.D. and Abbott,J.E., 1977, Initial Movement of a Grain on a Stream Bed: The Effect of Relative Protrusion, *Proc. Roy. Soc. London, A*, Vol.352, 523-537
90. Ferguson,R.I., Prestegaar,K.L. and Ashworth,P.J., 1989, Influence of Sand on Hydraulics and Gravel Transport in a Braided Gravel Bed Rivers, *W.R.R.*, 25(4), 635-643
91. Ferguson,R.I, 1992, Selective Transport and Downstream Fining of River Gravel, Interim Report, GR 3/7407, University of Sheffield
92. Ferguson,R.I and Hoey,T., 1992, Bedload Exchange Process in Gravel-bed Rivers, Research Report, University of Sheffield
93. Fischer,H.B., List,E.J., Koh,R.C.Y., Imberger,J. and Brooks,N.H., 1979, *Mixing in Inland and Coastal Waters*, Academic Press, New York, 1979, 80-147
94. Fletcher,C.A.T., 1991, *Computational Technique For Fluid Dynamics*, Springer-Verlag, Vol.II
95. Fread,D.L., 1974, Numerical Properties of Implicit Four-point Finite Difference Equations of Unsteady Flow, *Nat. Weather Service, TM HYDRO-18*, Washington, USA
96. Fread,D.L. and Smith,G.F., 1978, Calibration Technique For 1D Unsteady Flow Models, *J. Hydr. Div. ASCE*, 104(7), 1027-1044
97. Fread,D.L., 1980, Two Finite-Difference Models Used For River Flood Forecasting By The National Weather Service, Lecture Notes, Short Course on Comp. Hyd., Texas A & M University., College Station
98. Fukuoka,S. and Fujita,K., 1990, Prediction Method of Flow Resistance In Rivers With Compound Channels and Application To River Course Design, *Int. Conf. On River Flood Hydraulics*, ed by White,W.R., John Wiley & Sons Ltd
99. Galappatti,G. and Vreugdenhil,C.B., 1985, A Depth Integrated Model For Suspended Sediment Transport, *J. Hydr. Res.* 23(4), 359-377
100. Garcia,M. and Parker,G., 1991, Entrainment of Bed Sediment Into Suspension, *J. Hydr. Engrg. ASCE*, 117(4), 414-435
101. Garrad,P.N. and Hey,R.D., 1987, Boat Traffic, Sediment Resuspension and Turgidity in Broadland River, *J. of Hydrology*, 95, 289-297
102. Gessler,J., 1970, Self Stabilizing Tendencies of Alluvial, *Proc. ASCE*, 96(WW2), 225-249
103. Gessler,J., 1990, Friction Factors of Armoured River Beds, *J. Hydr. Engrg*, 116(4), 531-543

104. Gibbs,C.J. and Neill,C.R., 1972, Interim Report On Laboratory Study of Basket-Type Bedload Samplers, Research Council of Alberta, REH/72/2
105. Gibbs,C.J. and Neill,C.R., 1973, Laboratory Testing of Model VUV Bedload Samplers, Research Council of Alberta, REH/73/2
106. Graf,W.H., 1971, Hydraulics of Sediment Transport, McGraw-Hill
107. Griffiths,G.A., 1989, Form Resistance In Gravel Channels With Mobile Beds, J. Hydr. Engrg. ASCE, 115(3), 340-355
108. Han,Q.W. and He,M.M., 1987, Mathematical Model of Non-equilibrium Transport of Non-uniform Sediment (MI-NEWS), A Model of Alluvial Process and Reservoir Sedimentation, Lecture Notes of Advanced Course on Mathematical Modelling of Alluvial Rivers, Vol.2
109. Hantz,P.A., 1980, Low Sediment Transport Rates Over Flat Beds, J. Hydr. Div., ASCE, 106(7),1173-1190
110. Hardwick,R.I. and Willetts,B.B., 1991, Changes With Time of the Transport Rate of Sediment Mixtures, J. Hydr. Res. IAHR, 29(1), 117-127
111. Havno,K. and Brorsen,M., 1986, A General Mathematical Modelling System For Flood Forecasting and Flood Control, Proc. Inter. Conf. on Hydraulics of Floods and Flood Control, Cambridge, UK
112. Henderson,F.M., 1966, Open Channel Flow, The Macmillan Co., London, UK
113. Hetchkiss,R.H. and Parker,G., 1991, Shock Fitting of Aggradational Profiles Due To Backwater, J. Hydr. Engrg. ASCE, 117(9), 1129-1144
114. Hey,R.D., 1979, Flow Resistance in Gravel Bed Rivers, J. Hydr. Div., 105(4), 365-379
115. Hey,R.D., 1979, Dynamic Process-Response Model of River Channel Development, Earth Surface Process, Vol.4, 59-72
116. Hey,R.D. and Thorn,C.R., 1986, Stable Channels With Mobile Gravel Beds, J. Hydr. Engrg. ASCE, 112(8), 671-689
117. Hey,R.D., 1988, Mathematical Models of Channel Morphology, Modelling Geomorphologic Systems, ed by Anderson,M.G., John Wiley & Sons Ltd
118. Hey,R.D., 1988, Bar Form Resistance In Gravel Bed Rivers, J. Hydr. Engrg. ASCE, 114(12), 1498-1508
119. Hey,R.D., 1992, River Dynamics, Flow Regime and Sediment Transport, Dynamics of Gravel-bed Rivers, ed by Billi,P. et al, John Wiley & Sons Ltd, 17-37
120. Hirano,M., 1971, River Bed Degradation With Armouring, Proc. Japan Society of Civil Engineers, N0.195, 55-65
121. Hoey,T.B. and Ferguson,R., 1994, Numerical Simulation of Downstream Fining By Selective Transport In Gravel Bed Rivers: Model Development and Illustration, Water Resource Research, 30(7), 2251-2260

122. Holly,F.M. Jr, 1985, Dispersion in River and Coastal Waters - 1. Physical Principles and Dispersion Equations, ed by Novak,P. Developments in Hydr. Engrg. - 3
123. Holly,F.M. and Rahuel,J.L., 1989, Advances in Numerical Simulation of Alluvial River Response To Disturbances,
124. Holly,F.M. Jr and Rahuel,J.L., 1990, New Numerical/Physical Framework For Mobile-Bed Modelling, J. Hydr. Res. 28(4), 401-416
125. Holly,F.M. Jr and Rahuel,J.L., 1990, New Numerical/Physical Framework For Mobile-Bed Modelling, J. Hydr. Res., IAHR, 28(5), 545-564
126. Holtorff,G., 1982, Resistance To Flow In Alluvial Channels, J. Hydr. Div., ASCE, 108(9), 1010-1028
127. Holtorff,G., 1983, Steady Bed Material Transport In Alluvial Channels, J. Hydr. Engrg., ASCE, 109(3), 368-383
128. Hosseinipour,Z., 1989, Development and Application of A fluvial Hydrodynamic and Sediment Transport Model, Int. Conf. Paper, ed by Falconer,R.A. et al
129. Hung,C.S. and Shen,H.W., 1976, Stochastic Models of Sediment Motion On Flat Bed, J. Hydr. Div., ASCE, 102(12), 1745-1759
130. Ikeda,S., 1981, Self-formed Straight Channels in Sandy Beds, J. Hydr. Div. ASCE, 107(4), 389-406
131. Ikeda,S. and Nishimura,T., 1986, Flow and Bed Profile in Meandering, J. Hydr. Engrg. ASCE, 112(7), 562-579
132. Ippen,A.F., 1971, A New Look at Sedimentation in Turbulent Streams, J. of the Boston Society of Civil Engineers, 58(3)
133. Isaacson,D.L. and Madsen,R.W., 1976, Markov Chains Theory and Applications, John Wiley & Sons
134. Itakura,T. and Kishi,T., 1980, Open Channel Flow With Suspended Sediments, J. Hydr. Div. ASCE, 106(8), 1325-1343
135. James,C.S., 1985, Sediment Transport To Overbank Sections, J. Hydr. Res. IAHR, 23(5), 435-452
136. Keller,R.J. and Rodi,W., 1988, Prediction of Flow Characteristics in Main Channel/Flood Plain Flows, J. Hydr. Res. 26(4), 425-441
137. Kerssens,P.M.J., Prins,Ad and Rijn,L.C.van, 1979, Model For Suspended Sediment Transport, J. Hydr. Div., ASCE, 105(5), 461-476
138. Kikkawa,H., Ikeda,S. and Kitagawa,A., 1976, Flow and Bed Topography in Curved Open Channel, J. Hydr. Div, 102(9), 1327-1342
139. Kirchner,J.W., Dietrich,W.E, Iseya,F. and Ikeda,H., 1990, The Variability of Critical Shear Stress, Friction Angle and Grain Protrusion in Water Worked Sediments, Sedimentology, 37, 647-672

140. Knight,D.W. and Macdonald,J.A., 1979, Hydraulic Resistance of Artificial Strip Roughness, J. Hydr. Div. ASCE, 105(6), 675-690
141. Knight,D.W., Samuels,P.G. and Shiono,K., 1989, River Flow Simulation: Research and Developments, IWEM Conf. Paper
142. Kobayashi,N. and Seo,S.N., 1985, Fluid and Sediment Interaction Over A Plain Bed, J. Hydr. Engrg., ASCE, 111(6), 903-920
143. Komar,P.D. and Shih,S.M., 1992, Equal Mobility Versus Changing Bedload Grain Sizes in Gravel-bed Streams, Dynamics of Gravel-bed Rivers, ed by Billi,P. et al, John Wiley & Sons Ltd, 73-93
144. Koutitas,C. and O'Connor,B., 1981, Turbulence Model For Flow Over Dredged Channels, J. Hydr. Div. ASCE, 107(8), 989-1002
145. Kuhnle,R.A., 1989, Bed Surface Size Changes in Gravel Bed Channel, J. Hydr. Engrg. ASCE, 115(6), 731-743
146. Kuhnle,R.A., 1992, Fractional Transport Rates of Bedload on Goodwin Creek, *Dynamics of Gravel Bed Rivers*. ed by Billi,P. et al, 141-155
147. Kuhnle,R.A., 1993, Incipient Motion of Sand-Gravel Sediment Mixtures, J. Hydr. Engrg. ASCE, 119(12), 1400-1415
148. Lam,D.C.L. and Simpson,R.B., 1976, Centred Differencing and The Box Scheme For Diffusion-Convection Problems, J. Computational Physics, 22, 486-500
149. Lamberli,A. and Paris,E., 1992, Analysis of Armouring Process Through Laboratory Experiments, Dynamics of Gravel Bed Rivers, ed by Billi,P. et al, 205-225
150. Lau,Y.L., 1983, Suspended Sediment Effect On Flow Resistance, J. Hydr. Engrg., ASCE, 109(5), 757-763
151. Launder,B.E. and Spalding,D.B., 1974, The Numerical Calculation of Turbulent Flows, Computer Methods in Applied Mechanics and Engineering, Vol.3, 269-289
152. Leopold,L.B., Welman,M.G. and Miller,J.F., 1964, Fluvial Process in Geomorphology, Freeman and Company, San Francisco
153. Li,Q., Lu,Z.C. and Xu,X.H., 1989, Mathematical Approach To The Sediment Transport In The Lower Yellow River, Geographical Research, 8(2), 55-63
154. Li,Q. and Lu,Z.C., 1989, Mathematical Approach To The Effect of Change of River Caused By The Longitudinal and Upstream Deposition In The Lower Reaches of Huanghe River, Scientia Geographica Sinica, 9(4), 336-345
155. Li,Q., Pender,G. and Ervine,D.A., 1992, Morphological Calculation With Sediment Sorting and Armouring, Glasgow University
156. Li,Q., 1994, Applications of Hiding Functions On Experimental Test of Armouring Development, British Hydrological Society Fourth Postgraduate Symposium, University of Birmingham

157. Li,R.M., Simons,D.B. and Stevens,M.A., 1976, Morphology of Cobble Streams In Small Watersheds, J. Hydr. Div., ASCE, 102(8), 1101-1117
158. Liggett,J.A. and Cunge,J.A., 1975, Numerical Methods of Solution of The Unsteady Flow Equations, Unsteady Flow In Open Channels, Vol.1, ed. by Mahmood et al, Water Resource Publication, USA, 89-182
159. Limerinos,J.T., 1970, Determination of The Manning Coefficient From Measured Bed Roughness in Natural Channels, Water Supply, US Geological Survey, Paper 1898-B
160. Lin,P.N., Huan,J.Q. and Li,X.Q., 1983, Unsteady Transport of Suspended Load At Small Concentrations, J. Hydr. Engrg. ASCE, 109(1), 86-98
161. Lin,P.N. and Shen,H.W., 1984, Two-D flow With Sediment By Characteristics Method, J. Hydr. Engrg., ASCE, 110(5), 615-626
162. Little,W.C. and Mayer,P.G., 1976, Stability of Channel Beds By Armouring, J. Hydr. Div., ASCE, 102(11), 1647-1661
163. Low,H.S., 1989, Effect of Sediment Density On Bed Load Transport, J. Hydr. Engrg, ASCE, 115(1), 124-138
164. Lyn,D.A., 1987, Unsteady Sediment Transport Modelling, J. Hydr. Engrg., ASCE, 113(1), 1-15
165. Marivoet,J.L. and Craenenbroeck,W.V., 1986, Longitudinal Dispersion In Ship-canals, J. Hydr. Res., 24(2), 123-132
166. Mayerle,R., Nalluri,C. and Novak,P., 1991, Sediment Transport in Rigid Bed Conveyances, J. Hydr. Res. IAHR, 29(4), 475-495
167. McDowell,D.M., 1989, An General Formulae For Estimation of Rate of Transport of Non-cohesion Bed Load, J. Hydr. Res., 27(3), 355-361
168. McNulty,A.J. and Wood,I.R., 1984, A New Approach To Predicting The Dispersion of A Continuous Pollutant Source, J. Hydr. Res. 22(1), 23-34
169. Morse,B. and Townsend,R.D., 1990, Modelling Channel Bed Transients Using Explicit F-D Schemes, J. Hydr. Engrg, ASCE, 1345-1356
170. Morton,K.W. and Baimes,M.T., 1982, Numerical Methods For Fluid Dynamics, Academic Press
171. Myers,W.R.C. and Brennan,E.K., 1990, Flow Resistance In Compound Channels, J. Hydr. Res., 28(2), 141-155
172. Nakagawa,H. and Tsujimoto,T., 1980, Sand Bed Instability Due To Bed Load Motion, J. Hydr. Div. ASCE, 106(12), 2029-2051
173. Nakagawa,H., Tsujimoto,T. and Murakami,S., 1987, Convolution-Integral Modelling of Non-equilibrium Sediment Transport, Advances in Hydro-Sciences and Engineering, ed. by Sam S.Y. Wang, 1, 566-571
174. Needham,D.J., 1992, Dynamic Modelling of Bed Waves, Dynamics of Gravel-bed Rivers, ed by Billi,P. et al, John Wiley & Sons Ltd, 401-414

175. Niekerk,A.van, Vogel,K.R., Slingerland,R.L. and Bridge,J.S., 1992, Routing of Heterogeneous Sediments Over Movable Bed: Model Development, *J Hydr. Engrg. ASCE*, 118(2), 246-262
176. Novak,P. and Nalluri,C., 1984, Incipient Motion of Sediment Particles Over Fixed Beds, *J. Hydr. Res.*, 22(3), 181-197
177. Odgaard,A.J., 1982, Bed Characteristics In Alluvial Channel Bends, *J. Hydr. Div., ASCE*, 108(11), 1268-1281
178. Onishi,Y., 1981, Sediment Contaminator Transport Model, *J. Hydr. Div., ASCE*, 107(9), 1089-1107
179. Paintal,A.S., 1971, A Stochastic Model of Bedload Transport, *J Hydr. Res., IAHR*, 9(4), 527-554
180. Parker,G., Klingeman,P.G. and McLean,D.G., 1982, Bedload and Size Distribution in Paved-bed Streams, *J. Hydr. Div., ASCE*, 108(4), 544-571
181. Parker,G., Diplas,P. and Akigama,J., 1983, Meander Bends of High Amplitude, *J. Hydr. Engrg., ASCE*, 109(10), 1323-1337
182. Parker,G., 1990, Surface-based Bedload Transport Relation For Gravel Rivers, *J. Hydr. Res*, 28(4), 417-436
183. Parker,G. and Sutherland,A.J., 1990, Fluvial Armour, *J. Hydr. Res., IAHR*, 28(5), 529-544
184. Pasche,E. and Rouve,G., 1985, Over bank Flow With Vegetability Roughened Flood Plains, *J. Hydr. Engrg., ASCE*, 111(9), 1262-1278
185. Pemberton,E.L, 1972, Einstein's Bedload Function Applied To Channel Design and Degradation, *Sedimentation*, ed by Shen,H.W., Chapter 16, Water Resource Publications, Littleton, Colorado
186. Pender,G., 1992, Maintaining Numerical Stability of Flood Plain Calculations By Time Increment Splitting, *Pro. Instn. Civ. Engrg. Wat.*, 96, 35-42
187. Pender,G., Li,Q. and Ervine,D.A., 1993, A Development of Hiding Function For Van Rijn's Sediment Transport Formulae, *Advances in Hydro-Sciences and Engineering*, ed. by Sam S.Y. Wang, 1, 697-702
188. Pender,G. and Li,Q., 1994, Verification of A Numerical Model For Graded Sediment Transport, Glasgow University, CE-HY93-30
189. Pender,G. and Li,Q., 1994, Comparison of Two Hiding Function Formulations For Non-uniform Sediment Transport Calculations, Accepted by *Proc. Instn Civ. Engrs Wat. Marit & Energy*
190. Phillips,B.C. and Sutherland,A.J., 1985, Numerical Modelling of Spatial and Temporal Lag Effects in Bedload Transport, 21th IAHR Cong., Melbourne, Australia
191. Ponce,V.M. and Simons,D.B., 1977, Shallow Water Propagation in Open Channel Flow, *J. Hydr. Engrg. ASCE*, 103(12), 1461-1476

192. Ponce, V.M., Garcia, J.L. and Simons, D.B., 1979, Modelling Alluvial Channel Bed Transients, *J. Hydr. Div. ASCE*, 105(3), 245-256
193. Proffitt, G.T. and Sutherland, A.J., 1983, Transport of Non-uniform Sediments, *J. Hydr. Res., IAHR*, 21(1), 33-43
194. Rahuel, J.L., Holly, F.M. Jr., Chollet, J.P., Belleudy, P. and Yang, G., 1989, Modelling of River bed Evolution For Bedload Sediment Mixtures, *J. Hydr. Engrg. ASCE*, 115(11), 1521-1542
195. Rakoczi, L., 1987, Selective Erosion, A Key Problem In Numerical Modelling of River-Bed Materials and Their Movement. *Sediment Transport Modelling*. ed by Sam S.Y. Wang, 33-38.
196. Ranga Raju, K.G., 1985, Transport of Sediment Mixtures, 21st IAHR Congress, Melbourne, Australia
197. Raudkivi, A.J. and Ettema, R., 1982, Stability of Armour Layer in River, *J. Hydr. Div. ASCE*, 108(9), 1047-1057
198. Raudkivi, A.J., 1991, *Loose Boundary Hydraulics*, Pergaman Press
199. Reichert, P. and Wanner, O., 1991, Enhanced One-Dimensional Modelling of Transport in Rivers, *J. Hydr. Engrg. ASCE*, 117(9), 1165-1183
200. Rijn, L.C. van, 1984a, Sediment Transport, Part 1: Bedload Transport, *J. Hydr. Engrg. ASCE*, 110(10), 1431-1453
201. Rijn, L.C. van, 1984b, Sediment Transport, Part 2: Suspended load Transport, *J. Hydr. Engrg. ASCE*, 110(11), 1613-1641
202. Rijn, L.C. van, 1986, Mathematical Modelling of Suspended Sediment in Non-uniform Flows, *J. Hydr. Engrg. ASCE*, 112(6), 433-455
203. Rijn, L.C. van., Rossum, H. van and Termes, P., 1990, Field Verification of 2-D and 3-D Suspended-sediment Models, *J. Hydr. Engrg. ASCE*, 116(10), 1270-1288
204. Rodi, W., 1980, *Turbulence Models and Their Application in Hydraulics - A state of The Art Review*, Monograph, Int. Asso. for Hydr. Res. Delft, The Netherlands
205. Rokoczi, L., 1987, Selective Erosion, A Key Problem in Numerical Modelling of River Bed Changes, *Sediment Transport Modelling*, ed by Sam S.Y. Wang,
206. Saad, M.B.E.A., 1987, Critical Shear Stress of Armour Coat, *Sediment Transport Modelling*, ed by Wang S.Y. Sam, 308-313
207. Samuels, P.G. and Skeels, C.P., 1990, Stability Limits For Preissmann Scheme, *J. Hydr. Engrg. ASCE*, 116(8), 997-1012
208. Sauvaget, P., 1983, Dispersion In River and Coastal Waters, Numerical Computation of Dispersion, Chapter 2 in *Developments in Hydraulics*. edited by Novak, P., Elsevier Applied Science Publishers
209. Sauvaget, P., 1985, Dispersion in River and Coastal Waters - 2. Numerical Computation of Dispersion, ed by Novak, P. *Developments in Hydr. Engrg.* - 3

210. Scarlatos,P.D. and Partheniades,E.M., 1986, Numerical Simulation of Fine Sediment Motion In estuaries, Pro. 2nd Int. Conf. Paper
211. Schaffranek,R.W., Baltzer,R.A. and Goldberg,D.E., 1981, A Model For Simulation of Flow In Singular and Interconnected Channels, Chapter 3, Book 7, USGS, Techniques in Water-Resources Investigations
212. Schamber,D.R. and Larock,B.E., 1981, Numerical Analysis of Flow in Sedimentation Basins, J. Hydr. Div. ASCE, 107(5), 575-590
213. Schoellhamer,D.H., 1988, Two-Dimensional Lagrangian Simulation of Suspended Sediment, J. Hydr. Engrg, ASCE, 114(10), 1192-1209
214. Schumm,S.A., 1977, The Alluvial System, John Wiley & Sons Ltd
215. Seal,R., Parker,G. and Paola,C., 1993, The effect of Local Patchness of Gravel Grain Size Distributions on Bedload Transport in Braided Rivers, Advances in Hydro-Science and - Engineering, ed by Wang, S.Y. Sam, Vol.1, 1081-1088
216. Shimizu,Y., Yamagachi,H and Itakura,T., 1990, Three-Dimensional Computation of Flow and Bed Deformation, J. Hydr. Engrg. ASCE, 116(9), 1090-1108
217. Silvio,G.DI., 1992, Modelling Sediment Transport Under Different Hydrological and Morphological Circumstances, Dynamics of Gravel Rivers, ed. by Billi et al, John Wiley & Sons, 363-371
218. Silvio,G.DI., 1993, Larger-Scale Morphological Modelling of Fluvial and Coastal Systems, Advances in Hydro-Sciences and Engineering, ed. by Sam S.Y. Wang, 1, 157-165
219. Simons,D.B. and Simons,R.K., 1987, Differences Between Gravel and Sand-bed Rivers, Sediment Transport in Gravel Bed Rivers, ed by Thorn,C.R. et al, 3-15
220. Sloff,C.J., 1993, Study on Modelling The Morphology of Torrents On Volcano Slopes, J. Hydr. Res. IAHR, 31(3), 333-345
221. Sod,G.A., 1985, Numerical Methods in Fluid Dynamics, Cambridge University Press
222. Soni,J.P., Gardè,R.J. and Raju,K.G.R., 1980, Aggradation in Stream Due To Overloading, J. Hydr. Div. ASCE, 106(1), 117-232
223. Stein,C.J. and Rouve,G., 1989, 2D Depth-averaged Numerical Predictions of the Flow in a Meandering Channel With Compound Cross Section, Hydrosoft, Vol.2(1)
224. Sutherland,A.J., 1991, Hiding Function To Predict Self Armouring, Research Report, University of Canterbury, New Zealand
225. Sutherland,A.J., 1992, Static Armour Layers by Selective Erosion, Dynamics of Gravel-bed Rivers, ed by Billi,P. et al, John Wiley & Sons Ltd, 243-260
226. Tait,S.T., Willetts,B.B. and Maizels,J.K., 1992, Laboratory Observations of Bed Armouring and Changes in Bedload Composition. *Dynamics of Gravel Bed Rivers*. ed by Billi,P. et al, 205-225.

227. Tamai,N., 1992, Sediment Concentration in Unsteady Open-channel Flow, Proceeding of 8th Hydrodynamics Meeting, 1301-1310
228. Taylor,C. and Morgan,K., 1980, Recent Advances in Numerical Methods in Fluid, Pineridge Press Limited, Swansea, UK., Vol.1
229. Thomas,W.A. and Prasuhn,A.L., 1977, Mathematical Modelling of Scour and Deposition, J. Hydr. Div., ASCE, 103(8), 851-864
230. The Task Committee On Computational Hydraulics, 1980, Sources of Computer Programs In Hydraulics, J. Hydr. Div., ASCE, 106(5), 915-922
231. Tingsanchali,T. and Maheswaran,S., 1990, 2D Depth-Averaged Flow Computation Near Groyne, J. Hydr. Engrg. ASCE, 116(1), 71-86
232. Tsujimoto,T., 1987, Instability of Bed Surface Composition Due To Sorting Process In a Stream Composed of sand and Gravel, Sediment Transport Modelling, ed by Sam S.Y. Wang, 302-307
233. Thompson,G., 1993, Mathematical Models and Engineering Design, J. IWEM, 18-23
234. Townson,J.M., 1991, Free-Surface Hydraulics, Unwin Hyman
235. USWES, 1935, Studies of River Bed Materials and Their Movement With Special Reference To The Lower Mississippi River, Paper 17.
236. Vanoni,V.A. and Brooks, 1957, Laboratory Studies of the Roughness and Suspended Load of Alluvial Streams, Report E-68, Sedimentation Lab., California Ins. of Tech., California
237. Vanoni,V.A., 1984, Fifty Years of Sedimentation, J. Hydr. Engrg., ASCE, 110(8), 1022-1057
238. Vogel,K.R., Niekerk,A.van, Slingerland,R.L. and Bridge,J.S., 1992, Routing of Heterogeneous Sediments Over Movable Bed: Model Verification, J Hydr. Engrg. ASCE, 118(2), 263-279
239. Wang,Sam S.Y., Combs,P. and Hu,K.K., 1987, New Development in Modelling 3-D Sedimentation Phenomena, Sediment Transport Modelling, ed by Sam S.Y. Wang, 33-38
240. Wang,S.Q. and Zhang,R., 1987, Sediment Transport Rate For Non-Uniform Sand, Sediment Transport Modelling, ed by Sam S.Y. Wang, 588-593
241. White,W.R., Milli,H. and Grabbe,A.D., 1975, Sediment Transport Theories: A Review, Pro. Int. Civ. Engrg. Part 2, Vol.59, 265-292
242. White,W.R. and Day,T.J., 1982, Transport of Graded Gravel Bed Material. *Gravel-Bed Rivers*, ed. by Hey,R.D. et al, John Wiley & Sons Ltd, 181-213.
243. White,W.R., Paris,E. and Bettess,R., 1980, The Frictional Characteristics of Alluvial Streams: A New Approach, Proc. Instn. Civ. Engrs, 69, 737-750
244. Wiberg,P.L. and Smith,J.D., 1989, Model For Calculating Bed Load Transport of Sediment, J. Hydr. Engrg., ASCE, 115(1), 101-123

245. Wilcock,P.R., 1988, Methods For Estimating The Critical Shear Stress of Individual Fractions in Mixed-size Sediment, W.R.R., 24(7), 1127-1135
246. Wilcock,P.R. and Southard,J.B., 1988, Experimental Study of Incipient Motion in Mixed-size Sediment, W.R.R., 24(7), 1137-1151
247. Wilcock,P.R., 1992, Experimental Investigation of the Effect of Mixture Properties On Transport Dynamics, *Dynamics of Gravel Bed Rivers*. ed by Billi,P. et al, 109-139
248. Willetts,B.B., Maizels,J.K. and Florence,J., 1987, The Simulation of Stream Bed Armouring and Its Consequences, Pro. Instn. Civ. Engrg. Part 1, 82, 799-814
249. Willetts,B.B., Maizels,J.K. and Florence,J., 1988, The Simulation of Stream Bed Armouring and it Consequences, Discussion, Pro. Instn Civ. Engrg. Part 1, 84, 615-617
250. Willetts,B.B., 1992, Transport Rate: Considerations of Bed State, Aberdeen University
251. Willis,J.C., 1979, Suspended Load From Error Function Models, J. Hydr. Div. ASCE, 105(7), 801-816
252. Wendt,J.F., 1992, Computational Fluid Dynamics, An Introduction, Springer-Verlag
253. Yalin,M.S. and Finlayson,G.D., 1972, On the Velocity Distribution of the Flow Carrying Sediment in Suspension, ed. by Shen, 8-11
254. Yalin,M.S., 1977, Mechanics of Sediment Transport, Pergaman Press
255. Yalin,M.S. and Karahan,E., 1979, Inception of Sediment Transport, J. Hydr. Div., ASCE, 105(11), 1433-1444
256. Yalin,M.S., 1992, River Engineering, Pergamon Press
257. Yang,C.T. and Molinas,A., 1982, Sediment Transport and Unit Stream Power Function, J. Hydr. Div., ASCE, 108(6), 774-794
258. Yang,C.T. and Kong,X.B., 1991, Energy Dissipation Rate and Sediment Transport, J. Hydr. Res. IAHR, 29(4), 457-474
259. Zhang,H. and Kahawita,R., 1990, Linear Hyperbolic Model For Alluvial Channels, J. Hydr. Engrg. ASCE, 116(4), 478-493

